Anode Work Function Changes Caused by Sublimation from Barium Oxide Coated Cathodes.

Thesis presented for the degree of Doctor of Philosophy at the University of Southampton

by

Kevin Ross, B.Sc., Grad. Inst. P.

Physics Department,
Southampton University,
September 1963.

CONTENTS

INTRODUCTION

It has been known for many years that low work function anodes are frequently associated with efficient thermionic emitters. One of the best thermionic emitters, the oxide cathode, always contaminates the anode to such an extent that sometimes its work function (which may originally have been that of clean nickel, molybdenum, or tungsten) appears to be lower than that of the oxide cathode. During the lifetime of such a cathode, the anode surface becomes sufficiently contaminated by sublimed materials from the cathode for its work function to have fallen by several electron volts.

The present work was initially undertaken to investigate the work function changes that take place at the anode of a diode containing a barium oxide cathode, during the course of decomposition and activation of the cathode. Anode work functions have been measured by three independent methods: the Richardson line, the displacement of retarding potential characteristic, and the Zisman modification of the Kelvin technique. Most of the measurements were made at indicated pressures of better than 10^{-9} mmHg.

The anode work function measurements have made possible calculations of the activation energy of sublimation of barium

oxide and of the binding energy of barium oxide adsorbed on a tungsten substrate. A two phase model is proposed for the adsorption of barium oxide on tungsten at room temperature, and evidence is also presented for the existance of a third activated binding state.

Some measurements, reported in the appendices, have also been made on the work functions of uranium and zirconium carbides, and niobium.

CHAPTER I.

GENERAL PROPERTIES OF THE OXIDE COATED CATHODE

1.1. Introduction.

The discovery of the oxide coated cathode as an important thermionic emitter of electrons is due to Wehnelt(1904). In the course of experiments on gas discharges, he observed the emission of cathode rays from some areas of a platinum filament at relatively low temperatures and low anode voltages. At these low temperatures the emission could not have been directly from the platinum, but might have been the result of some impurity on the platinum surface. Wehnelt thought these impurities might be metal oxides originating from the stop-cock grease of the vacuum system. Systematic examination of the electron emission from various metal oxides showed that the most copious emitters of electrons were the alkaline earth oxides. This accidental discovery subsequently led to the modern oxide cathode which remains the most important of thermionic emitters.

Experiments carried out over the last fifty years have not yet presented a clear picture of the mechanism providing the high electron emission of the oxide coated cathode. Early work furnished the oxide coated cathode with a reputation for

poor reproducibility which was due largely to poor experimental conditions, especially those of vacuum. Improved vacuum techniques resulting from the introduction of diffusion pumps and liquid air traps and helped to eliminate many of the experimental difficulties. Later, with the arrival of Wilson's theory of semi-conductors many of the observations on oxide cathodes could be correlated under a coherent, though still inadequate theory.

As a result of recent research which will be described in detail below, and still further improved vacuum techniques which enable pressures of 10^{-10} mmHg. to be attained, a more satisfactory model of the oxide cathode is emerging.

In spite of the tremendous inroads made by transistors on the use of thermionic valves, the great reliability and long life of electron tubes containing oxide coated cathodes continues to makes their study of prime technological importance.

1.2. Preparation of the oxide cathode.

The term oxide coated cathode can embrace a variety of different cathodes. Essentially all comprise a base metal which is used to support either a layer of one alkaline earth oxide or a mixture of two or more oxides. In normal practice the thickness of this oxide layer can range from a minimum of 10^{-5}cm. to

a maximum of 10^{-2}cm. Cathodes generally operate at a temperature of about 1100°K, and can be heated either indirectly, in which case the base is in the form of a tube or box, or directly by depositing the coating on a wire or metal strip.

The demands made on the base metal are many and only a few metals and alloys are suitable. Such materials must have low vapour pressures at the normal operating temperature of the cathode, and melting points well above this temperature, be chemically inert towards the oxide and any gases or vapours associated with it, be readily outgassed during the processing of the cathode, and have adequate mechanical strength at high temperatures.

For directly heated cathodes, tungsten is preferred as a base material, although it has a disadvantage that at high temperatures a chemical reaction takes place with the alkaline earths to form a high resistance layer. When current is drawn through the oxide cathode a considerable voltage gradient can exist across this layer and the net effect is to shorten the life of the cathode. Platinum is particularly suitable as a base material where long life is a desirable feature of the cathode. Platinum is chemically inert towards the oxide coating and thus avoids any decomposition and the build up of a high resistance interface.

A third metal commonly used as a base material is nickel. In the pure state this is like platinum, chemically stable and has no effect on the emission. To improve the low tensile strength of pure nickel an alloy known as '0' nickel has been developed having the approximate composition:-

Co	0.5%	Fe	0.2%	Si	0.1%	C	0.4%
Mn	0.15%	Mg	0.1%	Cu	0.1%	S	0.005%

The impurity agents present in '0' nickel, besides resulting in a stronger cathode base, have been found to enhance the emitting properties of the cathode. At the same time silicon and manganese produce high resistance interface layers thus tending to shorten the life of the cathode.

Care is necessary in cleaning the base material before application of the coating of oxide. Washing the base in an organic solvent removes any grease present; oxides that might exist on the surface can usually be reduced by furnacing in dry hydrogen at 1300°K.

Emission measurements on the pure oxides of barium, strontium, and calcium at the same temperature give current densities approximately in the ratio 100:10:1. A mechanical mixture of any of these oxides has an emission current density equal to the sum of the emission current densities of the seperate components, but an oxide of mixed crystals gives a

higher emission current density than the mechanical mixture. Mixed crystals of barium/strontium oxide, (BaSr)O, have good emission properties, but by adding calcium to form (BaSrCa)O so that the crystals have a composition BaO:SrO:CaO of 49:44:7, the emission is optimised.

The alkaline earth oxides are unstable in air being rapidly converted into the hydrate and carbonate by water vapour and carbon dioxide. The formation of these compounds, which is accompanied by a change in volume, effects the bonding between base and coating, usually resulting in the coating flaking away from the base. For this reason the oxide is now generally prepared in vacuum, the alkaline earth being applied to the base as a carbonate and decomposed to oxide by pyrolysis in vacuum.

The carbonate can be prepared as a white precipitate by the addition of ammonia to a solution of the pure alkaline earth nitrate. The size of the precipitated particles depends on the temperature of the nitrate solution, and its concentration. After drying, the precipitate is mixed with an organic binder dissolved in a volatile solvent and ball-milled for several hours. Nitrocellulose is commonly used as a binder in a solution of amyl acetate. This helps the coating adhere to the base but can, under some circumstances, have adverse effects on the performance of the cathode.

The carbonate may be applied to the base by one of three methods; spraying, painting, or electrophoresis. When painting is used, successively thin layers of carbonate are super-posed until the required coating thickness is reached. This method, which is sometimes used for directly heated cathodes, does not normally lead to a uniform coating. Indirectly heated cathodes are generally coated by spraying the carbonate suspension onto the base. The physical properties, particularly density, of the carbonate deposit, vary widely in this process; gas pressure during the spraying, the ambient temperature, the distance of the spray gun from the base, and the concentration of the carbonate solution can all effect the final result. In general, surfaces prepared by spraying tend to be very porous. Application by electro-proresis is preferred where careful control of the coating thickness and a less porous structure are desired.

When sealed into an envelope and mounted on the vacuum system, the carbonate is converted to oxide by raising the temperature of the cathode to 1300^{o}K over a period of about 30 seconds. The gases evolved from the cathode during this process are pumped away as fast as possible. Decomposition of the carbonate can be judged complete when the pressure in the system falls below 10^{-6}mmHg. During decomposition large quantities of gas are absorbed on the walls of the envelope

and on the valve components; this absorbed gas can only be removed from the system by a rigorous outgassing programme involving baking at 450°c together with eddy current heating of metallic components

1.3. Activation.

After decomposition of the carbonate the emission obtainable from the cathode is usually low. Added to this there are wide variations in the emission characteristics from cathode to cathode. A higher and more stable emission can be obtained by processes called activation. The net effect of activation (which will be discussed in Chapter II) is thought to be to produce an excess of free barium in the oxide. Oxide cathodes can be activated in any one, or a combination of at least five distinct methods.

(1) Thermal activation.

Heating the cathode momentarily to a temperature (1350°K) well above its normal operating temperature can produce an excess of alkaline earth metal by increasing the rate of chemical reaction between the oxide and reducing agents; these can arise from two sources: (1) carbon and carbon dioxide originating from the decomposition of the binder material and the conversion of the carbonate coating to oxide, (2) any

reducing impurities that may be present in the base material. To investigate the possibility of reduction by carbon alone, Huber(1941) examined two types of cathode; one was prepared with a paste containing an organic binder and the other with a water paste. The presence of carbon was found to have no effect on the process of activation by reduction, though it may react with carbon dioxide to produce carbon monoxide: $CO_2 + C \rightleftharpoons 2CO$. Carbon monoxide may also be produced by the reaction:- $2CO_2 \rightleftharpoons 2CO + O_2$. The reduction of barium oxide by carbon monoxide is quite straight foreward:-

$$BaO + CO \rightarrow Ba + CO_2.$$

After a theoretical study of the chemistry of the oxide cathode, Rittner(1953) suggests that Th, Mg, Be, Zr, U, Al, Si, should all be good activators of barium oxide, while Fe, Mo, Cr, W, Mn, Ta, C, Ti, are only moderate activators. Ni, Cd, Cu, Pb, Au, Pt, Rh, are relatively inert and should not produce any activation.

(2) Activation by drawing current.

By raising the cathode temperature to 1000°K and applying a voltage to the anode it is possible to increase the emission current by as much as a factor of 10^3. This process is generally thought to produce electrolytic dissociation in the oxide. Detailed consideration will be

given to electrolytic dissociation and associated effects in Chapter II.

(3) Activation by external reduction.

Small quantities of reducing gases such as methane also produce activation in oxide cathodes. Free barium can be produced by the reaction: $BaO + CH_4 \rightarrow Ba + CO + 2H_2$

In this method the gas is introduced to the cathode at a pressure of 10^{-2} mmHg. and the cathode temperature then raised to 1300°K for five or ten minutes. Hannay, MacNair and White(1949) have used this method successfully. Hydrogen also acts as a reducing agent, but White(1949) has found that methane at 10^{-2} mmHg. is 100 times more effective in its reduction of barium oxide than hydrogen even at atmospheric pressure. However, at elevated temperatures methane is found to be unstable, dissociating spontaneously:

$$CH_4 \rightarrow C + 2H_2.$$

The carbon produced can deposit onto the cathode and thus result in a reduced emission.

Activation by external reduction is only used in experimental investigations with oxide cathodes.

(4) Activation by barium evaporation.

The excess barium required to activate the oxide cathode can be produced by evaporating barium metal directly onto the surface of the cathode. This method, like the previous one,

is not used commercially but is an experimental tool, Beese(1930). Cathodes activated in this way can be deactivated in a few minutes by raising the temperature to 1200°K thereby re-evaporating the deposited barium. At lower temperatures the barium deposited onto the cathode surface diffuses into the bulk of the cathode matrix thus causing activation.

(5) Activation by electron and ion bombardment.

Bombarding an unactivated cathode with electrons is found to have an activating effect. Electrons accumulating at the surface of the cathode lead to a change in surface potential which may give rise to an ionic current in the oxide layer and so produce activation by drawing current through the oxide. Bombardment by relatively low energy positive ions produces a similar effect.

1.4. The activated state.

Whichever of the five methods of activation are employed, the cathode emission finally reaches a steady state, although in this steady state the emission from the cathode is not uniform over the whole of the cathode area. Heinze and Wagener(1936) have taken electron images of the oxide cathode at various stages of activation which show that in the initial

stages of activation there are few emitting centres, but as activation proceeds the number of emitting patches increases to cover a large part of the cathode. Further activation produces little alteration in the size and distribution of the emitting patches.

A considerable volume of work on the activation of oxide cathodes leads to the conclusion that the activated coating contains an excess of alkaline earth metal, (see for example Hermann and Wagener(1950). Wagener (1954) found that the quantity of excess alkaline earth metal has an optimum value beyond which the emission does not increase. However, an attempt by Wooten et al.(1955) to correlate emission with barium content failed. For an activated cathode Wooten et al.gave a figure of 1 atom of barium in 10^6 oxide molecules. The poor emission sometimes observed in cathodes with a high excess barium content indicates that other factors effect emission. Most important among these are probably the preparation proceedure and the residual gas content of the final assembly.

1.5. The physical structure of the oxide cathode.

The completed cathode can be divided for convenience into four regions; the metal base, an interface layer, the oxide coating, and the vacuum interface, each region having

an important effect on the electrical performance of the cathode.

The base metal is important in determining the nature of the interface layer which results from reduction of the oxide coating by any reducing impurities diffusing out of the base metal. Reducing agents commonly used are silicon, titanium, manganese, magnesium, aluminium, and carbon. All of these react with barium oxide to form oxides, and many of the oxides in turn react with barium oxide to form higher compounds at the interface. Rooksby(1940) (1940a) (1947) reported the formation of barium aluminate $BaAl_2O_4$, barium orthosilicate Ba_2SiO_4, and barium orthotitanate Ba_2TiO_4.

Despite the fact that the interface layer gives a much stronger bond to the base metal, its growth during cathode operation often limits the life of the cathode by retarding the diffusion of reducing agents from the base into the oxide. This, together with the high resistance of the interface layer can limit the lifetime of the cathode.

Early investigations showed the electrical conductivity of the oxide coating to be very low compared with that of a metal. Further, all such measurements showed a general increase in the electrical conductivity with increasing temperature; substances having these properties are classified as semi-conductors. The semi-conducting properties of the

oxide coating are now well established and thought to result from the excess alkaline earth metal in the oxide. Detailed discussion of the semi-conducting properties of the oxide cathode will be given in Chapter II. A voltage drop does occur across this region of the cathode but it is small compared with the drop across the interface layer.

The exact nature of the vacuum interface is to a certain extent open to speculation. The resistance of this region is found to be strongly influenced by dissociated ions resulting from the application of external field.

1.6. The cathode and its environment.

In a diode containing an oxide cathode, materials evolved from the anode under electron bombardment can have a marked effect on the emission of the cathode, Young(1960). Under electron bombardment the anode is continually evolving gases deposited during decomposition and operation of the cathode. The residual ambient gas is found to be principally O_2, H_2O, H_2, CO, CO_2, and reaction between the cathode and these gases has been clearly demonstrated by Plumlee and Smith(1950) and Plumlee (1956). At a pressure of 10^{-7}mmHg. a number of gas atoms equivalent to a monolayer strike the cathode every 30 seconds so that condensation and re-evaporation must proceed

in dynamic equilibrium on the surface.

The effect of materials evolved from the glass envelope has been studied by Hamaker, Bruining, and Aten(1947) who found that the presence of chlorine on the cathode after activation could be accounted for by a reaction which took place during baking at 400°C:

$$2NaCl + SiO_2 + H_2O \rightarrow 2HCl + Na_2SiO_3.$$

The HCl produced then reacts with the carbonate of the cathode to form $BaCl_2$. During the pyrolysis of the carbonate the $BaCl_2$ evaporates onto the anode. Electrons with energies greater than 10 volts are able to decompose the chloride, and the chlorine atoms produced can then find their way back to the cathode and cause poisoning.

1.7. Preconversion of the oxide cathode.

Many effects resulting from the liberation of large quantities of gas during decomposition of an oxide cathode can be eliminated by 'preconverting' the cathode. To do this the cathode is mounted in a seperate envelope, evacuated, and decomposed in the usual way. When the time comes to mount the cathode in the final tube, the envelope is opened and the cathode remounted. While the cathode is exposed to the air it should be maintained at a temperature of 150°C, since this

allows the conversion of the oxide into the hydroxide only. Formation of the hydrate which occurs at lower temperatures, leads to a change in volume and hence to cracking and flaking of the coating. Heating also prevents the carbonate reforming from carbon dioxide present in the air. Preconverted cathodes have been observed by Haas and Jensen(1959) to give better emission than cathodes processed in the normal way.

CHAPTER II.

THE MECHANISM OF THE OXIDE CATHODE

2.1. Early emission theories.

The introduction of a satisfactory semi-conductor theory in 1931 led to an important advance in understanding the mechanism of the oxide cathode. By this time a theory accounting for the thermionic emission from pure metals had been established, the temperature dependance of emission being represented by Richardson's equation (see section 2.4.). The phenomena observed with oxide cathodes were not easily explained. Their high thermionic current density per watt of heater power (activity) surpassed even the more active contaminated metals such as thoriated and caesiated tungsten, but an explanation was initially sought by analogy with these systems.

The necessity for a process of activation to produce a fully active cathode, which could be effected thermally or by drawing current through the cathode, was demonstrated by Becker(1929). His experiments established that during either of these activation processes free metallic barium was produced, and that this resulted in the work function of the cathode being lowered.

The necessity for a process of activation to produce a fully active cathode, which could be effected thermally or by drawing current through the cathode, was demonstrated by Becker(1929). His experiments established that during either of these activation processes free metallic barium was produced, and that this resulted in the work function of the cathode being lowered.

At the time of Dushman's review (1930), two theories existed concerning the location of the barium and hence the emitting surface of the cathode. Becker's theory (1929) held that the activity depended on a surface concentration of free metallic barium. The free barium on the barium oxide coating was considered to lower the work function in a way analogous to barium on tungsten. At the same time Lowry(1930) considered the source of emission to be a layer of metallic barium or other alkaline earth metal on the surface of the base metal or alloyed with it. Electrons emitted from this composite surface would have to diffuse through the coating before being released into the vacuum. Apart from the source of emission, these two theories differed further regarding the role of the oxide coating. Becker considered it a good conductor, electrons passing easily to the surface, whereas Lowry suggested that the coating offered considerable resistance to the progress of electrons.

In support of his mechanism, Lowry pointed out the pronounced influence of different base materials on the cathode performance, and also the gradual decay in activity during operation which he thought was the consequence of a slow scintering effect in the oxide. Scintering would result in a closing of the pores, thereby increasing the resistance offered to the passage of electrons. By removing the coating completely, Becker and Sears(1931) found that the emission current dropped by three orders of magnitude. Jones(1936) removed just the outer surface of the coating in vacuum and observed a decrease in emission by three orders of magnitude which could be subsequently restored by thermal treatment. This indicated a marked dependance of electron emission on the external surface.

Darbyshire(1938) using electron diffraction techniques to examine surfaces of oxide cathodes, could find no positive evidence for the existance of a surface barium layer, but despite this he interpreted the results of his experiments as indicating such a layer. Other diffraction experiments by Huber and Wagener(1942) also failed to demonstrate conclusively the presence of surface barium. More recent theories concerning the emission sites in oxide cathodes are discussed in section 2.9.

With the advent of Wilson's theory of semi-conductors (Wilson 1931), and the application of this theory to oxide cathodes, many well established experimental facts concerning the oxide cathode could be explained and some measure of agreement was found between theoretical calculations and experiment. The theory is considered in greater detail below.

2.2. The band structure of solids; semi-conductor theory.

The behaviour of electrons in solids has been described quantitatively in terms of bands of allowed energy levels which may be seperated by gaps or forbidden energy regions. This theory can be approached by considering the discrete nature of energy levels in a free atom. When an assembly of atoms is condensed to form a crystal the energy levels of adjacent atoms interact, each discrete energy level being displaced such that a band of very closely spaced energy levels is formed. These allowed bands become wider with increasing energy and bands from different discrete levels in the individual atoms may overlap. A crystal may also have allowed energy bands which are normally unoccupied, corresponding to excited states in the isolated atoms. These empty bands are called conduction bands, and may overlap

with other vacant bands or with a filled band. The occupied band immediately below the conduction bands is called the valence band.

It follows from the Pauli Exclusion Principle and as a result of the two spin quantum states of each electron, that a band of energy levels formed from N atoms contains 2N possible electron energy states, so that when the atoms of a crystal only contribute one electron each to the valence band, the band is only half full. Electrons in such a crystal are easily accelerated by the application of low electric fields since there are levels of slightly higher energy to which the electrons can move. When the contribution to the valence band is two electrons from each atom, all the energy levels in the band will be filled. Such solids are said to be insulators provided the uppermost filled band does not overlap with an empty band, and the energy gap between it and the nearest empty band is about 10 eV. When this energy gap is only about 1 eV. electrons may be excited into the conduction band at temperatures a few hundred degrees above room temperature, and the solid is said to be an intrinsic semiconductor. For an energy gap EgeV, the number of electrons in the conduction band is given by

$$n = 2(2\pi m' kT)^{3/2} h^{-3} . \exp -E_g/2kT \qquad (2.1)$$

$$n = 5 \times 10^{15}\ T^{3/2}.\ \exp\ -E_g/2kT \qquad (2.2)$$

When E_g is 1 eV, the number of electrons in the conduction band is of the order 10^{15}. This is less than that of a metal by a factor of 10^7.

Semi-conductors usually contain impurities which can give rise to an enhanced conductivity if their concentration is sufficiently high. Such impurities can provide energy levels which lie in the forbidded region of the host crystal, and thus either supply electrons to the conduction band or accept electrons from the valence band much more readily than in the case of a pure semi-conductor.

Impurity levels fall into two distinct classes. Where the impurity has one or more valence electron than the host element then the impurity energy levels are located just below the bottom of the conduction band. Ionisation of these impurity centres by relatively low energy phonons contributes an electron to the conduction band which is then free to move in the crystal. Such impurity centres are called donors, and since the charge carriers are negatively charged, the crystal is said to be an 'n'-type semi-conductor. When the impurity atom has one or more valence electrons less than the host element, the impurity levels are slightly above the valence band, so that at a temperature greater than absolute zero a valence bond electron may have enough energy

to leave its normal state and enter the impurity level. These impurity levels are called acceptors, and conductivity takes place in the crystal as a result of electron vacancies or holes in the filled band. In this case the crystals are called 'p'-type semi-conductors.

It has been pointed out in Chapter I that considerable evidence is available for attributing the semi-conducting properties of the oxide cathode to a stoichiometric excess of free alkaline earth metal in the crystal lattice ('n'-type semi-conduction). This excess could result from: (1) Excess alkaline earth atoms deposited either interstitially or at lattice points; in view of atomic size considerations a very distorted lattice would result from the interstitial arrangement. (2) The existance of vacant oxygen sites in the lattice; this would provide an explanation for all the electronic behaviour without leading to a very distorted lattice.

Measurements using the Hall effect should make it possible to verify the 'n'-type semi-conductor theory of the oxide cathode. Wright(1951), Foreman(1954), and Isikawa(1951) have measured the Hall effect in barium films. 'N'-type semi-conduction was generally observed in all cases, although the introduction of impurities into the cathodes produced negative Hall coefficients corresponding to 'p'-type semi-conduction.

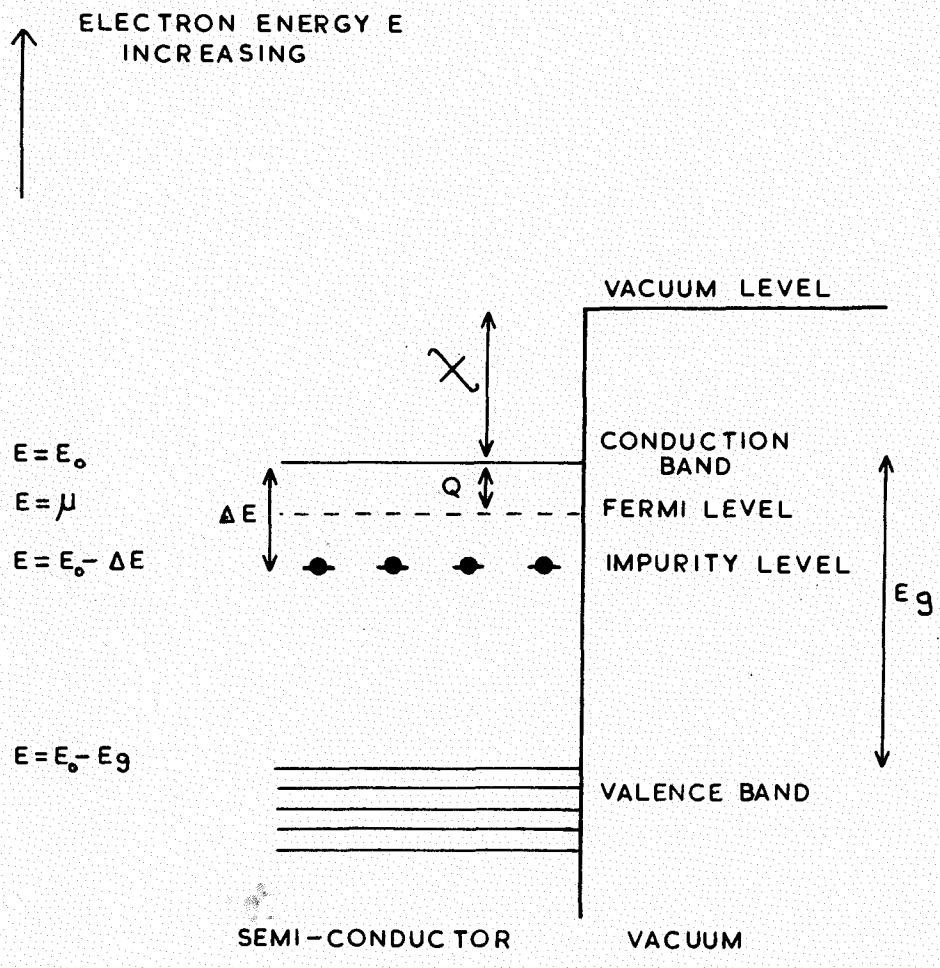

FIG. 1.
ENERGY LEVELS FOR AN 'n'-TYPE SEMI-CONDUCTOR

The energy level configuration of an 'n'-type semi-conductor is shown in Fig.1. The energy at the bottom of the conduction band is E_o. μ, the electrochemical potential level is called the Fermi level of the 'n'-type semi-conductor, and represents the partial free energy of the electrons. The exact position of μ between the conduction band and the impurity levels is determined by the relative number of impurity centres, and the temperature of the crystal (see below). E_g is the energy gap between the valence band and the conduction band.

The removal of an electron from the crystal into vacuum requires a total energy $Q + \chi$. Q is the energy necessary to raise an electron from the Fermi level into the conduction band, called the inner work function; χ is the surface work function, and represents the difference in energy between the bottom of the conduction band and a position just outside the surface. The total quantity $Q + \chi$ is known as the thermionic work function ϕ.

The basic features of an 'n'-type semi-conductor have been discussed by Seitz(1940). Taking the case of a single impurity level it is assumed that there are n_b bound electron states per unit volume having energy $(E_o - \Delta E)$, and that these levels are completely occupied at absolute zero temperature

by n_e electrons. In addition there is a conduction band of levels above these bound states which is completely unoccupied at absolute zero. Thermal transitions from the filled valence band to the conduction band are to be neglected on the assumption that $E_g \gg \Delta E$.

The location of the Fermi level is given by

$$\mu = E_o - \Delta E/2 + kT/2.\ \ln.n_b h^3/2(2\pi m' kT)^{3/2} \qquad (2.3)$$

where k is the Boltzmann constant, T is the absolute temperature, h is Planck's constant, and m' is the effective mass of an electron in the conduction band. For normal densities of bound electrons the last term on the right of Eq. 2.3. is of the order of magnitude kT, so that for $\Delta E \gg kT$

$$\mu = E_o - \Delta E/2.$$

The number of free electrons per unit volume in the conduction band, n_f is given by:

$$n_f = n_b{}^{1/2}\ 2^{1/2}(2\pi m' kT)^{3/4}\ h^{-3/2}.\ \exp - \Delta E/2kT. \qquad (2.4)$$

If kT is large compared with ΔE, all the impurity levels will be ionised and $n_f = n_b$.

2.3. The contact potential difference.

When two electrical conductors 1,2, are in contact,

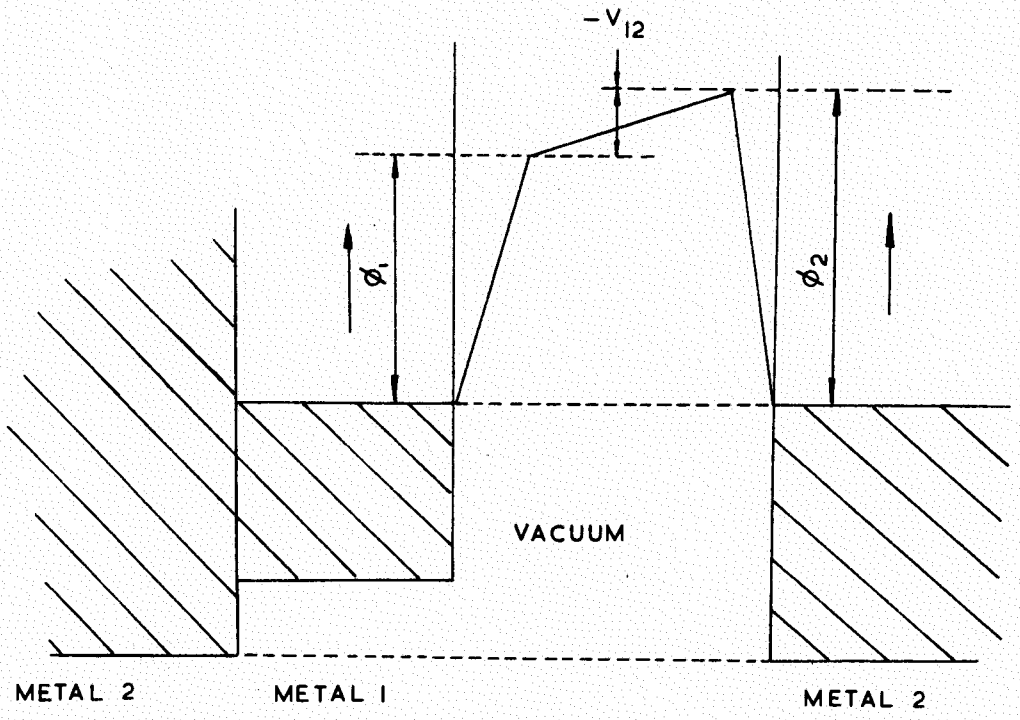

FIG. 2

POTENTIAL VARIATION BETWEEN TWO DIRECTLY CONNECTED METAL ELECTRODE

electron flow takes place across the junction between the two metals until the two Fermi levels reach a common energy level. Under these circumstances the potential variation across a vacuum gap between the two metals is shown in Fig.2. V_{12}, the potential across the vacuum, is known as the contact potential difference between the two surfaces of the conductors and is given by the expression

$$-V_{12} = \phi_2 - \phi_1, \qquad (2.5)$$

where ϕ_1 and ϕ_2 are the work functions of the two surfaces concerned.

2.4. Thermionic emission.

In considering the thermionic emission from oxide cathodes based on the model of an 'n'-type semi-conductor, it is important to remember that the oxide is in contact with its base metal. Fig.3 shows the energy level diagram when contact is made to the base. Immediately the semi-conductor makes contact with the metal, electron donors near the surface of the semi-conductor lose their electrons to the metal until the two Fermi levels coincide. This results in a layer of positive space charge in the semi-conductor called the Schottky depletion layer (Schottky 1939).

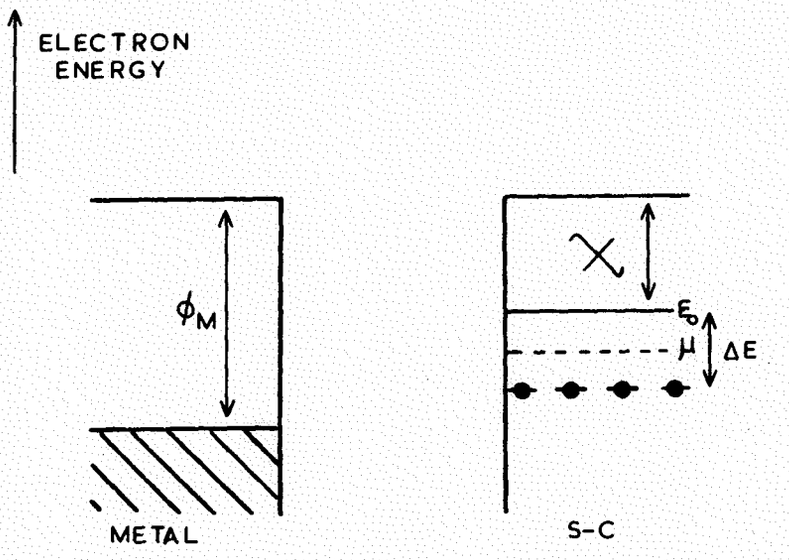

(a)

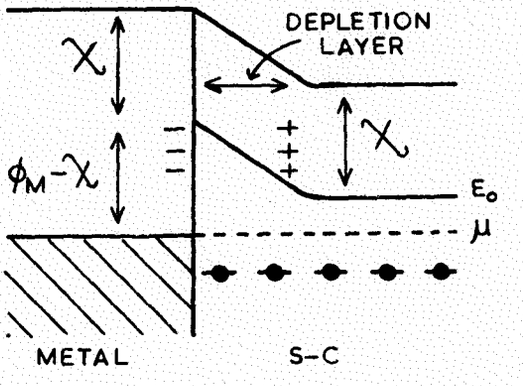

(b)

FIG. 3.
ENERGY LEVEL DIAGRAMS OF METAL TO SEMI-CONDUCTOR CONTACT. (a) PRIOR TO CONTACT, (b) AFTER CONTACT.

The emission current density equation for this model has been shown by Schottky(1940) to be similar to the Richardson-Laue-Dushman equation for emission from metals

$$j_o = A(1 - r)T^2. \exp -e\phi/kT. \qquad (2.6)$$

j_o is the saturated current density, r is the electron reflection coefficient at the emitting surface, ϕ is the thermionic work function $(\chi + E_o - \mu)$, and A is a constant given by:

$$A = 4\pi m'k^2e/h^3 = 120 \text{ amps/cm}^2\text{/deg.}^2 \qquad (2.7)$$

Substituting the value for $(E_o - \mu)$ from Eq.2.3. gives

$$j_o = B(1 - r)n_b^{1/2} T^{5/4} \exp. -(\Delta E/2 + \chi) \qquad (2.8)$$

where $$B = 2ek^{5/4} (2\pi m')^{1/4}/h^{3/2}. \qquad (2.9)$$

Fowler has pointed out that these equations are only valid provided normal internal equilibrium is maintained in the solid; emission is not an equilibrium process and therefore these equations should never apply. In addition, the effects of the high resistance interface and the depletion layer formed at the base to oxide coating contact have been ignored. Some discussion will be given to these two points at the end of this section.

A so called Fowler emission plot obtained from Eq. 2.8 by plotting log $j_o/T^{5/4}$ as a function of (1/T) will have a

slope whose value is $-(\Delta E/2 - \chi)$. From the energy diagram in Fig. 1 it can be seen that this quantity represents the thermionic work function at absolute zero. Similarly from Eq. (2.4) the so-called Richardson plot of log j_o/T^2 as a function of 1/T should provide a measurement of the thermionic work function ϕ. However, account must be taken of the fact that the work function ϕ may be dependent on temperature (Becker and Brattain 1934). If the linear relationship $d\phi/dT = a$ is assumed, then $\phi = \phi_R + aT$, where ϕ and ϕ_R are the values of the work function at T^o and 0^oK, respectively. Substituting this value of ϕ into Eq. 2.6 gives

$$j_o = A(1 - r)T^2 . \exp -e(\phi_R + aT)/kT \qquad (2.10)$$

$$j_o = A(1 - r).\exp -e(a/k). T^2 . \exp -e(\phi_R/kT) \qquad (2.11)$$

The Richardson plot is therefore a straight line whose slope provides a measurement of the thermionic work function at 0^oK, ϕ_R, and whose intercept gives a value of the thermionic constant

$$A_o = A(1 - r). \exp -e(a/k). \qquad (2.12)$$

In addition to determining the thermionic work function at absolute zero, a Fowler plot can provide an estimated value of the donor concentration from the intercept on the log j_o/T^2 axis, $\log A' = \frac{2ek^{5/4}(2\pi m')^{1/4}}{h^{3/2}} n_b(1 - r).$ (2.13)

Direct calculation of either r or n_b being impossible, Nottingham(1956) has estimated a value of 0.175 for (1 - r). A calculation based on the emission data of Hung(1950) then leads to a donor density of 2.4×10^{17} per cm^3. By using the emission data of Prescott and Morrison (1938) and their value for n_b of 10^{20}, Eisenstein(1948) finds a value of 0.05 for (1 - r), r = 0.95. Wooten's(1946) value of 10^{18} per cm^3 for n_b gives a value of 0.5 for (1 - r).

On account of the very porous nature of the oxide cathode, accurate emission current density evaluation is very difficult since the actual emitting area is unknown. Estimates of the external surface area will probably bear little relation to the total emitting area of the cathode, so that measured values of log A_o are unreliable.

In his analysis of Hung's emission data, Nottingham applied corrections to the theory to include the effect of multiple reflections on the diode characteristics and obtained a value of 112 amps/cm^2/deg.^{2} for A, this value being in good agreement with the theoretical value of 120 amps/cm^2/deg.^{2}

Interesting results are obtained by considering the emission from a cathode having zero reflection coefficient, a thermionic work function of 1.0 eV., with $n_b = 10^{18}$ per cm^3. Substitution of these valuesinto Eq.2.8 gives an emission

density at 1000°K of 55 amps/cm^2. Such high current densities have been observed only under microsecond pulse conditions, see Thomas(1930), Sproull(1945), Coomes(1946), and Wright(1947). From these observations it might be concluded that pulsed emission represents the true emission current density predicted by Eq.2.8, and that measured D.C. emission current densities represent a decayed state of the cathode. Emission decay effects will be discussed in detail in section 2.8.

The introduction of a depletion layer at the metal-coating interface, modifies the model of the oxide cathode (Fig.3b) and leads to a possible explanation of the rectification properties observed in oxide cathodes by Wright(1947) and Mutter(1947). The high resistance interface compounds also found in oxide cathodes have been discussed in Chapter I. When emission is drawn from the cathode surface the effect of the above interface layers is to reduce the potential applied to the cathode surface by an amount equal to the potential drop across the interface layer; this latter drop in potential may be a large fraction of the applied anode potential.

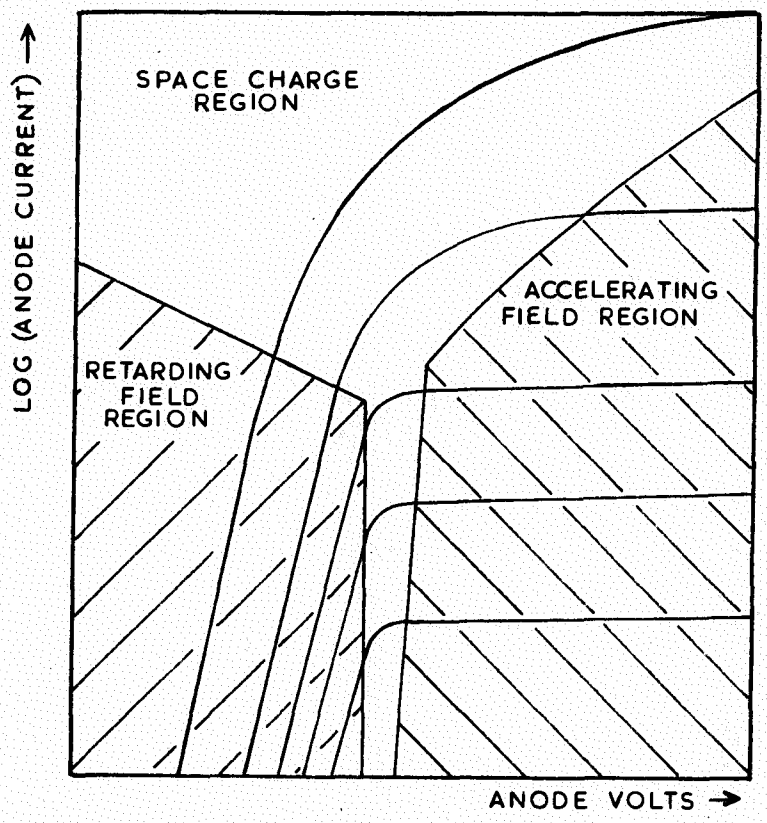

FIG.4.

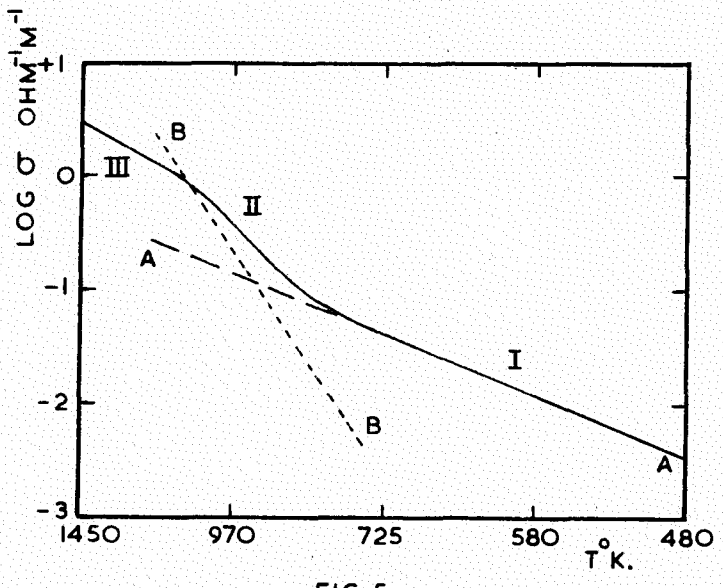

FIG.5.

REGION I, SEMICONDUCTOR CONDUCTIVITY IN CRYSTALS. RANGE II, PORE CONDUCTIVITY PREDOMINANT. RANGE III, PORE CONDUCTIVITY INHIBITED BY SPACE CHARGE. CURVE AA SEMI-CONDUCTOR CONDUCTION ALONE, CURVE BB PORE CONDUCTION ALONE WITHOUT SPACE CHARGE.

2.5 Voltage characteristics.

The general form of thermionic emission versus anode voltage curves for different cathode temperatures is shown in Fig.4, and can be divided into several distinct regions.

(a) Retarding potential region.

The retarding potential is the work required to carry an electron from a point just outside the emitter surface to a point just outside the collector surface, and may result from an externally applied negative voltage, or from the contact potential difference between the anode and the cathode. For a plane parallel diode the current density j_r collected at an applied anode-cathode voltage V is given by

$$j_r = A(1 - r)T^2 C.\exp -(V + \phi_A)/kT \qquad (2.14)$$

where ϕ_A is the anode work function, and C the anode electron reflection coefficient.

(b) Accelerating field region.

At low cathode temperatures where the emission current density is low enough for space charge effects to be neglected, there is a point where the retarding field changes abruptly to an accelerating field as the anode voltage is increased. The behaviour in the accelerating field region has been investigated by Schottky(1914) who assumed that mirror image forces exist between the cathode

interior and the emitted electrons. A reduction of work function resulting from a field E at the cathode surface was shown to be

$$\phi = (eE)^{1/2}. \qquad (2.15)$$

and the emission current density in this region j_a given by

$$j_a = j_o \exp (e^{3/2} E^{1/2})/kT. \qquad (2.16)$$

where j_o is the emission current density for zero applied field.

(c) Space charge region.

At higher cathode temperatures the space charge limited region becomes extended. Emission in this region range obeys the Langmuir-Child law, Childs(1911), Langmuir(1913),

$$j_{sp} = b. V^{3/2} \qquad (2.17)$$

where j_{sp} is the space charge limited current, b is a constant depending on the electrode arrangement, and V is the anode voltage.

2.6. Electrical conductivity.

Few reliable measurements on the electrical conductivity of oxide cathodes had been made prior to 1949, and these were frequently at varience. Despite experimental difficulties in making these measurements, it was generally accepted in the early work that the variation of electrical conductivity

σ with temperature T was of the form:

$$\sigma = a.\exp -b/T. \qquad (2.18)$$

a and b being constants.

In 1949 Loosjes and Vink made a careful investigation of the electrical conductivity of a (BaSr)O cathode over the temperature range 500° to 1200°K. Their results showed that the conductivity over this temperature range could be divided into the three regions shown in Fig.5. Below 800°K the temperature dependance is small, the value of a the so-called activation energy in Eq.2.18, varying from 0.6 to 0.09 eV. with increasing cathode activity, while in the range 800° to 1000°K there is a higher dependance of conductivity on temperature with activation energies from 2.2 to 0.8 eV. Above 1000°K the slope is again reduced.

Loosjes and Vink explained these results in terms of two conduction mechanisms acting in parallel with one another. Low temperature conduction was attributed to normal conduction through the particles of the oxide crystals, whereas conduction in the range 800° - 1000°K was explained by electron movement between the electron emitting grains of the porous oxide coating. At temperatures above 1000°K this conduction mechanism becomes inhibited by the formation of a space charge in the pores.

The electrical conductivity of an 'n' type semi-conductor σ_c, is proportional to n_f, the number of electrons in the conduction band, and u, their mean mobility, so that

$$\sigma_c = n_f e u. \qquad (2.19)$$

Expressing σ_c in terms of electrical mean free path l which has a constant value l_o at a temperature T,(Maurer, 1945),

$$\sigma_c = \frac{4 n_f l_o e^2}{3(2\pi m' kT)}^{1/2} \qquad (2.20)$$

Substituting for n_f from Eq.2.4 gives:

$$\sigma_c = \frac{4}{3} 2^{1/2} n_b^{1/2} (2\pi m' kT)^{1/4} \cdot \frac{e^2 l_o}{h^{3/2}} \cdot \exp(-\Delta E/2kT) \qquad (2.21)$$

Providing $\Delta E/2 \gg kT$, σ_c will be almost independant of the term in $T^{1/4}$ and can be written:

$$\sigma_c = K \exp -\Delta E/2kT \qquad (2.22)$$

The plots of log σ against 1/T in the temperature range below 800°K which were found by Loosjes and Vink to be linear, will then have a gradient $\Delta E/2$. As the temperature is increased above 800°K, conduction of the electron gas in the pores of the oxide coating gradually swamps the semi-conduction component.

The pore conduction process has been examined theoretically by Loosjes and Vink(1949), Hensley(1952), and Foreman(1954). The magnitude of the conduction current for

a given applied potential and cathode temperature depends on the mean free path of the electrons, the pore size, the space charge in the pores, and the Schottky effect at the pore surface resulting from the applied field. The expression derived for the pore conductivity is of the form

$$\sigma_p = K' \exp(-\phi_1/kT) \qquad (2.23)$$

ϕ_1 is a work function, which, by comparison with external thermionic emission, Loosjes and Vink identify as the Richardson work function, K' is a constant.

The combination of these two conduction mechanisms can be represented by:

$$\sigma = A\sigma_p + B\sigma_c = C \exp(-\phi/kT) + D \exp(-\Delta E/2kT) \qquad (2.24)$$

where A,B,C,D, are constants. If ϕ_1 is the Richardson work function,

$$\phi_1 \simeq \chi + \Delta E/2, \quad \text{so that} \quad \phi_1 > \Delta E/2.$$

Over the whole temperature range these two processes act in parallel, but at low temperatures the solid semi-conduction mechanism dominates. In the high temperature range plots of log σ as a function of 1/T must be corrected for the semi-conduction process acting in parallel if an accurate value of ϕ_1 is to be obtained from the gradient.

An alternative explanation for the break in the conductivity curves might be the existance of two seperate impurity levels below the bottom of the conduction band.

However, if this was the case, activation energies in the high temperature region would be much less than the Richardson work function, as energy would only be required to take electrons from the donor levels into the bottom of the conduction band. Loosjes and Vink(1949) and Nakai, Inuishi, and Tsung-Chi(1955) reported values of the activation energy for the high temperature conductivity which agree with the Richardson work function for thermionic emission in the same activation state. However, both these results should be considered cautiously. Loosjes and Vink measured the conductivities by pressing two cathodes into contact with one another. Emission measurements were made by seperating the cathodes and inserting an anode between them; this process of seperation could almost certainly be expected to modify the cathode surfaces. On the other hand, the conductivity measurements by Nakai, Inuishi, and Tsung-Chi (1955) have not been corrected for the parallel acting low temperature conductivity mechanism. Many workers obtain agreement to within 20% between the activation energy for high temperature conductivity and the Richardson work function, and this might be regarded as satisfactory since the emitting surfaces may be different for the two mechanisms.

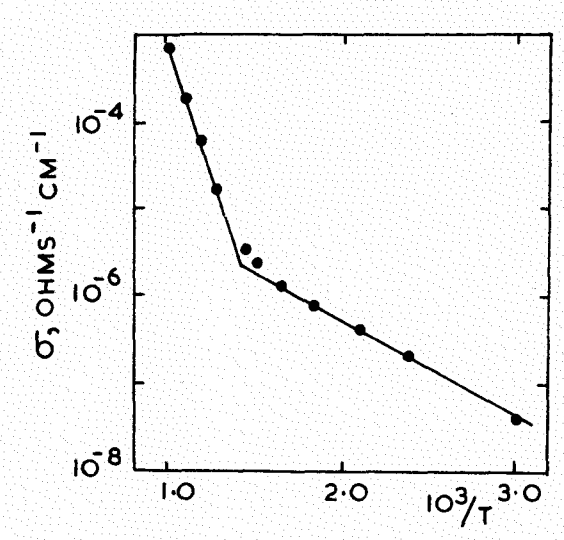

(a)
ELECTRICAL CONDUCTIVITY
VS. RECIPROCAL TEMPERATURE.
YOUNG (1952)

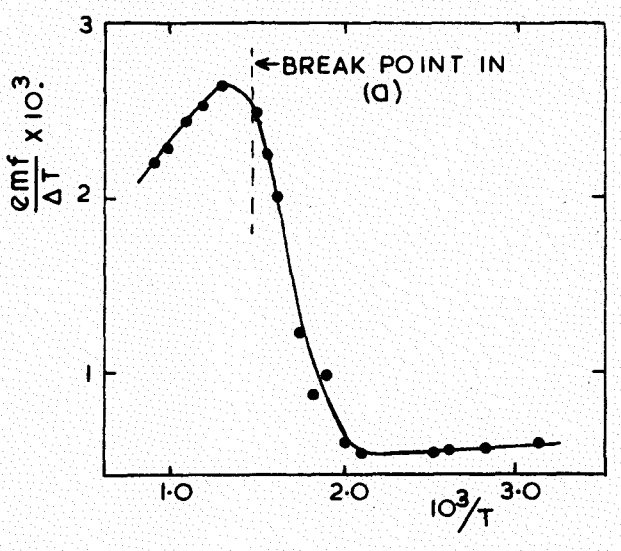

(b)
THERMOELECTRIC POWER
VS. RECIPROCAL TEMPERATURE
YOUNG (1952)

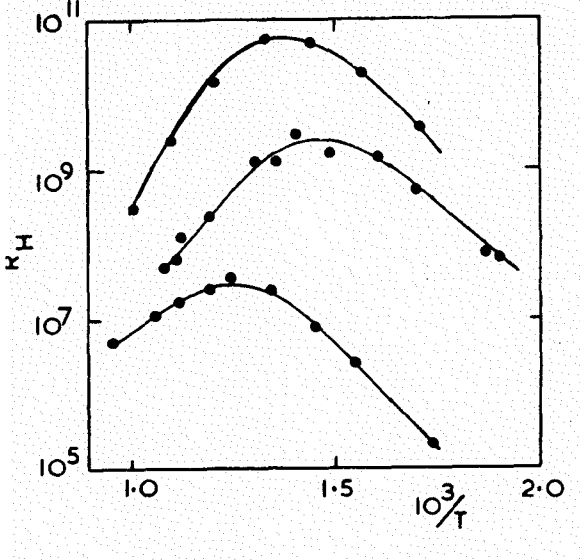

(c)
HALL COEFFICIENT VS.
RECIPROCAL TEMPERATURE
FORMAN (1954)

FIG.6.

Measurements of the Hall coefficient and thermoelectric power provide other means of studying these conduction processes. Theoretical models based on the pore conduction and semi-conduction suggested by Loosjes and Vink have been studied by Foreman(1954) and Hensley(1952), and these theoretical results are in good agreement with the experimental observations of Foreman(1954) and Young(1952). Both the Hall coefficient and the thermoelectric power show a distinct changes (Fig.6) in the temperature region corresponding to a transition from pore to semi-conduction.

Closely allied to the Hall effect is the phenomenon of magnetoresistance; this is the change of electrical resistance brought about in a conductor or semi-conductor by the application of an external field. In agreement with theoretical predictions based on the Loosjes-Vink model, oxide cathodes have been shown (by Foreman 1954, and Metson 1958b) to exhibit strong megnetoresistive properties only when conduction is by way of the vacuum pores.

Pore conduction will involve successive collisions of electrons with the oxide particles, and the nature of such collisions, i.e. whether they are elastic, or non-elastic involving an energy transfer, has been investigated by Metson (1957)d. These investigations show clearly that the collisions are non-elastic, and indicate that the conducting

electrons are thermionically emitted at the cathode base and travel to the surface, suffering regular non-elastic collisions with the pore walls.

The results of experimental investigations in the region below 800°K have not been in quantitative agreement with the theoretical predictions. Measurements of the thermoelectric power by Young, although in qualitative agreement with Hensley's theoretical analysis based on the semi-conductor model, fail to agree quantitatively, and an additional ionic conduction process was suggested by Hensley to account for the discrepancy. Evidence for such a process was provided by Higginson(1958). Metson was unable to detect the presence of this second semi-conduction process and attributes Higginson's results to gas contamination in the cathode.

Experiments with both inert gases and oxygen indicate that the solid semi-conduction mechanism in the oxide cathode is a surface phenomenon resulting from a layer of excess alkaline earth atoms, as in de Boer's model (1935). Hughes and Coppola(1952) and Hannay et al.(1949) have found exceptionally low activation energies of the order 0.05 eV. with the cathode below 800°K and surrounded by a high pressure inert gas. Upon introducing oxygen to an oxide cathode, Wright(1950) and Metson and Macartney(1959)a observed

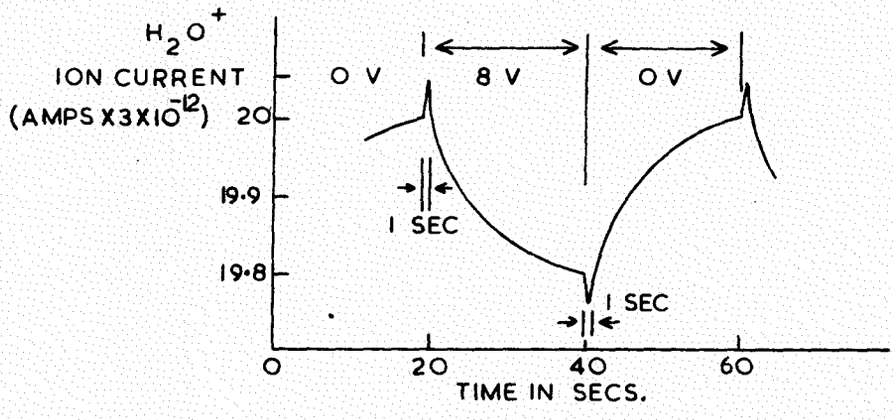

FIG. 7.
H_2O EVOLUTION FROM A BARIUM OXIDE CATHODE AT 1085°K

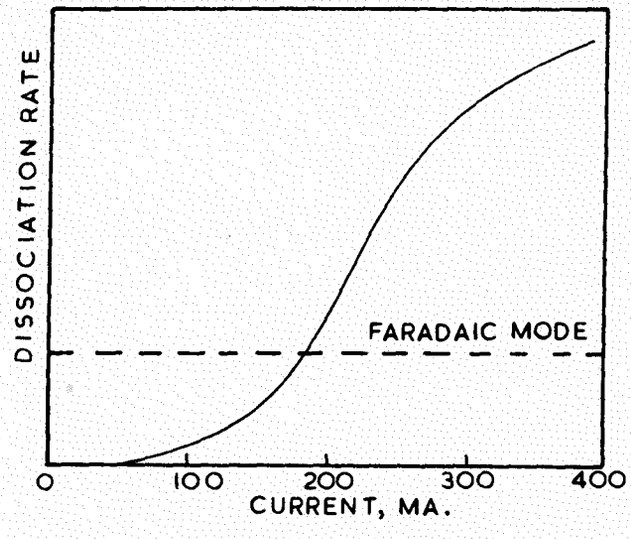

PROBABLE RELATIONSHIP BETWEEN DISSOCIATION RATE AND CURRENT

FIG. 8.

instantaneous poisoning. The effect of the inert gas would be to prevent residual oxidising gases reaching the alkaline earth atoms on the surface. Oxygen would immediately oxidise any excess alkaline earth atoms on the surface and hence produce the observed decay in conductivity.

2.7. Current dependant processes.

Electrolysis occuring in oxide coated cathodes was investigated by Becker(1929), and shown to produce free metallic barium and oxygen. Drawing temperature limited emission from the cathode resulted in oxygen evolution, whereas when the current had been reversed metallic barium was found on the surface. As a result of investigations to study the observed pulsed-emission decay in oxide cathodes, Sproull(1945) suggested a flow of barium ions away from the surface dependant on the thermionic current density.

Plumlee(1956) has described the evolution of H_2, H_2O, CO, O_2, and CO_2 from a cathode at 1035^{o}K under various applied potentials. Evolution of molecular oxygen was found to be proportional to the applied potential and inversly proportional to the state of activation of the cathode. Fig.7 shows the voltage dependant evolution of H_2O.

For a given applied field, the CO_2 evolved was found to be proportional to the residual CO_2 pressure in the system. A filament failure in the experimental system prevented detailed observations on H_2 evolution, although some voltage dependant effects were observed.

From these results Plumlee suggested that apart from the usual reaction of barium oxide with water vapour:

$$BaO + H_2O \rightarrow Ba(OH)_2 ,$$

at low vapour pressures another reaction might be expected of the form:

$$BaO + H_2O \rightarrow Ba(OH)^+ + O^{2+} + H^+$$
$$\rightarrow Ba(OH.e) + 1/2.O_2 + 1/2.H_2.$$

This reaction indicates the formation of a new type of hydroxyl ion having attached to it an extra electron which Plumlee suggests is the electron donor centre in the oxide cathode. However the above reaction has not been verified experimentally. Active electron donors of the (OH.e) type would require the partial pressure of H_2O in the system to be of the order 10^{-11}mmHg. which is not unrealistic.

The most exhaustive study of electrolitic and associated effects in the oxide cathode so far available is that carried out by Metson(Series of monographs starting in 1957). These investigations show that although current

dependant dissociation does occur in the oxide cathode, it is not Faradaic. Fig.8 shows the probable variation of dissociation rate with current (Metson and Macartney 1960a). The hypothesis presented by Metson to explain this dissociation is as follows; an applied field accelerates electrons through the vacuum pores of the cathode finally resulting in non-elastic collisions with the oxide particles. If during such a collision energy transfer raises the temperature of an oxide molecule above a critical temperature T_c, the molecule dissociates, and the dissociated ions are seperated by the applied field. In this hypothesis the seperation between oxide particles in the matrix is considered to be quite random, so that a lower critical field exists which will accelerate an electron over the longest free path in the matrix and produce dissociation when the electron collides with an oxide particle.

In one of Metson and Macartney's experiments a layer of (BaSr)O 200μ thick sandwiched between an 'O' nickel anode core and a pure platinum cathode core (the so-called S-type assembly), was operated at 800 mA. for 8 hours with both cores at 1020^{o}K. Upon examination barium and strontium were found to be alloyed into the cathode core, and the anode was covered with a layer of nickel oxide, thus providing good evidence in favour of an electrolytic process. It was generally found

that electrolytic dissociation produced a rise in the matrix resistance of an S-type assembly fitted with platinum cores, and that under steady current flow conditions the resistance finally acquired a constant value which was higher than that of the matrix under zero load conditions. When the current flow was removed from the matrix the resistance returned to its original value.

The increase in matrix resistance is attributed by Metson to an increase in the number of negative oxygen ions in the matrix. Under the influence of the applied field, dissociated barium and oxygen ions drift to the cathode and anode cores where they discharge to the atomic form. The increased concentration of the respective atoms at the anode and cathode cores gives rise to a slow diffucion back to the centre of the matrix resulting in their recombination as barium oxide molecules. The matrix resistance reaches a steady state when dynamic equilibrium exists between the dissociation and recombination rates.

Extending Metson's analysis to the conventional diode, oxygen ions arriving at the cathode surface cross the diode gap and discharge at the anode. Of the oxygen atoms leaving the anode, some will return to the cathode, the remainder will be lost in the vacuum. Thus an excess of barium will be built

up in the cathode matrix, and compared with the S-type assembly, the emission decay will be reduced. Removing the current load will result in a cathode of increased activity due to the excess barium produced by the electrolytic dissociation.

Okumura and Hensley (1963) have proposed a mobile acceptor theory to account for the activation of oxide coated cathodes. They suggest that in the initial stages of cathode processing Schottky vacancy pairs are produced, and that being positively and negatively charged, these vacancies act as acceptors and donors, respectively, in the oxide matrix. On the basis of their experimental results, Okumura and Hensley propose that during activation of the cathode free barium is produced by reaction of the barium oxide with the reducing agents in the nickel base, and that the presence of this free barium can result in anihilation of acceptors, thus increasing the cathode activity by removing the acceptors (barium vacancies) which compensate the donors (oxygen vacancies)

On this model activation by drawing current proceeds with a number of negatively charged acceptors being moved to the anode side of the oxide particles where they lower the Fermi level and are neutralised by charge transfer. Okumura and Hensley consider it possible that on reaching the surface

of an oxide particle, the neutral acceptor releases an oxygen atom, the net result being a fall in the acceptor concentration.

The above theory has no distinct advantages over other theories, but merely proposes an alternative mechanism by which a donor density can be established in the oxide cathode. The experimental results given by Okumura and Hensley by no means establish this theory, and it seems that in the light of evidence so far available, activation of the oxide cathode by drawing current is due to electrolytic dissociation of the oxide, the oxygen being evolved and leaving an excess of the alkaline earth metal in the matrix.

2.8. Thermal stability and evaporated products.

The only 'internal' investigations of the thermal stability of alkaline earth oxides are those of Metson(1961)a. Measurements of the electrical conductivity of an S-type assembly with platinum cores indicate that purely thermal dissociation does occur in a (BaSr)O matrix, and that under the influence of an applied field the dissociated products are accumulated in the anode and cathode sections of the matrix. Negative oxygen ions in the anode section produce a sharp rise in the anode-to-cathode resistance ratio, R_2/R_1.

Experiments with single oxides in the same system show a rise in R_2/R_1 as a result of purely thermal treatment at 1020°K, only in the case of strontium oxide. Barium oxide shows only a slight rise in R_2/R_1. indicating that barium oxide on a platinum base can be regarded as thermally stable. Thus in the case of the mixed oxides the observed dissociation is that of the strontium oxide component of the matrix.

Many observations have been made on the products evaporated from cathodes of mixed and single oxides, Plumlee and Smith(1950), Aldrich(1951), Pelchowitch(1954), Metson (1961)b. With the exception of the work by Metson, the evaporated products have been studied using high resolution mass spectrometric techniques. Metson identified the evaporants by their electrical conductivity, optical properties, and reactions on exposure to air. As Rittner (1953) suggested in his theoretical study of the chemistry of oxide cathodes, the products evaporated from any given alkaline earth oxide depend to a great extent on nature of the metal base.

Mixed oxides of (BaSrCa)O in the ratio 49:44:7 on active nickel have been investigated by Plumlee and Smith. At 1273°K the evaporation spectrum shows large amounts of barium and barium oxide together with strontium and a small amount of

calcium. On pure platinum or nickel the mixed oxides were shown by Pelchowitch and Plumlee and Smith to evaporate mainly as barium oxide.

(BaCa)O and (BaSr)O coated onto pure platinum or nickel have been found by Pelchowitch to evaporate mainly as barium oxide, although Metson's evaporation experiments showed the evaporation from a (BaSr)O system to be predominantly strontium.

When consideration is given to the products evaporated from single oxides on platinum the results are some to a extent surprising; the main evaporant from calcium oxide was found by Pelchowitch to be neutral calcium, and to a lesser extent calcium oxide and positive calcium ions, while strontium was observed to evaporate as strontium metal, strontium oxide, and positive strontium ions, in the same proportions as the calcium oxide evaporants. However, in the case of barium oxide dissociation does not take place, the only evaporant being barium oxide. At higher temperatures in the region 1500^{o}K, in addition to BaO, lesser quantities of Ba_2O^+, Ba_2O, and Ba_2O_2 are evaporated.

TABLE 2.1.

Oxide	L_s(eV.)	H (eV.)	H - L_s(eV.)
BaO	3.9	5.8	1.9
SrO	5.4	6.1	0.7
CaO	6.5	6.6	0.1
L_s heat of sublimation		H dissociation energy	

Table 2.1 gives the heats of sublimation L_s and the dissociation energies H of barium oxide, strontium oxide, and calcium oxide. From Table 2.1 it is not suprising to find that barium oxide is the more stable of the three oxides. As Metson(1963) has recently pointed out, the degree of dissociation as measured by the ratio of metal to oxide in the sublimate is dependant on the energy difference H - L_s rather than on H alone.

The combined effect of a hot cathode and an applied anode potential of about 30 volts has been shown by Metson and Woodgate(1962)a to have disasterous effects on the oxide matrix. The process of dissociation by non-elastic collisions of electrons with the oxide particles is greatly accelerated at these high voltages, increasing the energy gained by the

electrons between collisions, and causing intense heating and luminescence of the oxide particles. At still higher applied voltages this internal electron bombardment produced incandescence at small points in the cathode, resulting finally in a partially eroded cathode surface. During this latter process violet and less frequently green flashes were observed, indicating excited states of strontium and barium, respectively. Further increases in the electron energy were found to result in total disruption of the matrix. Fused, positively charged particles were ejected from the cathode leaving a fused oxide layer covered with strontium and barium metal. Observations of the trajectories of the ejected particles with and without the presence of magnetic fields indicate that the fused particles are carried out of the disrupting cathode in a jet of negative oxygen ions, and that they receive their positive charge from the dissociated metal ions.

The very high electron energies required to cause total disruption were obtained by holding the current through the coating I_A constant, and then decreasing the cathode temperature. Since

$$I_A = en\bar{v}$$

where n is the charge density and $\bar{v}$ the average drift velocity

of the electrons, decreasing the cathode temperature at constant I_A produces a decrease in the number of carriers and therefore an increase in $\bar{v}$.

2.9. Emission decay effects.

For a fixed cathode temperature and anode potential the emission current from a fully activated oxide cathode is observed to decay with time. The time scale of this decay allows a division into two catagories; long term emission decay and millisecond decay.

Long term emission decay is probably caused by the return of material from the anode and this has been mentioned in section (2.6). Such decay is observed for certain definite values of the anode potential in oxide cathode valves. Metson(1949) has reported emission poisoning at anode potentials of 5, 10, and 16 volts. From the work of Jacobs (1946) who derived a tentative relationship between minimum electron energy for dissociation and the heat of formation of the compound concerned, these voltages are thought to correspond to dissociation energies; the 5 volt effect to the dissociation of BaO or SrO, the 10 volt effect to the dissociation of either $BaCl_2$ or $SrCl_2$ and the 16 volt effect to the dissociation of $BaSO_4$ or $SrSO_4$, or to gaseous

ionisation phenomena. The electro-negative component formed by these dissociations may then result in the observed cathode poisoning.

A second emission decay phenomenon, having a time constant of the order of a few milliseconds, was first observed by Blewett(1939), and attributed to a depletion of barium atoms from the cathode surface. Later investigations by Sproull (1945) confirmed Blewett's findings. Nergaard(1952) proposed a mobile donor theory to account for the millisecond decay phenomenon. Under an applied field the partially ionised donors formally distributed uniformally throughout the coating, would drift away from the cathode surface, leaving a donor depletion layer. For a fixed anode potential the drift of charged donors is counterbalanced by a diffusion of donors under the influence of the newly created concentration gradient. The net result is a depletion of donors from the surface resulting in an increase in the work function of the cathode. On removing the applied field the former uniform distribution is restored by diffusion.

Confirmation of Nergaard's theory came from Hensley(1956) when it was observed that the saturation current density from an oxide cathode using a pulsed voltage was decreased when a direct current was drawn from the cathode at the same time. When the direct current was reversed in the opposite direction

to the pulsed current, the saturation current density was increased.

Hensley's mobile acceptor theory (1963) can also explain millisecond decay. All the essential features of Nergaard's theory are retained, except that, being negatively charged, the acceptors are attracted to the surface when a positive potential is applied.

2.10. Thin film emission.

All studies of thermionic emission from monolayer films of evaporated barium oxide indicate a similarity between the emission properties of such films and those of thick sprayed oxide coated cathodes. (see for example Davisson and Pidgeon 1920, Moore and Allison 1950, Russell and Eisenstein 1954, Metson 1957, Florio 1963)

The formation of a thin film of alkaline earth oxide on the metal base of an oxide cathode has been described by Metson(1958)a. When the base metal is sprayed with carbonate only about 50% of the carbonate is in contact with the base. During decomposition and thermal treatment of the cathode, alkaline earth oxide is evaporated from the porous coating to cover the previously bare areas of the base with a thin film of the oxide. Metson considers this film to be the source of

electrons thermionically emitted from the cathode. On this model the porous matrix has three functions; to limit the total emission by the space charge effect of electrons emitted from the pore walls, to maintain the thin emitting film which is being continually condensed and re-evaporated, and to protect the core emitter from gas attack.

Russell and Eisenstein consider that the thin film of oxide on the base metal only makes a contribution with the rest of the matrix to maintaining an electron gas density in the pores, these electrons being continually absorbed and re-emitted from the pore walls.

The presence of an interface layer between the oxide coating and the metal base does not necessarily upset the theory of thin film emission in oxide cathodes. Where such an interface is present it is probable that a thin film of matrix material may be condensed on the interface layer.

CHAPTER III

SUBLIMATION AND ADSORPTION PROCESSES.

3.1. Introduction.

The main interest of this work is the sublimation and adsorption of barium oxide. In this chapter consideration will be given to sublimation and adsorption processes, and the modification of the adsorbent work function by adsorbates. The various methods available for estimating the thickness of adsorbed films will also be discussed.

3.2. Sublimation.

Sublimation is said to take place when a solid changes directly to vapour without the presence of a liquid phase. The condition necessary for sublimation is that the solid should be maintained at a pressure below that corresponding to its triple point. If the solid is then heated, sublimation takes place.

During sublimation only those molecules whose thermal energies are greater than the heat of sublimation of the solid can escape from the surface. As the temperature of the solid is raised, the number of molecules able to leave the surface increases, leaving only the less energetic

molecules and so tending to lower the temperature of the solid. The energy necessary for a molecule to leave the surface is called the activation energy of sublimation, and this quantity can be related to the temperature of the solid and the rate of sublimation by an Arrehenius equation; in any reversible reaction the variation of the velocity constant c with the temperature $T^{o}K$ in either direction was shown by Arrehenius to obey a relation of the form:

$$d/dT.\ \ln(c) = A/kT^{2}, \qquad (3.1)$$

where k is Boltzmann's constant, and A can be considered as an energy of activation. Integrating Eq. 3.1 ;

$$c = C \exp -A/kT. \qquad (3.2)$$

where C is a constant of integration. Thus, taking the case of sublimation, where W is the rate of sublimation in grams per square centimeter per second, and L_S is the activation energy of sublimation,

$$W = C \exp -L_S/kT. \qquad (3.3)$$

The value of the activation energy of sublimation can be deduced from a graph of log W as a function of 1/T,

$$L_S = 1/5040.\ d(\log W)/d(1/T).\ eV. \qquad (3.4)$$

3.3 Condensation.

The early condensation experiments of Wood(1915, 1916),

Knudsen(1909), and Langmuir(1917), established that a lower critical substrate temperature was necessary before condensation could take place. From observations with cadmium and mercury vapour Wood and Knudsen concluded that when atoms strike a glass surface which is above the critical temperature for condensation, they are reflected from the surface. This reflection may result from either elastic or non-elastic collisions with the surface, but in either case the reflection is a direct result of the atom striking the surface initially.

The results of Langmuir's experiments indicated a process of condensation and re-evaporation, rather than reflection: by increasing the intensity of the vapour stream hitting the condensing surface Langmuir found that the critical temperature for condensation could be increased. On the basis of Langmuir's theory, condensed atoms would have a finite life on the condensing surface before being re-evaporated. For temperatures below the critical value, the life-time of an atom on the surface may be sufficiently long to enable another condensed atom to collide with it, and so form an atomic pair. The atomic pair forms a nucleus with a much longer mean life on the surface than the single atom.

Fraser(1931) attributed the observations of Wood, Knudsen,

and Langmuir to condensation on surface contaminated by gases and grease from the vacuum systems. When consideration is given to the vacuum conditions available for these early investigations, it is possible that such contamination did exist, and that it might have resulted in a lowering of the surface binding forces. On clean degassed metals the weakest vapour intensities should condense, and the structure of the deposited layer can be expected to be similar to the crystal lattice of the substrate.

A flux of atoms or molecules can be condensed either as mono-atomic or mono-molecularlayers, or aggregates. The conditions leading to either structure have been stated by Appleyard(1937):- "Let L be the latent heat of evaporation of condensed atoms or molecules from the substrate, and L_m the latent heat of evaporation from the condensing solid. Then, if $L < L_m$ the aggregate form has the lowest energy and is the most stable. If $L > L_m$ the monolayer form is the most stable." Observations made on thin films of cadmium and mercury by Estermann(1925), Cockcroft(1928), and Holland(1956) are in good agreement with this statement.

Aggregate formation is also governed by the mobility of the atoms or molecules on the substrate. The Lennard-Jones (1937) model of a crystal surface is one having a periodic structure; low potential pockets exist in which the condensed

molecules or atoms are trapped at low temperatures. Before the trapped molecules or atoms can be mobile over the surface they must have sufficient kinetic energy to surmount the potential barriers between pockets. Since this kinetic energy is much less than the energy required for re-evaporation, migration can occur at temperatures well below those at which re-evaporation takes place.

For relatively high intensity metal vapour beams, Levinstein(1949) observed a stronger tendency for the condensed films to form monolayers rather than aggregates. Levinstein explained these observations in terms of surface mobility. Atoms or molecules will move over the surface until they collide with other atoms or molecules and thereby loose their mobility. In the case of high intensity beams, atoms arriving on the surface either collide with each other, or with existing atom pairs; since there is a greater probability of collision between migrating atoms than between a migrating atom and an existing atom pair, many small new nuclei are formed. Atoms arriving at a slow rate collide more frequently with existing pairs and result in a few large patches.

3.4 Chemical and physical adsorption.

Adsorption phenomena are frequently divided into two classes; chemical adsorption (chemisorption), and physical adsorption. In principle these two processes can be distinguished by defining chemical adsorption as occurring when the binding of the molecule to the surface is caused by an exchange or sharing of electrons. The forces producing chemisorption are the same as those producing chemical combinations, so that during chemisorption the heat evolved (the heat of chemisorption) is the heat expected from a chemical reaction between the adsorbate and the adsorbent. Since chemisorption is a surface reaction taking place between the adsorbent and the adsorbate, it follows that only one chemisorbed layer can be formed; chemisorption is always unimolecular.

The forces of interaction in physical adsorption are Van der Waal's forces in their widest sense. This includes quadrupole, permanent dipole, and induced dipole attraction. Such forces are weak in comparison with chemisorption forces, the heat of physical adsorption being of the same order of magnitude as the heat of liquifaction of gases. When physical adsorption takes place the residual surface forces,

and the attraction of the already adsorbed atoms or molecules, enable more than one layer to be adsorbed.

Chemisorption and physical adsorption are most easily distinguished by determining the activation energy for re-evaporation of the adsorbate, since this activation energy is a measure of the surface binding energy. The equation governing re-evaporation is similar to Eq. 3.3; W becomes the rate of re-evaporation, and L_s the activation energy for re-evaporation. Interaction energies in chemisorption and physical adsorption processes usually differ by a factor of 10 or more; a typical value for the chemisorption of hydrogen on nickel is 1.3 eV. (Beeck 1950): the heat of physical adsorption for hydrogen is generally an order of magnitude smaller than this value.

3.5 Modification of the adsorbent electron work function by adsorbates.

The effect of an adsorbate on the work function of a metal surface is to produce a change in the work function by altering the surface dipole structure. In the case of monolayer formation such effects can be understood in terms of the dipole moment of the adsorbate; for films of increasing thickness the explanation generally lies in the bulk properties

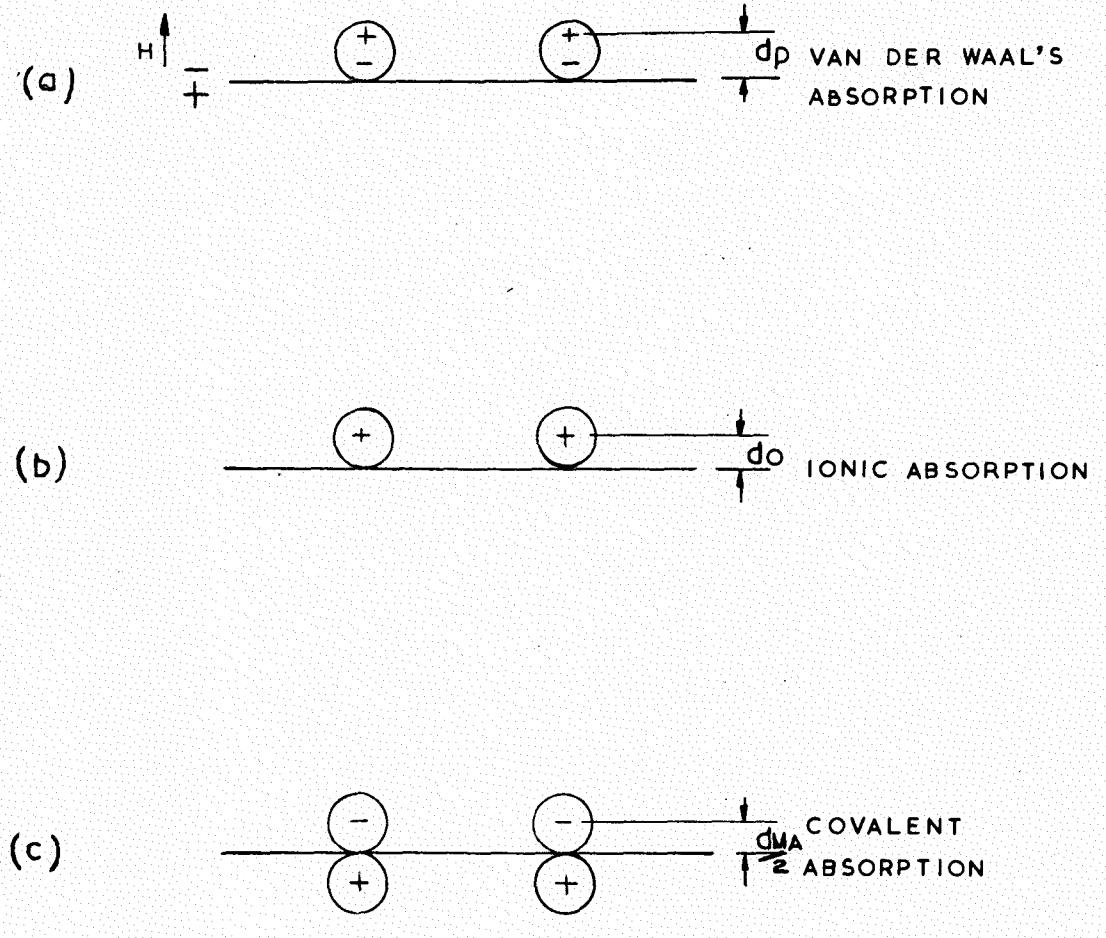

DIPOLES AT A METAL SURFACE

FIG.9.

of the adsorbate.

When the adsorbate is a monolayer having n dipoles per unit area aligned perpendicular to the adsorbent surface, the net effect is a double charge layer, each layer having a charge density (n.e) and a seperation d. Assuming each dipole has an effective moment M which is independent of the surface dipole density, the work function of the metal will then be changed by an amount $\Delta\phi = \pm 4\pi nM$, the sign of $\Delta\phi$ being positive or negative depending upon whether the dipoles are aligned with their negative charges outwards or not.

The three cases of dipoles at a metal surface are shown in Fig.9 (Culver and Tomkins 1959). The metal as a whole without the presence of an adsorbate layer is electrically neutral, but at the surface the atoms are unbalanced, having other atoms on one side only. Consequently electrons of the surface atoms are distributed unsymmetrically with respect to the positive ions; a spreading of electrons from the surface atoms into the space just outside the metal lowers the electron density immediately inside the surface, resulting in an electric double layer and a field H at the metal surface. Any non-polar particles adsorbed on this surface may be polarised by the surface field with positive charge outwards as shown in case (a) of Fig. 9; the resulting dipole moment

$M = ed_p$, produces a fall in the work function of the adsorbate. Alternatively the adsorbed particle may merely supress the electric double layer at the surface, the net result still being a reduction of the adsorbent work function.

When the adsorbate is completely ionised by the adsorbent the effective dipole results from the adion and its electrical image in the metal (Fig. 9, case b). The exact position of this image charge is subject to a certain amount of dispute, but it is thought by Coulson(1951) to lie on the surface opposite the adions thus leading to a dipole length d_o, and dipole moment $M = ed_o$. The sign of the change in work function resulting from ionic adsorption depends on the relative values of the adsorbent work function ϕ and the ionisation potential V_i of the adsorbate. Where ϕ is greater than V_i the outer electron of the adatom is usually captured by the adsorbent since this represents a more stable energy configuration. The result is a surface dipole with the positive sign outwards and $\Delta\phi$ is negative. Some adatoms whose ionisation potentials are slightly greater than the adsorbent work function can also produce a fall in the adsorbent work function, but in these cases the effect is reduced. This can be regarded as partial ionisation. When V_i is very much greater than ϕ, for example oxygen on

tungsten, electrons can transfer from the adsorbent to the adatoms and produce a change in work function $\Delta \phi$ which is positive.

Case (c) in Fig. 9 represents covalent adsorption where, assuming a metal surface, the dipole length is $d_{MA}/2$. The total effective dipole moment per adatom will be $M = 2e(d_{MA}/2)$

$$= ed_{MA}.$$

In the case of metal atoms adsorbed on a metal adsorbent, Stranski and Suhrmann(1947) have pointed out that the adatom distribution in a monolayer over a field emitter is such as to maximise the number of nearest neighbour contacts. This distribution is the same as that found for the surface atoms in the bulk adsorbate metal; the bonding is intermetallic (Ehrlich 1959) and gives rise to a dipole moment on the surface; the resultant change in work function $\Delta \phi$ is a function of the electronegativity of the adsorbate and the surface dipoles. Since the dipole moment produced by two dissimilar atoms has been shown by Pauling(1960) to be proportional to the difference in their electronegativities, $\Delta \phi$ is in fact only a function of the adsorbent and adsorbate electronegativities. A theoretical study of the work function variation of metals coated by metallic films has been made by Gyftopoulos and Levine(1962). In this work the dipole contribution to the change in work

function is taken as zero when the fraction of the surface covered θ is zero or unity. When θ is unity it is assumed that mutual dipole interactions result in zero net dipole moment, the work function ϕ with monolayer coverage being determined by the electronegativity of the adatoms according to the Gordy-Thomas(1956) relationship

$$\phi = 2.27x + 0.34 \text{ eV}, \qquad (3.5)$$

where x is the relative electronegativity. Excellent agreement is found by Gyftopoulos and Levine when their theoretical results are compared with available experimental data for tungsten coated by thorium, cesium, and strontium.

When non-polar molecules are physically adsorbed by a metal adsorbent, the distance between adsorbed molecules decreases as $\theta \rightarrow 1$, and the mutual interactions of the induced dipoles result in a certain amount of depolarisation. Clearly, as in the Gyftopoulos and Levine model for metal adsorbates, it is possible that when a monolayer is formed the net dipole contribution to the change in adsorbent work function is zero.

Polar molecules should behave in almost the same way, the only difference being a reduced mutual depolarising effect resulting from the interaction of the molecules' permanent dipole moments with the surface electric field.

This view is supported by the work of Mingolet(1950) and (1957). Values of work function changes for Xe, O_2, C_2H_2, CH_4, C_2H_6, N_2 physically adsorbed on metal surfaces were all found to be negative.

The application of a high electric field, in the direction of the surface field H (Fig. 9a), to an adsorbent on which a monolayer of polar molecules are adsorbed might be expected to result in complete polarisation of the adsorbate molecules and so produce a further reduction in adsorbent work function.

3.6 Work function variations of metals coated with barium oxide films.

The activation of a tungsten ribbon by material evaporated from a barium oxide coated cathode was first investigated by Davisson and Pidgeon(1920). The cathode used for these investigations was a tungsten filament coated with barium oxide; activation of the tungsten ribbon was attributed to barium oxide rather than to barium. The latter almost certainly evaporated with the barium oxide, being produced by the reaction of barium oxide with tungsten (Rittner 1953):

$$4/3.BaO + 1/3.W = 1/3.BaWO_4 + Ba.$$

It is only during the last thirteen years that systematic

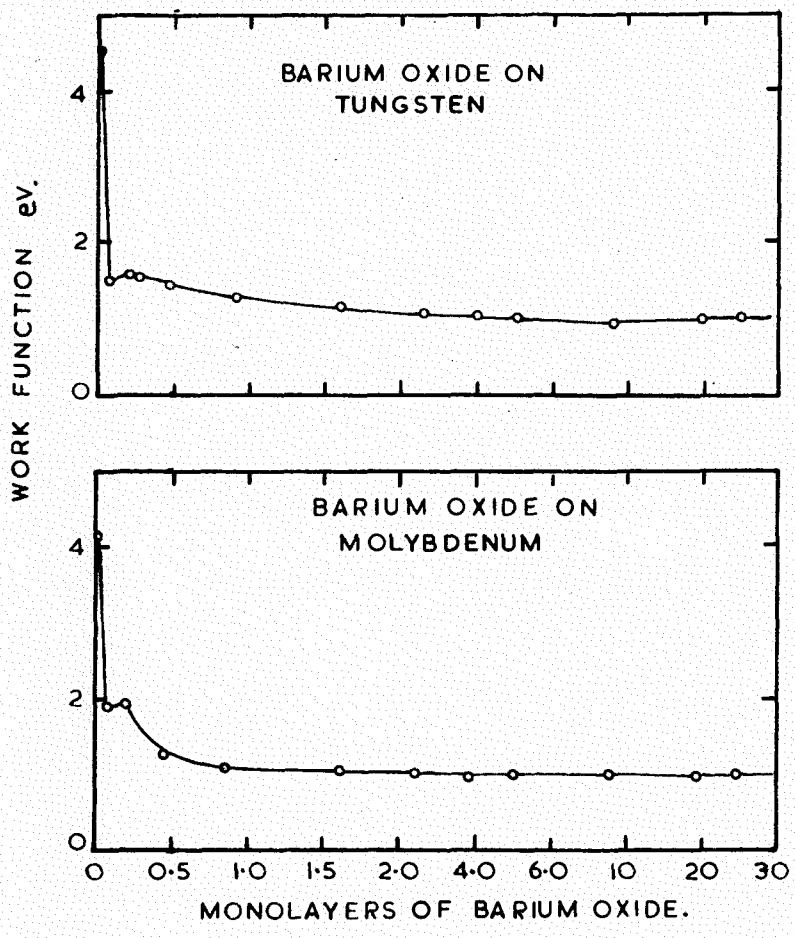

MOORE & ALLISON
(1950)

FIG. 10.

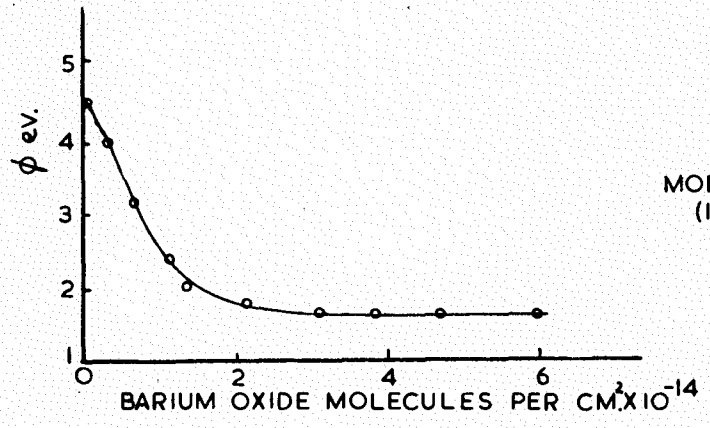

MORGULIS
(1960)

FIG. 11.

investigations have been made of the work function variation of metals coated by pure barium oxide. Fig. 10 shows the results of Moore and Allison(1950). Films of pure barium oxide, varying in thickness from 1 to 25 monolayers, were deposited onto thin ribbons of tungsten, molybdenum, tantalum, and zirconium, from a barium oxide coated platinum filament whose temperature could be determined pyrometrically to within an accuracy of $\pm$ 10^{o}K. Variations in work function were determined from Richardson plots, and the position of the monolayer could be estimated either by using radioactive tracer techniques, or by calculations based on the vapour pressure curves for barium oxide and the geometry of the experimental tube. Using the latter method a source temperature uncertainty of 10^{o} introduced a 50% error in the calculated sublimation rate. The radioactive tracer technique provided an estimate of the amount of vapour deposited to within 2%.

The results in Fig. 10 were intrepreted by Moore and Allison in terms of a polar barium oxide molecule being preferentially adsorbed with the oxygen atom adjacent to the adsorbent, and the molecule itself being perpendicular to the surface. As the surface concentration increases, depolarising fields of adjacent molecules tend to reverse the orientation of

some molecules resulting in a two diamentional crystal. No explanation was given for the mechanism operating in multi-layer films.

Fig. 11 shows the results of Morgulis(1960) for barium oxide deposited on platinum and tungsten. Work function changes were determined using the displacement of retarding potential characteristic technique (see Chapter IV). As in the paper of Moore and Allison, the vacuum conditions during these measurements are not quoted. Morgulis attributes the decrease in adsorbent work function to polar barium oxide molecules orientated on the adsorbent surface as in the Moore and Allison model.

Field emission studies of barium oxide on tungsten by Noga(1962) indicate a work function change $\Delta\phi$ of -2.3eV. with a maximum value of $\Delta\phi$ occurring when $\theta = 0.1$. Noga points out that whereas barium on tungsten has a minimum work function when $\theta = 1$, the larger dipole moment of the barium oxide molecules can be expected to produce mutual depolarisation at much lower coverages than in the case of barium atoms and so result in a maximum value of $\Delta\phi$ at relatively lower coverages.

Recently Florio(1963) has used the retarding potential method to measure the change in anode work function caused by

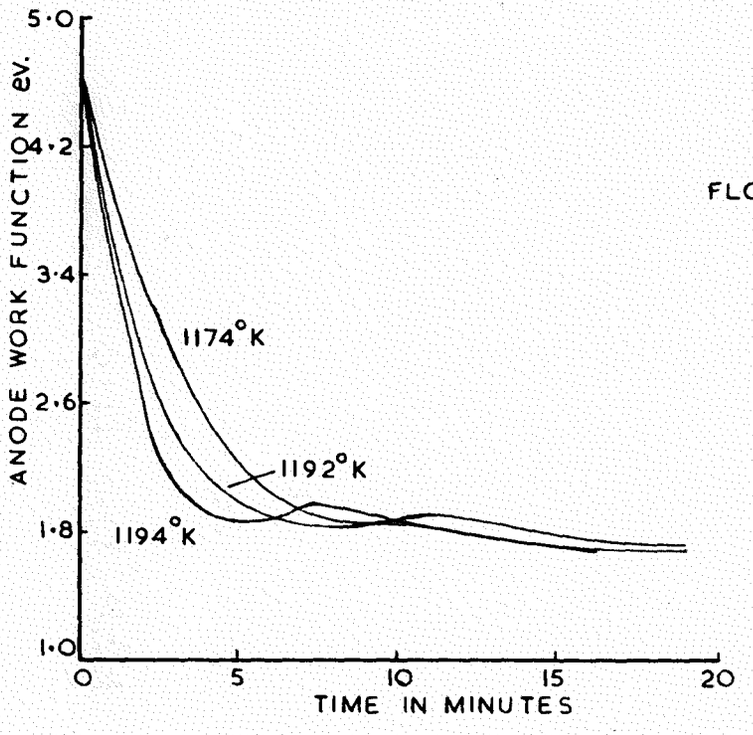

FLORIO (1963)

FIG. 12.

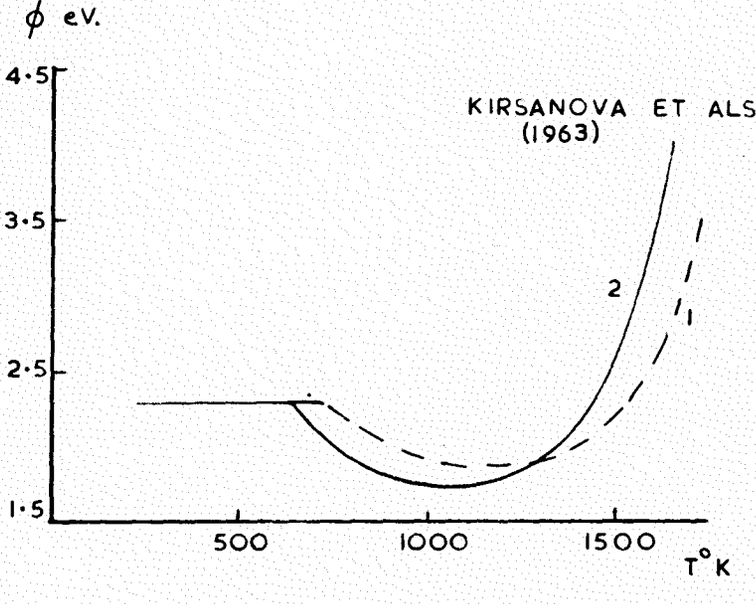

FIG. 13.

barium oxide sublimation from a platinum based barium oxide cathode. Sublimation curves obtained at different cathode temperatures (Fig. 12) initially either a minimum or an inflection point, followed by an asymptotic approach to an even lower value of the anode work function. From vapour pressure data for barium oxide and considerations of the diode geometry, Florio estimates the monolayer position to be at the first minimum.

The effect of depositing barium oxide onto a tungsten substrate which is held at different temperatures over the range 300° to 1200°K has been investigated by Kirsanova(1963). The observed variations in the tungsten work function are similar to those described above. However, when the final stable work function value is plotted as a function of temperature the result is as shown in Fig. 13, curve 1. Depositing the film of barium oxide onto a cold substrate and then heating the substrate to a higher temperature results in a stable work function value which is dependant on the temperature to which the substrate has been raised. Curve 2 in Fig. 12 shows the temperature dependence of the stable work function value in this latter case. From these results, Kirsanova deduces that the adsorption of barium oxide onto a hot tungsten substrate is two phase due to the participation in adsorption of

lower lying atoms together with the surface atoms. At relatively low temperatures only the surface atoms are considered active in the adsorption process.

Work function measurements and electron diffraction have been used by Russell and Eisenstein(1954) to investigate the structure of thin films of barium oxide deposited onto tungsten. Using radioactive tracer techniques to measure film thicknesses, they found that the emission of a deposited film increased up to a thickness of 20 monolayers, after which the emission stayed constant. Films deposited with the substrate temperature below 450^{o}K were found to be amorphous in structure, but when such films were subsequently heated to 800^{o}K a crystalline structure was produced. Films deposited onto substrates at 800^{o}K were crystalline at room temperature. Russell and Eisenstein interpret these results in terms of surface mobility. At temperatures below 450^{o}K the mobility of barium oxide on tungsten is considered too low to produce orientation of the deposited molecules into a crystal lattice.

3.7. Sublimation activation energy measurements for barium oxide on platinum.

Broadly speaking three techniques are available for measuring the sublimation activation energy of barium oxide:

(1) Barium oxide can be sublimed at a known temperature onto a neighbouring collector for a fixed period of time. The film condensed on the collector is then dissolved in H_2SO_4, and the precipitated $BaSO_4$ weighed. This proceedure is repeated for a number of different sublimation temperatures and the activation energy determined from a plot of log W as a function of 1/T as discussed in section 3.2. Values of L_s, the sublimation activation energy obtained by this (weight) method are shown in table 3.1.

TABLE 3.1.

Worker	Method	L_seV.	Temperature Range (^oK)
Classen 1933.	Weight	3.91	1223-1475
Herrmann 1937.	"	5.20	not given
Blewett et al.1939.	"	3.75	1200-1800
Aldrich 1951.	M.S.	3.75	1150-1400
Pelchowitch 1954	"	4.96	1150-1250
" "	"	4.08	1280-1350
Morgulis 1960.	"	3.89	1400-1600
Florio 1963.	W.F.	4.64	1170-1270

(2) Mass spectrometer techniques (M.S.) have provided a highly accurate means of measuring the sublimation rates from oxide

cathodes. The results of mass spectrometer measurements for barium oxide are shown in table 3.1. In particular, the measurements of Pelchowitch represent a very careful investigation of activation energies over a comparatively wide temperature range.

(3) Of particular interest to this thesis is the method used by Florio(1963) to determine L_s. Since sublimation rate is inversly proportional to time, a graph of log(1/t) as a function of (1/T), where t is the time required for a given mass of barium oxide to sublime, and T is the sublimation temperature, will enable L_s to be calculated from Eq. 3.3. Florio evaporated barium oxide from a platinum based barium oxide coated cathode onto a molybdenum anode; the work function variation of the molybdenum anode during the evaporation could be followed continuously by the displacement of retarding potential characteristic technique (see section 4.4.). The curves obtained from these measurements for a series of different sublimation temperatures are shown in Fig. 12 and the results from them are given in Table 3.1. L_s is obtained from a plot of log (1/time) against (1/T) for a particular work function value on each of the sublimation curves.

3.8. Estimation of film thickness.

A knowledge of film thickness is of major importance when

accounting for the physical phenomena observed in thin films. Furthermore, it may be desirable to deposit a film having a definite thickness, in which case, either the film can be monitored during deposition, or alternatively, the deposition time can be estimated from consideration of the substrate shape, the vapour source, and the position of the latter relative to the substrate.

Multiple beam interferometric techniques together with measurements of the absorption and transmission coefficients are convenient methods whereby thicknesses can be continuously followed during film deposition. Tolanski(1948) has described optical interference methods for the measurement of film thicknesses down to 3×10^{-7}cm. In the case of deposition on crystalline substrates, X-ray adsorption techniques have been used to determine film thicknesses in the range 10^{-5} to 10^{-2}cm. by Friedman and Birks (1946). Vapour deposits can be weighed directly using a torsion micro-balance; by this method sensitivities up to a microgram are possible and the deposits can be weighed in vacuum. Radioactive tracer techniques as mentioned in section 3.4 have been shown to give very accurate measurements of vapour deposits.

CHAPTER IV.

THE MEASUREMENT OF WORK FUNCTIONS

4.1. Introduction.

A number of important techniques are available for the measurement of work functions: (a) The work function of the surface under investigation can be determined from thermionic emission measurements. (b) The work function can be determined from a measurement of the contact potential difference between the unknown surface and surface of known work function (the reference surface). (c) The cooling produced when an electron is emitted from a surface can be used to determine the work function of the surface; this technique is sometimes called the calorimetric method. (d) The work function can be determined by photoelectric measurements. (e) Field emission can be used to determine the work function of a surface. Of these five methods only (a) and (b) have been employed for the measurements described in this thesis.

Work function measurements by these different techniques on the same surface are frequently found to be at variance. In addition to discussing the actual measuring techniques it will therefore be necessary to give some consideration to the significance of the measured work functions. The effect of

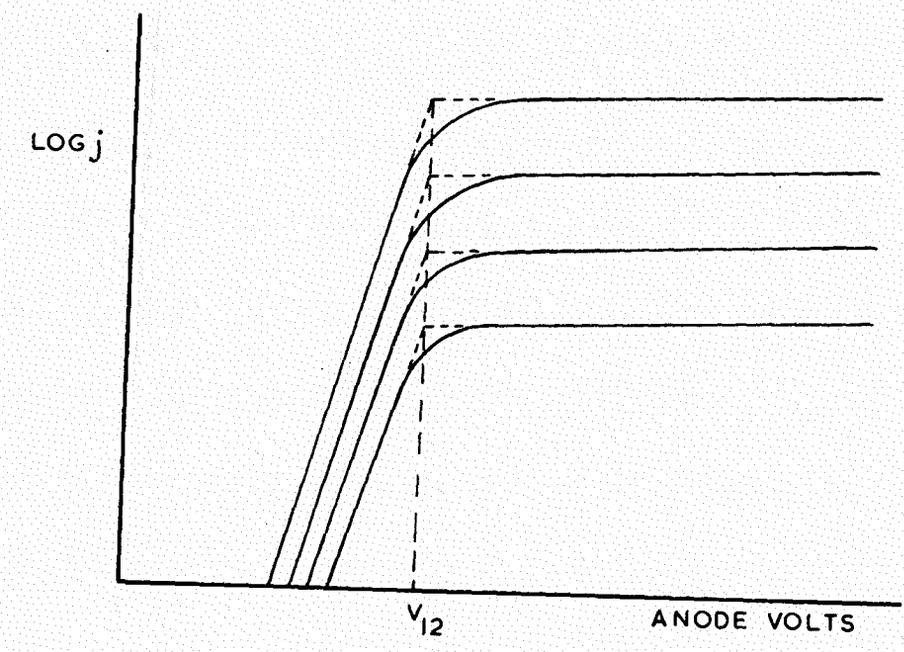

(a)

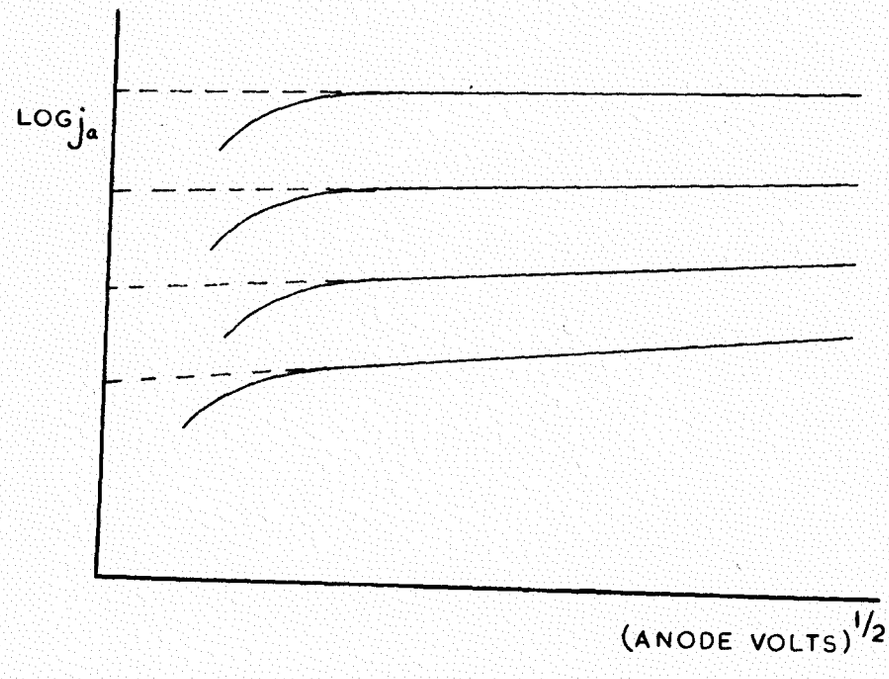

(b)

FIG. 14.

work function patches on the measured work function values will also be discussed.

4.2. The Richardson line method.

The slope of a plot of $\log(j_o/T^2)$ against $(1/T)$ has been shown in section 2.4 to provide a measurement of ϕ_R, the thermionic work function at absolute zero, and a value of the emission constant A_o can be obtained from the intercept. Such plots are called Richardson plots, and the work function values determined from such plots may be referred to as the Richardson work function (ϕ_R).

The value of j_o, the saturated current density with zero field at the cathode surface cannot be determined directly, but must be determined either from Schottky plots (which are obtained from Eq. 2.16 by plotting j_a as a function of $E^{1/2}$, Fig. 14b) by extrapolating back to zero field, or from current voltage characteristics as in Fig. 14a; the knee in the curves occurs when the anode voltage V_A is equal and opposite to the contact potential difference V_{12}, between the anode and cathode.

Herring and Nichols(1949) have discussed the effects of patches on Richardson plots. They consider the emission from patchy surfaces from two extremes; low field cases where the applied electric field is small compared with the field

resulting from the contact potential difference between adjacent patches, and high fields where the applied surface field is large compared with the patch field. In these two regions Schottky plots are found to have a slope given by

$$d(\ln j)/dE^{1/2} = e^{3/2}/kT \ , \qquad (4.1)$$

the theoretical slope for a uniform surface. In the intermediate region the Schottky plots are not straight and the average slope is greater than for a uniform surface.

Under the influence of a high electric field each patch emits independently of its neighbour. The total current is given by

$$j = \sum_i f_i j_i \qquad (4.2)$$

where f_i is the fraction of the surface occupied by the i^{th} patch and j_i is the emission per unit area from the i^{th} patch; the Richardson work function for the case of high fields is given by

$$\phi^{xx} = \sum_i w_i \phi_{Ri} \qquad (4.3)$$

where w_i is the fraction of the total field emission current from the i^{th} type of patch and ϕ_{Ri} is the Richardson work function of the i^{th} type of patch. Eq. 4.3 shows that ϕ can lie between a minimum value ϕ_{Rmin} and an upper limit less than $\bar{\phi} - T.d\bar{\phi}/dT$, where $\bar{\phi}$ is the arithmetic average work function at a temperature T given by:

$$\bar{\phi} = \sum_i f_i \phi_i . \qquad (4.4)$$

ϕ_i is the work function of the i^{th} patch. From Eq. 4.3 it can be seen that at lower temperatures emission currents from the low work function patches predominate and $\phi^{xx} \rightarrow \phi_{Rmin}$, resulting in the Richardson plot for non-uniform surfaces being concave upwards.

For the case of low applied electric fields where only electron energies normal to the surface are considered, all emitting areas having a work function less than $\bar{\phi}$ act as one patch whose work function is $\bar{\phi}$. Neglecting the reduction in work function resulting from the small applied field strength, the slope of the Richardson plot gives

$$\bar{\phi}^{xx} = \sum_{i \geq k} w_i \phi_{Ri} + w\bar{\phi}^{x} \quad , \qquad (4.5)$$

where all ϕ_{Ri} for $i \geq k$ are greater than $\bar{\phi}$, w_i is the fraction of the total emission from the i^{th} patch, and w is the fraction of the total emission from all patches with $\phi_i < \bar{\phi}$. Also $\bar{\phi}^{x} = \bar{\phi} - T.d\bar{\phi}/dT$. The value of the work function obtained from a low field Richardson plot is therefore higher than ϕ the value obtained in the case of high applied fields.

4.3 The effective work function.

Hensley[1961] has recently defined an effective work function

ϕ_E for a surface as the work function obtained when the temperature and the emission current density are substituted directly into the Richardson equation (Eq.2.6), taking the theoretical value of 120 amps/cm^2/$^oK^2$ for A, and assuming the reflection coefficient r is zero. Then,

$$\phi_E = kT. \ln(AT^2/j) \qquad (4.6)$$

determines the effective work function for a temperature T and an emission current density j. j can be measured by applying a voltage which is just sufficient to over come space charge effects. The emission current density so measured will differ from the value at zero field, but provided such measurements are made at a constant applied voltage and constant temperature, this difference remains constant.

Effective work functions measured at different temperatures and plotted as a function of absolute temperature enable $d\phi_E/dT$ to be determined, and by extrapolation a value of the effective work function at the absolute zero can be obtained. From Eqs. 2.6 and 4.6 it can be shown that

$$\phi_E = \phi_R + a_E T \qquad (4.7)$$

where $$a_E = d\phi_E/dT = k.\ln(120/A_o) \qquad (4.8)$$

and A_o is the emission constant A in the Richardson equation determined experimentally from the Richardson plot. From the above equations it can be seen that the effective work function at absolute zero obtained by extrapolation, is the Richardson

work function ϕ_R. In addition Eq. 4.8 shows that a value of A_o can be calculated from $d\phi_E/dT$.

Special graph paper is available for making effective work function plots on which the ordinate and abscissa are the effective work function and absolute temperature, respectively. Superimposed on the graph are lines of constant current density as calculated from Eq. 4.3.

In his paper, Hensley suggests that a useful and quick method of reporting cathode characteristics is to quote the effective work function at say, 1000°K, and the value of $d\phi_E/dT$.

4.4. Anode work functions by displacement of retarding potential characteristic.

The form of thermionic emission versus anode voltage curves has been discussed in section 2.5. For a plane parallel diode the current density collected at an applied anode-cathode voltage V in the retarding region is given by Eq. 2.15:

$$j_r = A(1 - r)\, T^2\, C \exp -(V - \phi_A)/kT$$

This equation contains both the anode work function ϕ_A and the anode voltage, so that providing j_r and T are maintained constant, any variation in ϕ_A, the anode work function, is reflected in a displacement of the retarding potential

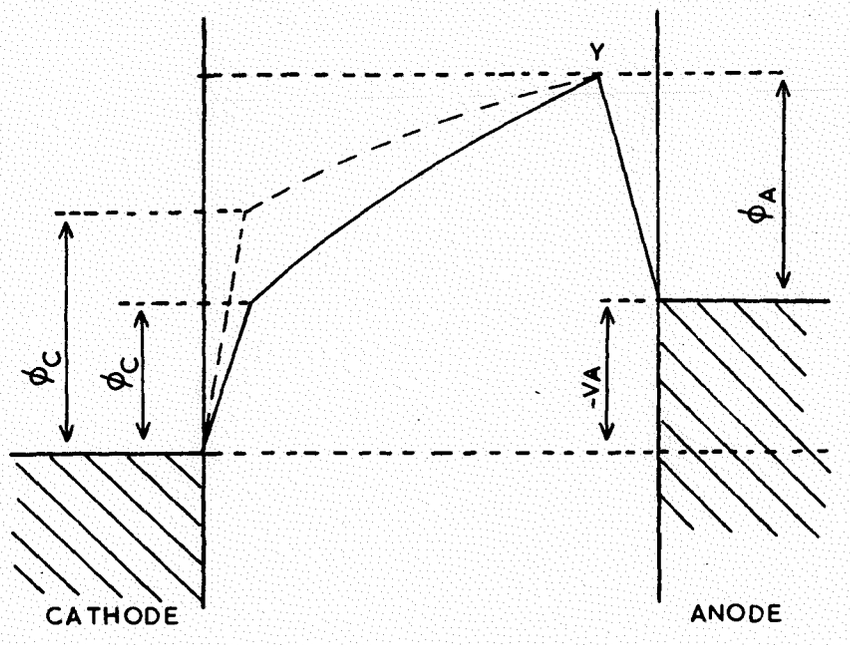

FIG 15
VARIATION OF POTENTIAL IN THE RETARDING FIELD REGION

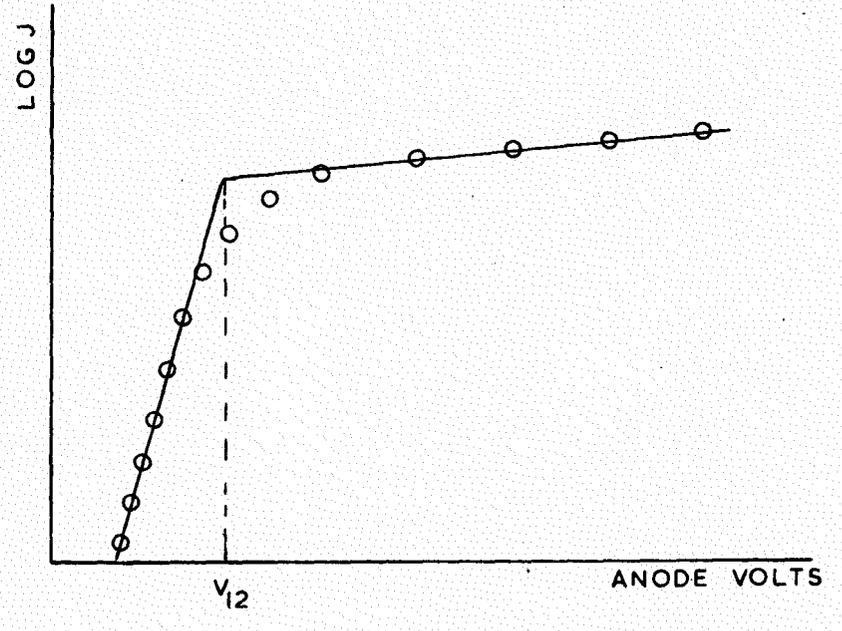

FIG. 16.

characteristic along the voltage axis. The change in V required to maintain j_r constant is exactly equal to the change in anode work function.

Fig. 15 shows the variation in potential across a diode in the retarding field region for two values of the cathode work function. Before a current can be registered electrons must pass over the potential maximum Y whose height is determined by the anode work function ϕ_A, and the applied anode-cathode voltage. Any variation in the cathode work function will clearly not effect the electron current flow across the diode since the potential that must be overcome before an electron can reach the anode is equal to the difference between the potential at Y and the potential of the Fermi level in the cathode. Changes in the cathode temperature will alter the current density in the retarding region by altering the energy distribution of electrons leaving the cathode surface.

A value of the cathode electron temperature can be obtained by measuring the slope of the log current-voltage plot in the retarding region; from Eq. 2.14,

$$T = 5040.\ dV_A/d\log(j_r). \qquad (4.9)$$

Electron temperatures determined in this way are greatly influenced by electrode geometry and the strength of the

retarding field. Ideally the diode should either have cylindrical symmetry or infinite plane parallel electrodes: all measurements should be confined to high retarding fields where the effects of patches on the cathode and space charge are reduced to a minimum.

Hung(1950), Fan(1943) and Heinze and Hass(1938) have found excellent agreement between the electron temperature determined from the slope of retarding potential plots and temperature measured by thermocouple and pyrometric techniques. On the other hand Ferris(1949) and Bulyginskii and Dobretsov(1956) find that electron temperatures calculated from retarding potential plots are higher than the measured temperatures. Actual values are not given by Ferris, but Bulyginskii and Dobretsov find a difference of 25° at $500^{\circ}K$, and 230° at $1000^{\circ}K$.

The displacement of retarding potential characteristic technique was used by Florio(1963) to follow continuously varying anode work functions. It has also been used by Comsa, Gelberg, and Iosifescu(1961) to measure the temperature dependence of the work functions of molybdenum and nickel, though the temperature range for such investigations must be limited to the region in which thermionic emission from the metals is practically absent.

Anderson(1935) determined the contact potential difference

between two surfaces by plotting retarding potential characteristics first to one surface and then to the other surface. By taking the difference in anode-cathode potential for a given value of j_r in the high retarding field region of the characteristics he obtained a measure of the contact potential difference between the two surfaces. For two uniform surfaces, the contact potential difference measured by this technique provides a value of the difference in thermionic work functions at the temperature of measurement. In the case of patchy surfaces, reflection effects resulting from the patch fields must be considered. Herring and Nichols have examined the case of a checkerboard anode whose patches have work functions ϕ_{A1} and ϕ_{A2} with $\phi_{A2} > \phi_{A1}$. For normal electron energies all patches with ϕ_{A1} will act as a single patch of work function $\bar{\phi}_A$ and the reference current j_r for these patches occurs at a retarding potential $V_r = V - V_{12}$, where $V_{12} = \bar{\phi}_C - \bar{\phi}_A$, $\bar{\phi}_C$ is the average work function of the cathode, and V is the externally applied anode-cathode potential. The current collected by the patches with work function ϕ_{A2} will be displaced by $d\phi_A/2$ where $d\phi_A = \phi_{A2} - \phi_{A1}$. Thus for a checkerboard anode, j_r occurs when $V - V_{12} = V_r + d\phi_A/4$. For a second checkerboard anode with ϕ'_A, and $d\phi'_A = \phi'_{A2} - \phi'_{A1}$, j_r occurs when $V' - V'_{12} = V_r + d\phi'_A/4$. Therefore the difference in anode-cathode potentials for a

current j_r is

$$V - V' = \bar{\phi}'_A - \bar{\phi}_A + 1/4.(d\phi_A - d\phi'_A). \qquad (4.10)$$

4.5 Measurement of contact potential difference by the intersection method.

In the absence of space charge and electrode reflection effects, a diode having uniform plane electrodes will show a sharp break in the plot of log j against V when the true anode potential is zero, i.e. when the externally applied anode potential V is equal and opposite to the contact potential difference V_{12} between the anode and cathode. If the anode work function ϕ_A is known, then the work function of the cathode ϕ_C can be calculated from the relationship:

$$\phi_C = \phi_A - V_{12} .$$

ϕ_C is related to the Richardson work function ϕ_{RC} by the expression,

$$\phi_{RC} = \phi_C - T.d\phi_C/dT \qquad (4.11)$$

Practical diodes never have uniform surfaces; reflection effects at the electrode-vacuum boundaries, together with space charge effects in the low retarding and accelerating field regions, produce a gradual turning over of the voltage characteristic in

the region of V_{12} rather than a sharp break (Fig. 16). The characteristic approaches a straight line again in the accelerating region when the anode potential is much larger than any difference in work function occurring on the cathode (Herring and Nichols 1949). The exact value of V_{12} can be determined from the intersection of tangents drawn to the two linear regions of the curve.

Heinze and Wagener(1938) examined the intersection method for the case of a patchy anode and a patchy cathode. Their analysis gives an intersection point when

$$V = -V_{12} = \bar{\phi}_A - \tilde{\phi}_C \qquad (4.12)$$

$\tilde{\phi}_C$ is an exponential average (average over emission) of the cathode work function at its operating temperature T, and is related to ϕ^{xx} in Eq. 4.3 by the expression

$$\phi^{xx} = \tilde{\phi}_C - T.d\tilde{\phi}_C/dT. \qquad (4.14)$$

By definition $\tilde{\phi}_C$ will be weighted on the low work function side so that

$$\tilde{\phi}_C < \bar{\phi}_C .$$

It follows from Eq. 4.12 that V, the intersection point on the voltage axis, varies with the cathode temperature, providing $d\tilde{\phi}_C/dT \neq 0$. Thus by plotting a series of current voltage characteristics for different cathode temperatures the observed shift in V provides a measure of $d\tilde{\phi}_C/dT$.

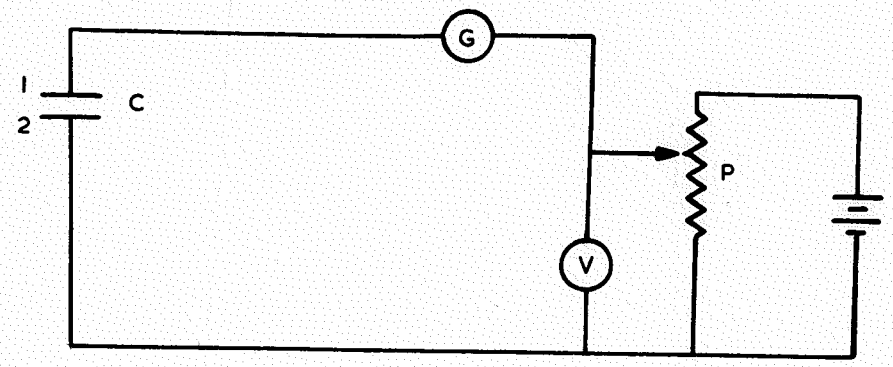

FIG. 17.

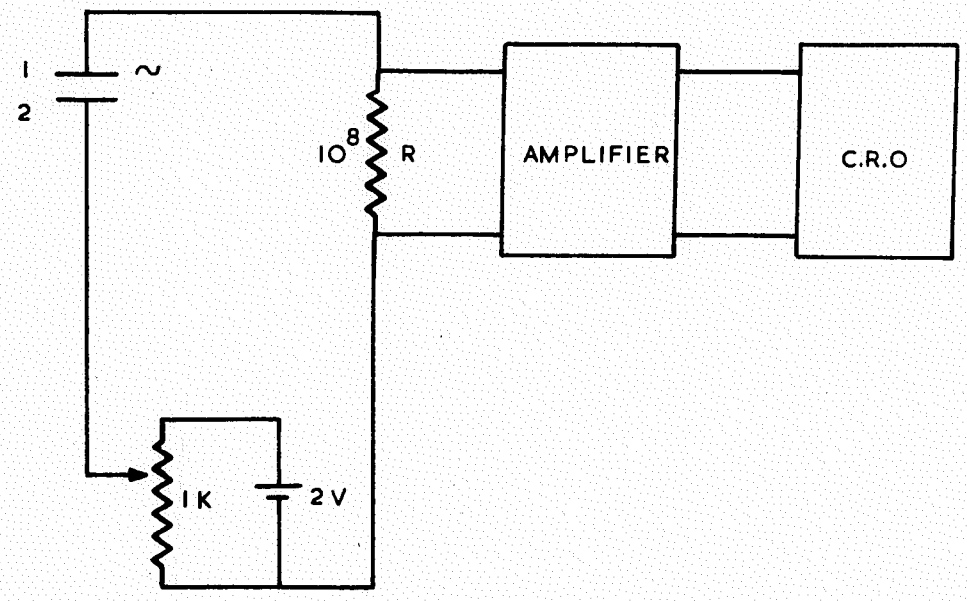

FIG. 18.

Emission characteristics in which the transition from retarding to accelerating field only extended over 20 mV. were obtained by Shelton(1957). Uniform emitting and collecting surfaces were provided in these investigations by the use of two (211) crystals of tantalum. A third intervening electrode fitted with a small hole reduced the space charge and kept the field at the emitter surface constant, and a strong axial magnetic field fixed the trajectories and conserved the tangiental components of the emitted electrons.

4.6. The Kelvin technique.

The oldest and one of the most reliable methods of determining contact potential differences is a technique described by Kelvin(1898). Fig. 17 shows the experimental arrangement. The two surfaces whose contact potential difference is to be determined are arranged to form a condenser c; plate 1 is a surface of known work function, 2 is the surface whose work function is to be determined. If C is the capacitance of the condenser, and V_{12} the contact potential difference between the two surfaces, then each condenser plate has a charge:

$$Q = CV_{12}. \qquad (4.15)$$

Sudden alteration of the plate seperation changes C, and consequently produces a change in Q, resulting in a flow of charge in the circuit and a deflection of the galvanometer G. When a voltage V, equal and opposite to V_{12} is applied to the condenser plates, altering their seperation does not produce a change in Q; the galvanometer deflection is zero. The voltmeter reading is then a measure of the contact potential difference V_{12} between the two surfaces.

An important modification of this technique due to Zisman(1932) has been used in the work described in this thesis. In this modification one of the two condenser surfaces is arranged to vibrate so that the capacitance of the condenser varies sinusoidally. Fig. 18 shows the experimental arrangements. The contact potential difference between the vibrating electrodes now results in a sinusoidally varying charge flow through the resistor R. This produces an alternating voltage across R which is amplified and may then be displayed on an oscilloscope screen. When a potential is applied to the condenser plates which is equal and opposite to V_{12}, the alternating voltage across R falls to zero; this condition can be observed on the oscilloscope. The work function of the surface under investigation is then determined from the measured contact potential difference V_{12}, and the work function of the reference surface ϕ_r, by the relation:

$$\phi = V_{12} + \phi_r \qquad (4.16)$$

In the case of two patchy surfaces, 1 and 2, then for a seperation which is large compared with their patch dimensions the contact potential difference is given by

$$V_{12} = \bar{\phi}_1 - \bar{\phi}_2, \qquad (4.17)$$

where $\bar{\phi}_1$ and $\bar{\phi}_2$ are the arithmetic average work functions defined by Eq. 4.4.

The Kelvin technique may be used to study the variation of work function with temperature. This is done by maintaining the temperature of the reference surface constant and measuring V_{12} with the second surface held at different temperatures. Care must be taken to make appropriate corrections for thermoelectric effects occurring in the circuit.

In comparing the Kelvin technique for measuring the contact potential difference between two surfaces, with the Anderson method described in section 4.4, it can be seen from Eqs. 4.10 and 4.17 that for measurements on patchy surfaces the results obtained from the two methods should differ slightly. Anderson(1952) made a direct comparison of these two methods when measuring the contact potential difference between barium and silver. Agreement to within an experimental error of $\pm$ 0.01 volts was found. This result led Anderson to suggest that this failure to find a difference between the two methods

reflects the inadequacy of the patch theory developed by Herring and Nichols(1949) in which only the normal electron energies are considered. In the case of strong fields, it does seem reasonable to expect that electrons close to a patch will be unaffected by the tangiental component of the patch field, but this may not be the case for slow electrons in retarding fields.

CHAPTER V.

THE APPARATUS AND TECHNIQUES

5.1. Introduction.

The work function of a surface can be greatly effected by the adsorption of small quantities of gas. At a pressure of 10^{-6}mmHg. residual gases form a monolayer on a clean surface in about 1 second. By reducing the pressure to 10^{-10}mmHg. the time required for a monolayer to form is increased to a few hours. Ultra-high vacuum conditions were therefore essential for the work described in this thesis; to meet this need two types of vacuum system were constructed and are described in this chapter.

The experimental tube designs used in these investigations were various, though a number of features were common to all the tubes constructed; these features, together with the general experimental proceedures, are described below.

5.2. The vacuum systems.

The two vacuum systems constructed during the course of this work were both of pyrex glass and mounted on a tubular

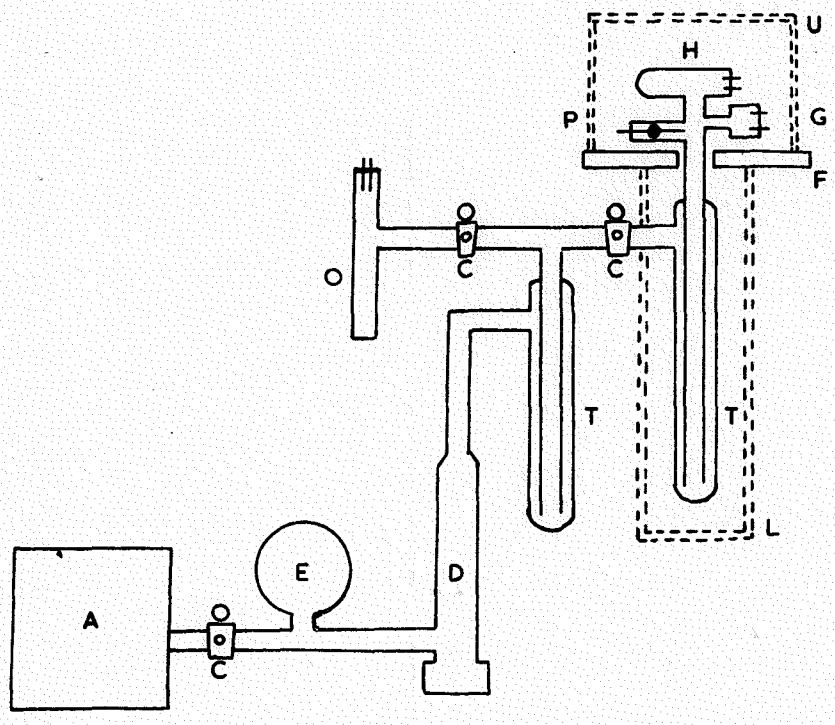

A TWO STAGE ROTARY PUMP
C TAP
D TWO STAGE MERCURY DIFFUSION PUMP
E RESERVOIR
F OVEN BASE
G BAYARD-ALPERT GAUGE
H EXPERIMENTAL TUBE
L LOWER OVEN
O OUTGASSING SYSTEM
P PENNING GAUGE
T COLD TRAP
U UPPER OVEN

FIG. 19.

CONVENTIONAL VACUUM SYSTEM

steel frame. Great care was taken in cleaning all the components which were to be used in building the vacuum systems; the pyrex glass was treated with nitric acid and then washed with carbon-tetrachloride and finally distilled water; the mercury used in the diffusion pumps was washed well with water and vacuum distilled; certain metal components were normally furnaced in either hydrogen or vacuum before being added to the system.

Initially a conventional high vacuum system was used. This was subsequently replaced by a continuously pumped ultra-high vacuum system of the type described by Venema and Bandringa(1958). The systems are described below.

5.2.1. The conventional vacuum system.

The system shown schematically in Fig. 19 was designed to achieve ultimate pressures in the range 10^{-6} to 10^{-8}mmHg. It consisted of a two stage mercury diffusion pump backed by a two stage rotary pump.

Included in the backing line was a phosphorous pentoxide water vapour trap and a three litre reservoir; the latter enabled the system to continue pumping without the rotary pump for several hours, should the necessity arise. Two cold traps, one either side of a large bore stop cock, prevented mercury and pump oils reaching the experimental tube. Wide bore tubing

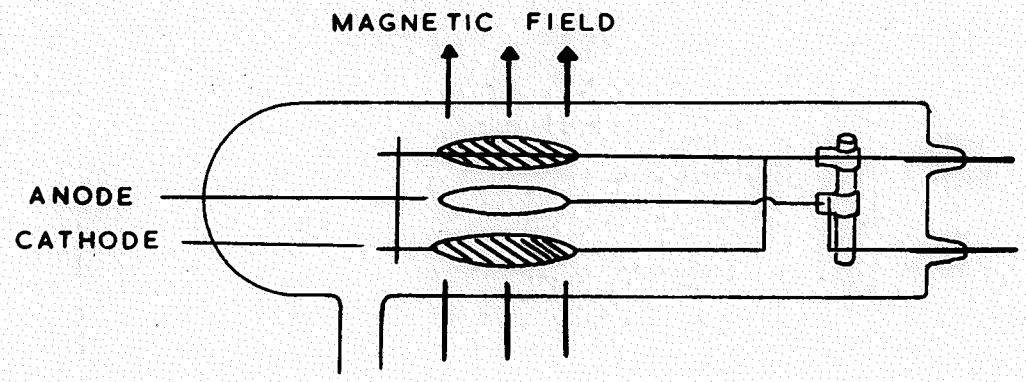

FIG.20.
PENNING GAUGE

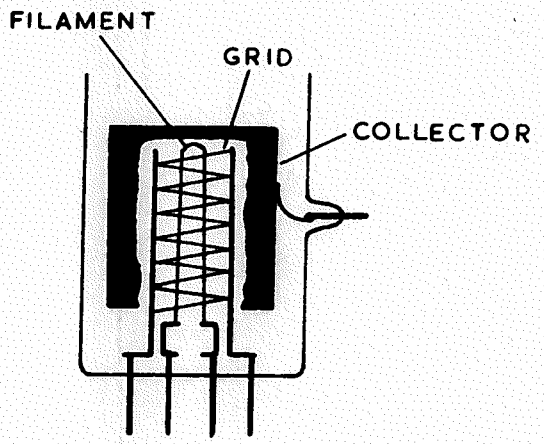

FIG.21.
CONVENTIONAL TRIODE
IONISATION GAUGE

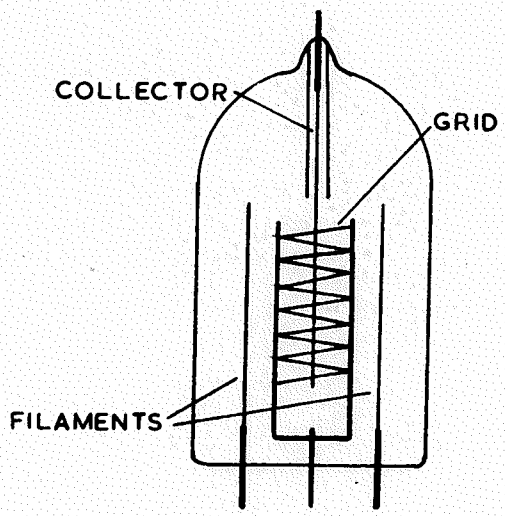

FIG.22.
BAYARD ALPERT
IONISATION GAUGE

(2.5cm.) was used through-out the high vacuum side of the system. Facilities were made available on the system for vacuum outgassing tube components prior to their assembly; when not in use, this part of the system could be isolated from the main pumping line.

A most essential requirement of any high vacuum system is that it may be baked at temperatures in the region of 450°C for extended periods in order to remove, as far as possible, any gases adsorbed on the walls. Two ovens were provided with the above system, one which could be lowered onto the asbestos working table to bake out the manifold and experimental tube, and a second which was used to bake the first cold trap.

Pressures in the system were monitored by two types of ionisation gauge. Penning(1937) gauges enabled pressures down to 10^{-6}mmHg. to be followed, while in the pressure range 10^{-6} to 10^{-10}mmHg., Bayard-Alpert gauges were used (Bayard and Alpert 1950).

The Penning gauge is a cold cathode ionisation gauge comprising a nickel ring anode between two nickel discs of 2 cm. diameter and 1 cm. apart, which form the cathode (Fig. 20). The glass envelope containing the electrodes is mounted between the pole pieces of a 600 oersted permanent magnet, and positioned such that the magnetic field is perpendicular to the plane of the electrodes. The gauge operates with a potential

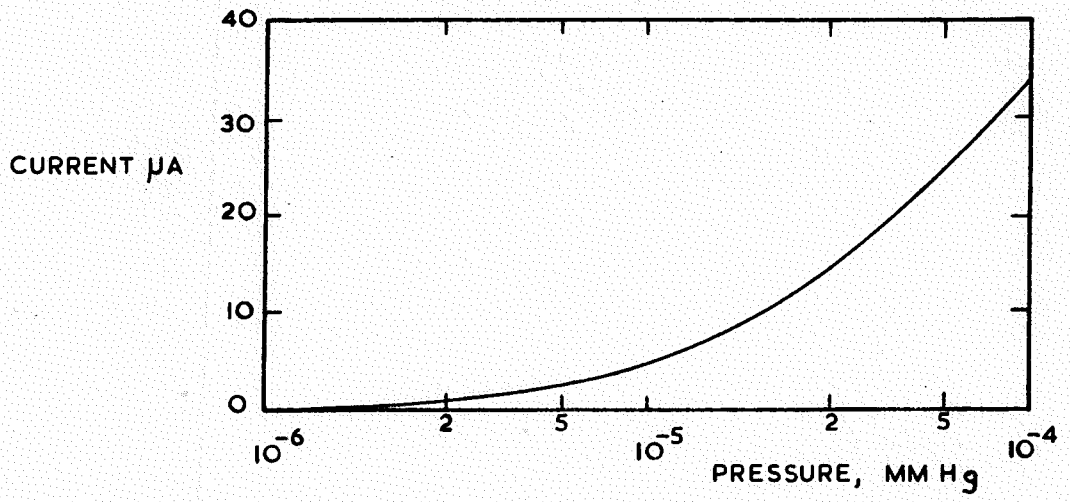

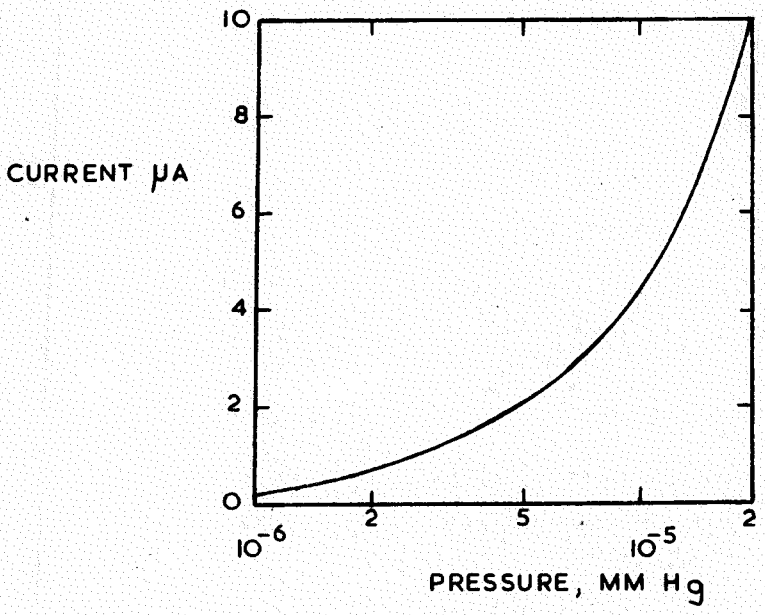

FIG. 23.
PENNING GAUGE CALIBRATION FOR AIR.

of 2000 volts applied between the anode and cathode. Once a discharge is initiated between the electrodes, electrons moving in long helical paths as a result of the combination of electric and magnetic fields cause greatly increased ionisation by collision with the residual gas molecules. The resulting ion current is an indication of the pressure; a calibration for such a gauge is given in Fig. 23.

The conventional triode-type ionisation gauge shown in Fig. 21 never indicated pressures lower than about 10^{-8}mmHg. Nottingham(1947) demonstrated the existance in such gauges of a residual ion current which is completely independent of pressure. This limitation was confirmed independently by Bayard and Alpert(1950), Lander(1950), and Metson(1951), who demonstrated that soft X-rays formed when electrons from the filament bombarded the grid strike the collector surface and release photoelectrons. These photoelectrons form the lower limit to the ion current that can be measured at the collector. Bayard and Alpert(1950) minimised the X-ray effect by constructing an inverted triode ionisation gauge (Fig. 22), so that the collector, which was in the form of a fine wire, was inside the grid, and the filament was placed outside. By this means the collector area exposed to X-rays was greatly reduced, and the lower limit of operation may be extended to

less than 10^{-11} mmHg. Commercial (Mullard-type 10G.1) Bayard-Alpert gauges were used for the work described in this thesis. These gauges have tungsten filaments and collectors, while the grid is of molybdenum wire. Typical electrode operating voltages are -100 volts on the collector and +200 volts on the grid. The magnitude of the ion current in the collector circuit I_c depends on three factors: (a) gas pressure p, and the type of gas, (b) grid current I_g, and (c) the sensitivity of the gauge S

$$S = \frac{I_c}{I_g} \cdot \frac{1}{p} \qquad (4.1)$$

For nitrogen S has a value of 18.5 $mmHg^{-1}$. Pressures were determined by measuring the collector current on an electrometer, when the grid current was set to 1 mA by adjustment of the filament voltage.

Ionisation gauges exhibit a pumping action (Schwarz 1944) at high values of grid current due to two processes, one chemical and the other electrical. The former process results from chemical reactions between active gases and the hot filament ($2500^{\circ}K$); electrical pumping appears to result from the glass walls of the gauge becoming negatively charged by electron inpact and causing positive gas ions to be trapped. The IOG.1 has an approximate pumping speed of 0.1

litres (air) per second when operating with a grid current of 10 mA., and this can be used to achieve pressures down to 10^{-11} mmHg.

When the system had been cleared of leaks using standard techniques, the rotary and diffusion pumps were switched on, and liquid nitrogen was applied to the second trap. The whole of the bakable region was then raised to a temperature of about 450°C for 24 hours, after which the lower oven was removed and liquid nitrogen applied to the first trap; baking of that part of the system above the asbestos table continued for a further 3 to 4 hours. When the bake-out was completed, components of the experimental tube were outgassed by either direct heating, electron bombardment, or eddy current heating; the grid and anode of the Bayard-Alpert gauge were outgassed by electron bombardment from the filament. The experimental tube and the Bayard-Alpert gauge could then be sealed off together from the systems. By using the gauge as a pump the pressure in the experimental tube could be further reduced to 10^{-10} mmHg.

5.2.1. The Venema and Bandringa ultra-high vacuum system.

The system described in section 5.2.1 suffered from the disadvantage that once the experimental tube and gauge has been sealed from the vacuum system, any large volumes of gas subsequently evolved from tube components produced a consider-

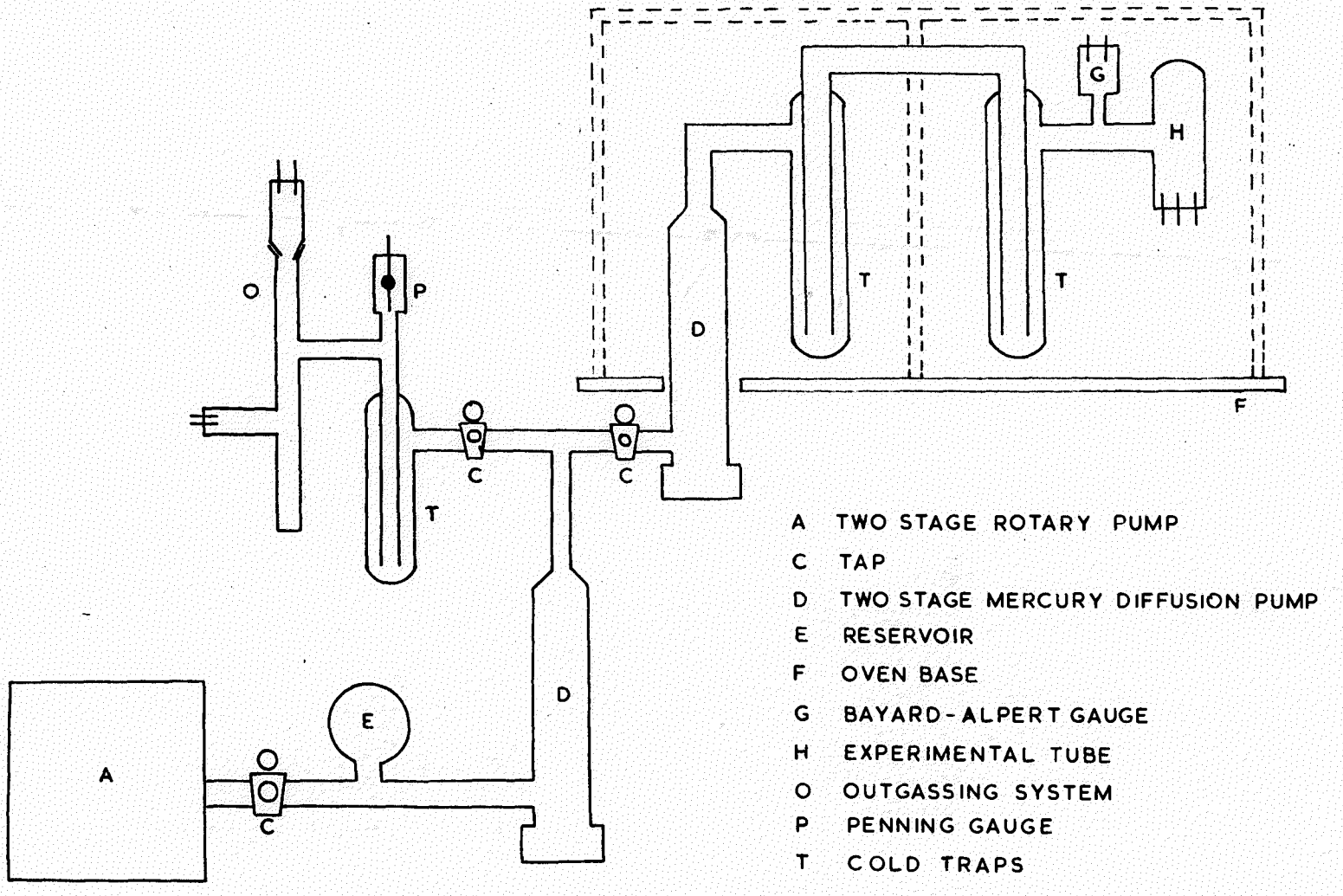

FIG. 24.

VENEMA AND BANDRINGA—TYPE VACUUM SYSTEM.

able rise in pressure which could only be reduced very slowly by the pumping action of the Bayard-Alpert gauge. The slow pumping speed of this arrangement can only be overcome by having a continuously pumped system capable of producing pressures in the region 10^{-10} mmHg. This requirement led to the adoption of the Venema and Bandringa system.

The Venema and Bandringa system, which is shown diagramatically in Fig. 24, consists of two double stage mercury diffusion pumps backed by a two stage rotary pump; back diffusion of gas against the vapour stream in the first diffusion pump is considerably reduced by minimising its outlet pressure by the second diffusion pump. The first diffusion pump passes through a hole in the asbestos table to enable the mouth and both jets of the pump to be baked, together with the cold traps and the experimental tube. The baking of the first diffusion pump ensures that all the glass on the high vacuum side of the first pump is outgassed; to obtain a high pumping speed at the experimental tube, 3.5 cm. diameter glass tubing was used for this part of the system. Baking was carried out in two stages; first the whole of the bakable part of the system was maintained at 450°C while being pumped by the second diffusion pump and the rotary pump; after 12 hours the oven section over the first diffusion pump and the

second cold trap was removed while baking of the other parts continued. The first diffusion pump was then switched on, and liquid nitrogen applied to the second trap. The remaining oven section was removed after a further two hours. At this stage the pressure measured by the Bayard-Alpert gauge was generally 10^{-7} mmHg.; after outgassing the tube components and applying liquid nitrogen to the first cold trap the pressure indicated by the Bayard-Alpert gauge was normally between 10^{-10} and 10^{-9} mmHg.

5.3. The experimental tubes.

The experimental tubes used in these investigations were designed primarily to measure anode work function changes caused by sublimation from a barium oxide coated cathode. In the early tubes, arrangements were made for the anode work function to be measured by both the intersection method and the Kelvin technique (see Chapter IV); a later modification in the tube design enabled the shift of retarding potential characteristic method to be used together with the intersection method and the Kelvin technique.

The diode geometry was in all cases approximately plane parallel. Ideally, with such an arrangement, the electrodes

should be very close spaced and as large as possible, since field distortion at the edges of the electrodes is then minimised. However, the need for movable anodes, and a uniform cathode temperature, made very close electrode spacing impossible, and necessitated the use of relatively small electrodes. The designs adopted were therefore a compromise between these conflicting requirements.

When the Kelvin technique was to be used, precautions were taken in the tube design to reduce stray capacitances between the moving electrode and the other surfaces in the experimental tube, especially the electrostatic screen, to a minimum. The reference surfaces that have been used for the Kelvin measurements were gold, molybdenum, and tungsten. Gold was evaporated from a bead onto a glass electrode, and was originally chosen on account of the stability of its work function in high partial pressures of oxygen. However, the number of fresh films which could be deposited from one bead was limited, and for this reason the use of gold was abandoned in preference to solid electrodes of molybdenum and tungsten which could be cleaned as required by 'flashing' to very high temperatures for brief periods.

During the course of the investigations four different anode materials were employed: nickel, molybdenum, tungsten, and niobium. The barium oxide was mounted on two types of cathode

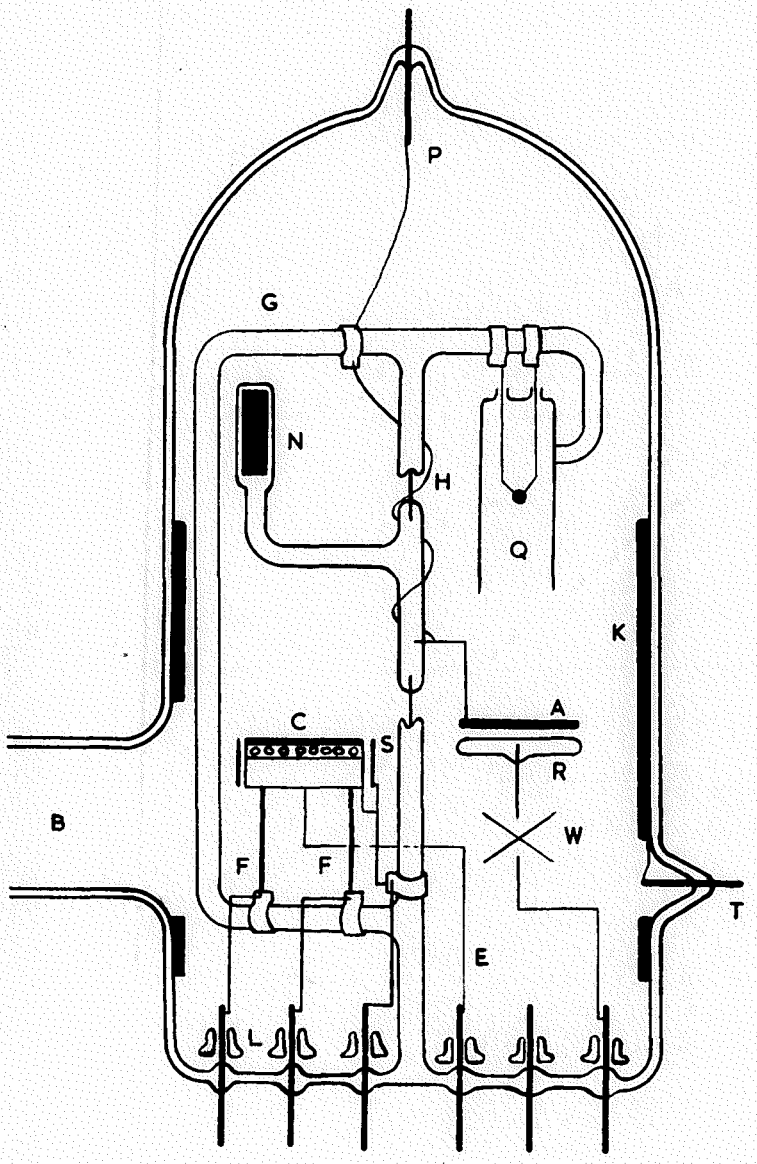

FIG. 25.
TYPICAL N SERIES TUBE

base: in the early experiments cylindrical 'O' nickel buttons were used, but excessive evaporation of nickel was found to take place and they were replaced by platinum boxes.

5.4. The construction of an experimental tube.

This section described the construction of the tube shown in Fig. 25. Although it was the first tube to be built, most of the techniques involved in its construction were subsequently employed.

Referring to Fig. 25, the cathode base (C) was made from sheet 'O' nickel stamped onto a cylindrical button 1.9 cm. in diameter. This button was fitted with a 0.05 cm. diameter nickel support wire welded externally to the wall, and a 0.01 cm. diameter thermocouple lead (E) which was welded inside the button to the centre of the disc. Equiping these buttons with heaters suitable for reaching a maximum temperature of 1300^{o}K proved a problem. This was solved using a 30 cm. long, non-inductive, ceramic insulated heating coil, of 0.05 cm. diameter tungsten wire (FF), pressed against the inside of the button by means of a molybdenum disc which also acted as a radiation shield. The cathode base assembly was then hydrogen furnaced at 1300^{o}K for five minutes. When this was completed, the cathode button was mounted in a cardboard screen and

sprayed with barium carbonate suspension to a thickness of about 500μ.

The glass vibrating electrode (R), associated with the Kelvin technique, was constructed by pressing molten pyrex glass against a carbon block to obtain a disc 2cm. in diameter. Electrical connection was made to the surface via a tungsten seal which was pushed through the disc while it was molten. The tungsten seal also serves as a support for the electrode. After careful annealing of these discs, the surface was ground flat with carborundum and water, washed in nitric acid and distilled water, dried, and finally flame polished. Oxidation of the end of the tungsten seal produced by the flame polishing was removed by electrolysis in caustic soda solution. The back of the glass electrode was painted with colloidal graphite solution to prevent charge localisation in the areas which would not be covered with the evaporated gold film. A vibrating spring (W) was constructed from two thin pieces of tungsten strip, and attached to the glass electrode so that it could vibrate in a plane perpendicular to its surface.

The source of evaporated gold was a gold bead on the end of a tungsten filament mounted inside a glass shield (Q). The bead was formed by winding 15cm. of 0.03cm. diameter high purity gold wire around the end of a tungsten hair-pin, and heating the tungsten in hydrogen. During this process the

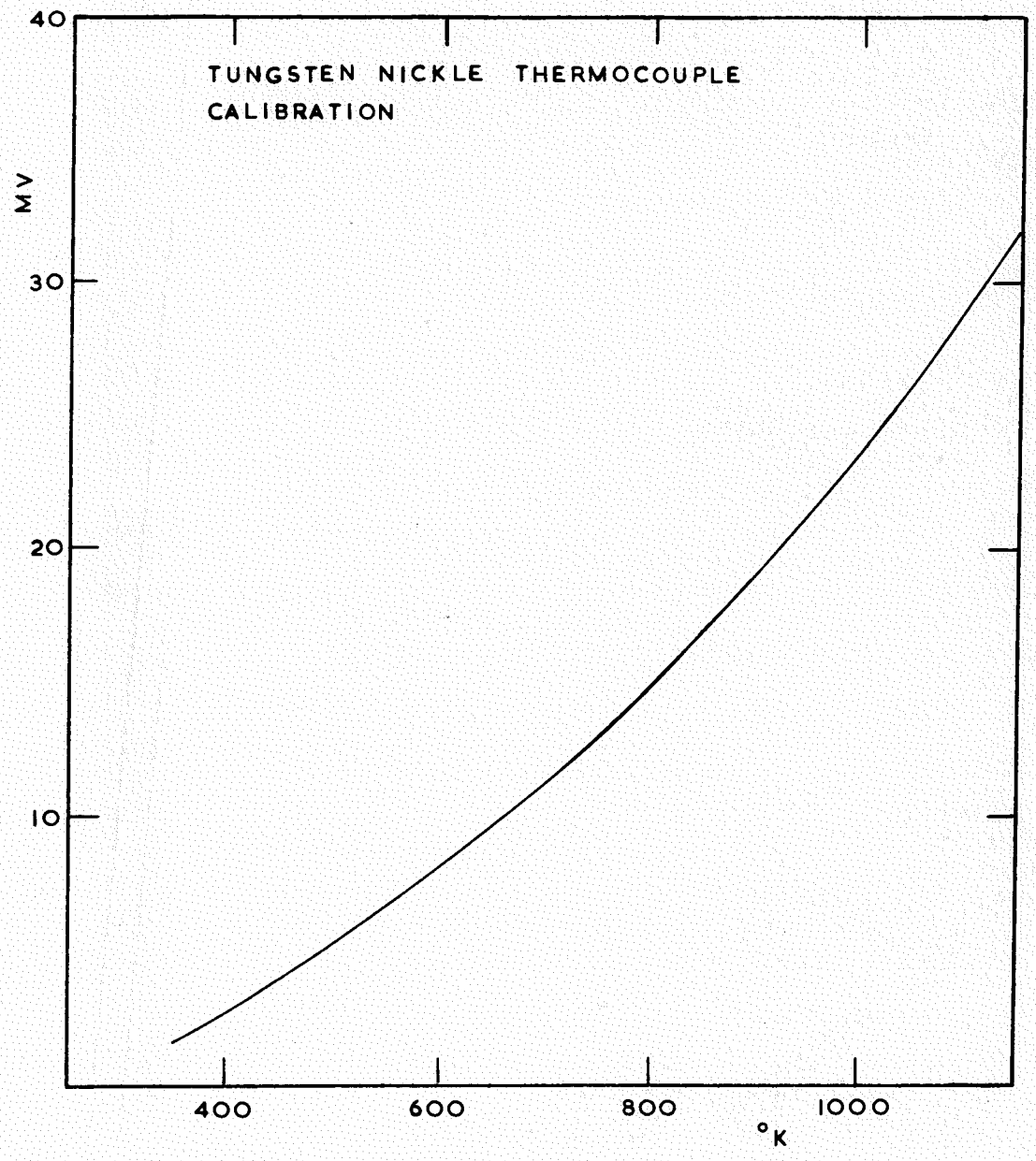
TUNGSTEN NICKLE THERMOCOUPLE
CALIBRATION
MV
40
30
20
10
400
600
800
1000
°K

FIG. 26.

bead was maintained at a temperature just below evaporation to remove as much dissolved gas as possible.

The anode (A) was made from 0.04cm. thick nickel sheet. This was cut into a 2cm. diameter disc, fitted with a nickel support wire, and hydrogen furnaced at 1300°K for 5 minutes.

The assembly was supported by a glass frame (G) sealed to the stem of a seven lead C.9 pinch; glass screens (L) were fitted to the leads of the pinch to prevent electrical short circuit by conducting films which might condense on the base. Nickel tags welded round the glass frame supported the cathode and the gold bead. When in position, the cathode was fitted with a nickel radiation shield (S). The anode was welded to a tungsten lead sealed into a glass hinge (H). By means of a glass encased soft iron slug (N) fixed to the hinge, the anode could be positioned either over the reference electrode, or over the cathode.

The completed assembly was sealed into a C.9 glass envelope fitted with a side arm (B) and two tungsten seals (T,P). One seal made contact to a conducting screen of graphite (K) painted on the walls of the envelope, and the other served as an electrical connection to the anode.

5.5 Temperature measurements.

Thermocouples were used to measure the cathode temperatures.

TABLE 5.1.

W/W - 26% Re mV	Pt/Pt - 10% Rh mV	Kaye & Laby Temp. ^{o}K
0.00 ± 0.05	0.00	295 ± 5%
0.40	0.60	390
0.75	1.00	440
1.25	1.50	505
1.76	2.00	560 ± 1%
2.40	2.50	615
3.08	3.00	670
3.80	3.50	720
4.55	4.00	775
5.30	4.50	825
6.20	5.00	875
7.85	6.00	970
9.55	7.00	1065
11.25	8.00	1160
12.95	9.00	1245
14.70	10.00	1330
16.35	11.00	1420
18.00	12.00	1500
19.55	13.00	1585
21.15	14.00	1665
22.70	15.00	1745
24.30	16.00	1830
25.80	17.00	1915
27.05	17.80	1980

In the case of the 'O' nickel bases a tungsten/nickel thermocouple was found to be most suitable; the hot junction was a tungsten wire welded to the inside of the base, as described in section 5.4; the cold junction was formed outside the tube, and could be maintained at 273°K when necessary. Emission measurements were unaffected by the cold junction being at room temperature; the results of these measurements depend on temperature differences rather than on the absolute temperature. The calibration curve for a tungsten/nickel thermocouple is shown in Fig. 26. The temperature of the platinum based cathodes was measured by a platinum/platinum-10% rhodium thermocouple which was welded to the back of the platinum box. Johnson and Matthey supplied the platinum/platinum - 10% rhodium thermocouple material to a standard specification; the calibration for this thermocouple was obtained from Kaye and Laby(1959).

During the later experiments it was desirable to measure anode temperatures up to 2700°K. A tungsten/tungsten-26% rhenium thermocouple is suitable over this temperature range, and was welded to the back of the anode. The calibration for this thermocouple, which was obtained in this laboratory by Mr. Blott, is shown in Table 5.1.

Thermoelectric e.m.f.s developed by the thermocouples were

FIG. 27.
THE ELECTROMETER CIRCUIT

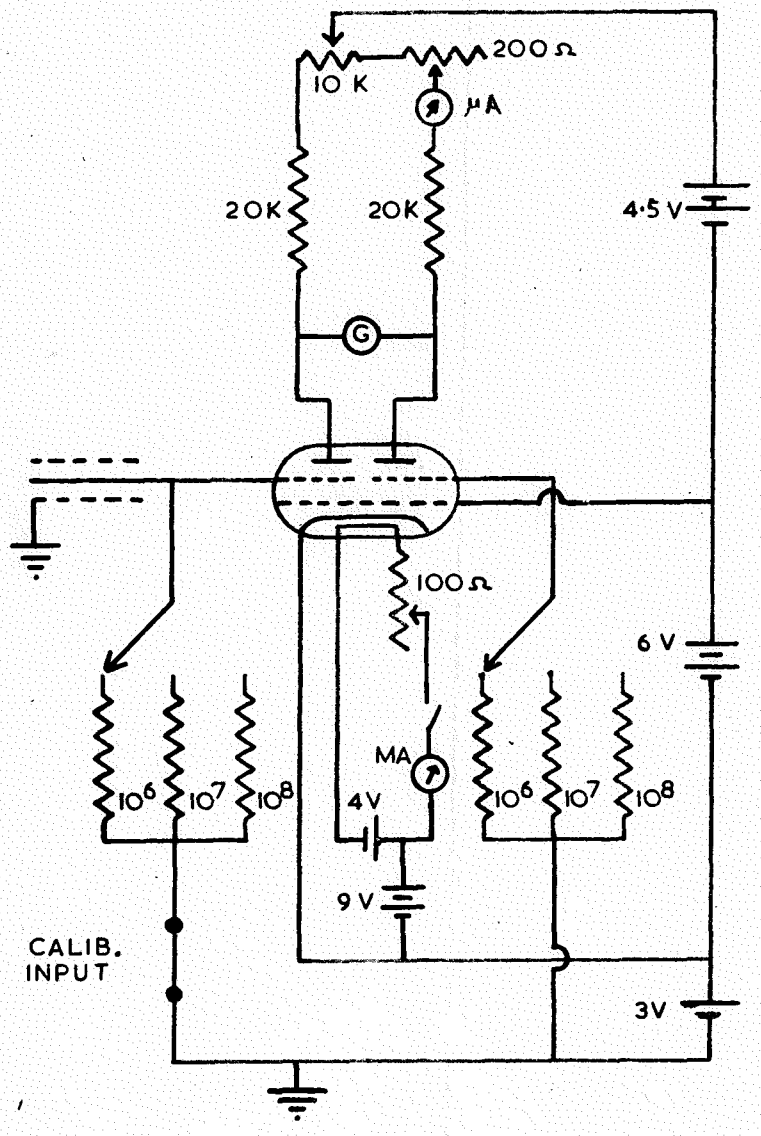

BDM.10.

measured with a Croydon Instruments potentiometer.

5.6. Emission measurements.

Emission currents down to 10^{-12} amps were measured by an electrometer with switched input resistors having values 10^6, 10^7, 10^8 ohms, together with a sensitive galvanometer. The electrometer circuit is shown in Fig. 27. One half of the electrometer valve (a Ferranti electrometer double beam tetrode, type B.D.M.10, now unavailable) is used as a reference circuit. A small current flowing through one of the input resistors produces a change in the control grid voltage, and causes an out-of-balance current to flow through the galvanometer G. The circuit is initially balanced by the two variable resistors in the anode circuit so that no current flows through the galvanometer. To obtain maximum stability, the on-of switch in the heater circuit, and all the anode circuit components were of high quality. A ceramic rotary switch was found to have adequate insulating properties for switching-over the input resistors. Heater power was supplied from a pair of 2 volt accumulators which were contained in a separate screened box; connections were made to the electrometer by screened coaxial cable. Grid bias batteries provided

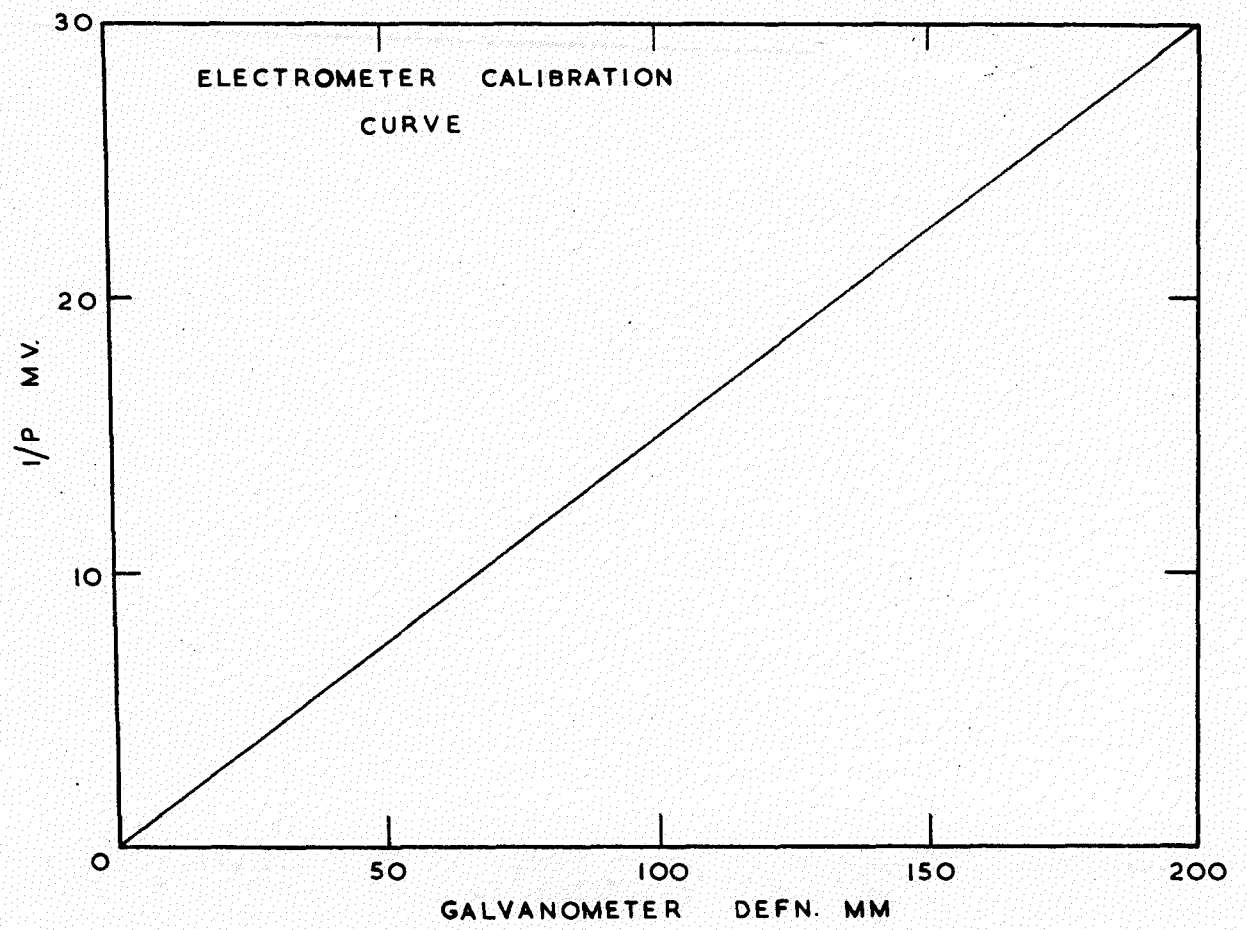
ELECTROMETER CALIBRATION
CURVE
30
20
10
0
I/P MV.
50
100
150
200
GALVANOMETER DEFN. MM

FIG. 28.

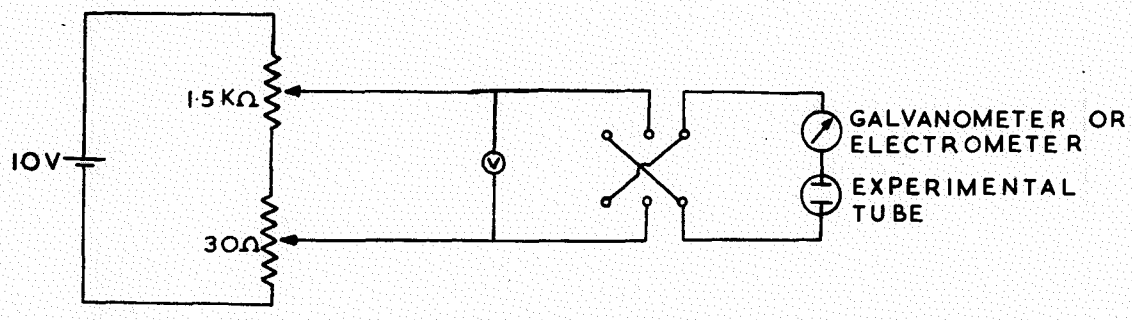

FIG. 29.

POTENTIOMETER UNIT CIRCUIT

the other voltage supplies; these were mounted inside the screened metal box containing the electrometer. Under normal operation, a heater current of 300 mA. resulted in an anode current of 150μA. The instrument was calibrated against a Croyden Instruments potentiometer. Using a Pye Scalamp Galvanometer of current sensitivity 4.8×10^{-8} amps per cm., a deflection of 1 cm. on the galvanometer corresponded to an input of 1.5 millivolts. A calibration curve for the electrometer is shown in Fig. 28.

Thermionic emission measurements for low applied fields were made by applying voltages from the potentiometer unit shown in Fig. 29. Voltages for the high field Schottky plots were taken from a 0-20 kV. Brandenburg high tension unit.

5.7. Kelvin measurements.

Referring to Fig. 18, the charge at any instant on each plate of the sinusoidally varying condenser is given by

$$Q = AV_{12} / 4\pi d(1 + a\sin wt)9.10^{11}. \text{ coulombs.} \qquad (5.2)$$

A is the area of the condenser plates, V_{12} is the contact potential difference between the plates, d is the normal seperation, a is the amplitude of vibration of the plates, and the frequency of vibration is given by $w/2\pi$. Differentiating Eq. 5.2 with respect to time :

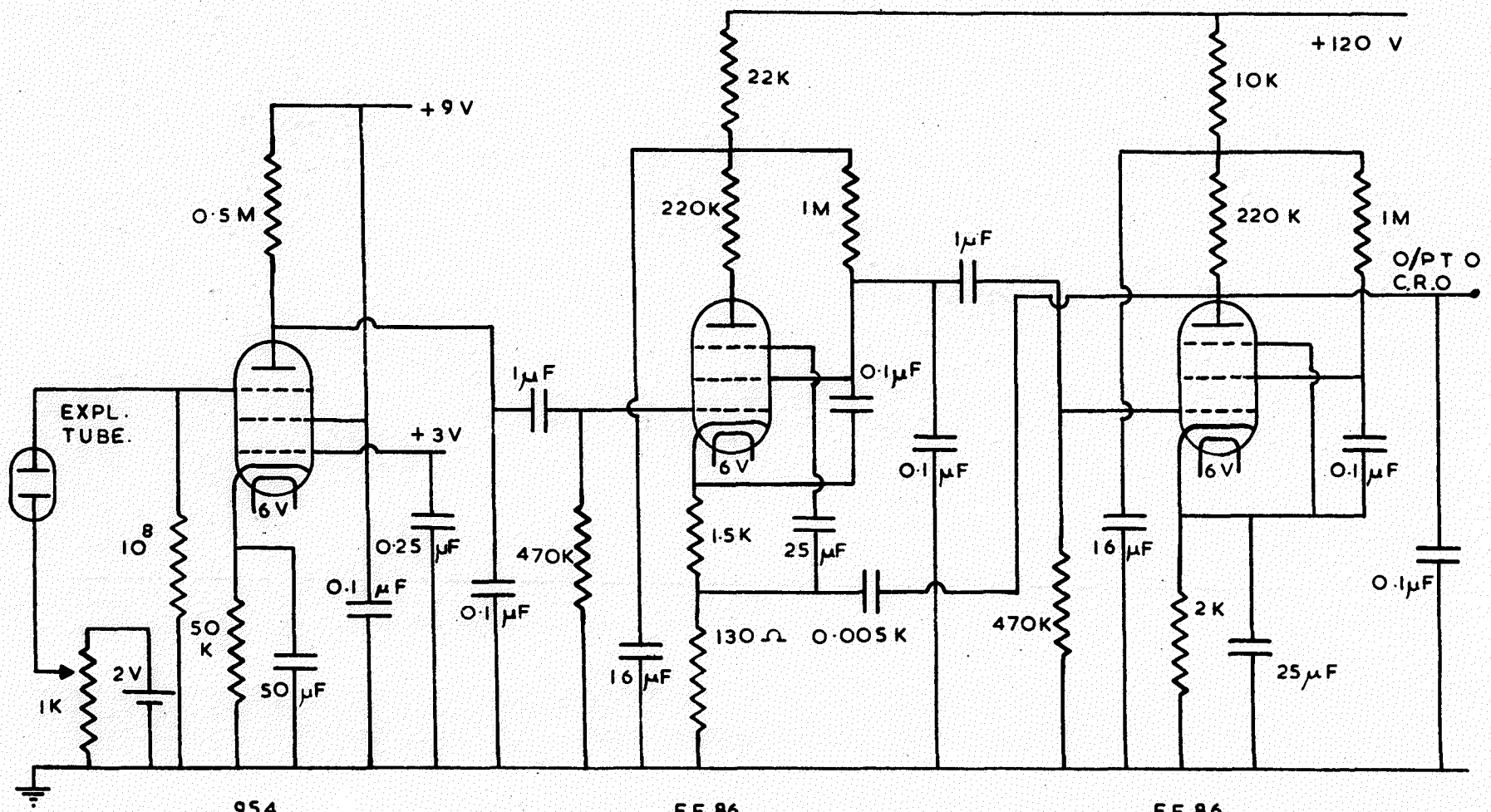

CONVENTIONAL LOW FREQUENCY AMPLIFIER.

FIG. 30.

$$dQ/dt = V_{12}Aaw \cos wt / 4\pi d(1 + a\sin wt)^2 9x10^{11} \qquad (5.3)$$

This is an expression for the current through the resistance R. The ratio of the alternating voltage across R to the contact potential V_{12} is therefore

$$dV/V_{12} = RAaw \cos wt/4\pi d(1 - a \sin wt)^2 \, 9x10^{11}. \qquad (5.4)$$

In the experimental tubes designed to measure contact potential differences by the Kelvin technique, typical values of the quantities in Eq. (4.4) were: $V_{12} = 0.2v$, $A = 1cm^2$, frequency of vibration 15c/s, d = 0.2 cm., a = 0.2 cm. On substitution these give for the maximum voltage across the resistance R

$$dV_{max} = R \times 5.8 \times 10^{-12}. \qquad (5.5)$$

If $R = 10^8$ ohms, $dV_{max} = 5.8 \times 10^{-4}$.

Initially Kelvin measurements were made with a low frequency amplifier circuit of conventional design (Fig. 30). This amplifier had a gain of 1000, and the output was fed into a Solartron oscilloscope which had a maximum sensitivity of 10 mv. per cm. Batteries were used to power the amplifier, and these, together with the amplifier and the experimental tube were contained in separate earthed metal boxes. All connections were made by screened coaxial cable. The backing off potential was also drawn from batteries via a 1000 ohm linear potentiometer and measured on a Croyden Instruments potentiometer. Despite the screening precautions, inter-

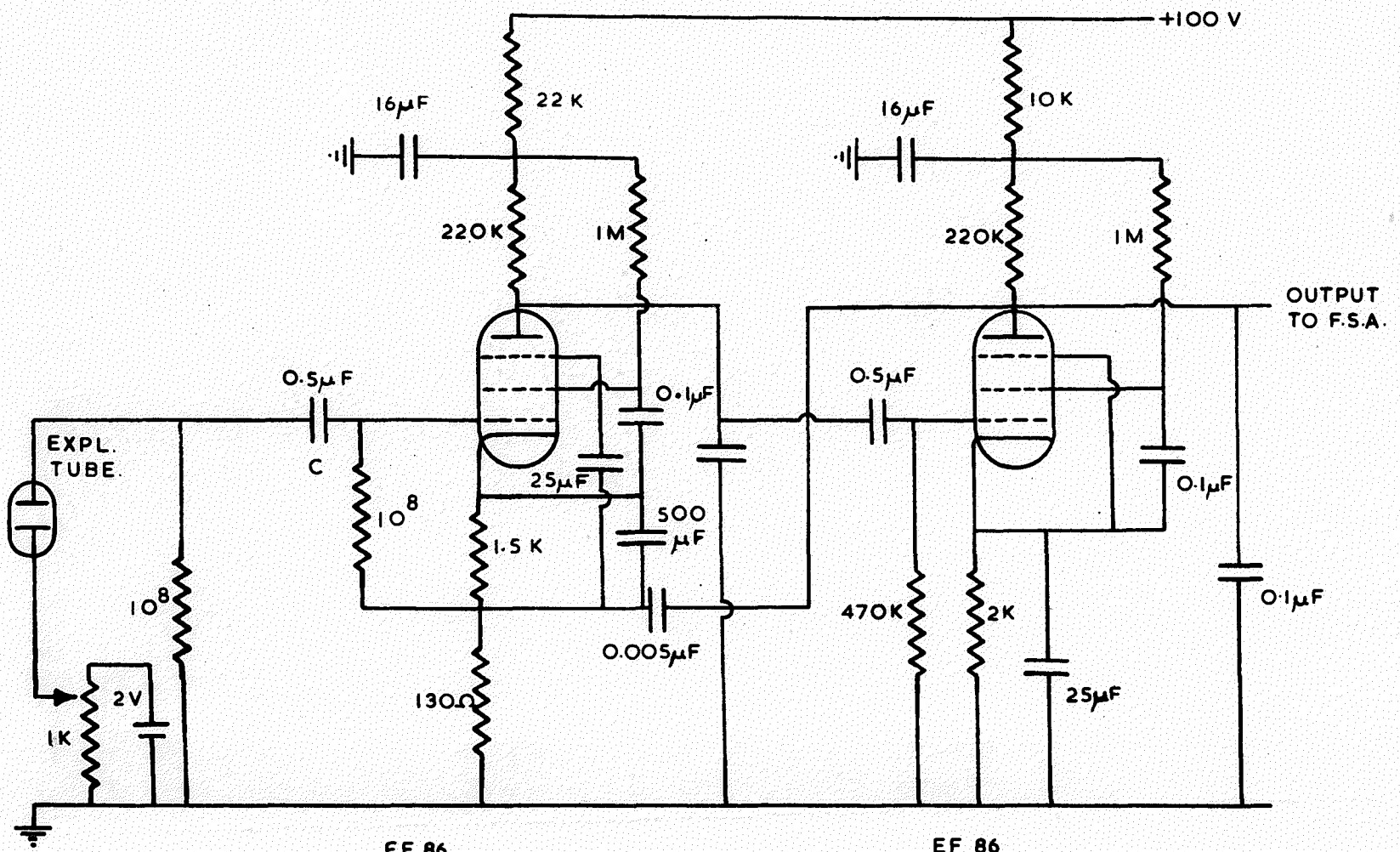

PRE-AMPLIFIER.

FIG. 31a.

ference from the mains 50 c/s supply was sufficient to limit the sensitivity of the measurements such that contact potential differences could only be determined to within $\pm$ 50 mv.

Much attention was given to the design of a more sensitive amplifier system for the Kelvin measurements. Macdonald(1961) has shown that ideally the shunt capacitance on the input of a Kelvin amplifier should be zero, or at least small enough for the load to be primarily resistive. This results in a higher conversion efficiency and reduces the harmonics present in the signal. In addition the amplifier must have a high input impedence.

An attempt to improve the input impedence was made by replacing the 954 valve in the first stage of the circuit shown in Fig. 30 by an MD 1402 electrometer valve. This gave the first stage a gain of less than unity and was eventually abandoned. The most satisfactory arrangement was achieved with the circuits shown in Fig. 31. The first two stages (Fig. 31a) formed a head amplifier which was mounted inside the screened metal box containing the experimental tube. In this manner lead capacitance was reduced to a minimum. A high input impedence was achieved with an EF 86 operating as a cathode follower but providing a gain of 25. The overall gain of the head amplifier was 1000. After passing through the head

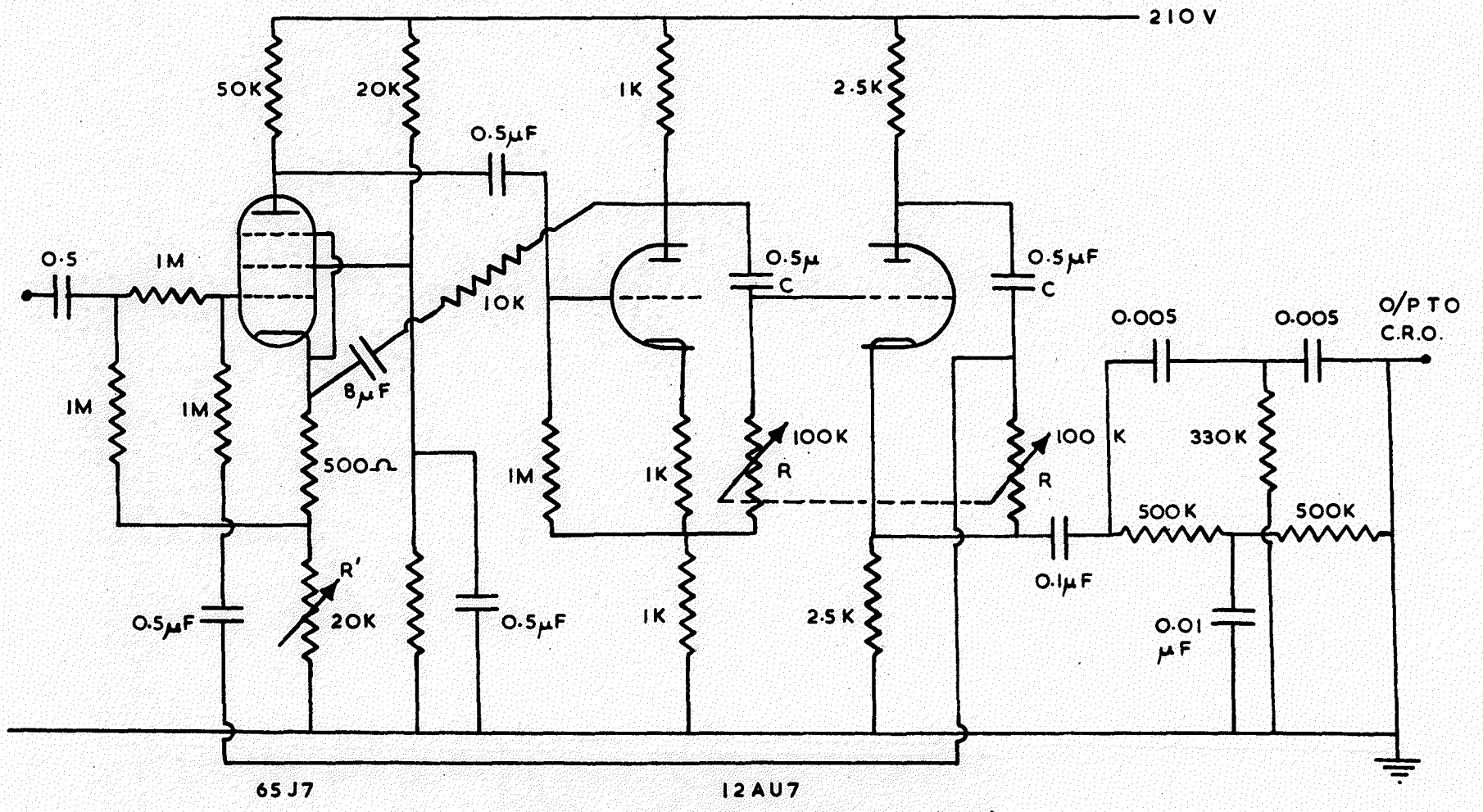

FREQUENCY SELECTIVE AMPLIFIER (F.S.A)

FIG . 31 b.

amplifier, the signal was fed into a frequency selective amplifier (Fig. 31b) which could be tuned to the frequency of the vibrating condenser by adjusting the ganged resistances R. The band width of the frequency selective amplifier was controlled by R'; for a band width of less than 2 c/s the time constant of the amplifier became inconveniently long. When necessary a 50 c/s twin-T filter could be added to the circuit to further reduce interference from the A.C. mains supply. These improvements enabled contact potential difference measurements to be made to an accuracy of $\pm$ 10 mv.

Most Kelvin signals were found to have a considerable harmonic content before they passed through the frequency selective amplifier. Macdonald(1961) showed in his theoretical analysis of the sinusoidially varying capacitance problem, that rich harmonic generation will occur when the condenser reactance at the vibrating frequency is comparable with the load resistance. Non-parallelism of the condenser plates has also been shown by Alexander(1952) to increase the harmonic content of the signal. In certain circumstances the use of a frequency selective amplifier might therefore be a disadvantage.

CHAPTER VI.

THE PRELIMINARY RESULTS.

6.1. Introduction.

The object of the preliminary investigations was to study the anode work function changes which occurred during the decomposition and activation of a barium oxide coated cathode.

The cathodes were decomposed by raising their temperatures to 1173°K over a period of about 30 seconds. They were maintained at this temperature for 48 hours after which they were said to be in the unactivated state. Positive potentials of 4, 20, 50, 75, and 100 volts were then successively applied to the anode for 24 hours each with the cathode at 1173°K.

The method adopted for referring to an individual tube and cathode activation state is as follows: First the type of tube is designated by one or more letters, followed by its number in the series. Finally a number in Roman numerals indicates the activation state of the cathode. Table 6.1 gives the cathode activation states.

TABLE 6.1.

Anode Voltage	Activation State
UD	I
D	II
4	III
20	IV
50	V
75	VI
100	VII

UD Undecomposed State
D Decomposed, but Unactivated State

6.2. The N series of tubes.

Initially a tube was designed to follow changes in the anode work function using the Kelvin technique and the intersection method (see Chapter IV). This resulted in the N series tube shown in Fig. 25. Detailed consideration was given to the construction of this type of tube in Chapter V; its distinguishing features were an 'O' nickel cathode base, a nickel anode, and the use of evaporated gold films as reference surfaces in the Kelvin measurements. Five such tubes were constructed, but on account of structural failures N.4 was the only tube in the series to give a full set of

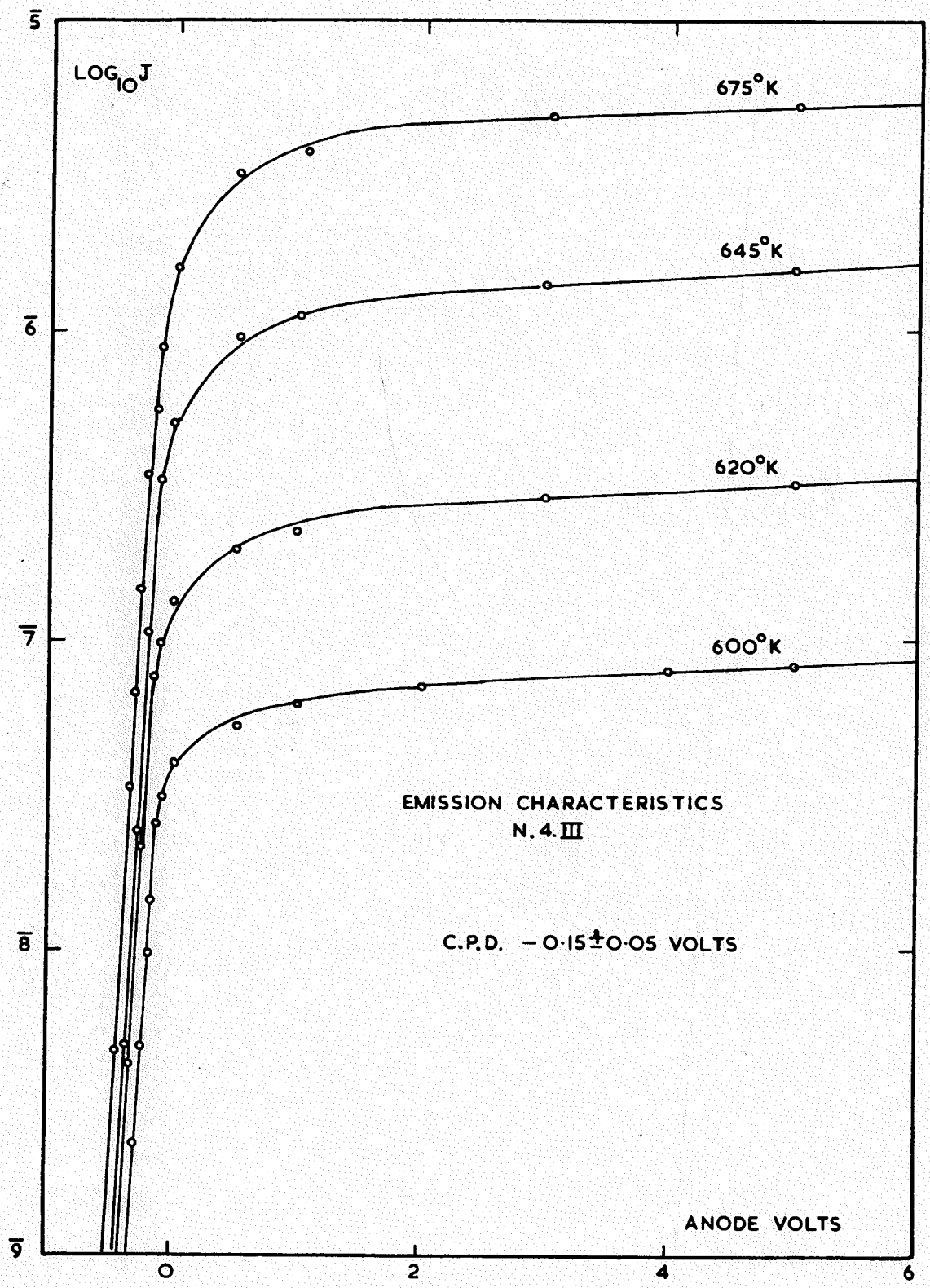
$\bar{5}$
$\log_{10} J$
675°K
645°K
620°K
600°K
$\bar{6}$
$\bar{7}$
$\bar{8}$
$\bar{9}$
EMISSION CHARACTERISTICS
N. 4. III
C.P.D. −0·15±0·05 VOLTS
ANODE VOLTS
0
2
4
6

FIG. 32.

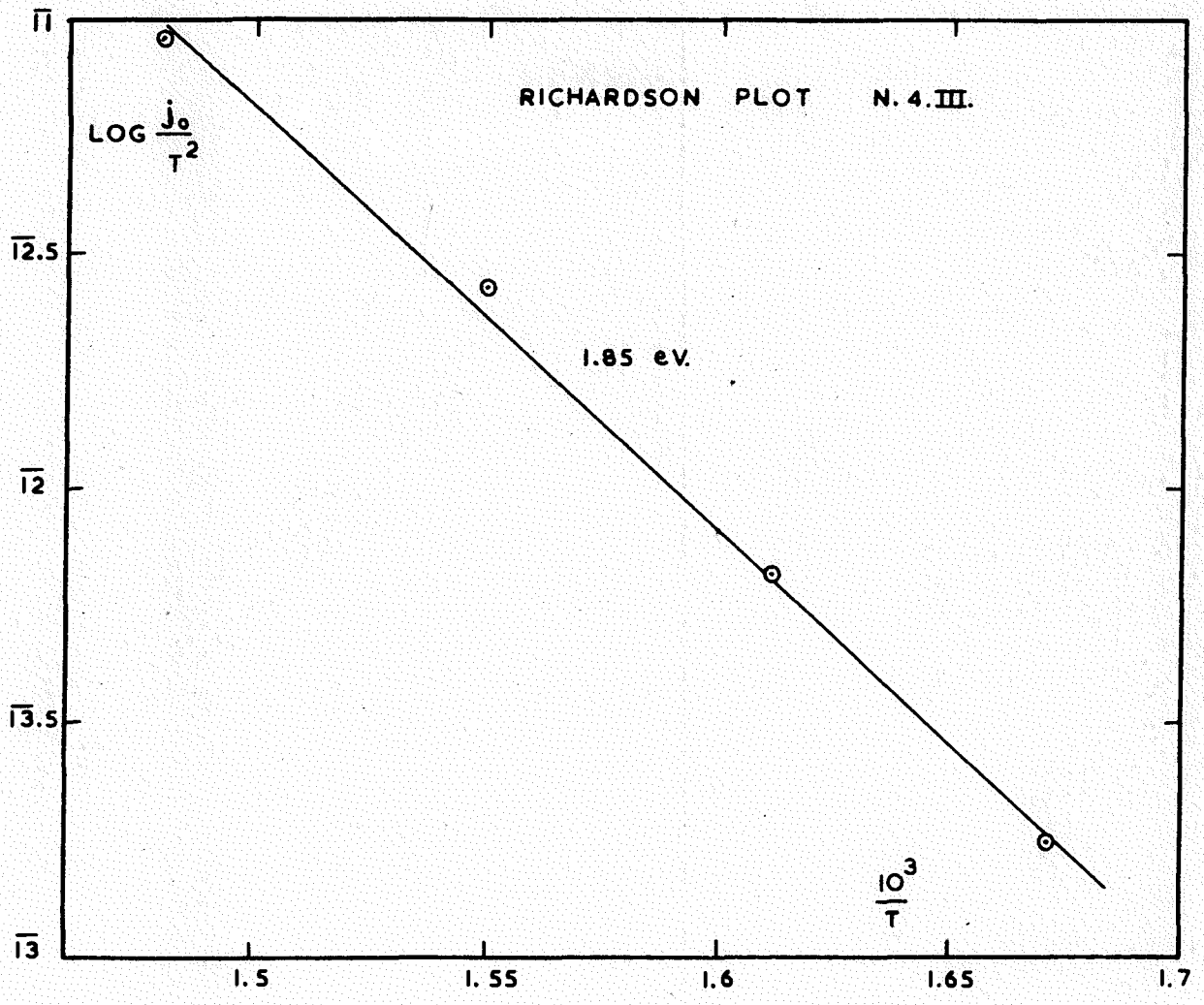
RICHARDSON PLOT N. 4. III.
LOG $\frac{j_0}{T^2}$
1.85 eV.
$\frac{10^3}{T}$
$\overline{11}$
$\overline{12.5}$
$\overline{12}$
$\overline{13.5}$
$\overline{13}$
1.5
1.55
1.6
1.65
1.7

FIG. 33.

results.

A set of emission characteristics for N.4.III. taken between 600°K and 675°K are shown in Fig. 32. The Richardson plot obtained from these emission characteristics is shown in Fig. 33, and indicates a cathode work function ϕ^{xx} of 1.85 eV. The anode-cathode contact potential difference indicated by the emission characteristics in Fig. 32 is -0.15 volts. To obtain an absolute value of the anode work function in a diode containing an oxide cathode, by the intersection method, corrections must be made for the thermoelectric effect, the potential gradient across the cathode matrix and interface layer, and the temperature coefficient of the cathode work function $d\phi_c/dT$. The uncorrected value of the anode work function, determined by the intersection method from the data in Figs. 32 and 33, is 1.7 eV. The importance of uncorrected values of the anode work function determined by the intersection method lies only in the change of anode work function that they may indicate. The full set of results obtained from N.4 are given in Table 6.2. Kelvin measurements made on the clean anodes prior to cathode decomposition gave the work function of nickel as 4.13, 4.60, 4.30, and 3.9 eV.

TABLE 6.2.

Cathode Activation State	Anode Work Function (eV)		Cathode Work Function Richardson Plot
	Intersection	Kelvin	
I	---	4.30	---
II	2.25	2.93	1.4
III	1.7	1.95	1.85
IV	1.8	2.13	1.9
V	1.65	2.00	1.75
VI	1.1	1.19	1.2
VII	1.1	2.20	1.1

Maintaining the cathodes in the N series tubes at temperatures of 1173°K for long periods of time caused appreciable evaporation from the 'O' nickel bases. Thick black deposits were found on the anodes of these tubes after the cathodes had been fully activated which chemical analysis indicated to be mainly nickel. Nickel was also found to be unsatisfactory as an anode material, mainly on account of outgassing difficulties. The eddy current heating used for outgassing gave rise to a high temperature gradient from the centre of the nickel anode discs to the edges, resulting in evaporation from the edges while the centre remained relatively cool.

To remove the effect of nickel evaporating from the cathode base a new tube was designed using platinum as the cathode base

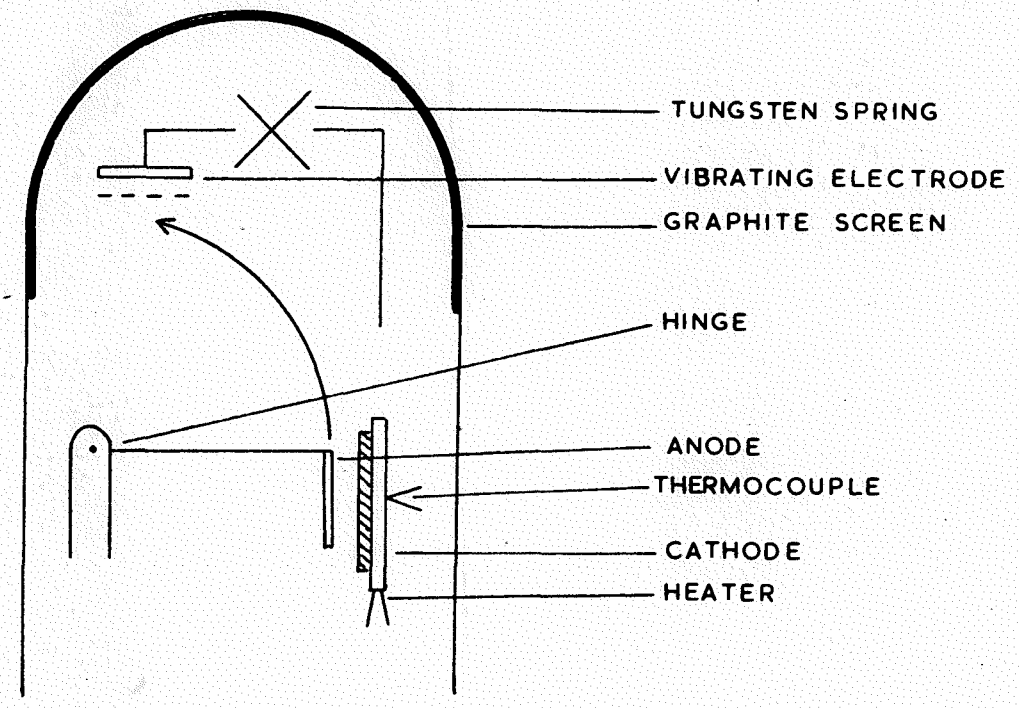

FIG. 34.

SCHEMATIC DIAGRAM OF A TYPICAL
K SERIES TUBE

material.

6.3. The K series of tubes.

A shematic diagram of a typical K series tube is shown in Fig. 34. The cathode base was a platinum box fitted with heaters and a platinum/platinum -10% rhodium thermocouple. The nickel disc anode could be rotated magnetically to face either the reference electrode or the cathode. The gold reference electrode was replaced in these tubes by a thin tungsten disc. Originally the work function of the tungsten reference electrode was taken as 4.52 eV., but all results have now been related to a tungsten work function of 4.54 eV., this being the value proposed by Hopkins and Riviere (1963) for polycrystalline tungsten foil.

Experimental results from K.2, K.3, and K.5 are given in Tables 6.3 and 6.4. Structural failures prevented any results being obtained from K.1 and K.4. The anode work function values given in Table 6.4 for the intersection method are again uncorrected.

TABLE 6.3.

Cathode Activation State	Anode Work Function, Kelvin Technique (eV)		
	K.2	K.3	K.5
I	4.69	3.92	4.65
II	4.07	3.58	3.67
III	4.02	4.17	3.87
IV	3.82	3.02	2.92

TABLE 6.3. (Continued)

Cathode Activation State	Anode Work Function, Kelvin Technique (eV)		
	K.2	K.3	K.5
V	2.3	2.92	3.68
VI	2.22	2.22	2.58
VII	2.42	2.32	2.72

The introduction of platinum as a cathode base material was expected to reduce considerably the cathode emission current density. This was not found to be so. Emission current densities from fully activated cathodes with both 'O' nickel and platinum bases were always between 25 and 30 mA. per cm^2.

TABLE 6.4.

Cathode Activation State	Anode Work Function, Intersection Method (eV)		
	K.2	K.3	K.5
I	-	-	-
II	5.19	5.22	3.38
III	4.73	4.56	3.18
IV	3.01	2.66	1.6
V	1.93	1.72	0.92
VI	2.24	1.93	1.95
VII	1.74	1.89	1.9

As a check on the anode work function measurements made by the Kelvin technique, a series of tubes were constructed (the M series), which enabled the anode work function to be measured

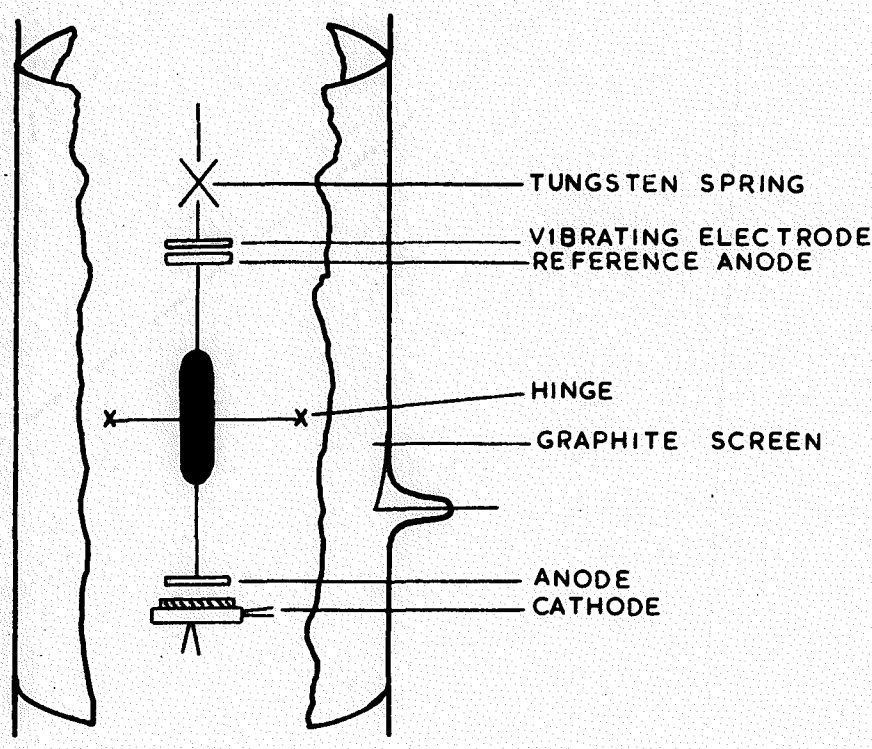

FIG. 35.

SCHEMATIC DIAGRAM OF A TYPICAL M SERIES TUBE

by a third method, the displacement of retarding potential characteristic method.

6.4. The M series of Tubes.

The M series tube is shown schematically in Fig. 35. Two anodes were incorporated in the design, and these could rotate about a hinge so that either anode could be made to face the cathode or the reference electrode. By this arrangement one of the anodes could always be kept as a clean reference surface, and hence the work function of the other contaminated anode could be found by the displacement of retarding potential characteristic (Anderson) method. Both the anodes and the vibrating reference electrode in these tubes were of thin molybdenum sheet. The contact potential difference between tungsten and molybdenum was taken from the measurements of Riviere (1957): the work function of molybdenum was then 4.24 eV.

The contact potential difference between the clean molybdenum electrodes was always less than 0.02 volts as measured by the Kelvin technique.

A typical set of emission characteristics obtained from the M series of tubes is shown in Fig. 36. The anode work function measurements made with tubes M.2-5 are summarised in

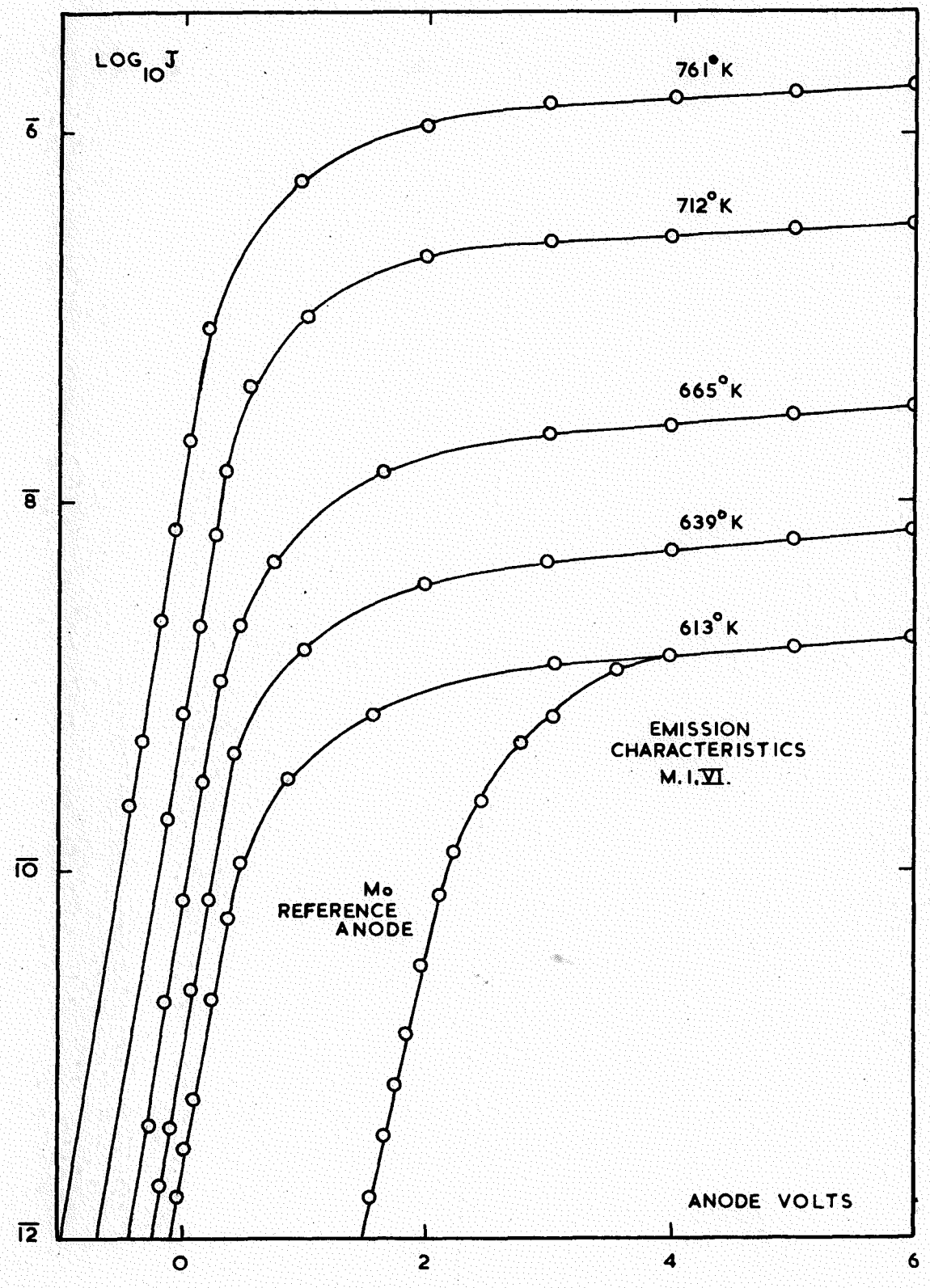
LOG10J
761°K
712°K
665°K
639°K
613°K
EMISSION
CHARACTERISTICS
M.I.VI.
Mo
REFERENCE
ANODE
ANODE VOLTS
6
8
10
12
0
2
4
6

FIG. 36.

Table 6.5. In this Table the arithmetic averages of the anode work function measurements for tubes M.2-5 in each cathode activation state, together with the corresponding average deviations, have been calculated.

TABLE 6.5.

Cathode Activation State	Anode Work Function (eV)		
	Kelvin	Anderson	Intersection
I	4.22 ± 0.02	---	---
II	3.51 0.13	3.54 ± 0.17	4.29 ± 0.46
III	3.48 0.09	3.37 0.14	4.06 0.28
IV	2.90 0.03	3.00 0.13	2.78 0.22
V	2.96 0.13	2.58 0.13	1.97 0.06
VI	3.00 0.18	2.78 0.15	1.85 0.29
VII	2.91 0.17	3.03 0.17	2.38 0.30

Three cathode work functions could be calculated from a set of emission characteristics such as those in Fig. 36, ϕ^{xx} ϕ_E, and $\tilde{\phi}$, where

$$\tilde{\phi} = \phi^{xx} + T.d\tilde{\phi}/dT. \qquad (4.14)$$

and $$\phi_E = \phi^{xx} + T.d\phi_E/dT \qquad (4.7)$$

Values of $d\phi_E/dT$ could be calculated from Hensley plots. A set of cathode data for tube M.3 is given in Table 6.6. The

random variations in work function shown in Table 6.6 are typical of the tubes in this series.

TABLE 6.6.

Cathode Activation State	Cathode Work Function			
	ϕ^{xx}	$\phi_E(600^oK)$	$\phi_E(0^oK)$	$\tilde{\phi}(650^oK)$
II	2.28	2.20	1.55	2.77
III	1.91	2.19	1.92	2.22
IV	2.80	2.48	2.80	2.77
V	1.98	2.18	1.98	2.42
VI	1.77	2.18	1.77	2.42
VII	2.42	2.13	1.86	2.55

Prompted by the agreement obtained between the Kelvin and Anderson methods, and the relative simplicity of the latter method, a new tube was designed (the T series tube) in which the anode work function was to be measured only by the Anderson method.

6.5. The T series of tubes.

The T series tube shown schematically in Fig. 37 was the last tube built for the preliminary investigations, and led the

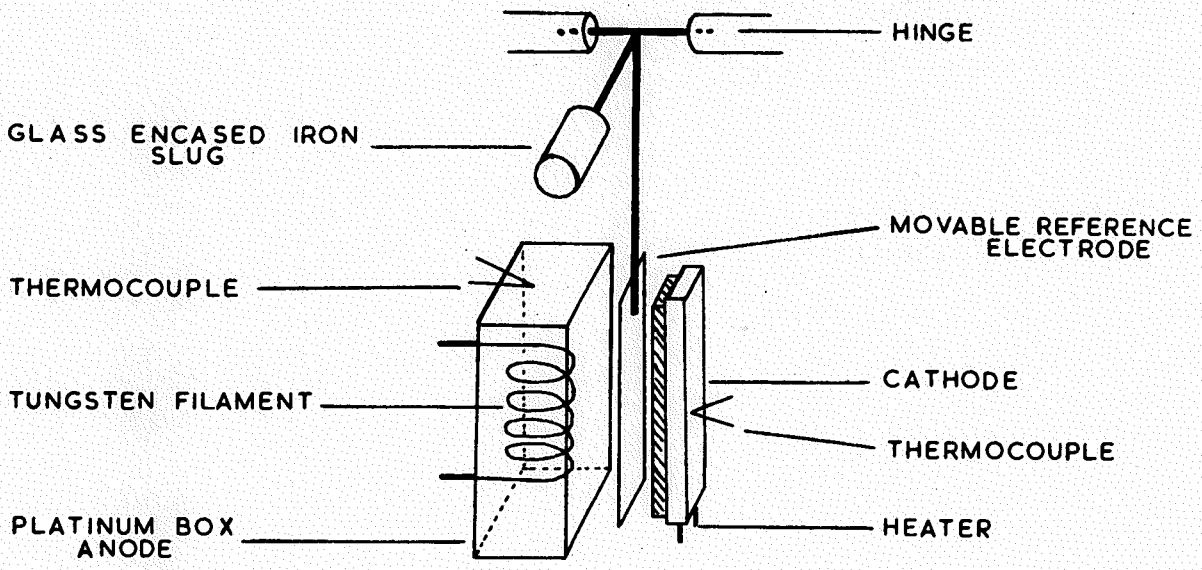

FIG. 37.

SCHEMATIC DIAGRAM OF THE ELECTRODE STRUCTURE IN A TYPICAL T SERIES TUBE

way to the tube design used for the experiments to be described in Chapter VII. It consisted essentially of a platinum box cathode coated with barium oxide and a platinum box anode. The latter was fitted with a heater and a platinum/platinum-10% rhodium thermocouple. A tungsten reference electrode could be inserted between the anode and cathode. This also served to screen either the anode or cathode while the other was being outgassed.

No further information regarding the nature of the anode films was obtained from the T series of tubes. Variation of the anode work function with temperature could not be investigated by the displacement of retarding potential characteristic method. The low work function of the anode films was found to result in electron emission from the anode at relatively low temperatures, and under these conditions the displacement of retarding potential characteristic technique could not be used.

Since the accepted work function for platinum could never be obtained in these tubes, platinum was thought to be unsuitable as an anode material. The anode work functions measured in the three tubes after heating at 1450^{o}K for 24 hours were 4.71, 4.74, and 4.11 eV. A reproducible value for the work function of platinum of 5.36 eV. was obtained by Oatley (1939) only after he had bombarded the platinum surface with positive ions of

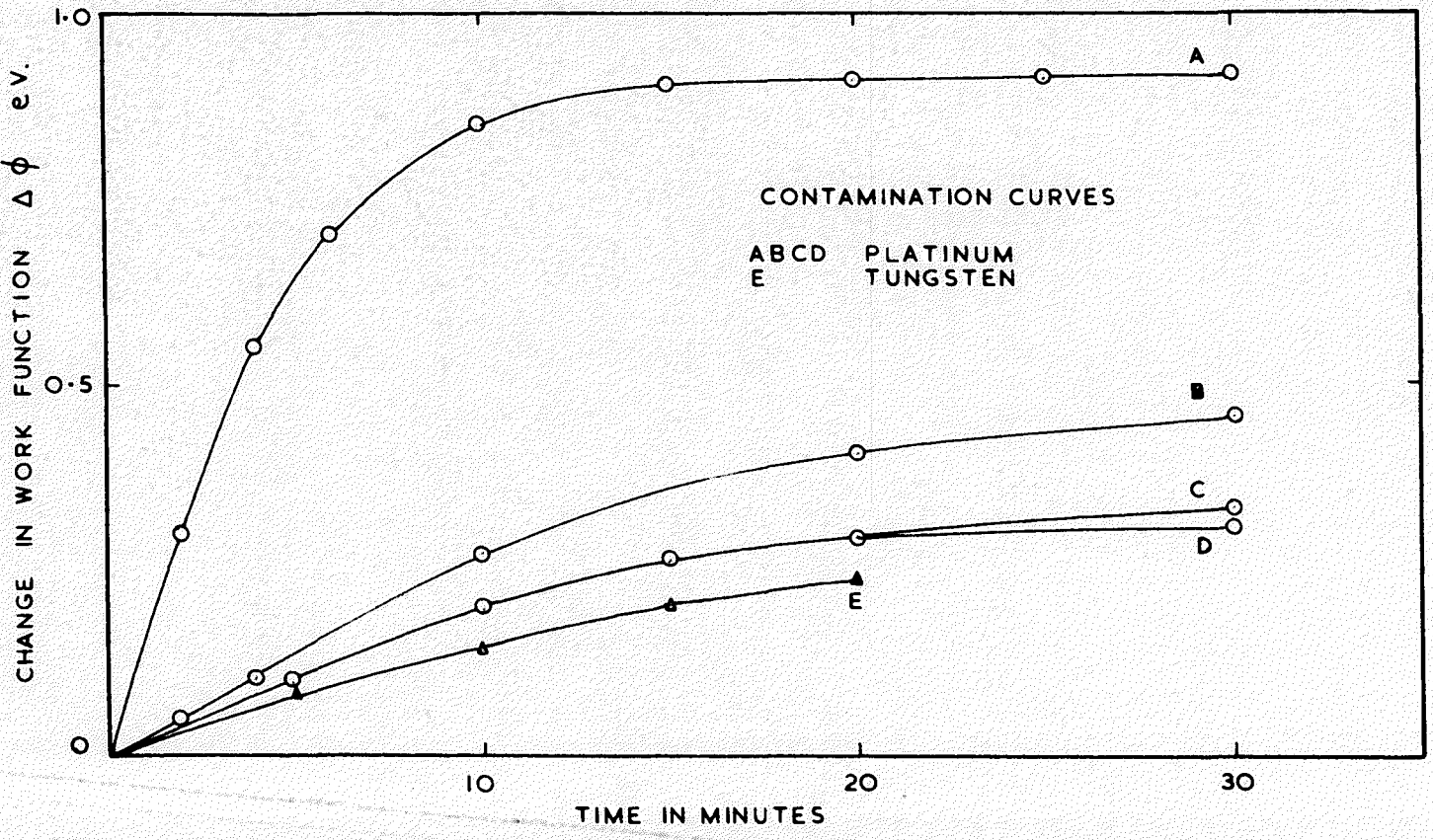
1·0
0·5
0
CHANGE IN WORK FUNCTION Δφ eV.
CONTAMINATION CURVES
ABCD PLATINUM
E TUNGSTEN
A
B
C
D
E
10
20
30
TIME IN MINUTES

FIG. 38.

oxygen and argon. After sublimation from the cathode onto the platinum it was never possible to return the work function of the platinum to a value higher than 3.0 eV.. Metson and Holmes (1960)b have reported a similar effect, and attribute it to barium metal dissolved in the platinum.

Fig. 38 shows the variations in the work function of the platinum anodes at a pressure of 10^{-9} mmHg. after various outgassing treatments. Curves A, B, and C were obtained from the anode of T.1; curve A was obtained after the anode had been at 1273°K for 24 hours, curve B after a further 7 hours at 1423°K, and curve C after three more hours at 1473°K. Air was accidently let into the system while the anode of T.2 was at 1573°K and no new information was obtained. The change in work function of the anode in T.3 after it had been maintained at 1573°K for 24 hours is shown by curve D of Fig. 38. Curve E shown the change in work function of clean tungsten at a pressure of 2×10^{-9} mmHg. after being outgassed at 2500°K.

6.6 The vacuum systems.

During the foregoing investigations a change was made from the conventional vacuum system to the Bandringa and Venema-type system described in Chapter V. Tubes M.2-5 and T.1-3 were

processed on the latter system.

During the first part of the bake-out proceedure associated with the Bandringa and Venema vacuum system the components of the experimental tubes were in an atmosphere of mercury vapour at 720°K for 12 hours. At this temperature little, if any, decomposition of the barium carbonate should take place, and any barium oxide formed should be stable in the mercury vapour at 720°K. A catalytic action by the mercury vapour in which the barium carbonate is reduced to oxide, and this in turn is reduced to free metallic barium is the only other possibility, and it is not very likely that this will occur (private communication, Dr. Fowles, Chemistry Department, Southampton University). Measurements of ϕ^{xx} for the barium oxide coated cathodes made in the decomposed state (II) before and after the introduction of the Bandringa and Venema vacuum system are given in Table 6.7.

TABLE 6.7.

ϕ^{xx} eV.	Conventional System				B & V system			
	2.6	2.4	2.5	2.4	2.4	2.3	2.3	2.7

These figures do not indicate any reaction of the mercury vapour with the cathodes.

6.7. Experimental errors.

(a) Richardson plots.

The average value of the probable error in cathode work functions determined by the Richardson line technique was found by the method of least squares to be ± 0.05 eV.

(b) Anode work functions.

Anode work functions determined by the intersection method are subject to the error in determining the cathode work function from the Richardson plot, and the error in determining the intersection point from the emission characteristics. The latter error had a maximum value of ± 0.1 volts. This results in a maximum error of ± 0.15 eV. in values of the anode work function determined by the intersection method.

Measurements made by the Kelvin technique in the N and K series of tubes were subject to an experimental error of ± 0.05 eV. Subsequent improvements in the Kelvin amplifier system enabled contact potential difference measurements to be made to an accuracy of ± 0.01 eV.

Contact potential differences determined by the displacement of retarding characteristic, or Anderson method, were uneffected by any systematic errors inherent in determing the cathode temperatures. A given cathode temperature could be reproduced to within $\pm 5^{\circ}$K. The effect of this temperature

uncertainty can be calculated from the retarding field equation (Eq. 2.15) :

$$j_r = A(1-r)\ T^2\ C \exp -(V - \phi_A)/kT.$$

Putting (1 - r) and C equal to 1, we have

$$\log j_r/T^2 = \log A + 5040(V - \phi)/T$$

Differentiating

$$d(V - \phi)/dT = 1/5040.(\log j_r/T^2 - \log A) - 2/5040$$

Substituting in this equation the experimental conditions $j_r = 10^{-11}$ amps, $T = 850^{\circ}K$, and the theoretical value of 120 amps/$cm^2/^{\circ}K$ for A, we have

$$d(V - \phi)/dT = (1/5040)(-19.23) - (2/5040).$$

$$= -21.23/5040$$

Therefore, $d(V - \phi)/(V - \phi) = (dT/T)(19.23/17.15)$.

Thus when ϕ = 4 eV., V = 2 V. and $dT = \pm 5^{\circ}K$, $d(V - \phi)$ is approximately ± 0.015 V. The experimental error in determining anode work functions from two retarding potential characteristics was therefore, ± 0.03 eV.

To this uncertainty must be added the uncertainty in making the actual current measurement, which was ± 0.02 V. The total experimental error in the Anderson measurements was ± 0.07 eV.

6.8. Conclusions from the preliminary results.

The most important conclusion to be arrived at from the preliminary investigations was that the anode should be cleaned after decomposing the cathode. It is thought that this would improve the reproducibility of the anode work function from tube to tube by eliminating the complicated effects due to cathode decomposition products. Further improvements in anode work function reproducibility were thought to be possible by cleaning the anode immediately before sublimation from the cathode took place in any one of the cathode activation states.

Eddy current heating of the reference electrodes in these experiments was most unsatisfactory, since it inevitably led to a rise in temperature of the anode, and the possibility of work function changes occurring on the anode as a result of these changes in temperature cannot be not overlooked. The fact that such changes did occur was later confirmed, and the results of experiments to investigate this effect will be described in Chapter VIII.

The lowest anode work function measured by the Kelvin technique was 1.19 eV. for N.4.VI. In the case of nickel based barium oxide cathodes the materials subliming have been reported by Plumlee and Smith (1950) to be barium and barium oxide in the ratio 9:11. These products, together with the

nickel found to sublime from the 'O' nickel bases, probably form a surface on the anode similar to a nickel matrix cathode; the nickel matrix cathode has been found to have a work function around 1.2 eV. (see for example Fane (1957)).

The low anode work functions observed in those tubes having platinum based cathodes could only be explained, either by the decomposition of barium oxide on the anode surface resulting from activating the cathode at potentials up to 100 volts, or by the formation of a barium oxide impurity semi-conductor on the anode surface.

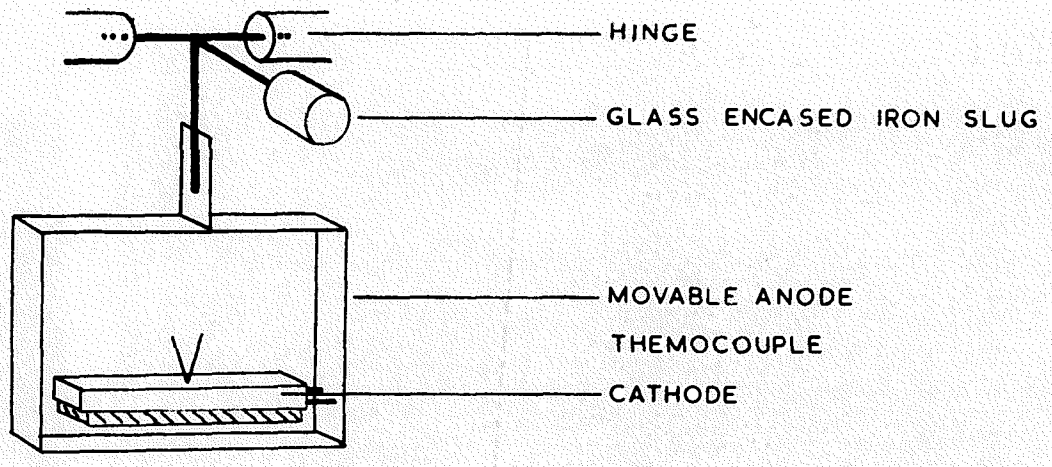

(A) MOVABLE ANODE, FIXED CATHODE.

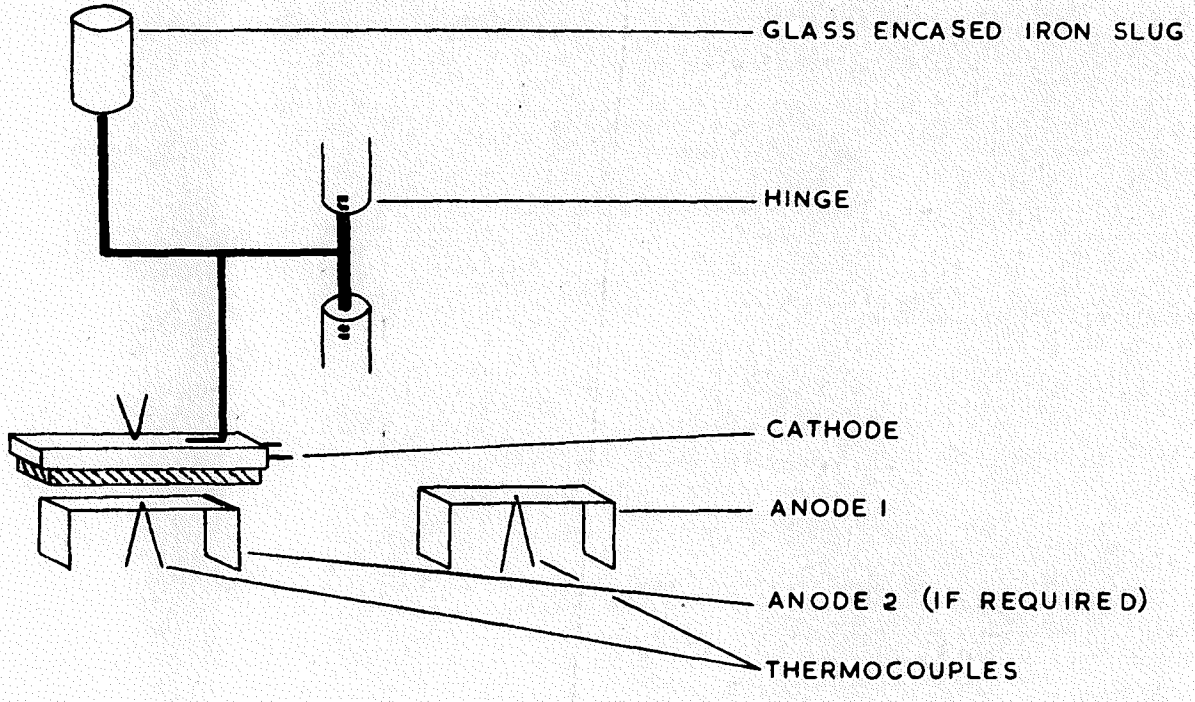

(B) MOVABLE CATHODE, FIXED ANODE.

FIG. 39.
SCHEMATIC DIAGRAMS OF THE ELECTRODE STRUCTURE FOR TYPICAL SERIES-P TUBES

CHAPTER VII.

Results (i)

7.1. Introduction.

Following the tubes used for the preliminary investigations, six tubes were constructed (P series), all of which contained a platinum base-barium oxide cathode and a tungsten anode (Fig.39). Arrangements were made to remove the anode from the proximity of the cathode (Fig.39A), or vice-versa (Fig.39B). The displacement of retarding potential characteristic method was used exclusively to follow changes in the anode work function. All experimental tubes in the P series were used to measure the change in work function of clean tungsten caused by sublimation from the cathode in each of its activation states. The cathodes were activated in the manner described in section 6.1.

7.2. Electron temperatures.

The measuring technique employed for these investigations was similar to that used for the low temperature data of Florio(1963); sublimation from the cathode took place at an

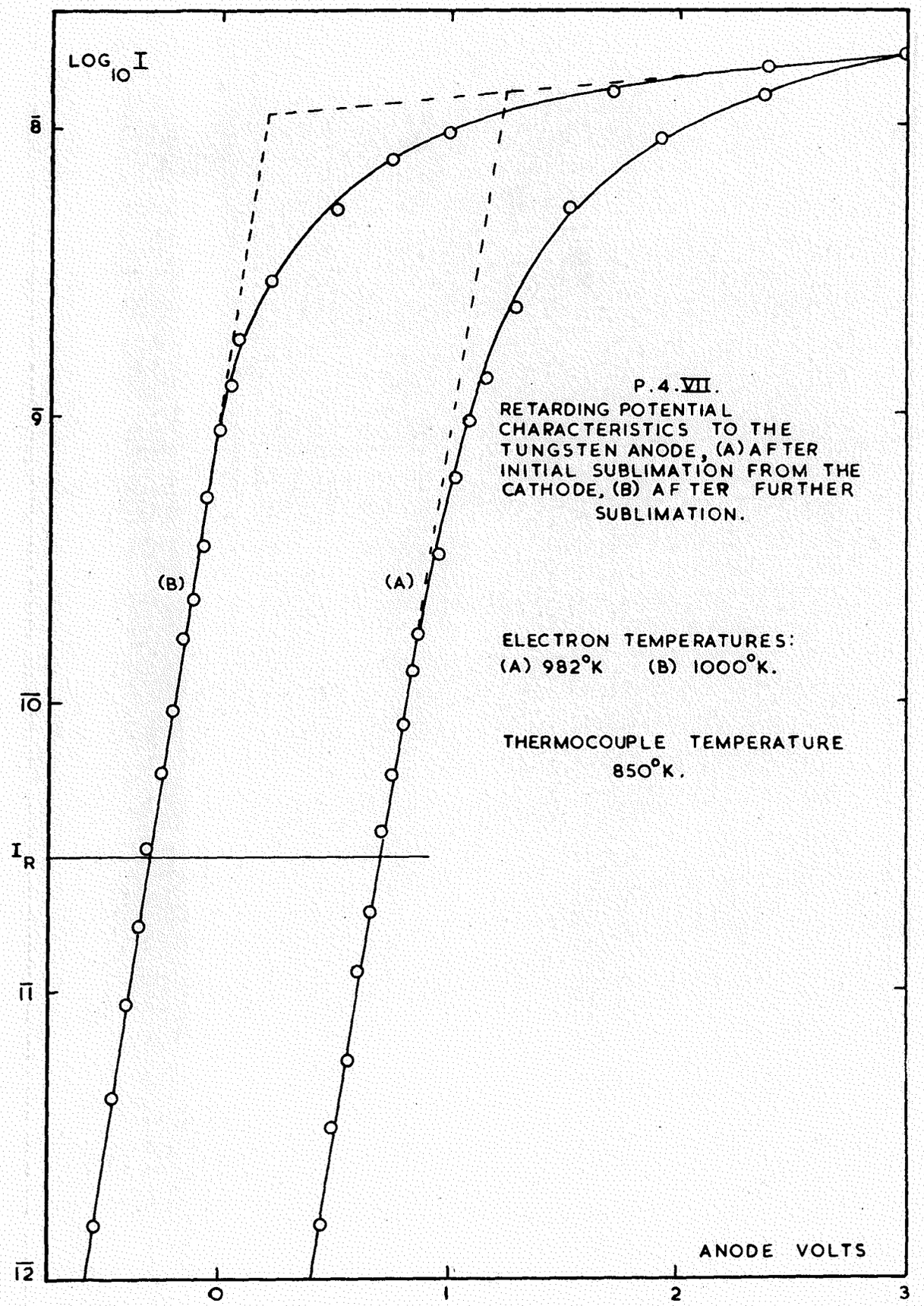
LOG10 I
$\bar{8}$
$\bar{9}$
$\bar{10}$
I_R
$\bar{11}$
$\bar{12}$
(B)
(A)
P.4.VII.
RETARDING POTENTIAL CHARACTERISTICS TO THE TUNGSTEN ANODE, (A) AFTER INITIAL SUBLIMATION FROM THE CATHODE, (B) AFTER FURTHER SUBLIMATION.
ELECTRON TEMPERATURES:
(A) 982°K (B) 1000°K.
THERMOCOUPLE TEMPERATURE 850°K.
ANODE VOLTS
0
1
2
3

FIG.40.

elevated temperature for a fixed period of time, after which the cathode was cooled to obtain the retarding potential point for a plot of anode work function (ϕ_A) against time. The conditions necessary for the successful use of this method have been considered in section 4.4. Most important for the accurate measurement of anode work function changes is constancy of the electron temperature during sublimation measurements. Retarding potential plots taken at different stages of anode contamination were always parallel, and indicated that the electron temperature remained constant to within 5%. Agreement between the electron temperature and the thermocouple temperature was usually better than 15%. Two such retarding potential plots are shown in Fig. 40. These measurements were always made at a cathode temperature of 850°K and with a retarding field current of 3×10^{-11} amps. Unless otherwise stated, all sublimation plots are for the cathode at 1173°K.

7.3. Sublimation curves for cathode activation states II to VII.

Immediately following the decomposition of the carbonate to oxide, sublimation curves such as the one shown in Fig. 41, curve (a), were obtained. The position of the first minimum

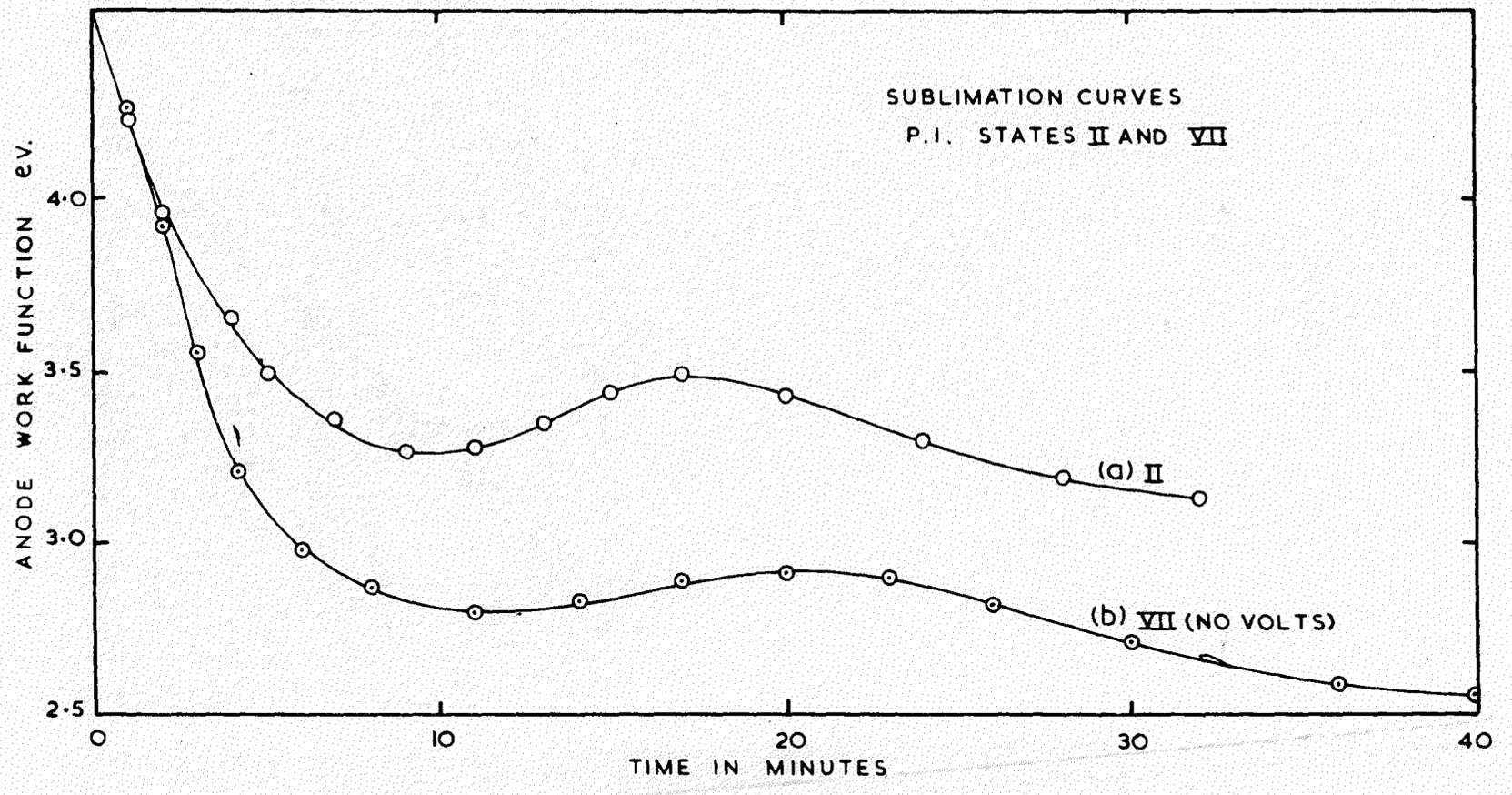
SUBLIMATION CURVES
P.I. STATES II AND VII
ANODE WORK FUNCTION eV.
4·0
3·5
3·0
2·5
0
10
20
30
40
TIME IN MINUTES
(a) II
(b) VII (NO VOLTS)

FIG. 41.

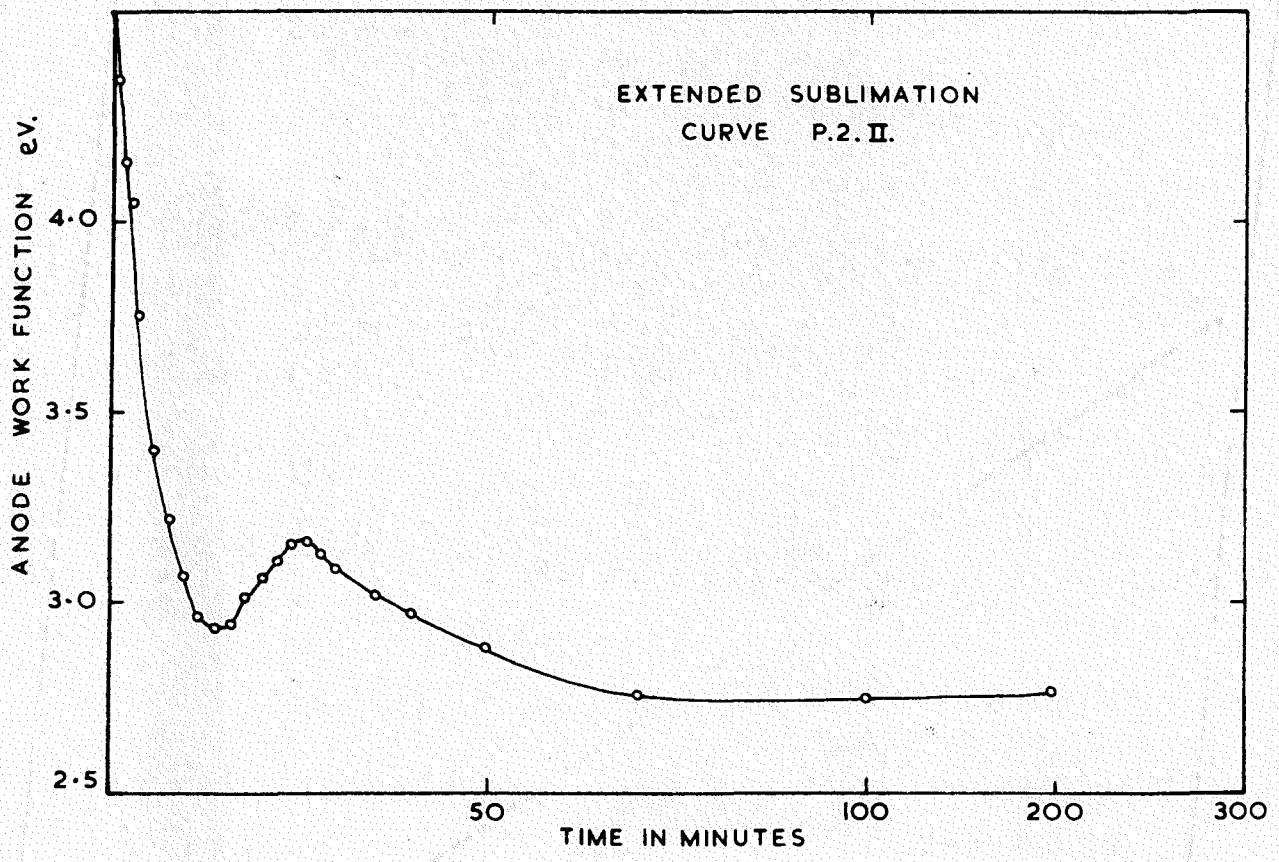
EXTENDED SUBLIMATION
CURVE P.2.II.
ANODE WORK FUNCTION eV.
4·0
3·5
3·0
2·5
50
100
200
300
TIME IN MINUTES

FIG. 42.

on the time axis was found to vary from tube to tube between the limits of 8 and 15 minutes. The ratio of the time to reach the first minimum and the time to reach the peak was always between 0.5 and 0.6 . The position of the first minimum varied between 1.3 eV. and 1.6 eV. on the ϕ_A scale from tube to tube. Fig. 42 shows an extended plot for P.3.II. The height of the peak above the first minimum of the sublimation curves obtained in state II was always a little over 0.2 eV..

After finally activating the anode with 100 volts on the anode (state VII), then removing the anode potential and allowing sublimation to take place as before, curve (b) of Fig. 41 resulted. All such curves were lower than those in the unactivated state by about 0.4 eV., the height of the peak above the first minimum was reduced by a factor of two, and the whole curve appeared to shifted slightly along the time axis. In all these curves, the ratio of the time to reach the first minimum and the time to reach the peak was between 0.5 and 0.6, as in the sublimation curves for state II.

All the points on any one sublimation curves have a constant error which arises from the spread of $\pm$0.075 volts found in fixing the retarding potential point for clean tungsten. The maximum experimental error for points on the sublimation curves is $\pm$0.07 eV. on the ϕ_A axis (see section 6.7), and $\pm$ 5 secs. on

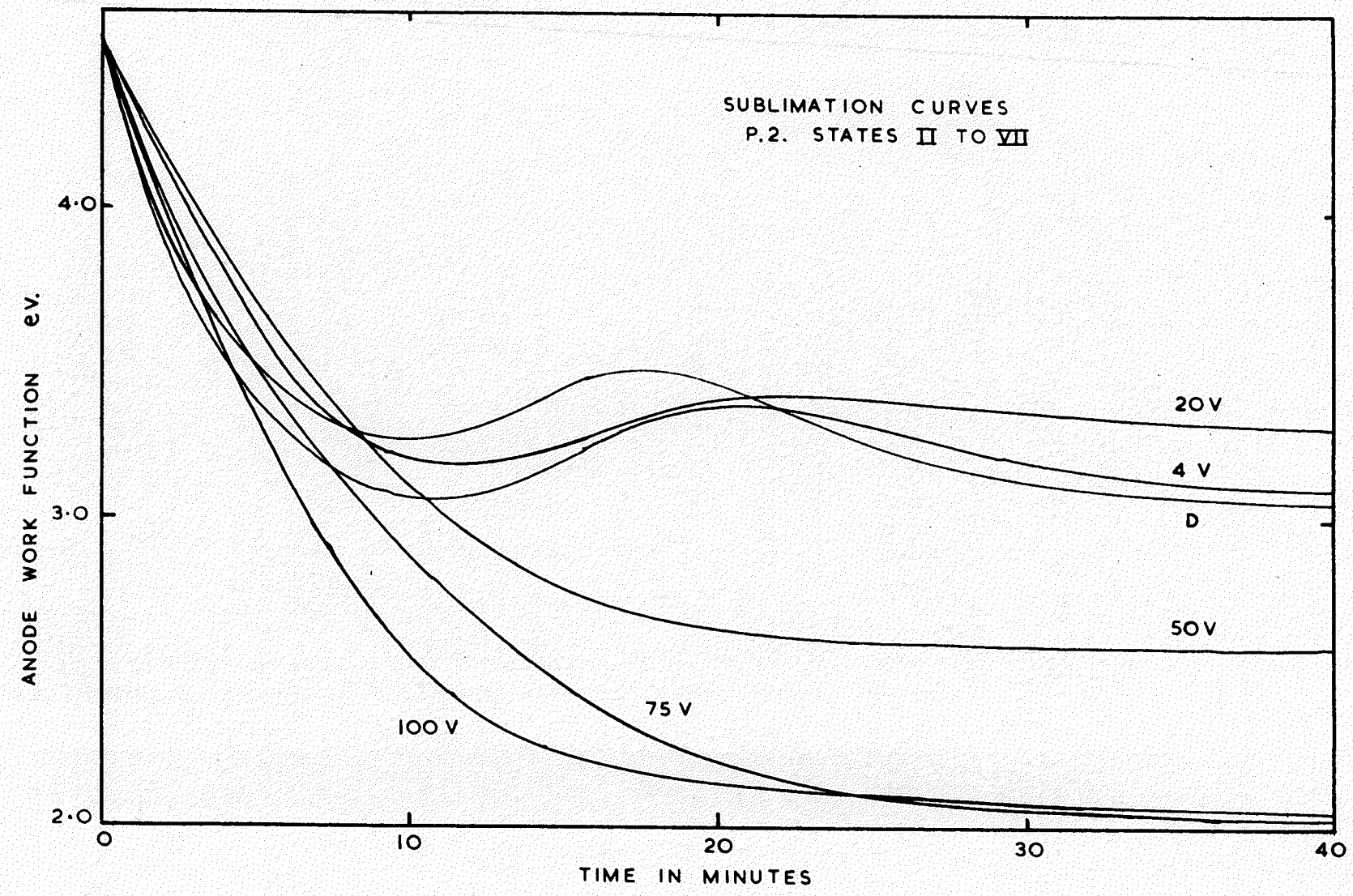
SUBLIMATION CURVES
P.2. STATES II TO VII
ANODE WORK FUNCTION eV.
4·0
3·0
2·0
0
10
20
30
40
TIME IN MINUTES
20 V
4 V
D
50 V
75 V
100 V

FIG. 43.

the time axis. Points on sublimation curves for all the P series of tubes showed virtually no spread. The spread of points shown on the curves of Figs. 41 and 42 is typical.

The shape of the ϕ_A versus time curve has been found to be dependant on the potential applied to the anode during sublimation. Sublimation curves obtained for each activation state with the activating voltage applied to the anode are shown in Fig. 43. No significant difference was found between the sublimation curves obtained with anode potentials from 0 to 20 volts. All such curves were found to be similar to those obtained in the unactivated state (II), and tended to show saturation at about 3.0 eV.. The application of 50 volts to the anode during sublimation removed the peak which occurred at lower voltages, and produced a lower final minimum work function of 2.5 eV.. Anode potentials of 75 and 100 volts lowered the final minimum work function still further: the mean final value for both the 75 volt and 100 volt curves was 2.0 eV. with a spread of $\pm$0.1 eV. The 75 and 100 volt curves for any one tube always had the same final minimum value, and showed saturation after between 35 and 40 minutes in all cases. The initial rate of fall in anode work function during sublimation with 100 volts applied to the anode always exceeded the initial rate of fall of the 75 volt curve.

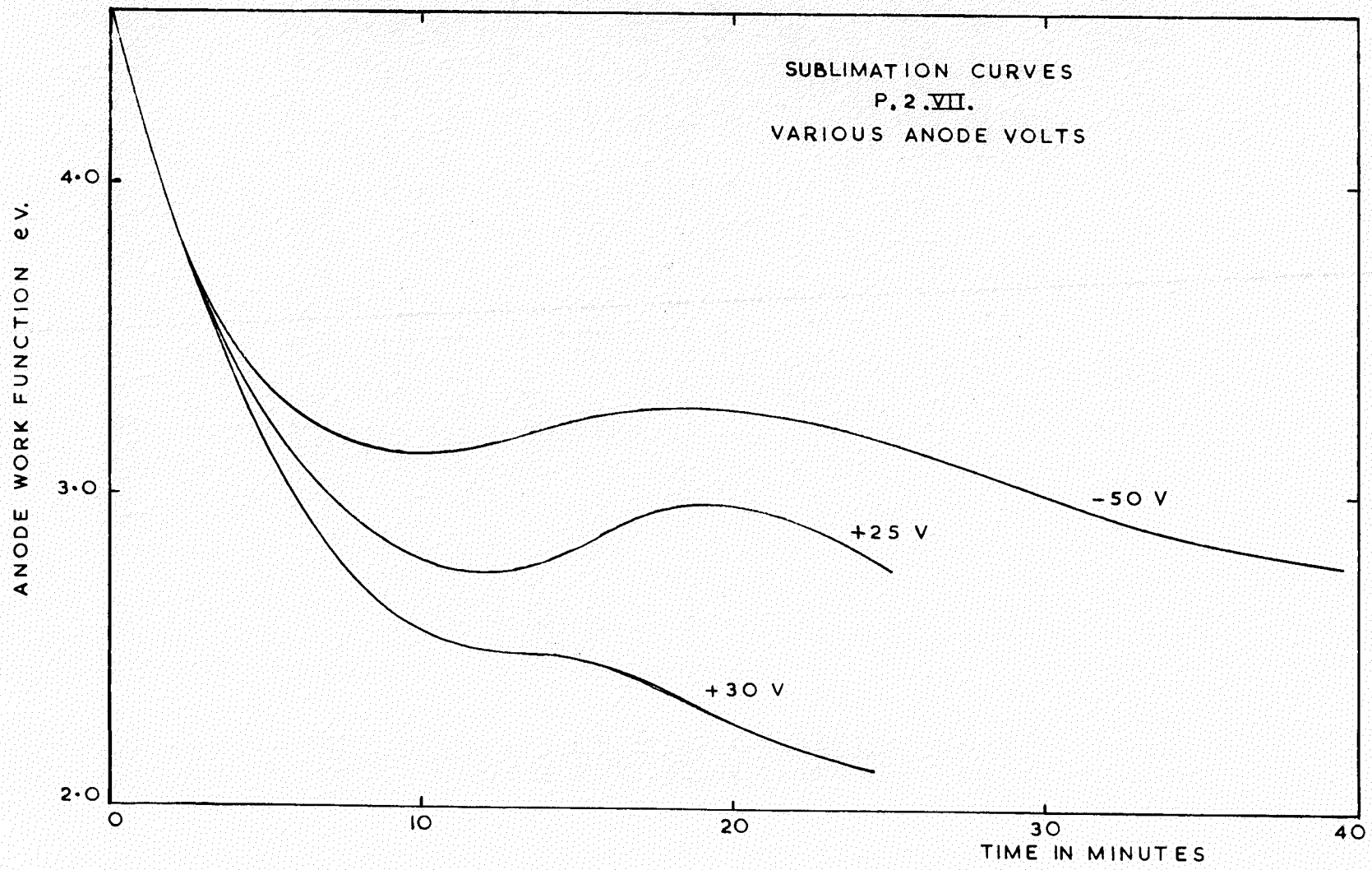
SUBLIMATION CURVES
P. 2. VII.
VARIOUS ANODE VOLTS
ANODE WORK FUNCTION eV.
4·0
3·0
2·0
0
10
20
30
40
TIME IN MINUTES
-50 V
+25 V
+30 V

FIG. 44.

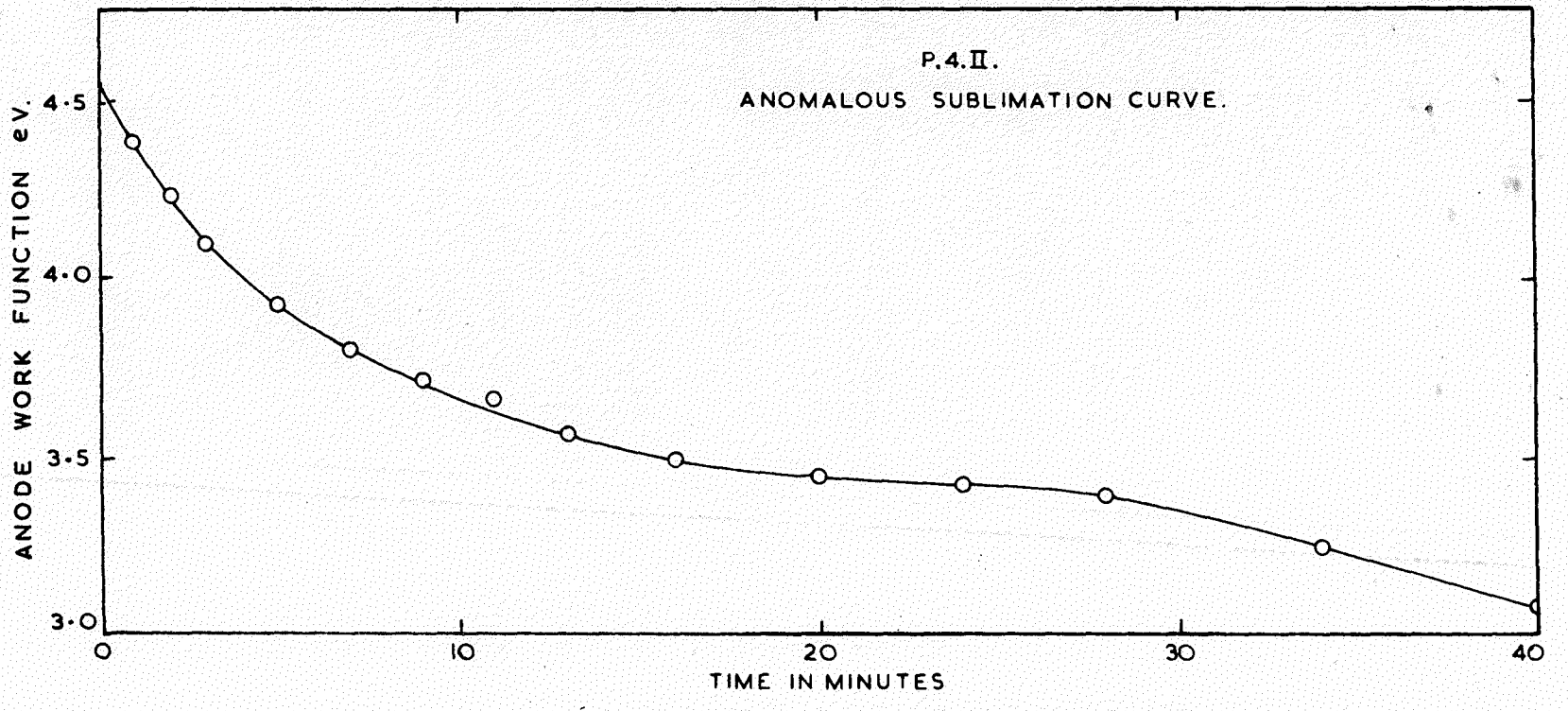
P.4.II.
ANOMALOUS SUBLIMATION CURVE.
ANODE WORK FUNCTION eV.
4·5
4·0
3·5
3·0
0
10
20
30
40
TIME IN MINUTES

FIG . 45.

The peak observed for anode potentials up to +20 volts was investigated in P.2 by taking sublimation data for anode potentials between -100 and +30 volts. Applying negative volts to the anode during sublimation did not remove the peak; only when the anode potential exceeded +30 volts was the peak completely removed (Fig. 44).

7.4. Anomolous sublimation curves.

Two of the tubes, P.4 and P.6, produced anomolous sublimation curves. Fig. 45 shows the anomolous curve obtained in the unactivated state (II); the curves for both tubes were identical, and showed excellent reproducibility. Sublimation curves for P.4 with anode potentials between 0 and 100 volts were not reproducible.

Anomolous curves were always observed with P.4. In the case of P.6 the anomolous behaviour first appeared 24 hours after the cathode had been decomposed, and disappeared after the cathode had been finally activated at 100 volts.

7.5. The anode temperature during activation and sublimation.

By fitting the anode in P.5 with a tungsten/tungsten-

26% rhenium thermocouple it was possible to measure the anode temperature with the cathode at 1173°K and 0, 50, 75, and 100 volts applied to the anode. The results are shown in Table 7.1.

TABLE 7.1.

Anode Volts	0	50	75	100
Anode Temperature (°K)	360	382	396	412

A film was then deposited on the anode by maintaining the cathode at 1173°K for 15 minutes. The change in anode work function was recorded, and then the anode was heated to 360, 382, 396, and 412°K. After each increase in temperature the anode work function was measured in an attempt to detect any change that might occur as a result of raising the anode temperature. No such change could be detected.

7.6. The anode current.

Fully activated cathodes in the P series of tubes showed only a small variation in emission from tube to tube. Table 7.2. gives the anode current I_A for a cathode temperature of 1173°K and an anode potential of 100 volts. The mean value of I_A is 13.2 mA. Typical values of I_A for 4, 20, 50, and 75

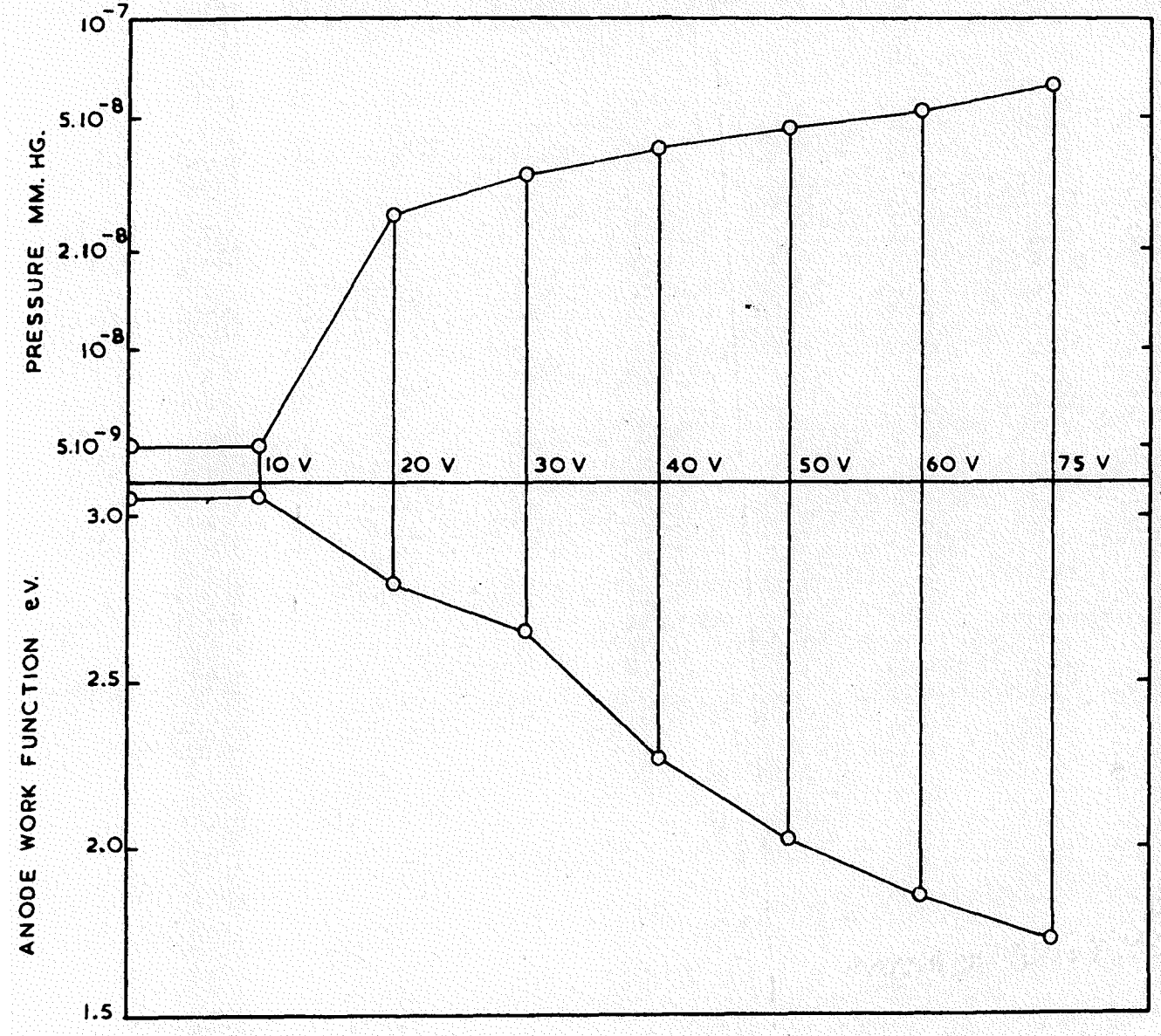
PRESSURE MM. HG.
10⁻⁷
5.10⁻⁸
2.10⁻⁸
10⁻⁸
5.10⁻⁹
10 V
20 V
30 V
40 V
50 V
60 V
75 V
ANODE WORK FUNCTION eV.
3.0
2.5
2.0
1.5

FIG . 46.

volts applied to the anode were 0.17, 3.0, 10.0, and 11.0 mA, respectively.

TABLE 7.2.

Tube	P.1	P.2	P.3	P.4	P.5
I_A mA.	12	12	15	14.5	14

Anode currents monitored during sublimation with a potential applied to the anode were always observed to decrease with time. With 50 volts applied to the anode during sublimation, the anode current normally fell from a value of 10 mA. corresponding to a clean anode, to a final stable value of 6 mA. after a period of 20 minutes; a change of 40%. The corresponding changes with 75 and 100 volts applied to the anode were 25% and 17%, respectively. With 20 volts applied to the anode during sublimation a slight decrease of about 5% was generally detected between the current to a clean anode and the current to an anode on which a film had been deposited.

7.7. Pressure variations during anode film bombardment.

The curve shown in Fig. 46 was obtained by first forming a film on the anode of P.5 by sublimation from the cathode for

15 minutes with the anode potential at 0 volts, resulting in an anode work function of 3.06 eV. With the cathode at 1173°K, positive potentials of 10, 20, 30, 40, 50, and 75 volts were then successively applied to the anode for one minute each. 55 seconds after a potential had been applied to the anode the pressure in the system was recorded, and after a further five seconds the anode potential was removed and the cathode temperature reduced to 850°K to obtain a retarding potential point. The cathode temperature was then restored to 1173°K and the next anode potential applied. Fig. 46 shows the fall in anode work function, and the increase in pressure, produced by applying each of the above anode potentials for one minute.

No change could be detected in either the anode work function or the pressure as a result of applying 10 volts to the anode. Increasing the anode potential above 10 volts did however produce considerable changes in both the anode work function and the pressure, the latter increasing with increasing anode potential, while the former decreased down to a minimum value of 1.7 eV. This value corresponds well with minimum value of the anode work function found when sublimation takes place with 75 or 100 volts applied to an initially clean anode. The increase in pressure produced by applying 75 volts to the anode was 5 times the increase generally observed as the result of applying 75 volts to a clean anode.

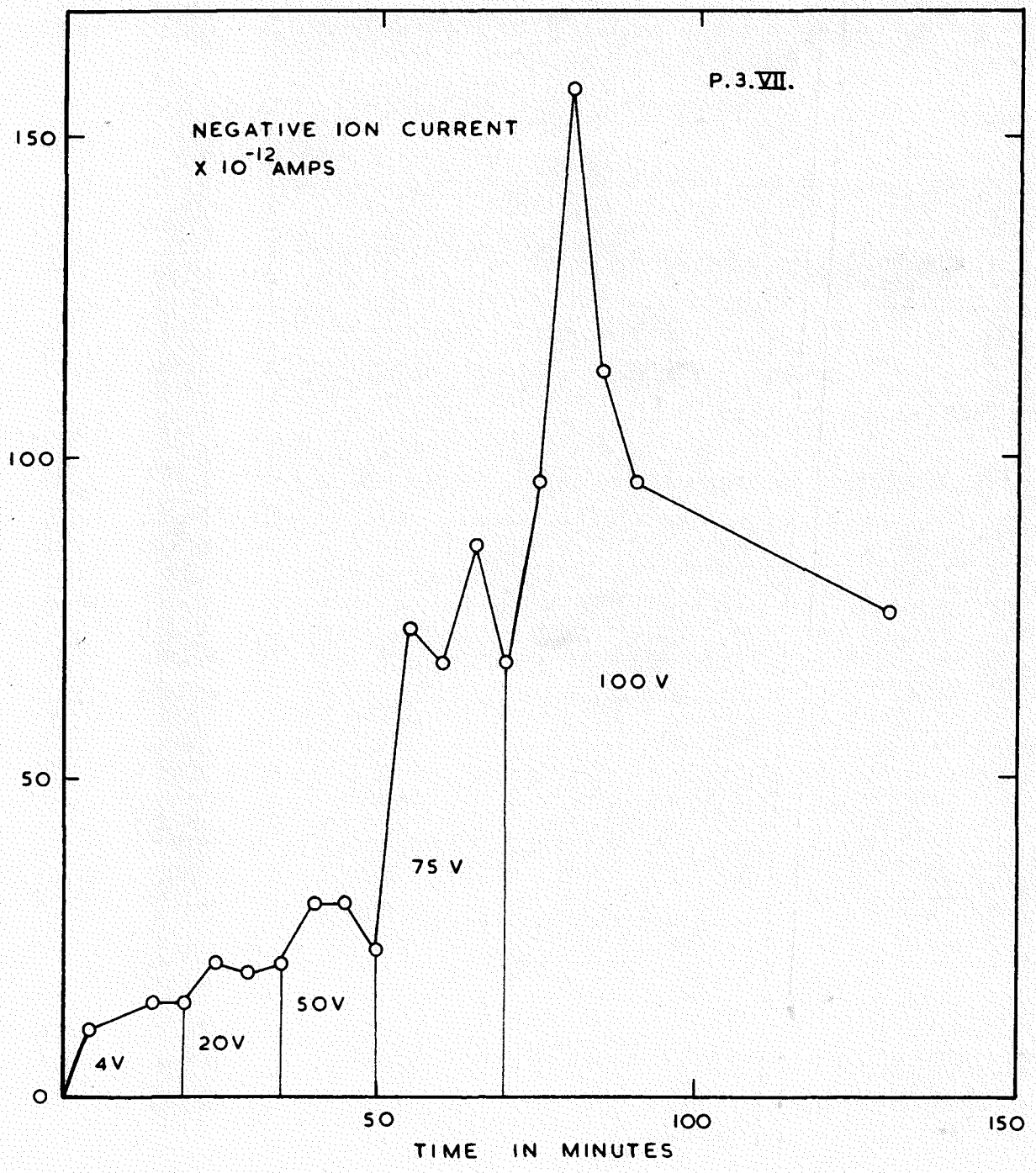
P.3.VII.
NEGATIVE ION CURRENT
X 10^-12 AMPS
150
100
50
0
4V
20V
50V
75 V
100 V
50
100
150
TIME IN MINUTES

FIG. 47.

Immediately the anode potential was removed in these experiments, the pressure returned to its original value.

7.8. Negative ion current.

The anode film resulting from operating the cathode at 1173°K for 12 hours with 100 volts applied to the anode was found to emit negative ions at room temperature. Alternatively negative ion emission could be produced by maintaining the cathode at 1173°K for 12 hours with the anode at zero potential, and then increasing the anode potential to 100 volts for 20 minutes with the cathode still at 1173°K. The first procedure always resulted in a stable negative ion current of 60 X 10^{-12}A. for a cathode potential of 10 volts. The same steady ion current was only reached by the latter method after the anode potential of 100 volts had been applied for 80 minutes.

The results of an experiment to investigate the ion current produced by anode potentials between 0 and 100 volts are shown in Fig. 47. A film was deposited on the anode by maintaining the cathode at 1173°K for 16 hours with zero anode potential. At this stage the negative ion current from the anode was absent. Anode potentials of 4, 20, 50, 75, and

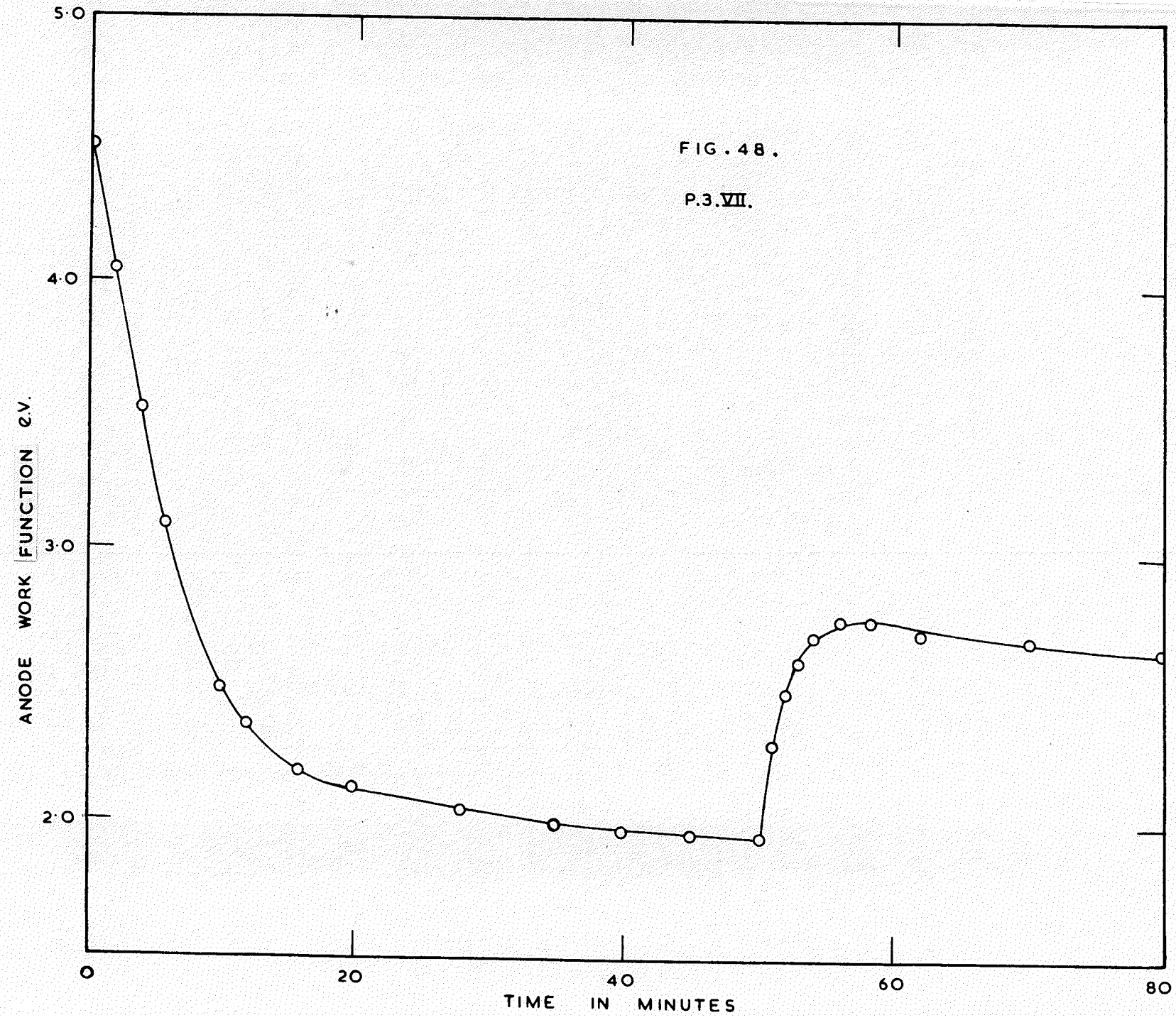

FIG. 48.

P.3.VII.

100 volts were then successively applied with the cathode at 1173°K for a total of 130 minutes. At five minute intervals the cathode temperature was reduced to room temperature and a measurement was made of the negative ion current with +10 volts applied to the cathode. The ion current increased only slowly with increasing anode potentials up to 50 volts. The biggest increments occurred with the application of 75 and 100 volts to the anode. The latter resulted in an initial maximum ion current of 157 X 10^{-12}A., and subsequently tended towards the saturation value of 60 X 10^{-12}A.

Negative ions were also found to be emitted by the cathode when it was at room temperature. In the fully activated state (VII) the negative ion current registered with an anode potential of +10 volts was always between 7 and 8 X 10^{-12}A..

7.9. Effect of varying the anode potential during sublimation.

A reduction of the anode potential from +100 volts to zero during a sublimation run was found to cause the change in work function shown in Fig. 48. The anode potential was removed after 50 minutes. The final shape of the sublimation curve then followed closely that of curve (b) in Fig. 41. The anode work function could be returned to its original value by

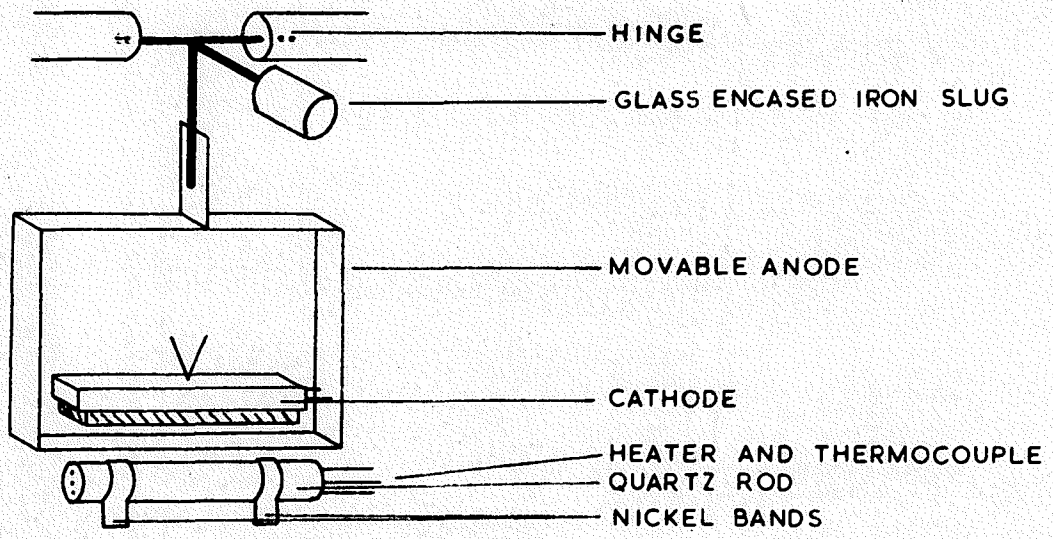

FIG. 49.

SCHEMATIC DIAGRAM OF TUBE P.3.

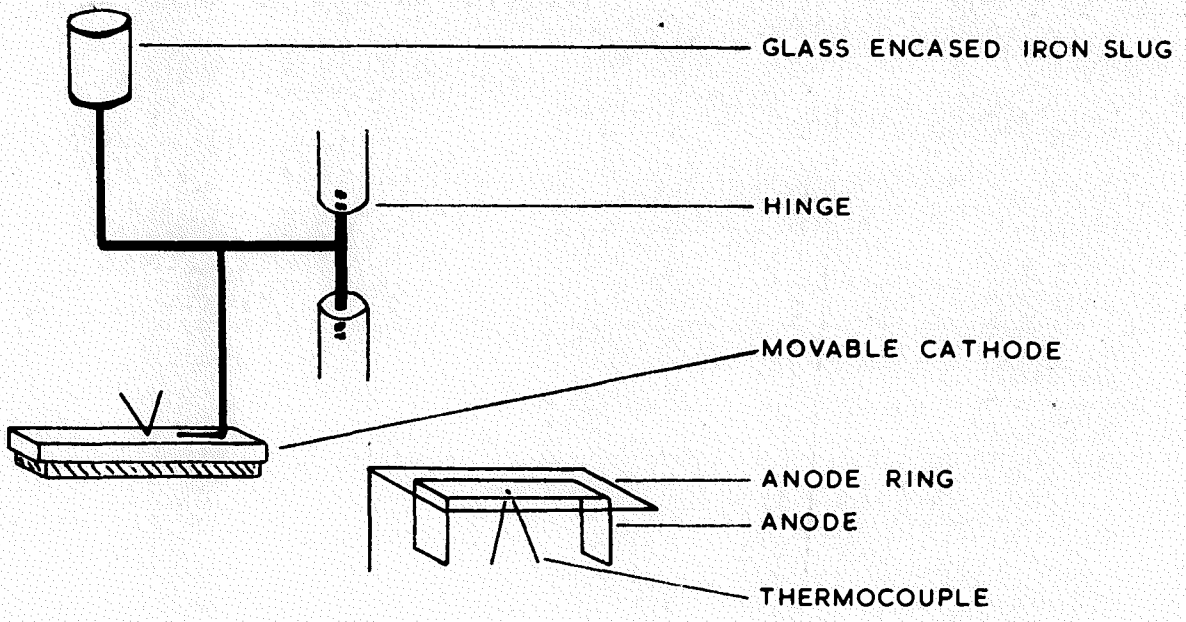

FIG. 50.

SCHEMATIC DIAGRAM OF P.6.

increasing the anode potential to 100 volts for 1 minute. The reverse effect was also found to exist; increasing the anode potential from 0 to 100 volts during a sublimation run with zero anode potential produced a drop in anode work function after 1 minute of 0.8 eV., after which the curve was the normal sublimation curve with 100 volts applied to the anode.

7.10. Conductivity of the anode films.

Arrangements were made in P.3 (Fig. 49) to measure the electrical conductivity of the anode films. A quartz rod 3 mm. diameter and 25 mm. long was fitted with two thin nickel foil supporting bands and positioned in front of the cathode but behind the movable anode. Four 0.5 mm. diameter holes through the rod carried a tungsten heater and a platinum/platinum-10% rhodium thermocouple. After maintaining the quartz at 1000°K for 24 hours the resistance between the nickel bands was greater than 10^{14} ohms. A film was then deposited onto the quartz by maintaining the cathode at 1173°K for 24 hours with zero anode potential. No measurable decrease in the resistance between the nickel bands was observed.

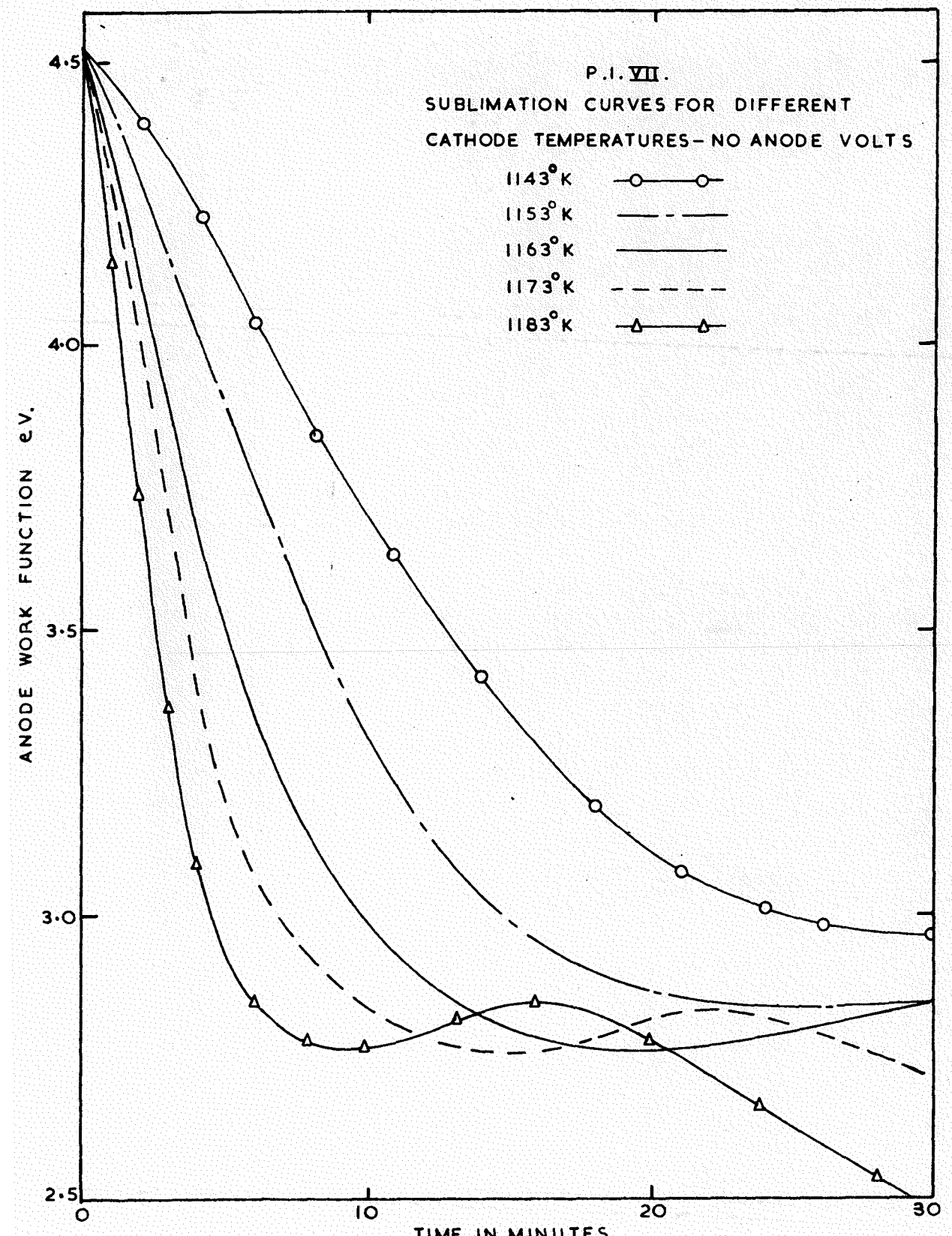
P.I. VII.
SUBLIMATION CURVES FOR DIFFERENT
CATHODE TEMPERATURES – NO ANODE VOLTS
1143°K
1153°K
1163°K
1173°K
1183°K
4·5
4·0
3·5
3·0
2·5
ANODE WORK FUNCTION eV.
0
10
20
30
TIME IN MINUTES

FIG. 51.

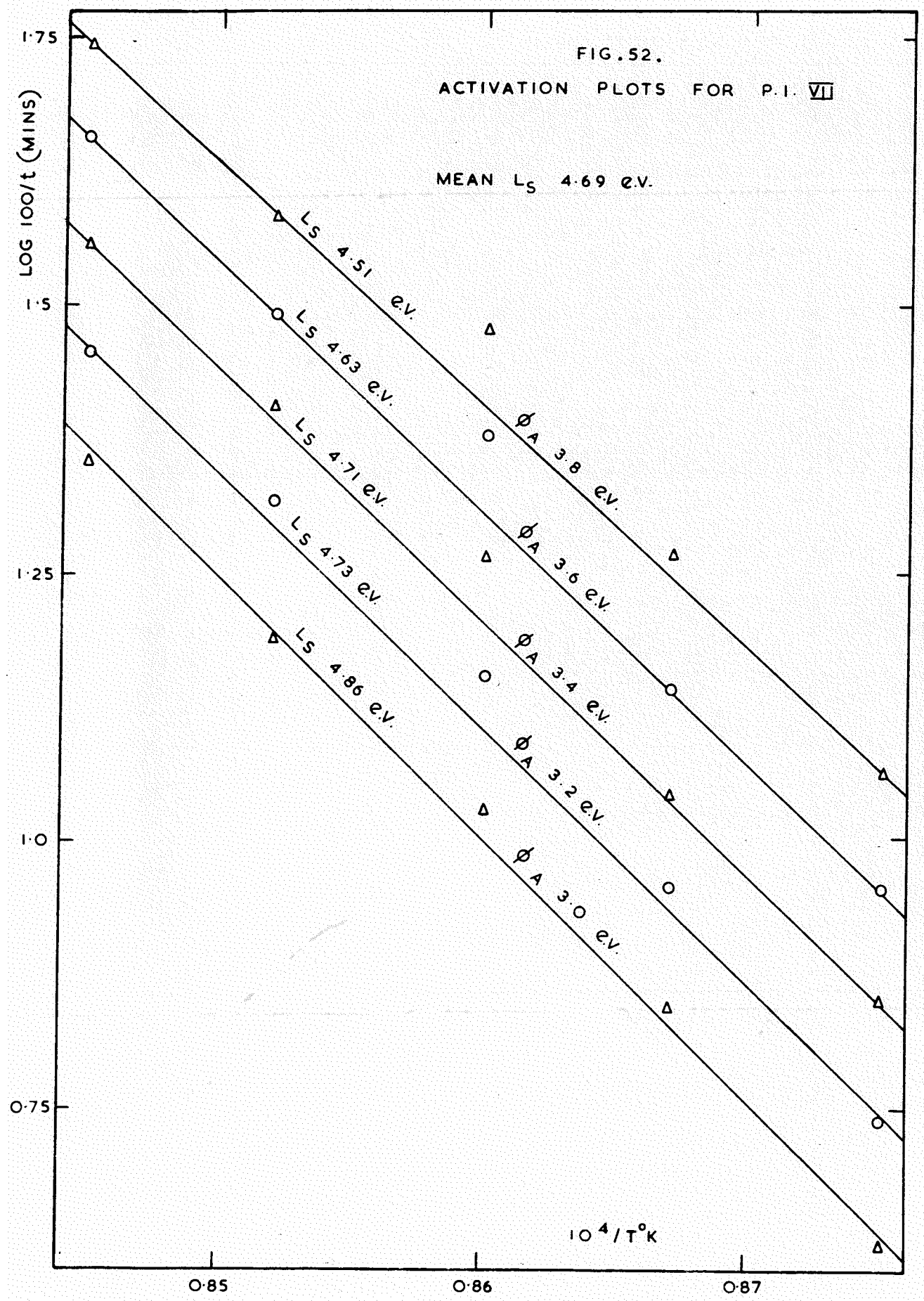
FIG. 52.
ACTIVATION PLOTS FOR P.I. VII
MEAN L_S 4·69 e.V.
LOG 100/t (MINS)
1·75
1·5
1·25
1·0
0·75
$10^4/T°K$
0·85
0·86
0·87
Ls 4·51 e.V.
Ls 4·63 e.V.
Ls 4·71 e.V.
Ls 4·73 e.V.
Ls 4·86 e.V.
ΦA 3·8 e.V.
ΦA 3·6 e.V.
ΦA 3·4 e.V.
ΦA 3·2 e.V.
ΦA 3·0 e.V.

7.11. Activation energy of barium oxide.

When the cathodes of P.1 and P.3 had been fully activated (state VII), sublimation data were prepared for the cathodes at various temperatures (Fig. 51). All the curves were of the same form as those in Fig. 41 (curves a and b), although at the lower temperature the first minimum had not been reached in Fig. 51. The most convenient range of cathode sublimation temperatures was found to be from 1143^{o}K to 1183^{o}K. The corresponding activation energy plots shown in Fig. 52 were obtained from the sublimation curves, using the method described in Chapter III, by measuring the time required at each temperature to reduce the anode work function by a fixed amount in the region before the first minimum. Activation plots were constructed for five different values of the anode work function, 3.8, 3.6, 3.4, 3.2, and 3.0 eV. The mean value for the activation energy was found to be 4.7 $\pm$ 0.2 eV in the case of P.1, and 4.4 $\pm$ 0.2 eV. for P.3.

7.12. Estimation of the monolayer position.

The object of this section is to estimate theoretically the mass of vapour deposited from a plane rectangular source onto a plane parallel receiver. Material subliming at a rate

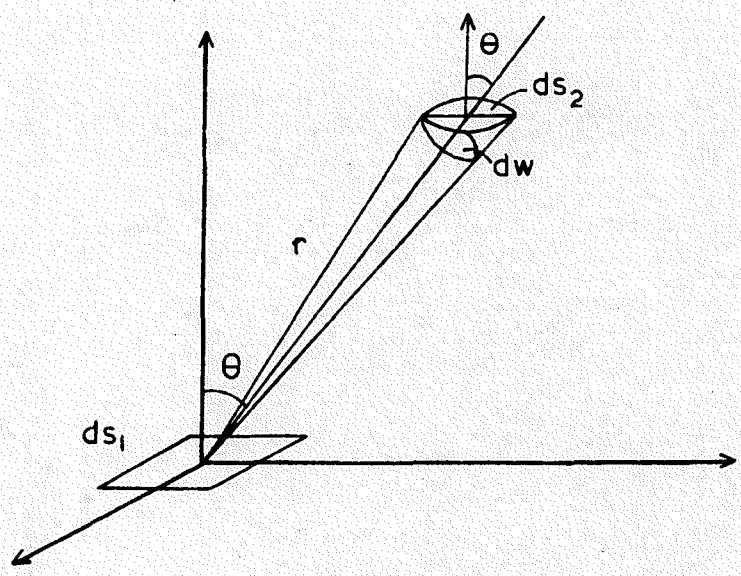

(a)

A IS AREA du dv.

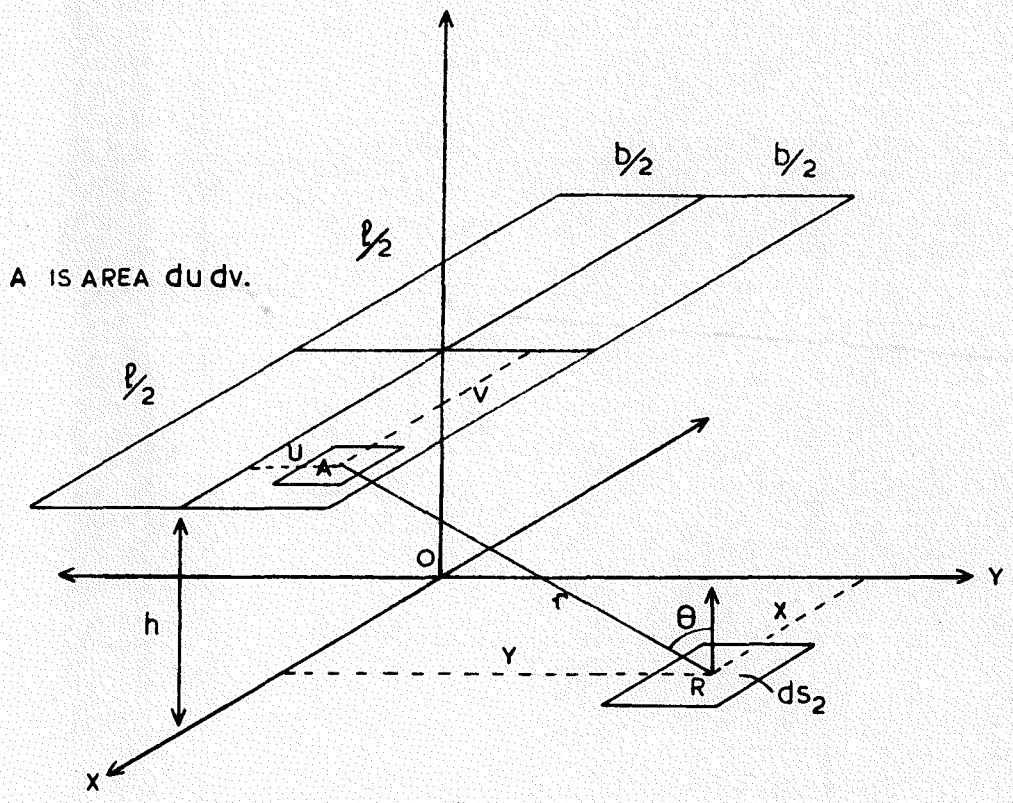

(b)

FIG. 53.

m gms. per second from a plane source area dS_1 will arrive on a plane parallel receiver area dS_2 (Fig. 53a) at the rate

$$dM = m/\pi \cdot \cos\theta \, dw, \qquad (7.1)$$

assuming evaporation takes place according to Knudsen's cosine law (1909).

So that

$$dM = m/\pi \cdot \cos^2\theta/r^2 \cdot dS_2. \qquad (7.2)$$

The mass deposited from an area dudv (Fig. 53b) on to dS_2 is

$$dM = m/lb\pi \cdot dudv \cos^2\theta$$

$$dM = \frac{m}{lb\pi} \frac{h^2 \, dudv}{(h^2 + (x - v)^2 + (y - u)^2)^2} \cdot dS_2.$$

The total mass deposited on dS_2 at a general point R (x,y) on the receiving plane in unit time is

$$M = \frac{mh^2}{lb\pi} \int_{-b/2}^{+b/2} \int_{-l/2}^{+l/2} \frac{du\,dv}{(h^2+(x-v)^2+(y-u)^2)^2} \cdot dS_2.$$

When R is at O, i.e. at x = y = 0,

$$M = \frac{m h^2}{l\, b\, \pi} \int_{-b/2}^{+b/2} \int_{-l/2}^{+l/2} \frac{du\, dv}{(h^2+u^2+v^2)^2} \cdot dS_2.$$

To integrate $\int_{-l/2}^{+l/2} \frac{dv}{(h^2+u^2+v^2)^2}$ put $h^2+u^2 = a^2$

$$\int_0^l \frac{dv}{(a^2+v^2)^2} = \left[\frac{v}{2a^2(a^2+v^2)}\right]_0^l + \frac{1}{2a^2}\int_0^l \frac{dv}{a^2+v^2}$$

$$= \frac{1}{2a^2}\left\{\frac{l}{a^2+l^2} + \left[\frac{1}{a}\tan^{-1}\frac{v}{a}\right]_0^l\right\}$$

$$= \frac{1}{2a^2}\left\{\frac{l}{a^2+l^2} + \frac{1}{a}\tan^{-1} l/a\right\}$$

$$\therefore M = \frac{m h^2}{2 l\, b\, \pi}\left(\int_0^b \frac{l\, du}{(h^2+u^2)(l^2+h^2+u^2)} + \int_0^b \frac{1}{(h^2+u^2)^{3/2}} \tan^{-1}\frac{l}{(h^2+u^2)^{1/2}}\, du\right) dS_2$$

Integration beyond this point has been carried out by a graphical method. It will therefore be convenient at this stage to introduce the values for l, h, and b based on the actual experimental conditions. Let l = 15 mm., h = 3 mm., b = 3 mm..

$$\int_0^3 \frac{15\,du}{(9+u)(234+u^2)} = 0.0034$$

$$\int_0^3 \frac{1}{(9+u^2)^{3/2}} \tan^{-1}\frac{15}{(9+u^2)^{1/2}}\,du = 0.054$$

$$M = \frac{m.9}{90\pi}\,(0.0034 + 0.054).dS_2$$

$$M = m \times 0.0018.\ dS_2.$$

Therefore the mass M gms. per minute arriving at area dS_2 = 0.0018 X m , where m is the total mass subliming per minute from a plane area of 45 mm^2. whose height is 3 mm. above the receiving plane.

It must be noted that no account has been taken in the

fore-going argument of reflection from the receiver surface. In addition, as stated in Chapter III, any calculations of deposited film thicknesses are very dependant on an accurate knowledge of m, and hence the source temperature.

Exact calculation of the number of barium oxide molecules on a tungsten surface which constitute a mono-molecular layer is difficult; at least two possibilities exist. The configuration chosen by Moore and Allison (1950) assumes that the molecules are adsorbed with their line of centres perpendicular to the tungsten surface, each molecule occupying a circle whose radius is equal to 2.75 $\mathring{A}$. (Slater 1939), the lattice spacing for barium oxide. A second configuration is one where the barium oxide molecules are adsorbed with their line of centres perpendicular to the tungsten surface, with the molecules occupying alternate adsorption sites on the tungsten with a spacing of 4.46 $\mathring{A}$. For these two models there will be $3.32 \times 10^{+14}$, and $5.06 \times 10^{+14}$ barium oxide molecules per cm^2. per monolayer, respectively.

The rate of sublimation from barium oxide at $1173^{\circ}K$ is 2.25×10^{-8} gms. per cm^2. per minute (Claasen and Veenemans 1933). For a temperature uncertainty of $\pm 5^{\circ}K$, the error in determining the amount of barium oxide deposited is $\pm 45\%$. Additional errors arise from estimating the area of the source.

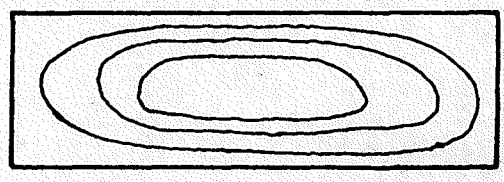

INTERFERENCE PATTERN OBSERVED
ON THE TUNGSTEN ANODES AFTER CATHODE SUBLIMATION

FIG. 54.

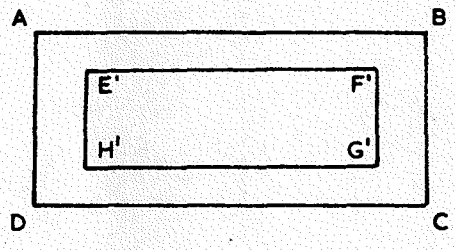

ABCD CATHODE AREA
E'F'G'H' ANODE AREA

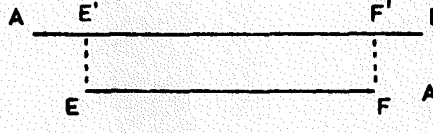

CATHODE AB 15·5 MM.
ANODE EF 12 MM.

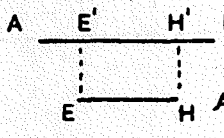

CATHODE AD 3·5 MM.
ANODE EH 2 MM.

FIG. 55.

Using Eq. 7.3 the time required to deposit a monolayer from a source 15 X 3 mm^2. onto a receiver 3 mm. below the source is 47 minutes when a barium oxide spacing of 5.5 Å is assumed, and 71 minutes assuming a spacing of 4.46 Å. This is well beyond the position of the hump in the sublimation curves (Fig. 41).

One tube, P.6 , was constructed with an anode-cathode spacing of 2 mm., and further, the anode area was made less than that of the cathode. Fig. 55 is a schematic of the anode and cathode arrangement in P.6. In this tube it seemed reasonable to assume that the mass of material arriving on the anode in unit time was equal to the mass subliming from an equivalent area E'F'G'H' on the cathode in unit time. However, not all the material subliming from those regions of the cathode near the edge of the anode area E'F'G'H' would arrive at the anode, but these losses were thought to be compensated by material arriving at the anode from that part of the cathode between E'F'G'H' and the edge ABCD of the cathode.

Again, using the data of Olaasens and Veeneman(1933), and assuming the barium oxide molecules to occupy only alternate sites on the tungsten, the calculated time for the formation of a monolayer is 58 minutes. Calculations based on the hypothesis that each barium oxide molecule occupies a circle

whose radius is 2.75 Å. indicate that the monolayer is formed after 3.8 minutes. Both these times are before the position of the first minimum on the time axis of the sublimation plots (see Fig. 41).

Films formed on the anode during sublimation from the cathode with the anode at zero potential were always transparent in vacuum, turning white on exposure to air. After sublimation from the cathode for a considerable period of time, Newtons rings by reflection could be seen in the anode film. The approximate spacing of these rings is shown in Fig. 54. Thick films formed on the anode after sublimation from the cathode with 100 volts applied to the anode still showed interference patterns, but had a darker appearance than those films obtained with zero anode potential.

CHAPTER VIII

Results (ii)

8.1. Introduction.

This chapter will be concerned only with results obtained from the last in the P series of tubes, P.6. This tube was constructed: (a) to measure the binding energy of the anode films, and (b) to differentiate between the effect of electron bombardment and the effect of the applied field in producing a low work function when sublimation from the cathode takes place with an applied anode potential of 100 volts. A schematic diagram of the electrode structure in P.6 is shown in Fig. 50. The cathode was hinged, and could be removed from the proximity of the anode. A tungsten strip 2 X 12 mm^2. and fitted with a tungsten/tungsten-26% rhenium thermocouple, formed the anode. A ring (in fact a rectangle 4 X 14 mm^2.) of 0.05 cm. diameter tantalum wire surrounded the anode. Electrical connection was made to the ring via a seperate terminal so that it was insulated from both the anode and cathode. The ring was easily outgassed by electron bombardment from the anode.

FIG . 56.

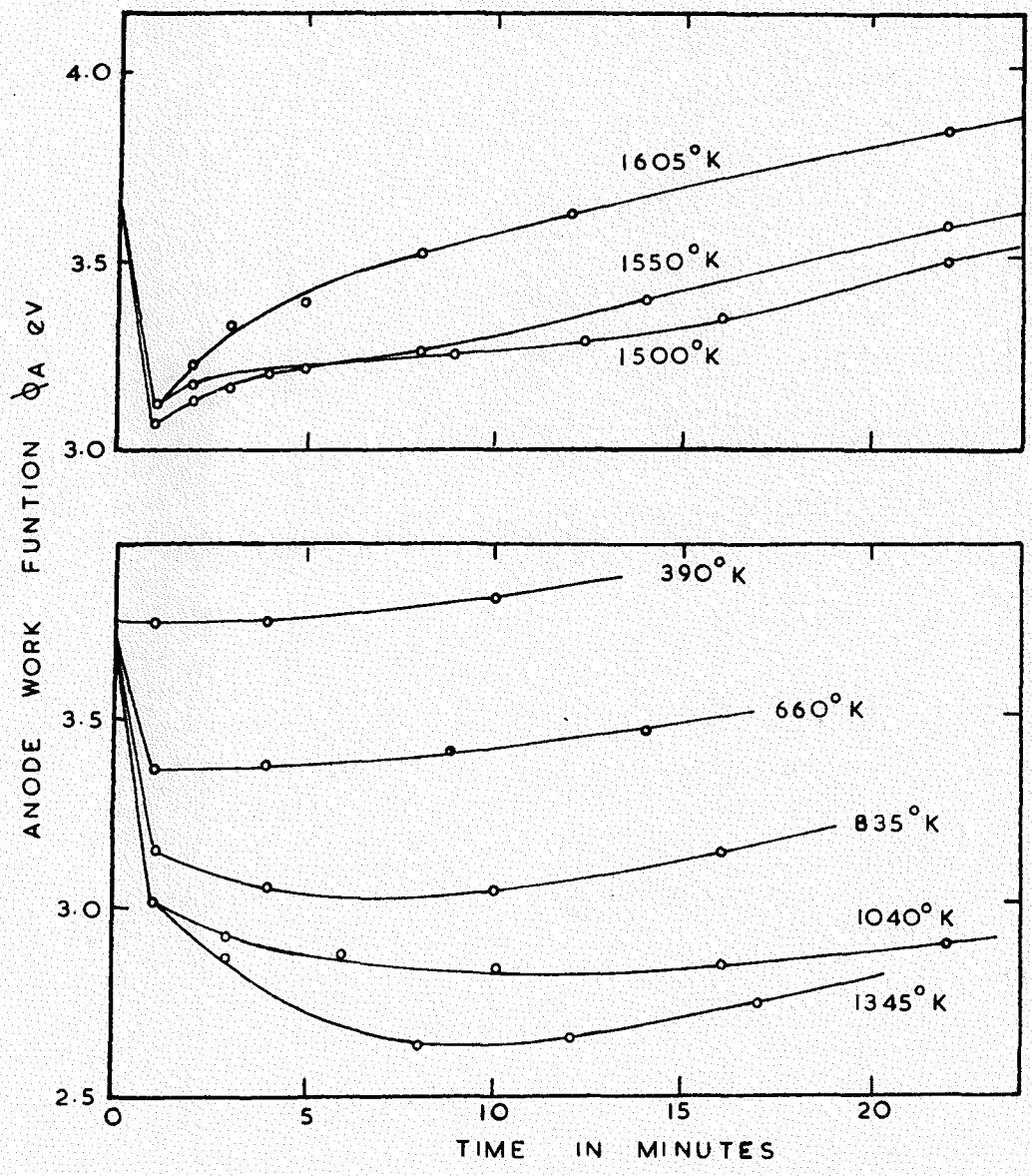
4.0
3.5
3.0
1605°K
1550°K
1500°K
ANODE WORK FUNTION φA eV
390°K
660°K
835°K
1040°K
1345°K
3.5
3.0
2.5
0
5
10
15
20
TIME IN MINUTES

8.2. Anode binding energies.

The first experiments carried out with P.6 were to observe the desorption of the anode films. This was done by the initial deposition of a film on the anode, followed by a raising of the anode temperature to re-evaporate the film. Retarding potential points taken during the re-evaporation enabled the work function of the anode to be plotted as a function of time as it returned to the value for clean tungsten. These experiments were carried out on films of two different thicknesses:

(i) Thin films.

Thin films were deposited on the anode by maintaining the cathode at 1173°K long enough to reduce the anode work function to 3.74 ± 0.04 eV. The anode was then raised to the temperature to be investigated. To make the retarding potential measurements it was necessary to return the anode to room temperature. When one such run had been made and the anode work function had returned to that of clean tungsten, the anode was further cleaned by raising it to a temperature in the region 2800°K for about 15 seconds. The whole process was then repeated for another anode re-evaporating temperature. Fig. 56 shows the results for anode temperature in the range

FIG. 57.

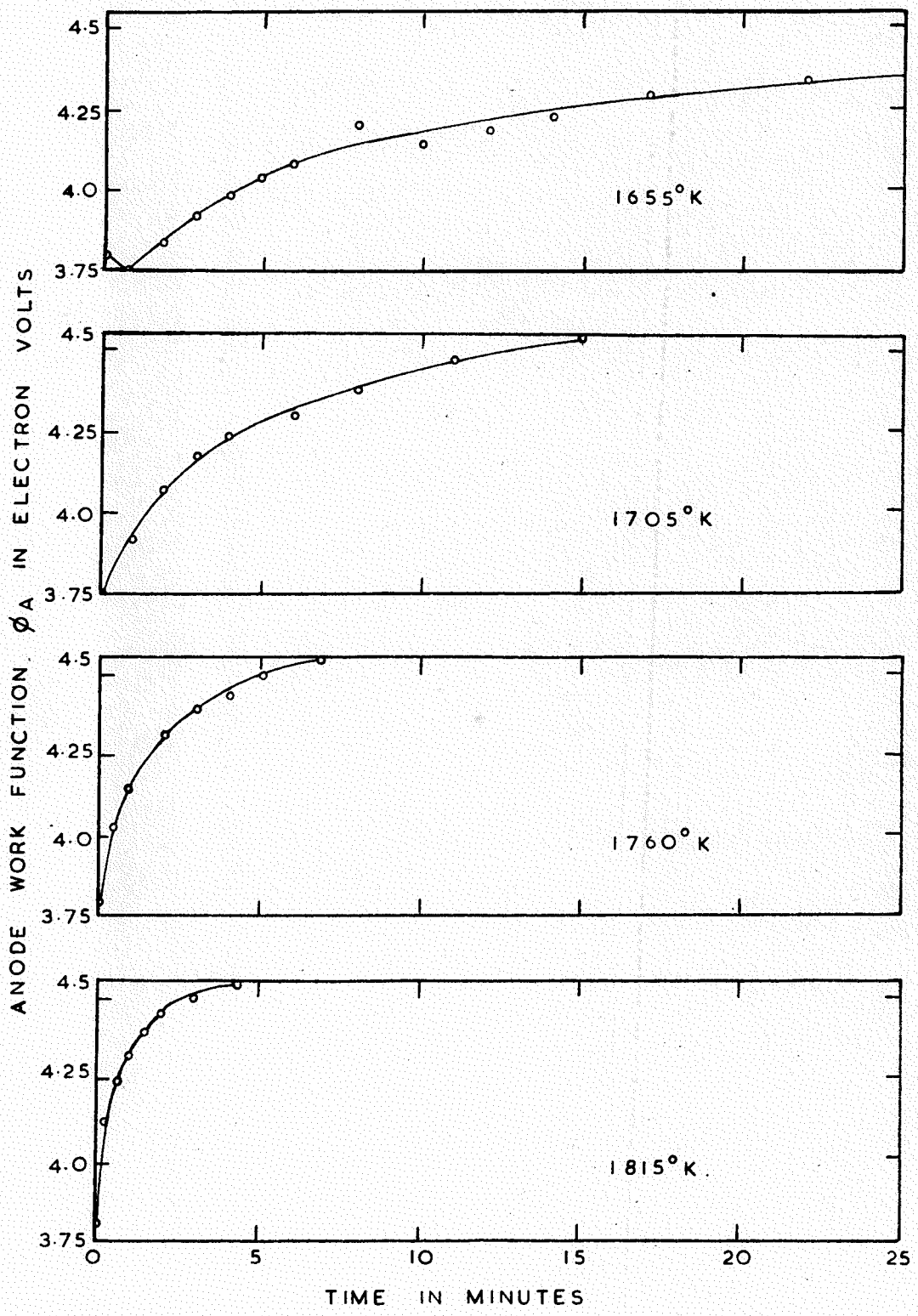
4·5
4·25
4·0
3·75
1655°K
1705°K
1760°K
1815°K.
ANODE WORK FUNCTION ϕ_A IN ELECTRON VOLTS
0
5
10
15
20
25
TIME IN MINUTES

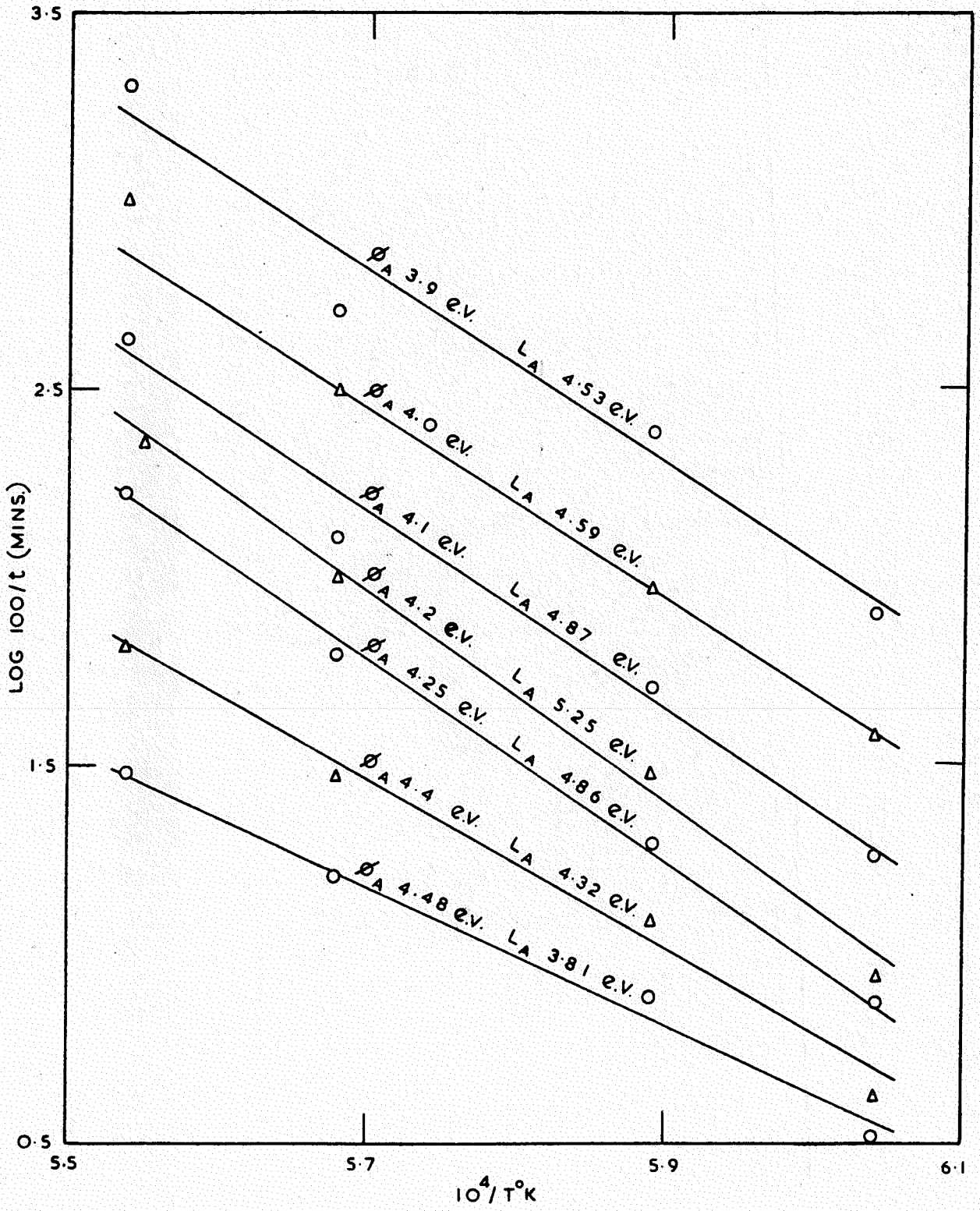
3·5
2·5
1·5
0·5
LOG 100/t (MINS.)
5·5
5·7
5·9
6·1
10⁴/T°K
ØA 3·9 e.V. LA 4·53 e.V.
ØA 4·0 e.V. LA 4·59 e.V.
ØA 4·1 e.V. LA 4·87 e.V.
ØA 4·2 e.V. LA 5·25 e.V.
ØA 4·25 e.V. LA 4·86 e.V.
ØA 4·4 e.V. LA 4·32 e.V.
ØA 4·48 e.V. LA 3·81 e.V.

FIG. 58.

390°K to 1605°K. Heating the anode with a condensed film to temperatures between 660°K and 1605°K for one minute always gave rise to a sharp fall in the anode work function. This fall appeared to be greatest for temperatures between 1000°K and 1500°K. No change was observed when the anode was raised to 390°K. A further fall in anode work function after heating for more than one minute was only recorded for anode temperatures 835°K, 1040°K, and 1345°K. The three highest temperature curves shown in Fig. 56, 1500°K, 1550°K, and 1605°K start to rise rapidly after one minute, at the rates 0.45, 0.68, and 1.03 eV. per minute, respectively. However, after 17 minutes, all three curves have a gradient of approximately 0.31 eV. per minute.

Fig. 57 shows the results obtained in these same experiments with anode temperatures in the range 1655°K to 1815°K. Except for an anode temperature of 1655°K, the curves do not show the initial fall in work function which was found at lower temperatures, but proceed, at rates depending on the anode temperature, to the work function of clean tungsten, 4.56 eV. From the curves in Fig. 57 it was possible to calculate the energy of adsorption L_A for the material re-evaporated from the tungsten using the method described in Chapter III. Data for log(1/t) against (1/T) curves were

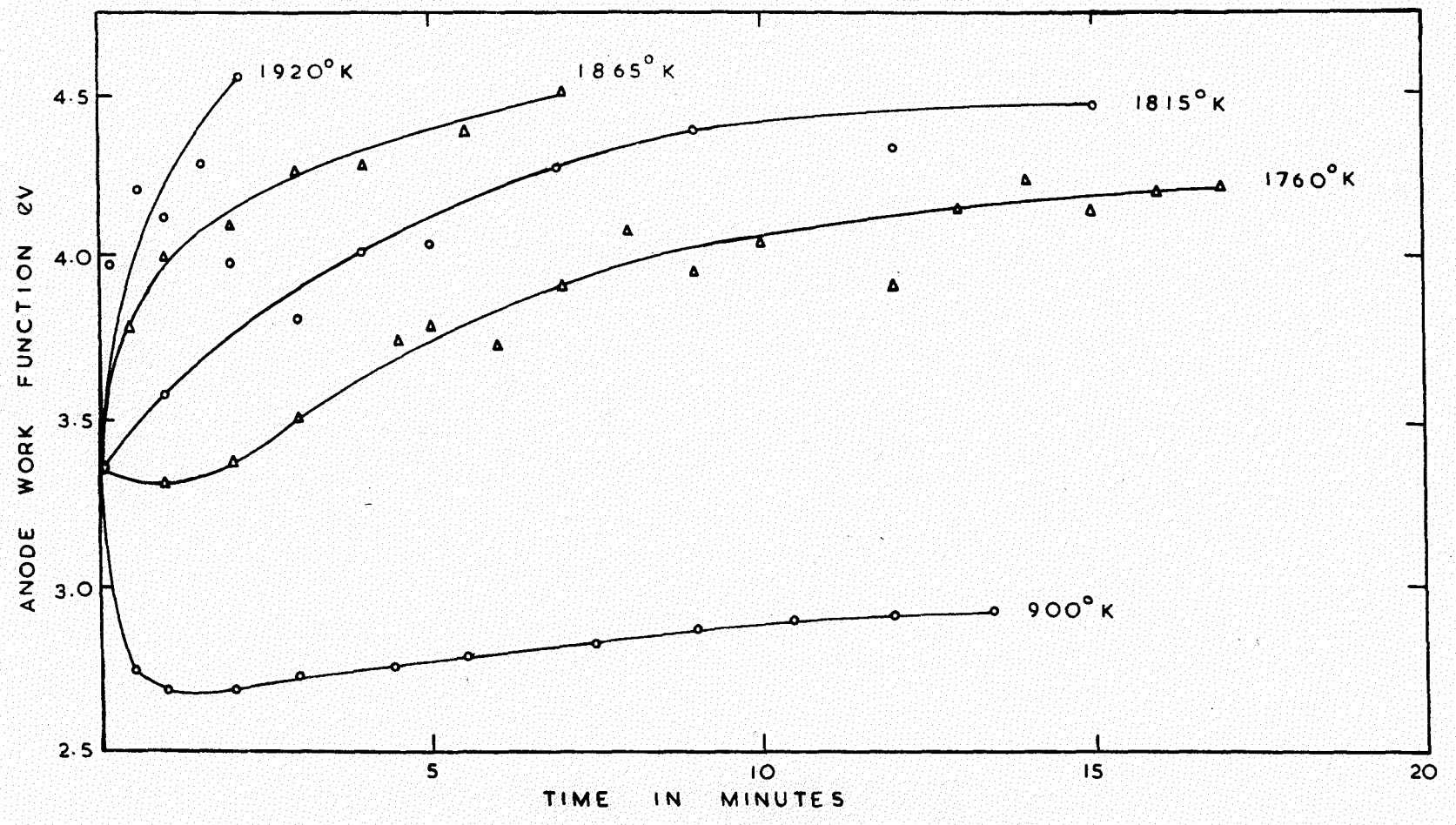
1920°K
1865°K
1815°K
1760°K
900°K
4·5
4·0
3·5
3·0
2·5
5
10
15
20
ANODE WORK FUNCTION eV
TIME IN MINUTES

FIG. 59.

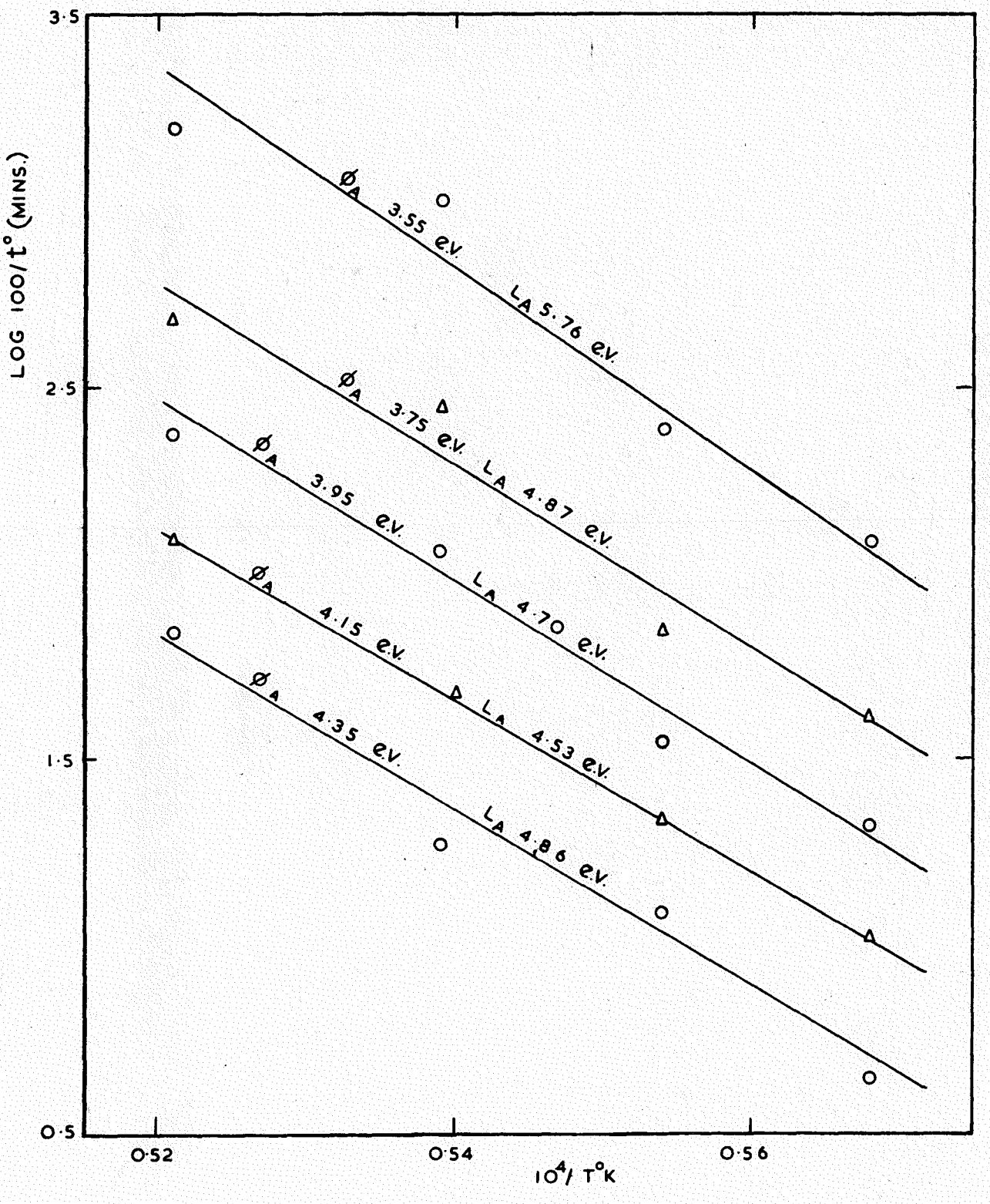
3·5
2·5
1·5
0·5
LOG 100/t° (MINS.)
0·52
0·54
0·56
10⁴/ T°K
φA 3·55 e.V.
LA 5·76 e.V.
φA 3·75 e.V.
LA 4·87 e.V.
φA 3·95 e.V.
LA 4·70 e.V.
φA 4·15 e.V.
LA 4·53 e.V.
φA 4·35 e.V.
LA 4·86 e.V.

FIG. 60.

prepared for different surface coverages (different anode work functions) and the results are plotted in Fig. 58. The gradients of the curves in Fig. 58, and hence the energies of adsorption, were calculated by the method of least squares. The average energy of adsorption is 4.6 eV.

(ii) Thick films.

The experiment described above was repeated for anode films deposited by maintaining the cathode at 1173^{o}K for 30 minutes. The anode work function resulting from the deposition of such a film was 3.35 $\pm$ 0.04 eV. Fig. 59 shows the changes in anode work function which resulted from heating the anode to temperatures in the range 900^{o}K to 1920^{o}K. The general pattern of the curves is similar to those in Figs. 56 and 57. The only obvious difference is the greater scatter of points on the plots for the four highest temperatures. Adsorption energies were again computed for different anode coverages. Fig. 60 shows the plots of log(1/t) as function of (1/T). Again the adsorption energies were calculated by the method of least squares. The average energy of adsorption for these thick films is 5.1 eV.

It was unfortunate that these measurements were made on a cathode in a state (II) which was subsequently found to be anomolous. However state (VII) of this same cathode was

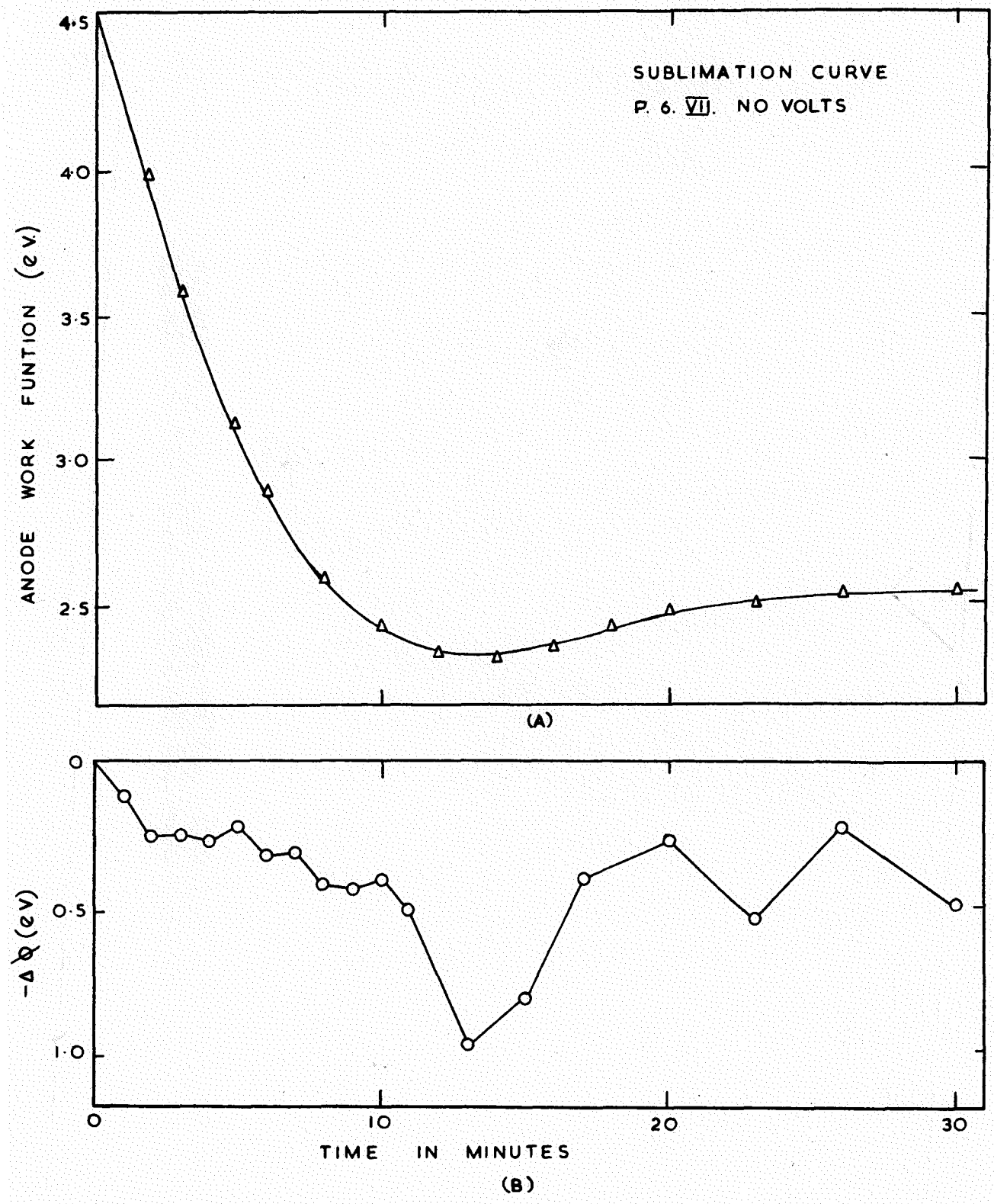
SUBLIMATION CURVE
P. 6. VII. NO VOLTS
ANODE WORK FUNTION (eV)
4·5
4·0
3·5
3·0
2·5
(A)
-Δφ (eV)
0
0·5
1·0
0
10
20
30
TIME IN MINUTES
(B)

FIG. 61.

normal and measurements indicated almost identical changes in anode work function with temperature.

In a further experiment with the cathode in state (VII), a film was formed on the anode by maintaining the cathode at 1173°K for one minute with no volts applied to the anode as in previous experiments. A measurement was then made of the change in anode work function produced by maintaining the anode at 1040°K for one minute. The anode was then cleaned and the process was repeated for cathode deposition times from 2 to 30 minutes. Fig. 61(B) shows the results of this experiment; the change of anode work function ϕ during one minute at 1040°K is plotted as a function of the cathode sublimation time. A sublimation curve obtained immediately after the experiment is shown in Fig. 61(A). The change in anode work function produced by raising the anode temperature appeared to increase with increasing deposition time up to about 13 minutes, resulting in an anode work function of about 1.4 eV.

An attempt was next made to investigate the adsorption energies of films sublimed from the cathode at 1173°K, and with an applied anode potential of 100 volts. Fig. 62 shows the sublimation curve obtained under these conditions. Films were deposited onto the anode down to the point Y in

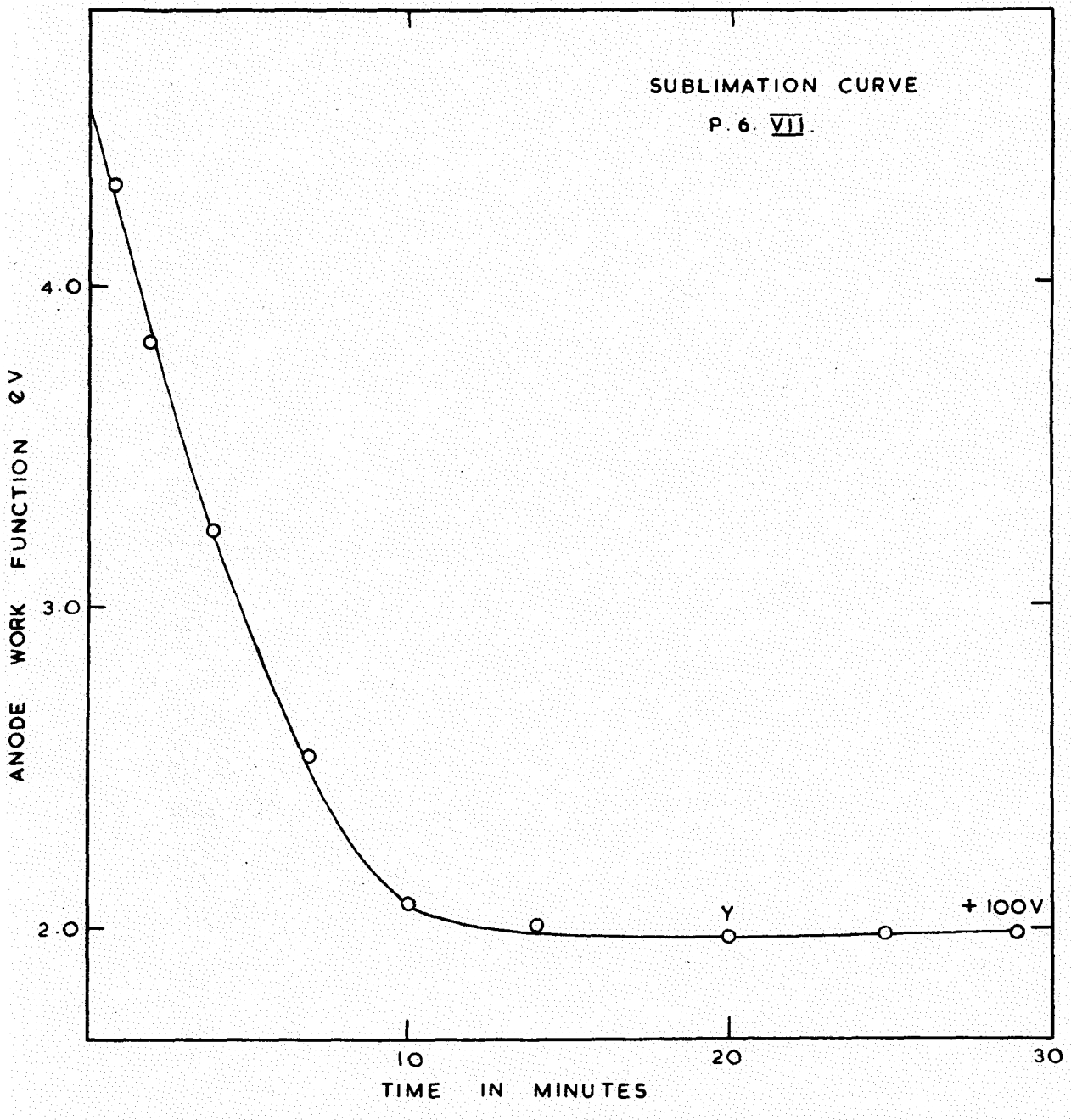
SUBLIMATION CURVE
P. 6. VII.
ANODE WORK FUNCTION ϕ V
4.0
3.0
2.0
Y
+ 100V
10
20
30
TIME IN MINUTES

FIG. 62.

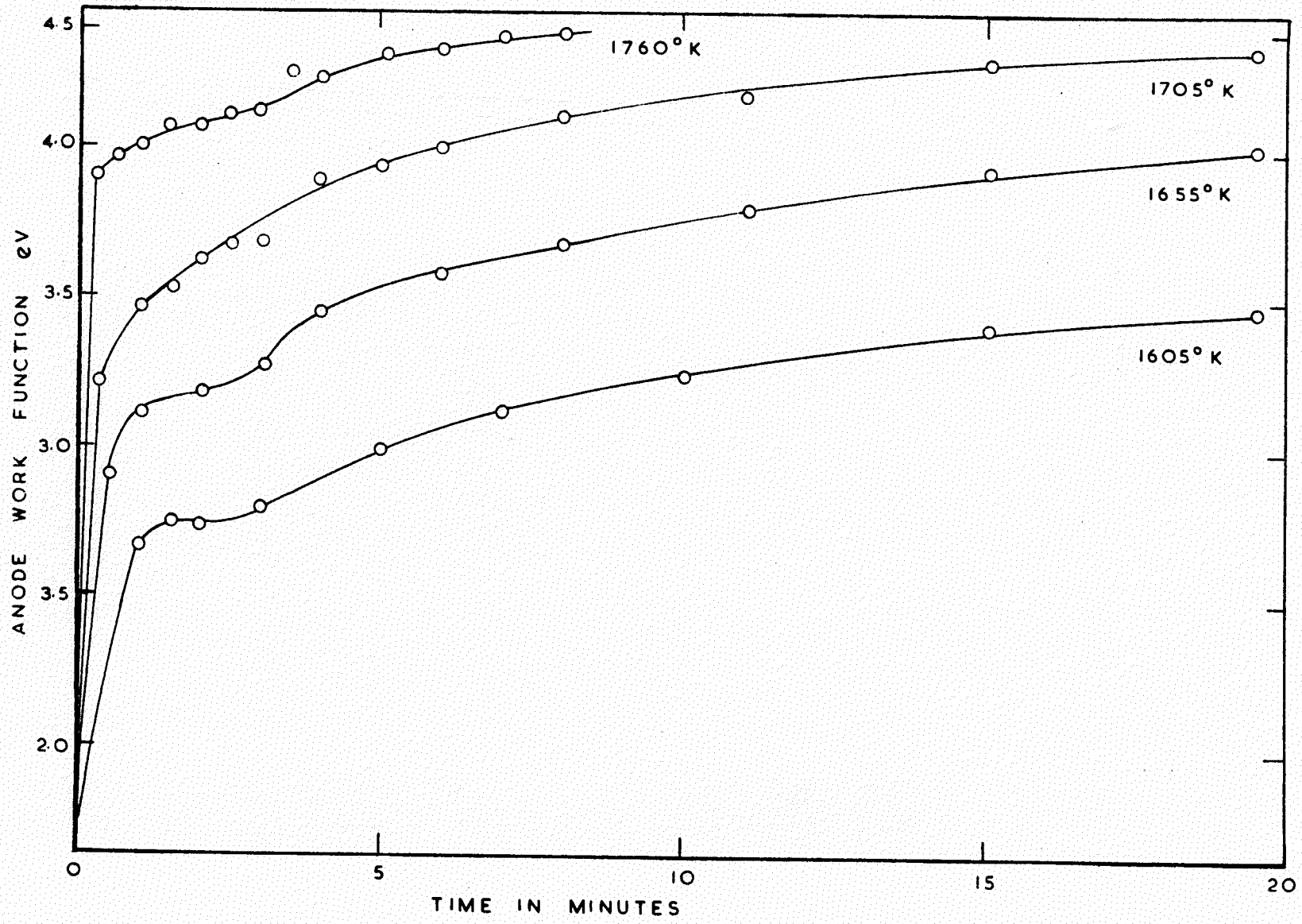
4.5
4.0
3.5
3.0
3.5
2.0
ANODE WORK FUNCTION eV
1760° K
1705° K
1655° K
1605° K
0
5
10
15
20
TIME IN MINUTES

FIG. 63.

Fig. 62, after which the anode temperature was raised and the subsequent change in work function was measured by the technique described previously. The results for four different anode temperatures are shown in Fig. 63. Only the initial part of these curves shows any definite temperature dependence. For anode work functions of 2.5 eV. the calculated adsorption energy L_A is 3.0 ± 0.3 eV. The shape of the curves for higher values of the anode work function does not allow a calculation of the adsorption energy. After five minutes the increase in anode work function appears to be independent of temperature.

8.3. The 100 volt effect.

Sublimation data obtained with the cathode at 1173^{o}K and the electrodes of P.6 at various potentials are shown in Fig. 64. Fig. 65 shows what is thought to be the corresponding electric field configurations for these different electrode potentials. The fields produced at the anode for curve C in Fig. 64 was thought to correspond to the case of a high field applied to the anode with respect to the cathode, but without electron bombardment from the cathode. This produced the same effect as maintaining all the electrodes at the same

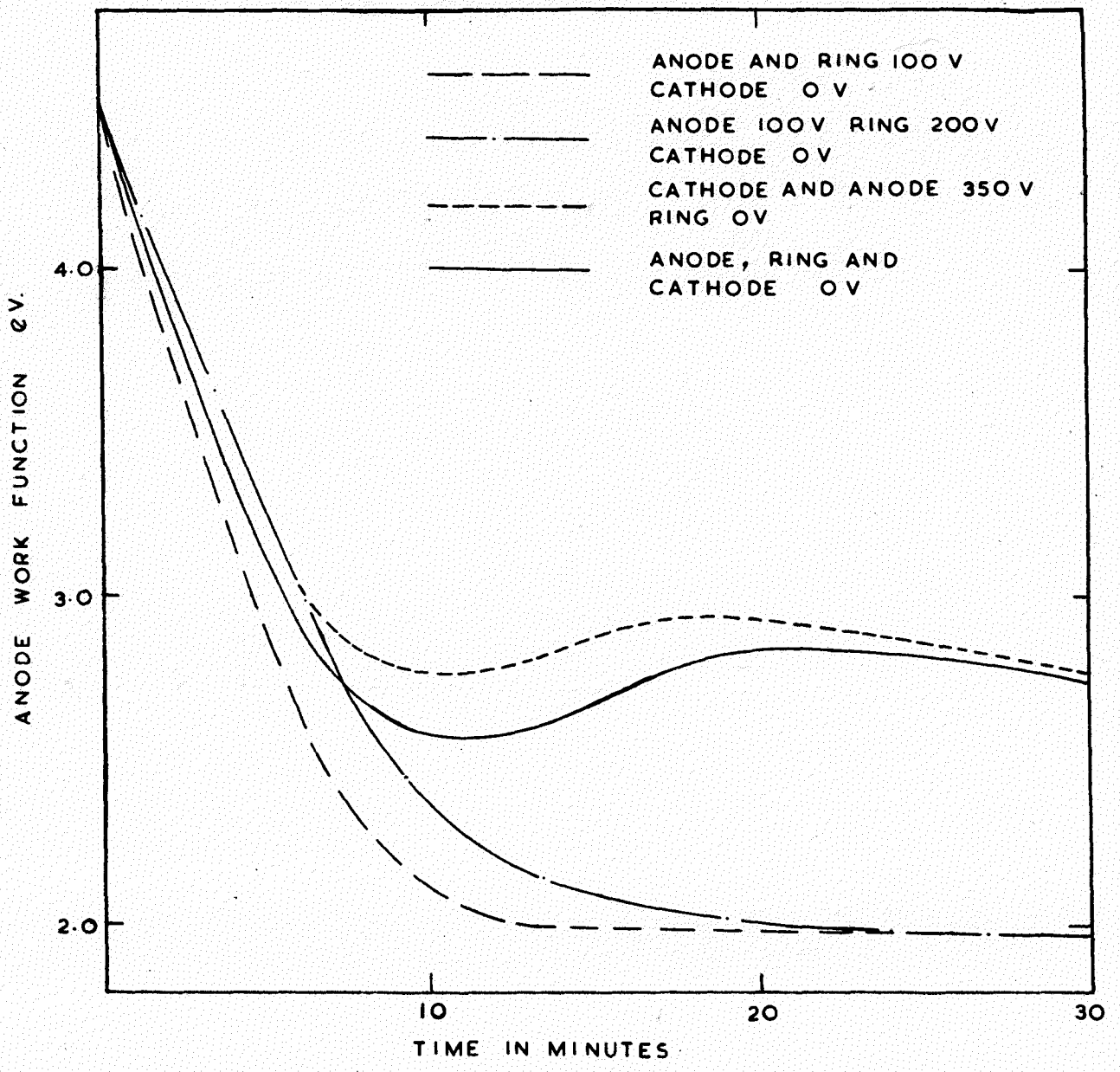
ANODE AND RING 100 V
CATHODE 0 V
ANODE 100V RING 200V
CATHODE 0 V
CATHODE AND ANODE 350 V
RING 0V
ANODE, RING AND
CATHODE 0 V
ANODE WORK FUNCTION eV.
4·0
3·0
2·0
10
20
30
TIME IN MINUTES

FIG. 64.

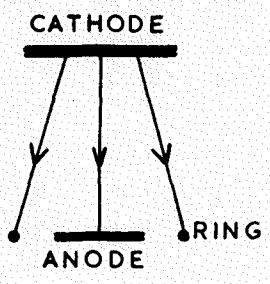

ANODE & RING 100 VOLTS
CATHODE 0 VOLTS

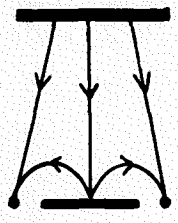

ANODE 100 VOLTS
RING 200 VOLTS
CATHODE 0 VOLTS

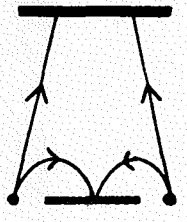

ANODE & CATHODE 350 VOLTS
RING 0 VOLTS

P.6. FIELD CONFIGURATIONS FOR VARIOUS ELECTRODE POTENTIALS.

FIG. 65.

potential. When after 30 minutes on curves C and D 100 volts was applied to the anode with the cathode at zero potential and 1173^{o}K, the anode work function dropped immediately to the level of curves A and B.

CHAPTER IX

9.1. Discussion of the results.

The application of an anode potential in a diode containing a hot barium oxide cathode can have several effects. Electron bombardment of any material deposited on the anode may result in its decomposition when the electron energy exceeds the dissociation energy. Metson (1949) has reported cathode poisoning in valves containing oxide cathodes for an anode potential of 5.56 volts which he attributed to the dissociation of barium oxide on the anode surface which had sublimed from the cathode. A similar effect was demonstrated by Wright (1954) which again indicated the presence of barium oxide on the anode. A further consequence of the applied anode potential might be to effect a current flow through the cathode matrix as discussed in Chapter II. Electrolytic dissociation can take place in the barium oxide matrix as a result of the applied anode potential: some of the dissociation products might then find their way to the anode surface.

It is also possible that the electric field between the anode and cathode might orientate the barium oxide molecules

which are deposited on the anode; though this possibility is thought to have been eliminated by the experiments described at the end of Chapter VIII.

The following hypothesis has been adopted by the author to explain the effects of applying various anode potentials during sublimation from the cathode: (1) There is a critical lower value of the ratio of barium to barium oxide on the anode below which the anode work function is characteristic of a tungsten surface covered by a barium oxide film. (2) An upper limit of the ratio of barium to barium oxide in the anode film exists, beyond which the anode work function is characteristic of barium on tungsten.

There is little doubt that the dependence of the shape of the sublimation curves in Fig. 43 on the potential applied to the anode during sublimation results from the decomposition of the anode deposits by electron bombardment. Sublimation curves obtained with anode potentials between 0 and 20 volts were all found to be similar, which indicates that, although decomposition of the anode deposit takes place when a potential of between 6 and 20 volts is applied to the anode during sublimation, the ratio of barium to barium oxide resulting from this decomposition is not high enough to effect the shape of the sublimation curve. An increase in anode potential beyond 20 volts correspondingly increases the energy of the

bombarding electrons and results in a rise in the ratio of barium to barium oxide on the anode. It is suggested that the barium content of the anode film is then high enough to alter the sublimation curve, resulting in a final anode work function which is lower than that of the barium oxide film. Sublimation with an anode potential of 75 volts further lowers the anode work function, again increasing the barium to barium oxide ratio on the anode. With 100 volts applied to the anode during sublimation, the initial fall in anode work function exceeds that of the 75 volt curve, indicating still further increases in the barium to barium oxide ratio of the anode film. However the increase in this ratio for the 100 volt curve over that of the 75 volt curve does not lower the final minimum work function beyond the final level of the 75 volt curve which might indicate that the proportion of barium to barium oxide is approaching infinity. The final minimum value for both the 75 and 100 volt curves if 2.0 eV, which is in good agreement with the measurements of Moore and Allison (1955) for barium tungsten who found the thermionic work function of tungsten covered with a monolayer of barium to be 1.9 eV.

Measurements of the anode current made during the sublimation support the above theory. Emission poisoning occurs during sublimation with anode potentials between 20 and

100 volts which could indicate the liberation of electro-negative constituents, probably oxygen, from the dissociated anode deposits. The percentage decrease in anode current during sublimation is found to be dependant on the applied anode potential. A maximum decrease of 40% was recorded with 50 volts applied to the anode, while the percentage decreases for 20 and 100 volts were only 5% and 17%, respectively. Two cathode effects must be considered in explaining this result. First, there is the poisoning effect of the anode decomposition products (oxygen), and second, there is the activating effect of the applied anode potential. For anode potentials less than 50 volts, the poisoning effect appears to be much greater than the activating effect, but for anode potentials greater than 50 volts, the effect of the poisoning is reduced by the parallel activating effect of the applied anode potentials.

The observed rise in pressure as the energy of electrons bombarding an anode film is increased (Fig. 46) supports the dissociation mechanism. In considering the pressure curve of Fig. 46 it should be remembered that the measurements were made in a continuously pumped system, had they been made in a sealed-off system, the total pressure rise would have been considerably higher, particularly in the region of higher anode potentials.

Assuming the observed negative ion current (section 7.8) to be negative oxygen ions produced by the dissociation of barium oxide in the anode film, then Fig. 47 shows that the amount of dissociation increases with the applied anode potential. Only by assuming 100% dissociation of the barium oxide deposited on the anode during a sublimation run with 100 volts applied to the anode, might the 100 volt peak in Fig. 47 be explained. Assuming that 75 volts applied to the anode does not decompose all the barium oxide arriving at the anode, increasing the anode potential to 100 volts would result initially in a very high negative ion current until all the barium oxide on the anode was dissociated, after which the negative ion current would return to a value dependant on the rate of arrival of barium oxide on the anode. However, the desorption curves in Fig. 63 indicate that the films formed during sublimation with 100 volts applied to the anode consist of both barium and barium oxide, so that not all of the deposited barium oxide is decomposed. As the ion emission is only observed after sublimation from the cathode for 12 hours, there should after that time be at least the equivalent of 12 mono-molecular layers of barium oxide deposited on the anode. Electron bombardment may therefore produce dissociation not only at the surface, but also deeper down in the anode film. The attainment of a constant negative ion current

might then represent an equilibrium state in the diffusion of dissociated ions to the surface of the film.

The effect of varying the anode potential during a sublimation run (section 7.9) is clearly accounted for in terms of dissociation.

Activation energies for the barium oxide subliming from a barium oxide coated cathode were found to be 4.7 ± 0.2 eV. and 4.4 ± 0.2 eV. in the temperature range $1143^{\circ}K$ to $1183^{\circ}K$, well within the lower linear region found by Pelchowitch (1954). These values agree well with the activation data for barium oxide cited in Chapter III. The activation energy for barium has been given by Dushman (1961) as 1.74 eV.

The conductivity measurements in which the barium oxide films were found to be insulating are in good agreement with the observations of Metson and Batey (1961)b. The measurements also indicate that little or no platinum is evaporated from the cathode base through the coating. Calculations by Moore and Allison (1950) based on the vapour pressure data of Claasen and Veeneman (1933) for barium oxide, and Jones, Langmuir, and Mackay (1927) for platinum, indicate that at $1173^{\circ}K$, about one platinum atom would evaporate for every 10^5 barium oxide molecules. The effect of the oxide layer on the metal is estimated to further reduce the rate of evaporation of the platinum by 30%.

The general shape of the sublimation curves obtained with zero anode potential is attributed to the deposition of barium oxide onto the tungsten anode. The displacement of the sublimation curves to lower work functions after the cathode has been fully activated undoubtedly results from the elimination of negative ions of carbon monoxide (Metson 1957b), and oxygen (Moore and Allison 1950), from the cathode during its activation.

Sublimation curves for barium oxide on polycrystalline tungsten similar to those in Figs. 41 and 42 (i.e. having an initial minimum followed by a rise to a maximum, and subsequently falling to a lower value) are to be found in the literature. The measurements of Moore and Allison (1950) show such an inflection at a calculated fractional coverage of $\theta = 0.2$ for barium oxide on both tungsten and molybdenum. Such inflections do not occur in their curves for barium oxide on tantalum or zirconium. In the investigations of Moore and Allison work functions were determined by the Richardson line technique. Results obtained by Morgulis (1960) using the displacement of retarding potential characteristic technique, also show a slight rise following an initial minimum in the sublimation curves. Using the same method as Morgulis, Florio (1963) obtained curves almost identical with those in Figs. 41 and 42, but with molybdenum as a substrate. Field

emission techniques have been used by Noga (1962) to investigate the adsorption of barium oxide on tungsten. Again, these measurements show an inflection in the sublimation curves for calculated fractional coverage of $\theta = 0.2$. Examination of the sublimation data of Kirsanova, Shul'man, and Dement'eva (1963), obtained by the Kelvin technique, also reveals that their curves have an initial minimum followed by a rise though they were not taken far enough to show a subsequent fall in the work function.

Measurements similar to those of Kirsanova, Shul'man, and Dement'eva (1963) have been carried-out by Kirsanova, Shul'man, and Gerasimova (1963) on the (110) face of a tungsten single crystal. Again, the sublimation curves show an initial minimum followed by a rise to a maximum about 0.2 eV. above the minimum. Unfortunately the exact crystallographic orientation of well aged polycrystalline tungsten foil is not well established, but the surface is generally found to consist predominantly of (100) planes orientated with the [100] direction within 25° of the normal to the surface.

The reduction in work function of polycrystalline tungsten by adsorbed barium oxide molecules has generally been attributed to the polar barium oxide molecules being preferentially adsorbed with their lines of centre

perpendicular, and the oxygen atom adjacent, to the tungsten surface.

Since the author has found the ratio of the time to reach the first minimum of the sublimation curves to the time to reach the following maximum is always between 0.5 and 0.6, it is possible that at the first minimum of the curves half of the tungsten surface is covered with evenly distributed barium oxide molecules orientated with their oxygen atoms adjacent and perpendicular to the surface. A strong mutual depolarising field would then exist, and may result in all the admolecules required to fill the remaining half of the surface being orientated with their barium atoms adjacent to the surface, thus cancelling the effective dipole on the surface and resulting in a tungsten surface covered by a two dimentional barium oxide lattice. The addition of further molecules to the surface would build up multilayers of barium oxide on the tungsten surface, and the fall in work function observed after the maximum may represent an approach to the work function of bulk barium oxide.

An alternative explanation for the shape of the sublimation curves can be found from the adsorption studies of gases on solids by Ehrlich (1963), who has shown that at low temperatures ($300^{o}K$) dynamic adsorption processes can occur in which admolecules are held to the surface by a

multiplicity of binding states. These states have been investigated by field emission and flash desorption techniques, and are attributed either to adsorption on planes with different crystallographic orientations and on steps or edge between the planes (Ehrlich 1959), or to the formation of gaps in the immobile adsorbed film (Roberts 1935).

No such investigations have been carried out for the adsorption of barium oxide on tungsten, and similarly, measurements have not been made of the binding energies of such a system. The conclusions deduced below must therefore be regarded as purely tentative.

Consider, as a model the case of a tungsten surface having two states of binding for the barium oxide molecules, Q_1 and Q_2, with energies of 5.5 and 4.6 eV., respectively. Barium oxide molecules arriving at the empty surface can do one of two things: (i) They can be incident on, and strongly bound to, a Q_1 site. (ii) An incident molecule may be adsorbed on a Q_2 site of low binding energy, and migrate from there to a more tightly bound Q_1 site. Molecules incident on a full Q_1 site will similarly migrate to a vacant Q_1 site. When the Q_1 fraction of the surface is fairly well filled up, the more weakly bound states begin to form. Fig. 66 represents the probability of these two states being occupied as a function of surface coverage θ. The molecules initially

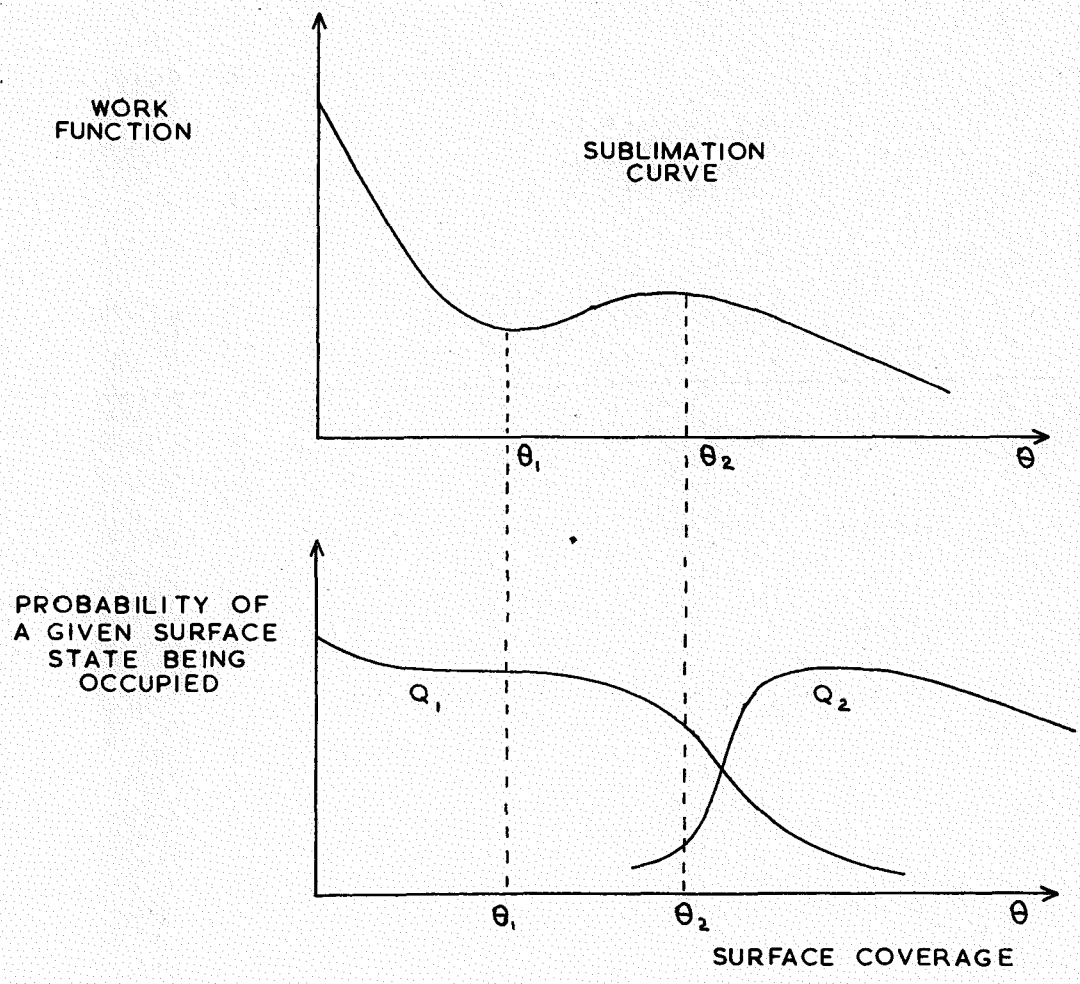
WORK FUNCTION
SUBLIMATION CURVE
θ1
θ2
θ
PROBABILITY OF A GIVEN SURFACE STATE BEING OCCUPIED
Q1
Q2
θ1
θ2
θ
SURFACE COVERAGE

FIG. 66.

adsorbed on the Q_1 sites are orientated with their oxygen atoms adjacent to the surface. As in the single state model, mutual depolarisation occurs on the Q_1 sites as they fill up, and this leads to an increase in work function after a coverage, say, θ_1. As adsorption on the Q_1 state nears completion, the Q_2 state starts to form, the barium oxide molecules being adsorbed in a similar way to those in the Q_1 state above. Binding energies for molecules arriving on top of the filled Q_1 states can be expected to be high (ionic binding, 4-5 eV.), and being comparable with that of the Q_2 state, there is now an almost equal probability of barium oxide being adsorbed anywhere on the surface. Mutual depolarising effects in the Q_2 regions may now be compensated by the building up of lower work function multi-molecular layers in the Q_1 region similar to those proposed in the single state model. A constant work function should be reached when every part of the surface is covered by at least two or three molecular layers of barium oxide.

It is difficult even to speculate as to the exact nature of the different binding sites for barium oxide adsorbed on tungsten. The choice in the light of present knowledge, as stated earlier, is between singularities or gaps in the adsorbed films, and different crystal planes and edges or steps on the tungsten surface. The latter seems more

attractive in view of our present knowledge of the surface structure of polycrystalline tungsten foil.

This model requires complete mobility of barium oxide over the tungsten surface at 300°K, evidence against the migration of barium oxide below 1000°K has been presented by Noga (1962). The experiments carried out by Noga, in which barium oxide was deposited onto a tungsten field emitter, and the temperature of the tungsten was then raised to 1700°K, indicate the following:

(a) Migration of the adsorbed molecules over the surface does not occur substantially below 1000°K.

(b) The chemical reaction $6BaO + W \rightarrow Ba_3WO_6 + 3Ba$ between barium oxide and tungsten, proceeds rapidly between 1073°K and 1173°K, with an activation energy of 3.3 eV.

(c) At about 1173°K the reaction ceases, the products of the reaction being stable on the surface until the temperature is raised above 1273°K.

(d) Above 1273°K the products of the reaction dissociate and evaporate.

(e) Above 1673°K all adsorbed substances are evaporated from the surface.

The migration experiments of Noga (1962) were carried out with a barium oxide film thickness of 0.05 monolayers. Over the temperature range 903°K to 968°K the activation

energy for migration was found to be 4.6 eV. The result of raising the tungsten and barium oxide film to these temperatures was to produce an increase in the work function. Similar measurements by the author (Fig. 56) do not show this same effect. As the tungsten in Noga's experiments was only outgassed at 2000°K, compared with 2800°K in the authors' experiments, the migration observed by Noga may possibly have been caused by the diffusion of impurities in the tungsten. On the basis of the author's model with Q_1 and Q_2 sites, however, any migration which may occur at coverages of 0.05 monolayers would be migration of the molecules between the strongly bound Q_1 states which would require an activation energy approaching the binding energy of the Q_1 sites and might be as high as 4.6 eV.

Heating the tungsten anodes when covered by different thicknesses of barium oxide leads to a rapid initial decrease in the work function for temperatures in the range 600°K to 1605°K (Fig. 56). Similar effects have been reported by Kirsanova, Shul'man, and Dement'eva (1963) for barium oxide on polycrystalline tungsten, using ~~field emission and~~ the Kelvin technique, ~~respectively~~, but the effect was not reported in the paper of Moore and Allison (1950). Further consideration will be given to this paper later. Kirsanova, Shul'man and Dement'eva (1963) do not consider the possibility

of a reaction between the adsorbed barium oxide and the tungsten substrate, but attribute the decrease in work function of the barium oxide coated tungsten upon heating (see Fig. 13) to the formation of an activated binding state. Their published data provides no evidence to suggest that such a reaction takes place.

The author considers that the initial fall in anode work function produced by raising the temperature of the anode (Fig. 56) is due to the formation of an activated surface binding state. Deposition of the barium oxide molecules onto the less densely packed (100) planes of the tungsten surface at 300°K results in the single or two phase binding discussed earlier in this Chapter; when the temperature of the tungsten is raised, activated adsorption takes place in which bonds are formed between the barium oxide molecules and the lower lying tungsten atoms which can be "seen" by the barium oxide molecules through the surface atoms of the (100) planes. From this point of view, Kirsanova, Shul'man and Dement'eva (1963) consider the adsorption of barium oxide on tungsten analogous to the adsorption of oxygen on tungsten, in which an oxygen atom adsorbed between four tungsten atoms constituting a unit cube face in the (100) plane, touches five tungsten atoms simultaneously, and is more strongly bound than it would be on the (110) plane. Once sites of this

kind are occupied, oxygen atoms on the (100) plane can only make contact with two tungsten atoms and are consequently less strongly bound to the surface (Gomer and Hulm 1957). Kirsanova, Shul'man and Gerasimova (1963) have investigated the adsorption of barium oxide on the (110) face of a tungsten single crystal and have not detected the presence of an activated binding state on this closely packed face. Desorption was also found to take place at lower temperatures than in the case of the polycrystalline surface.

The difference in the anode work function after heating for one minute at different temperatures (lower curves, Fig. 56) could be due to migration of the barium oxide molecules to vacant sites where activated adsorption can take place. However, such a process would be exponentially dependent on temperature and all the lower curves in Fig. 56 would be expected eventually to reach the same level provided desorption does not take place. For temperatures above 1500^{o}K (upper curves Fig. 56) there is a differential effect between activated binding and desorption. The activation energy for desorption determined from the curves in Figs. 57 and 59 was found to be 4.6 and 5.1 eV., respectively.

The measurements of Moore and Allison (1950) were made by the Richardson line technique. Their data indicates that

emission measurements were always made at temperatures of at least 600°K; at these temperatures, activated binding of the barium oxide molecules to the tungsten could take place, so that their measurements probably represent the actively bound state. This would account for the very low work functions which they obtained (see Fig. 10). It is fortunate that each set of emission characteristics must have been taken starting at the highest temperature.

The desorption curves in Fig. 63, obtained for a film deposited on the tungsten anode with an applied anode potential of 100 volts, indicate the presence of two different species adsorbed on the tungsten, one of high binding energy, and the other of a lower binding energy. Examination of the curves for 1605°K and 1655°K shows a step which probably corresponds to the point where all the species of the lower binding energy is desorbed from the surface.

Earlier in this chapter it has been suggested that films deposited on the anode with the anode at a potential of 100 volts consist of a mixture of barium and barium oxide. The calculated activation for the first part of the desorption process in Fig. 63 was 3.0±0.3 eV. Measurements of the activation energy for desorption of barium from tungsten by Moore and Allison (1955) indicate a value between 3.45 and

3.7 eV. It would seem therefore, that when the 100 volt layer is heated to about 1600°K the barium produced by dissociation is desorbed very rapidly, while at the same time the barium oxide is desorbed, but at a much slower rate.

In conclusion, the measurements indicate that the potential applied to a tungsten anode during sublimation from a barium oxide cathode effects the shape of the anode work function versus time curves, causing dissociation of the anode deposits by electron bombardment. It is thought that there exists a critical lower value of the ratio of barium to barium oxide on the tungsten anode below which the work function is characteristic of a tungsten surface covered by a film of barium oxide, and similarly, that there is an upper limit to the ratio of barium to barium oxide on tungsten beyond which the work function is characteristic of barium on tungsten. A two phase model is proposed for the adsorption of barium oxide on tungsten at room temperature, and evidence is also presented for the existance of a third activated binding state.

9.2. Suggestions for future work.

The conclusions from the preliminary results indicate the lack of reproducability inherent in the anode film deposited during the initial decomposition of the cathode. A more reliable study of the continuous changes in anode work function which occur during the activation of a barium oxide cathode could be made with an M-type tube, providing the anode is cleaned after decomposing the cathode. The results to two such sets of experiments would be a valuable addition to the results in Chapter VI.

The results in Chapters VII and VIII pose a number of interesting problems. Clearly the proposition that there is a lower limit to the ratio of barium to barium oxide on the anode, below which the anode work function is characteristic of barium oxide on tungsten, and similarly, that there is an upper limit to this ratio, beyond which the anode work function is characteristic of barium on tungsten, requires verification. Initially the investigation of sublimation from a barium oxide cathode with anode potentials greater than 100 volts should be made. Such experiments might show that above a critical anode potential the sublimation curves for a given cathode temperature are identical. The effect of bombarding the anode film from an independant filament might also be investigated.

A more useful approach to the above problem may be by way of studying the desorption of the anode films. Curves of the type shown in Fig. 63 should show a marked change as the anode potential during sublimation is varied. For anode potentials greater than 100 volts, the inflection, which is most predominant in the 1605°K curve, should move to higher values of the anode work function; finally the activation energy determined from any part of the desorption curve should be characteristic of the desorption of barium from tungsten. Similarly as the anode potential during sublimation decreases, the inflection should move to lower anode work functions until it again disappears, and the activation energy is characteristic for the desorption of barium oxide from tungsten.

There are many ways in which the two phase absorption suggested for the adsorption of barium oxide on tungsten at 300°K can be investigated. Such adsorption would be accompanied by a decrease in the binding energy with increasing surface coverage. Providing it is possible to construct an anode of sufficiently low heat capacity, it may be possible to detect a decrease in the heat produced by adsorption as the surface coverage increases. More careful measurements of desorption characteristics, such as those in Figs. 57 and 59 may also show a variation in the binding energies, providing

the binding energies can be determined to within an accuracy of at least 0.1 eV.

Further investigation of the activated adsorption is also called for. This may best be done by studying the change in resistance of the tungsten filament as the activated adsorption takes place. When such adsorption takes place, the bonding with lower lying atoms should produce an increase in the resistance of the filament.

Information concerning the adsorption of barium oxide on the different crystallographic planes of tungsten can be obtained from field emission studies. The field emission studies of Noga (1962) were unsatisfactory; as the barium oxide could only be deposited onto one side of the tungsten emitter tip a full field emission pattern of barium oxide adsorbed on tungsten at room temperature could not be obtained, but by heating the tip the barium oxide could be made to migrate and cover the whole of the tip surface. An emission tube in which barium oxide could be deposited over the whole of the emitter tip would enable sites of preferential adsorption to be detected, and, the sites where activated adsorption of barium oxide on tungsten occurs could be readily observed. A detailed study of the binding energy of different adsorption sites could be made by experiments in which the barium oxide is desorbed from the emitter tip

at successively increasing temperatures.

The results obtained from field emission experiments might then be compared with measurements similar to those described in Chapters VII and VIII using tungsten single crystals in place of polycrystalline tungsten foil.

APPENDIX I. Some work function measurements in experimental tubes containing uranium and zirconium carbides, and niobium.

A.1.1. Introduction.

During the three years required for the completion of this thesis there was considerable speculation concerning a device for converting heat directly into electrical energy known as the 'thermionic direct converter'. Such a device is essentially a heat engine in the thermodynamic sense, with an electron gas as a working fluid. The heat source is the cathode in some sort of diode arrangement. Electrons emitted from the cathode have sufficient kinetic energy to overcome the potential energy barrier and arrive at the colder anode where they transform their high kinetic energy into potential energy. This potential energy can then be utilised by connecting the anode and cathode through an external load.

Because of the great interest in this device the author undertook some experiments with materials which have been suggested as possible emitters. These materials were uranium and zirconium carbides, and niobium.

At least three reports of measurements of the work function of uranium carbide had appeared in the literature

prior to those of the author. Richardson line determinations had been reported by Pidd et al. (1959), and Hass and Jenson (1960), which gave 4.57 and 2.94 eV., respectively, for the work function of uranium carbide. Using the Kelvin technique Hopkins (1962) obtained a value of 3.97 eV.

Richardson lines had also been reported for zirconium carbide which varied from 2.1 eV. (Haddad et al. 1949) and 2.3 eV. (Wright 1953) for the powdered material, to 3.8 eV. (Pidd et al. 1959) and 4.0 eV. (Danforth and Williams 1961) for the fused carbide.

Only two measurements of the work function of niobium have been reported in the literature to the knowledge of the author. Using thermionic methods, Wahlin and Sordahl (1934) reported a value of 3.96 eV., and Reimann and Kerr Grant (1936) a value of 4.01 eV.

In view of the unsatisfactory state of the published data for these materials the measurements described below were undertaken. Work function measurements of uranium and zirconium carbides were made by the Richardson line technique and the Kelvin technique. Only the Kelvin and displacement of retarding potential characteristic methods were used for the measurements on niobium. The reference surface normally used in this work was that of tungsten, though on one occasion

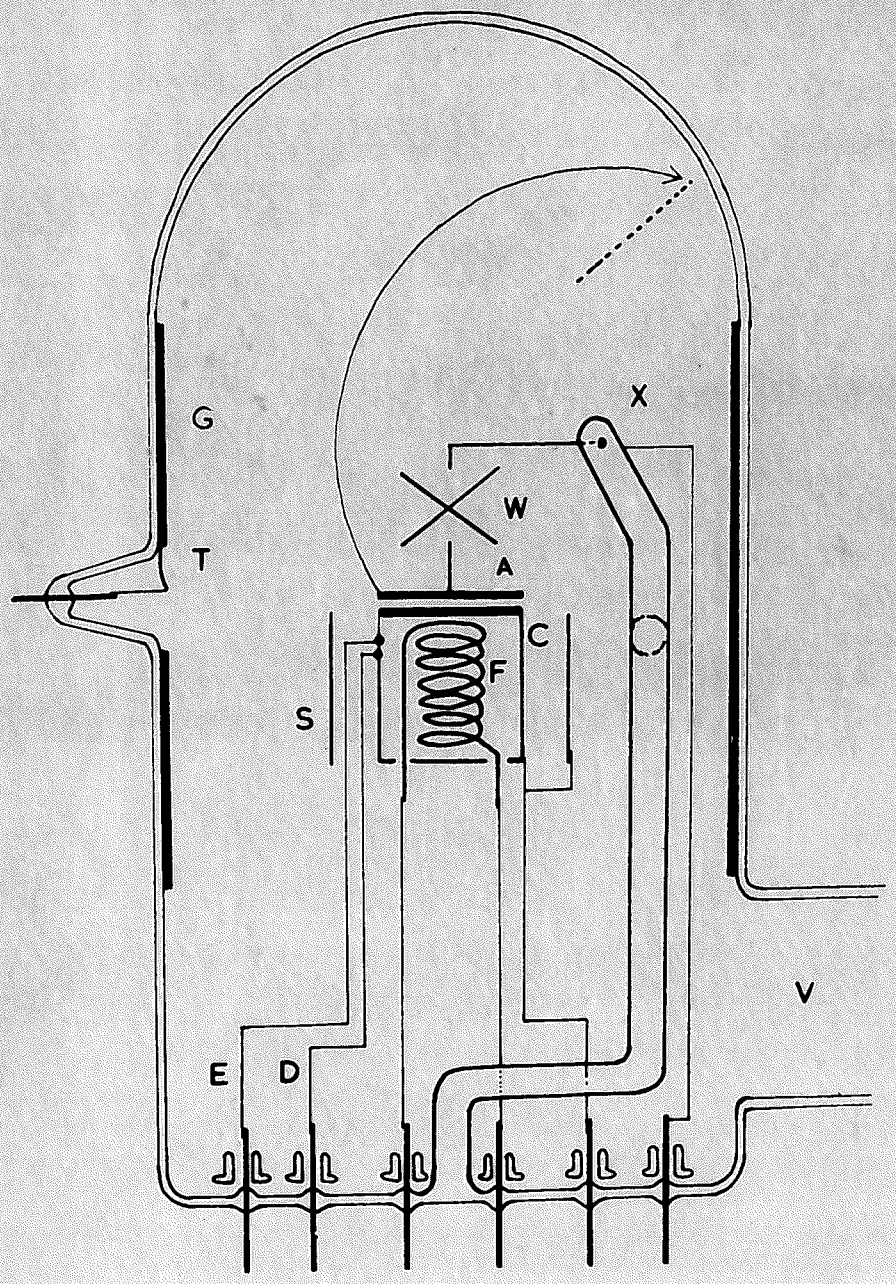

FIG. A.I.

molybdenum was substituted. The work function of the tungsten surface was assumed to be 4.54 eV. (Hopkins and Riviere 1963). In the single tube where molybdenum was used as a reference surface the contact potential difference between tungsten and molybdenum was taken from the measurements of Riviere (1957); the work function of molybdenum was then 4.24 eV.

In the case of the uranium carbide cathodes, the necessary zero field conditions were obtained from retarding potential characteristics. With two of the zirconium carbide cathodes Schottky plots were used to obtain the zero field data for the Richardson plots.

A.1.2. Experimental: uranium and zirconium carbides.

A schematic diagram of the type of tube used for these investigations is shown in Fig. A.1. The anode (A) could be rotated about a tungsten-glass hinge (X) and hence removed from the cathode proximity during outgassing. By means of a tungsten spring arrangement (W), the anode could be made to vibrate in a vertical plane above the cathode.

Three cathode designs were tested during this work; the first of these was a simple disc of tantalum 1.5 cm. in

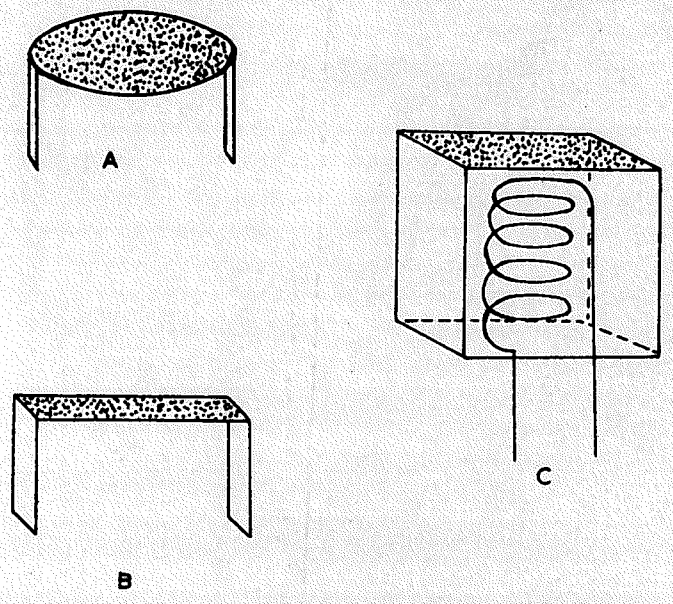

FIG. A.2.

diameter fitted with two mounting flanges (Fig.A.2A). Heating was either via an external R.F. heater or by electron bombardment from an auxiliary filament inside the tube. A very uneven temperature distribution was common with these cathodes, nor was it possible to measure the low emission currents necessary for accurate retarding potential plots. Directly heated tantalum strips (Fig.A.2B) 1.5 X 0.3 cm^2 were much more satisfactory in both these respects. In order to measure the temperature coefficient of the work function using the Kelvin technique, voltage gradients over the cathode surface due to the heater current had to be eliminated. The final cathode design (see Fig. A.1 and Fig.A.2C) was therefore an indirectly heated tantalum box (C in Fig. A.1) 1.5 X 1.5 X 1.5 cm^3, and heated by radiation from a tungsten filament (F) inside the box. The maximum temperature achieved with this type of cathode when fitted with a radiation shield (S) was about 2100^{o}K. The cathode temperatures were followed by using a tungsten/tungsten-26% rhenium thermocouple (ED) welded immediately under the emitting surface in the case of the disc and strip cathodes, and welded to the side of the box cathodes.

The surfaces of these cathodes to be coated were initially carburised by heating to about 2300^{o}K in a flux of carbon

vapour. The carbide was then deposited electrophoretically, the cathode dried, sintered, and stored in argon until required. Sealing into the experimental tubes took place in a stream of dry nitrogen with the cathode cold. The completed tubes were sealed via a 25 mm. arm (V) to the Venema and Bandringa vacuum system. Pressure readings throughout the measurements were usually within the range 10^{-9} to 10^{-10} mmHg.

A.1.3. Results: uranium and zirconium carbides.

Table A.1 shows the results obtained from the measurements on cathodes of uranium and zirconium carbide by both the Kelvin and Richardson line techniques.

TABLE A.1

Cathode work function eV.

	Tube No.	ø Kelvin	ø Richardson	dø/dT
Uranium Carbide	U1	3.99 ± 0.015	-	-
	U2	3.76 ± 0.01	2.8 ± 0.1	5×10^{-4}
		3.73 ± 0.01	2.8 ± 0.1	6×10^{-4}
		3.76 ± 0.01	-	-
	U3	3.94 ± 0.01	3.3 ± 0.1	2×10^{-4}
		-	3.1 ± 0.1	5×10^{-4}
		-	2.6 ± 0.1	5×10^{-4}
		-	2.7 ± 0.1	5×10^{-4}
		-	2.8 ± 0.1	5×10^{-4}
Zirconium Carbide	Z1	3.63 0.01	-	-
	Z2	3.64 0.01	2.6 0.1	6×10^{-4}
		-	2.2 0.1	6×10^{-4}
		-	2.7 0.1	9×10^{-4}
	Z3	3.63 0.01	-	-
	Z4	3.64 0.01	-	-

The three sets of measurements made with tube U2 were separated by several days during which emission was drawn from the cathode at 1800°K. With tube U3 the first state

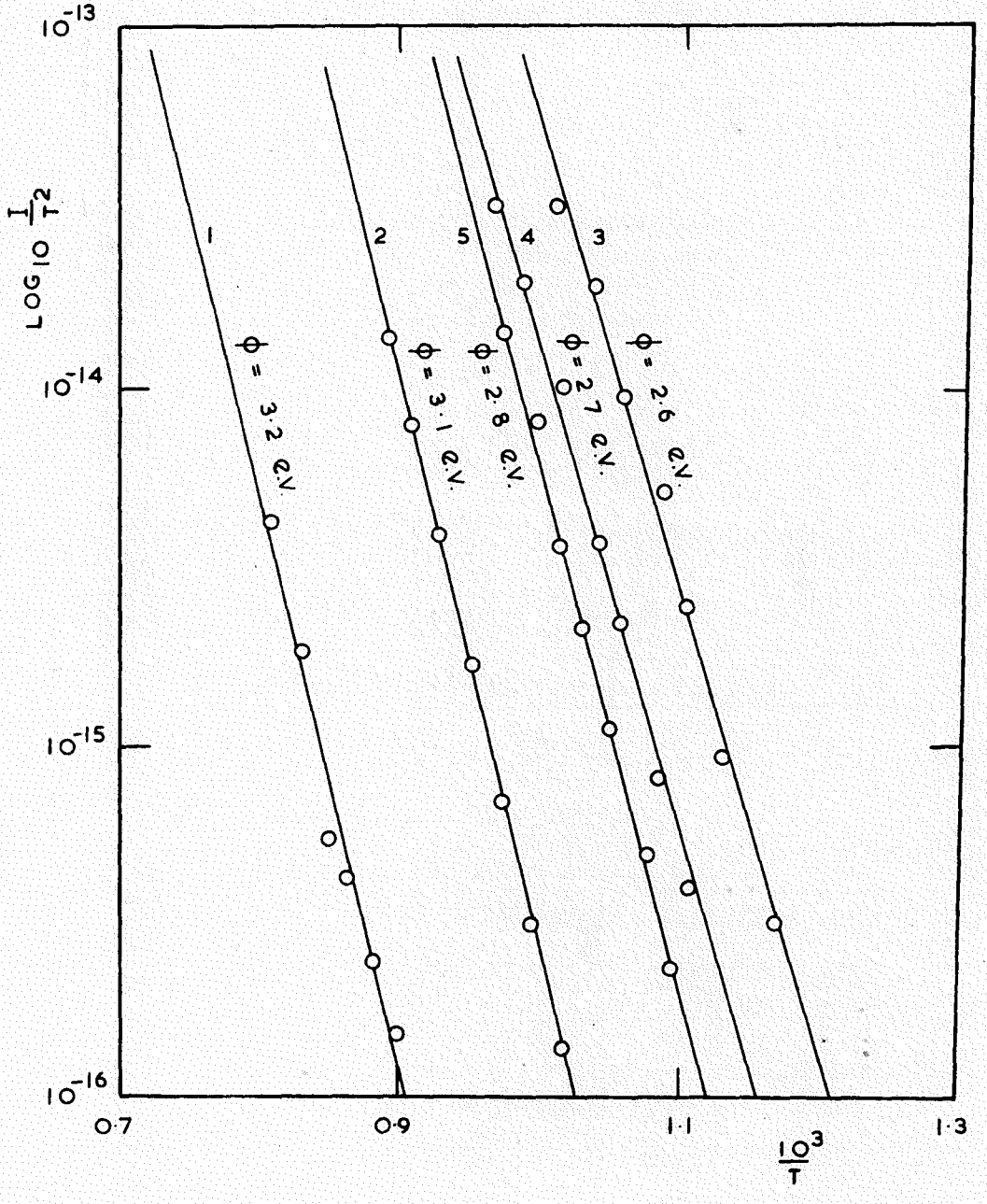

FIG. A.3.

RICHARDSON PLOTS FOR U.3.

was immediately after an ultra-high vacuum had been attained, the second was after 15 hours further outgassing at 1800°K. The last three states were achieved after emission had been drawn from the cathode at a temperature of 1800°K and were separated by periods of 24 hours. The Richardson lines corresponding to tube U3 are shown in Fig. A.3. Unfortunately, because of distortion on tube U3 it was only possible to measure the Kelvin work function immediately after outgassing the cathode.

The data for the temperature coefficient of the work function was obtained either from Richardson plots or from effective work function plots, in both cases assuming the theoretical value of A.

A.1.4. Discussion of results: uranium and zirconium carbides.

After a temperature correction has been applied to the work function measurements derived from the Richardson line technique so that they apply to 300°K, a considerable discrepancy still exists with the results from the Kelvin measurements; averages of 3.0 as compared with 3.8 eV. in the case of uranium carbide, and 2.7 compared with 3.6 eV. for zirconium carbide. An obvious explanation of these results is in terms of work function patches on the cathode

surfaces. The Kelvin method measures the arithmetic average over the area of the high and low work function patches, while the emission measurements reflect an average work function but heavily weighted towards the areas of greatest emission (see Chapter IV).

Since the above measurements were made two more measurements of the work function of uranium carbide have appeared in the literature. Elcombe and Wright (1963) using the Richardson line method in unspecified vacuum conditions obtained a value of 3.3 eV. for the work function of uranium carbide containing an excess of carbon. Measurements by Bainton (1963) on uranium carbide, again containing a slight excess of carbon, gave a value of 3.11 eV. for the Richardson work function, at a pressure between 5×10^{-7} and 2×10^{-6} mmHg. An obvious conclusion to be drawn from a consideration of these results is that at present workers have not yet achieved uniform uranium or zirconium carbide surfaces. If it is assumed that the surfaces have two distinct constituants, one of high and one of low work function, then by alloting an arbitrary value to the high work function patches it is possible to calculate the areas occupies by the two components. If the arbitrary value is 4.5 eV. for both the uranium and zirconium carbides then the emitting

areas of the cathodes are about 50% of the total area.

A.1.5. Experimental: niobium.

Two experimental tubes were used for these measurements. In one of the P series of tubes, P.3, a second niobium anode was included (Fig.39B) By making retarding potential plots first to the tungsten anode and then to the niobium, the contact potential difference could be determined by the displacement of retarding potential characteristic method. The second experimental tube was of the type used for the uranium and zirconium carbide investigations, (see Fig. A.1). A directly heated niobium strip 3 X 20 mm^2 formed the cathode. The anode arrangement was identical to that in Fig. A.1.

The niobium was outgassed by maintaining it at 2300°K for 24 hours followed by several short periods at 2700°K. The latter temperature could not be maintained for any length of time as it gave rise to copious evaporation from the niobium. Outgassing was judged complete when raising the niobium to temperatures in the region 2300°K did not cause the pressure in the vacuum system to rise above 5×10^{-9} mmHg.

A.1.6. Results: niobium.

The contact potential difference between niobium and tungsten measured by the displacement of retarding potential characteristic method was 0.17±0.03 volts. Adopting the value of 4.54 eV. for the work function of tungsten (Hopkins and Riviere 1963), the work function of niobium is 4.37±0.03 eV.

The contact potential difference between tungsten and niobium measured by the Kelvin technique was found to be 0.2±0.05 V. The work function of niobium determined by this technique is therefore 4.34±0.05 eV.

REFERENCES

Aldrich, L.T., 1951, J. Appl. Phys., 22, 1168.

Alexander, A.E., and Anderson, J.R., 1952, Austral.J.Appl. Sci., 3, 201.

Anderson, P.A., 1935, Phys. Rev., 47, 958.

Anderson, P.A., 1952, Phys. Rev., 88, 655.

Anderson, P.A., 1959, Phys. Rev., 115, 553.

Appleyard, E.T.S., 1937, Proc. Phys. Soc. Lond. 49, 118.

Bainton, K., 1963, Adv. Energy Conversion 3, 273.

Bayard, R.T., Alpert, D., 1950, Rev. Sci. Instr. 21, 571.

Becker, J.A., 1929, Phys. Rev., 34, 1323.

Becker, J.A., and Sears, R.W., 1931, Phys. Rev., 38, 2193.

Becker, J.A., and Brittain, W.H., 1934, Phys. Rev., 45, 694.

Beeck, O., 1950, Discuss. Farad. Soc., 8, 118.

Beese, N.C., 1930, Phys. Rev., 36, 1309.

Blewett, J.P., 1939, Phys. Rev., 55, 713.

Blewett, J.P., Liebhafsky, H.A., and Hermelly, E.F., 1939, J.Chem. Phys., 7, 478.

Bulyginskii, D.G., Dobretsov, D.N., 1956, Zh. tech. Fiz., 26, 977.

Childs, C.D., 1911, Phys. Rev., 32, 492.

Claasen, A., and Veenemans, C.R., 1933, Z.Phys., 80 342.

Cockcroft, J.D., 1928, Proc. Roy. Soc., A, 119 293.

Comsa, G., Gelberg, A., and Iosifescu, B., 1961, Phys. Rev., 122, 1091.

Coulson, C.A., 1951, "Electricity", Oliver, London

Coomes, E.A., 1946, J. Appl. Phys., 17, 647.

Culver, R.V., and Tomkins, F.C., 1959, Adv. in Catalysis XI, 67.

Darbyshire, J.A., 1938, Proc. Phys. Soc. Lond., 50 635.

Danforth, W.E., and Williams, A.J., 1961, J. Appl. Phys., 32, 1181.

Davisson, C., and Pidgeon, H.A., 1920, Phys. Rev., 15, 553.

De Boer, J.H., 1935, Electron Emission and Adsorption Phenomena, C.U.P.

Dushman, S., 1930, Rev. Mod. Phys., 2, 381.

Dushman, S., 1961, Scientific Foundations of Vacuum Technique, Wiley.

Ehrlich, G., 1963, Anual. Acad. Sci., New York, 101 722.

Ehrlich, G., 1959, Structure and Properties of Thin Films, ed. Neugebauer, C., Newkirk, J., and Vermilyea, D., Wiley.

Eisenstein, A.S., 1948, Adv. in Electronics, 1, 1.

Elcombe, A.D., and Wright, D.A., 1963, Adv. in Energy Conversion, 3, 199.

Estermann, J., 1925, Z. Phys., 33, 320.

Fan, H.Y., 1943, J. Appl. Phys., 14, 557.

Fane, R.W., 1957, Brit. J. Appl. Phys., 9, 149.

Ferris, W.R., 1949, R.C.A. Review, 10 134.

Florio, J.V., 1963, J. Appl. Phys., 34, 200.

Forman, R., 1954, Phys. Rev., 96, 1479.

Fowler, R.H., 1936, Statistical Mechanics, C.U.P.

Fraser, R.G.J., 1931, Molecular Rays, C.U.P.

Friedman, H., and Birks, L.S., 1946, Rev. Sci. Instr., 17, 99.

Gomer, R., Hulm, J.K., 1957, J. Chem. Phys., 27, 1363.

Gordy, W., and Thomas, W., 1956, J. Chem. Phys., 24, 439.

Gyftopoulos, E.P., and Levine, J.D., 1962, J. Appl. Phys. 33, 67.

Haddad, R.E., Goldwater, D.L., and Morgan, F.H., 1949, J. Appl. Phys., 20, 886.

Hamaker, H.C., Bruining, H., and Alen, A., 1947. Phil. Res. Rep., 2, 171.

Hannay, N.B., MacNair, D., and White, A.H., 1949. J.Appl.Phys., 20, 669.

Haas, G.A.,,and Jensen, J.T., 1960, J. Appl. Phys., 31, 1231.

Haas, R., and Jensen, J.T., 1959, Rev. Sci. Instr., 30, 562.

Heinze, W., and Wagener, S., 1936, Z. Tech. Phys., 17 645.

Heinze, W., and Hass, W., 1938, Z. Tech. Phys., 19, 166.

Heinze, W., and Wagener, S., 1938, Z. Phys., 110, 164.

Hensley, E.B., 1952, J. Appl. Phys., 23, 1122.

Hensley, E.B., 1956, J. Appl. Phys., 27, 286.

Hensley, E.B., 1961, J. Appl. Phys., 32, 301.

Herring, C., and Nichols, M.N., 1949,
Rev. Mod. Phys., 21 185.

Hermann, G., 1937, Z. Phys. Chem., 35B 298.

Hermann, G., and Wagener, S., 1950, The Oxide Coated Cathode,
Vols I and II, Chapman and Hall.

Higginson, G.S., 1958, Brit. J. Appl. Phys., 9, 106.

Holland, L., 1956, Vacuum Deposition of Thin Films,
Chapman and Hall.

Hopkins, B.J., 1962, Nature, 193, 668.

Hopkins, B.J., and Riviere, J.C., 1963, Proc. Phys. Soc.,
81, 590.

Huber, H., 1941, Thesis, University of Berlin.

Huber, H., Wagener, S., 1942, Z. Tech. Phys., 23, 1.

Hughes, R.C., and Coppola, P.P., 1952, Phys. Rev., 88, 346.

Hung, C.S., 1950, J. Appl. Phys., 21, 37.

Isikawa, Y., Sato, T., Okumura, K., and Sasaki, T., 1951,
Phys. Rev., 84, 371.

Jacobs, H., 1946, J. App. Phys. 17 596.

Jones, T.J., 1936, Thermionic Emission, Methuen and Co., London.

Jones, T.J., Langmuir, I., and Mackay, G.M.J., 1927,
Phys. Rev., 30, 201.

Kaye, G.W.C., and Laby, T.H., 1959, Physical and Chemical
Constants, Longmans.

Kelvin, Lord, 1898, Phil. Mag., 46, 82.

Kirsanova, T.S., Shul'man, A.R., and Dement'eva, A.V., 1963,
Soviet Physics: Solid State 4, 1918.

Kirsanova, T.S., Shul'man, A.R., and Gerasimova, A.P., 1963.
Soviet Physics: Solid State, 4, 1920.

Knudsen, M., 1909, Ann. Phys. Lpz., 28, 999.

Lander, J.J., 1950, Rev. Sci. Instr., 21, 672.

Langmuir, I., 1913, Phys. Rev., 2, 450.

Langmuir, I., 1917, Proc. Nat. Acad. Sci. Wash. 3. 141.

Lennard-Jones, J.E., 1937, Proc. Phys. Soc. Lond., 49, 140.

Levinstein, H., 1949, J. Appl. Phys., 20, 306.

Loosjes, R., and Vink, H.J., 1949, Phil. Res. Rep., 4, 449.

Lowry, E.F., 1930, Phys. Rev., 35, 1367.

Macdonald, J.R., and Edwardson, D.E., 1961,
Proc. I.R.E., 49, 453.

Maurer, R.J., 1945, J. Appl. Phys., 16 563.

Metson, G.H., 1949, Proc. Phys. Soc. Lond. 62B, 589.

Metson, G.H., 1951, Vacuum, 1, 283.

Metson, G.H., 1951, Brit. J. Appl. Phys. 2, 46.

Metson, G.H., 1957a, I.E.E. Monograph No. 211R.

" 1957b, " " " 243R.

" 1957c, " " " 268R.

" 1957d, " " " 269R.

" 1958a " " " 289R.

" 1958b " " " 317R.

Metson, G.H., and Macartney, E., 1959a, I.E.E. Monograph No. 347E.

Metson, G.H., and Macartney, E., 1960a, I.E.E. Monograph, No. 357E.

Metson, G.H., and Holmes, M.F., 1960b, I.E.E. Monograph, No. 397E.

Metson, G.H., 1961a, I.E.E. Monograph, No. 443E.

Metson, G.H., and Batey, H., 1961b, I.E.E. Monograph, No. 444E.

Metson, G.H., 1961c, I.E.E. Monograph, No. 473E.

Metson, G.H., and Woodgate, E., 1962a, I.E.E. Monograph No. 499E

Metson, G.H., 1962b, I.E.E. Monograph No. 529E.

Metson, G.H., 1962c, I.E.E. Monograph No. 530E.

Metson, G.H., 1963, Proc. I.E.E. 110, 845.

Mingolet, J.C.P., 1950, Farad. Soc. Discuss. 8, 105.

Mingolet, J.C.P., 1957, Chemisorption, ed. Garner, W.E., Butterworths, London.

Moore, G.E., and Allison, H.W., 1950, Phys. Rev., 77, 246.

Moore, G.E., and Allison, H.W., 1955, J. Chem. Phys., 23, 1609.

Morgulis, N.D., 1960, Soviet Physics: Solid State, 1, 1029.

Mutter, W.E., 1947, Phys. Rev., 72, 531A.

Nakai, J., Innuiski, Y., and Tsung-Che, Y., 1955,
J. Phys. Soc. Jap., 10, 437.

Nergaard, L.S., 1952, R.C.A. Rev., 13, 464.

Noga, K., 1962, J. Phys. Soc. Jap., 17, 950.

Nottingham, W., 1947 Conference on Physical Electronics.

Nottingham, W., 1956, Handbuch der Physik 11, 1.

Oatley, C.W., 1939, Proc. Phys. Soc. Lond., 51, 318.

Okumura, K., and Hensley, E.B., 1963, J. Appl. Phys., 34, 519.

Pauling, L., 1960, Nature of the Chemical Bond,
Cornell University Press.

Penning, F.M., 1937, Phil. Tech. Rev., 2 201.

Pelchowitch, I., 1954, Phil. Res. Rep., 9, 42.

Pidd, R., et al., 1959, J. Appl. Phys. 30, 1575.

Plumlee, R.H., and Smith, L.P., 1950, J.Appl. Phys., 21, 811.

Plumlee, R.H., 1956, R.C.A. Rev., 17, 190.

Prescott, G.H., and Morrison, J., 1938, J Amer. Chem. Soc.,
60, 3047.

Reimann, A.L., and Kerr Grant, C., 1936, Phil. Mag., 22, 34.

Rittner, E.S., 1953, Phil. Res. Rep., 8, 184.

Riviere, J.C., 1957, Proc. Phys. Soc. Lond., 70B, 676.

Roberts, J.K., 1935, Proc. Roy. Soc. Lond., 152A, 464.

Rooksby, H.P., 1940, J. Roy. Soc. Arts, 88 318.

Rooksby, H.P., 1940a, G.E.C. Journal, 11, 83.

Rooksby, H.P., 1947, Nature, 159, 609.

Russell, P.N., and Eisenstein, A.S., 1954, J. Appl. Phys., 25, 954.

Rutledge, W.C., and Rittner, E.S., 1957, J. App. Phys., 28 167.

Schottky, W., 1914, Ann. Phys. Lpz., 44, 1011.

Schottky, W., 1939, Z. Phys., 113 369.

Schottky, W., 1940, Das Freie Elektron in Physik and Technique, Springer, Berlin.

Schwarz, H., 1944, Z. Phys., 122, 437.

Seitz, F., 1940, Modern Theory of Solids, McGraw-Hill.

Shelton, H., 1957, Phys. Rev., 107, 1153.

Slater, J.C., 1939, Introduction to Chemical Physics, McGraw-Hill.

Sproull, R.L., 1945, Phys. Rev., 67, 166.

Stranski, I.N., and Shurmann, R., 1947, Ann. Phys., 1, 169.

Thomson, B.J., 1930, Phys. Rev., 36, 1415.

Tolanski, S., 1948, Multiple Beam Interferometry of Surfaces and

Films, Clarendon Press.

Venema, A., and Bandringa, M., 1958, Phil. Tech. Rev., 20, 145.

Wagener, S., 1954, Proc. Phys. Soc. Lond., 67B, 369.

Wahlin, H.B., and Sordahl, L.O., 1934, Phys. Rev., 45, 886.

Wehnett, A., 1904, Ann. Phys. 14, 425.

White, A.H., 1949, J. Appl. Phys., 20, 856.

Wilson, H.A., 1931, Proc. Roy. Soc. Lond., A134, 277.

Wood, R.W., 1915, Phil. Mag., 30, 300.

Wood, R.W., 1916, Phil. Mag., 32, 364.

Wooten, L.A., 1946, Phys. Rev., 69, 248.

Wooten, L.A., Moore, G.E., and Guldner, W.G., 1955, J. Appl. Phys., 26, 937.

Wright, D.A., 1947, Proc. Roy. Soc. Lond., A190, 394.

Wright, D.A., 1950, Brit. J. Appl. Phys., 1, 150.

Wright, D.A., 1951, Phys. Rev., 82, 574.

Wright, D.A., 1953, Proc. I.E.E., Pt. 3, 100, 125.

Wright, D.A., 1954, Brit. J. App. Phys., 5, 108.

Young, J.R., 1952, J. Appl. Phys., 23, 1129.

Young, J.R., 1960, J. Appl. Phys., 31, 921.

Zisman, W.A., 1932, Rev. Sci. Instr., 3, 367.

ACKNOWLEDGEMENTS.

The author wishes to thank his supervisor, Dr. B.J. Hopkins for his invaluable encouragement, guidance, and accessibility for discussion.

Thanks are also due to the following:-

Professors A.M. Taylor and G.W. Hutchinson for providing the laboratory facilities.

My colleagues of the Physics Department, Southampton University, for their helpful discussion during the course of the work.

Dr. G.H. Metson of the Post Office Research Station for the gift of the platinum cathode bases.

Mr. A.A. Fuller of Research and Development Services, Wareham, Dorset, England, who prepared the cathode surfaces for the work described in Appendix 1.

The Department of Scientific and Industrial Research for financial assistance.

Miss J. Cooper for her patience in typing this thesis.

Reprinted from
Proceedings of the Physical Society, Vol. 79, Part 2, No. 508
1962
Printed in Great Britain by J. W. Arrowsmith Ltd., Bristol 3

The Work Function of Zirconium Carbide

A number of reports have appeared recently which are concerned with the thermionic emission from cathodes containing uranium carbide and zirconium carbide (Pidd *et al.* 1959, Haas and Jensen 1960, Danforth and Williams 1961, Abrams and Jamerson 1961). Interest in such materials has been stimulated by some experiments and considerable speculation concerning the conversion of heat into electricity by means of thermionic emission. Much of the published experimental work relates to measurements of the emission current at a series of temperatures followed by a Richardson plot interpretation of the data. Richardson line slopes have been reported for zirconium carbide which vary from 2·1(6) ev (Haddad *et al.* 1949) and 2·3 ev (Wright 1953) for the powdered material to 3·8 (Pidd *et al.* 1959) and 4·0 ev (Danforth and Williams 1961) for the fused carbide. Objections to the Richardson line technique for the determination of work functions have been detailed by Nottingham (1956) and by Herrmann and Wagener (1951); they are particularly relevant under the vacuum conditions reported in these measurements.

A study is being made in this laboratory of the variations in anode work function that take place in diodes containing cathodes of uranium carbide, zirconium carbide and mixtures of the two. In some of the experimental tubes it has been possible to determine the cathode work function at the same time. Such a determination for uranium carbide will be reported elsewhere; the purpose of this letter is to record the measurements with zirconium carbide.

The method employed, which was the Zisman vibrating condenser modification of the Kelvin technique, serves as a measure of the contact potential difference between the unknown surface and a reference surface of known work function. Either tungsten or molybdenum is used in this laboratory for the reference electrode material; molybdenum was used in these particular experiments. If the zirconium carbide is assumed to have a uniform surface, then this technique is a measure of the true work function of the zirconium carbide. But if the surface is patchy (this is more probable) then an average work function defined by

$$\bar{\phi} = \sum_i f_i \phi_i$$

(where f_i is the fraction of the surface occupied by the ith patch of work function ϕ_i)

is determined (Herring and Nichols 1949). Unlike the Richardson slope this value is the work function of the unknown surface at the temperature of measurement (~ 300 °K).

The zirconium carbide was deposited electrophoretically on to a carburized tantalum disk. Heating to temperatures in the region 2000 °K could be achieved either by a simple electron gun or by radio-frequency induction. The reference electrode was hinged so that it could be moved away from the zirconium carbide during outgassing; the possibility of contamination between the two electrodes was thus eliminated. When suitably positioned the reference electrode could be made to vibrate at its natural frequency (about 20 c/s) by tapping the tube wall.

A continuously pumped hard glass ultra-high vacuum system of the type described by Venema and Bandringa (1958) was used in the present work. All the usual precautions were observed and the pressure throughout the measurements was within the range 10^{-9} to 10^{-10} mmHg.

Three zirconium carbide cathodes have been studied in separate experimental tubes. In tube 1 a single determination of the contact potential difference was made; in tube 2 six determinations over a period of 24 hours were obtained. Three determinations were made with tube 3. The results are as follows:

Tube 1	single determination	$0{\cdot}60 \pm 0{\cdot}01$ ev
Tube 2	six determinations	$0{\cdot}61 \pm 0{\cdot}01$ ev
Tube 3	three determinations	$0{\cdot}61 \pm 0{\cdot}01$ ev.

Operation of the zirconium carbide cathode for 24 hours at a temperature of 1500 °K produced no change in the contact potential difference with tube 2. It is concluded from this observation that no liberation of free zirconium metal (as observed by Wright 1953 for uncarburized tantalum) took place at the cathode by chemical reaction between the carbide and the tantalum base.

Adopting Rivière's value for the work function of molybdenum (Rivière 1957) the work function of the zirconium carbide is $3{\cdot}62 \pm 0{\cdot}01$ ev. If it is assumed that the zirconium carbide surface is uniform then the value of 3·62 ev represents the true work function at 300 °K. If the carbide is patchy then 3·62 is an arithmetic average over the area of any high or low work function patches on the surface.

The authors are pleased to acknowledge the help and advice of the Direct Conversion Group of the Atomic Energy Research Establishment, Harwell, who also financed the work. Thanks are due to Professors A. M. Taylor and G. W. Hutchinson for the facilities provided.

The Physical Laboratory,
The University,
Southampton.
15th December 1961.

B. J. Hopkins.
K. J. Ross.

Abrams, R. H., Jr., and Jamerson, F. E., 1961, *J. Appl. Phys.*, **32**, 1783.
Danforth, W. E., and Williams III, A. J., 1961, *J. Appl. Phys.*, **32**, 1181.
Haas, G. A., and Jensen, J. T., 1960, *J. Appl. Phys.*, **31**, 1231.
Haddad, R. E., Goldwater, D. L., and Morgan, F. H., 1949, *J. Appl. Phys.*, **20**, 886.
Herring, C., and Nichols, M. H., 1949, *Rev. Mod. Phys.*, **21**, 185.
Herrmann, G., and Wagener, S., 1951, *The Oxide Coated Cathode*, Vol. 2 (London: Chapman & Hall).
Nottingham, W. B., 1956, 'Thermionic Emission', *Handb. d. Phys.*, Vol. 21 (Berlin: Springer).
Pidd, R. W., *et al.*, 1959, *J. Appl. Phys.*, **30**, 1575.
Rivière, J. C., 1957, *Proc. Phys. Soc.* B, **70**, 676.
Venema, A., and Bandringa, M., 1958, *Philips Tech. Rev.*, **20**, 145.
Wright, D. A., 1953, *Proc. Instn Elect. Engrs*, Pt. 3, **100**, 125.

Reprinted from

ADVANCED ENERGY CONVERSION

An International Journal

PERGAMON PRESS

OXFORD · LONDON · NEW YORK · PARIS

Advanced Energy Conversion. Vol. 3, pp. 265–271. Pergamon Press, 1963. Printed in Great Britain

WORK FUNCTION MEASUREMENTS IN EXPERIMENTAL TUBES CONTAINING CATHODES OF URANIUM AND ZIRCONIUM CARBIDES

B. J. HOPKINS, K. J. ROSS and B. H. BLOTT*

Summary—Work function measurements are reported for carburized tantalum cathodes coated electrophoretically with uranium and zirconium carbides. Thermionic methods for the determination of work function have been used together with the Zisman modification of the Kelvin technique. The poor agreement found between the two sets of results is thought to indicate that thermionic emission takes place from only a fraction of the total cathode area. Work function measurements have also been made on the thin films that evaporate from these cathodes during their operation at high temperatures on to fixed anodes. When the cathode is uranium carbide, our measurements can be interpreted in terms of an evaporated film of uranium metal and uranium monoxide on the anode surface. All of this work has been performed under ultra-high vacuum conditions.

The mean work function values for tubes containing uranium carbide cathodes are as follows: the work function from the Kelvin measurements at 300°K is 3·81 ± 0·01 eV and that from the slope of a Richardson line plotted from retarding field data and applying to 0°K is 2·9 ± 0·1 eV. The temperature coefficient of the work function of uranium carbide is 5×10^{-4} eV per deg.

For zirconium carbide cathodes the mean values are: 3·62 ± 0·01, 2·5 ± 0·1 eV and 7×10^{-4} eV per deg.

The work function of the anode in a tube containing a uranium carbide cathode reaches a constant value in a few hours of 3·0 ± 0·1 eV. This, like the Kelvin results quoted above, is an arithmetic average over the area of any high and low work function patches and in this case applied to the unmeasured temperature of the anode when the cathode was operating at 1300°K.

1. INTRODUCTION

A NUMBER of reports have appeared recently which are concerned with work function measurements on refractory cathode materials containing uranium compounds. Emission measurements at a variety of temperatures under high accelerating field conditions are generally extrapolated to the zero field condition followed by a Richardson line interpretation of the data. The significance of the Richardson line slope used as a measurement of work function has been questioned by several workers [1, 2] and the aim of the investigations described in this paper was to establish the work functions of uranium and zirconium carbides using some alternative to the Richardson line technique. The method chosen was the Zisman vibrating condenser modification of the Kelvin technique which is a measure of the contact potential difference between the unknown material and a surface the work function of which is either assumed, as in this work, or measured by some other method—frequently photoelectric. The reference surface normally used in this work was tungsten, though on occasion molybdenum was substituted. As there is no accepted average work function for polycrystalline tungsten at 300°K, we have followed Anderson [3] in assuming that the thermionic measurements of Dushman *et al.* [4] represent a reference level for the comparison of contact potentials. Accordingly the work function of the tungsten surface after suitable ageing at elevated temperatures was assumed to be 4·52 eV. In the single experimental tube cited below where molybdenum was used as a reference surface the contact potential difference between molybdenum and tungsten was taken from the measurements of Rivière [5]; the work function of molybdenum was then 4·22 ± 0·05 eV.

* The Physical Laboratories, The University, Southampton, England.

During these investigations the Richardson line slope for any given cathode was measured either immediately before or after the contact potential measurements. The necessary zero field conditions were obtained from retarding potential characteristics.

One type of experimental tube was designed specifically to follow the work function changes taking place at the anode as films were evaporated from the cathode during operation. This could be done by one of two methods; by the Kelvin technique or by the displacement of the retarding potential characteristic along the voltage axis resulting from the introduction of a reference surface.

Determinations of the temperature coefficient of the work function should be possible in some of these experimental tubes using the Kelvin technique; unfortunately such measurements have not been made with sufficient accuracy to justify publication at this stage. Only data from effective work function plots are therefore recorded in this paper.

2. EXPERIMENTAL

Schematic diagrams of the two types of experimental tubes used in this work are shown in Figs. 1 and 2. Three cathode designs were tested during the work; the first of these was a simple disk of tantalum 1·5 cm in diameter fitted with two mounting flanges. Heating was either via an external R.F. heater or by electron bombardment from an auxiliary fila-

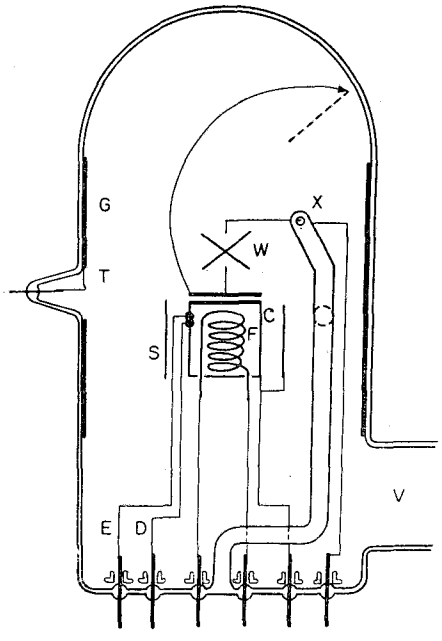

FIG. 1. Experimental tube used for the cathode work function measurements.

ment inside the tube. A very uneven temperature distribution was common with these cathodes nor was it possible to measure the low emission currents necessary for accurate retarding potential plots. Directly heated tantalum strips (1·5 × 0·3 cm) were much more satisfactory in both these respects. These are shown in Fig. 2. In order to measure the temperature coefficient of the work function using the Kelvin technique, voltage gradients over the cathode surface due to the heater current had to be eliminated. The most recent

cathode design (see Fig. 1) was therefore an indirectly heated tantalum box (*C*) (1·5 cm side) heated by radiation from a tungsten filament (*F*) inside the box. The maximum temperature so far achieved with these cathodes when fitted with radiation shields (*S*) was about 1800°C.

The surfaces of these cathodes to be coated were initially carburized by heating to about 2000°C in a flux of carbon vapour. The carbide was then deposited electrophoretically, the cathode dried, sintered and stored in argon until required. Sealing into the experimental tubes took place in a stream of dry nitrogen with the cathode cold.

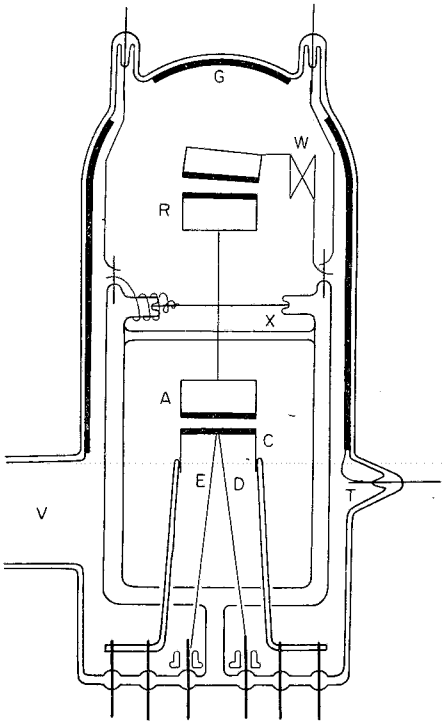

FIG. 2. Experimental tube used for the anode work function measurements.

Movement in both types of experimental tubes took place about the axis of the tungsten–glass hinges *X*; the rotor was turned when the tube was fixed in position on the vacuum system by the action of an external magnet on a glass-encased iron slug inside the tubes. In tubes of the type shown in Fig. 1, the reference electrode was also the anode for any emission measurements; in the tubes of Fig. 2 a specific molybdenum anode was provided together with two reference electrodes, one of which was attached to the rotor for use in the displacement of the characteristic technique. The reference surface for use with the Kelvin technique was mounted on a tungsten spring arrangement (*W*) so that it could vibrate at its natural frequency of about 15 c/s when stimulated electromagnetically from outside the tube. All non-conducting surfaces inside the tubes, except those required for insulation purposes, were coated with a conducting film of colloidal graphite (*G*) which could be earthed externally via a tungsten seal (*T*) through the hard glass envelope. The temperature of the cathode was followed by using a tungsten/tungsten–26 per cent rhenium

[6] thermocouple (*ED*) spot welded immediately under the emitting surface. This thermocouple was calibrated up to 1800°K against a platinum/platinum–rhodium thermocouple and carried beyond that point using data supplied by the manufacturers. The completed tubes were sealed via a 25 mm arm (*V*) to a pumping system of the type first described by Venema and Bandringa [7]. Pressure readings throughout the measurements were usually within the range 10^{-9} to 10^{-10} mm Hg.

The Kelvin contact potential difference measurements were made at room temperature in the usual manner of backing off the signal by the application of a measured potential in series with the electrodes. A conventional low frequency amplifier was used with an electrometer first stage. Screening from 50 c/s pick-up had to be arranged carefully and the final output to the oscilloscope was filtered.

3. RESULTS

Table 1 shows the results obtained for the measurements on cathodes or uranium and zirconium carbides by both the Kelvin and the Richardson line techniques.

TABLE 1. CATHODE WORK FUNCTIONS (eV)

	Tube No.	ϕ Kelvin	ϕ Richardson	$d\phi/dT$
Uranium carbide	U1	$3{\cdot}97 \pm 0{\cdot}015$	—	—
	U2	$3{\cdot}74 \pm 0{\cdot}01$	$2{\cdot}8 \pm 0{\cdot}1$	5×10^{-4}
		$3{\cdot}71 \pm 0{\cdot}01$	$2{\cdot}8 \pm 0{\cdot}1$	6×10^{-4}
		$3{\cdot}74 \pm 0{\cdot}01$	—	—
	U3	$3{\cdot}92 \pm 0{\cdot}01$	$3{\cdot}3 \pm 0{\cdot}1$	2×10^{-4}
		—	$3{\cdot}1 \pm 0{\cdot}1$	5×10^{-4}
		—	$2{\cdot}6 \pm 0{\cdot}1$	5×10^{-4}
		—	$2{\cdot}7 \pm 0{\cdot}1$	5×10^{-4}
		—	$2{\cdot}8 \pm 0{\cdot}1$	5×10^{-4}
Zirconium carbide	Z1	$3{\cdot}61 \pm 0{\cdot}01$	—	—
	Z2	$3{\cdot}62 \pm 0{\cdot}01$	$2{\cdot}6 \pm 0{\cdot}1$	6×10^{-4}
			$2{\cdot}2 \pm 0{\cdot}1$	6×10^{-4}
			$2{\cdot}7 \pm 0{\cdot}1$	9×10^{-4}
	Z3	$3{\cdot}61 \pm 0{\cdot}01$	—	—
	Z4	$3{\cdot}62 \pm 0{\cdot}01$	—	—

Typical emission characteristics used in the calculation of the Richardson work functions are shown in Fig. 3. The three sets of measurements with tube U2 were separated by several days during which emission was drawn from the cathode at 1800°K. With tube U3 the first state was immediately after an ultra-high vacuum had been attained, the second was after 15 hr further outgassing at 1800°K. The last three states were achieved after emission had been drawn from the cathode at a temperature of 1800°K and were separated by periods of 24 hr. The Richardson lines corresponding to tube U3 are shown in Fig. 4. Unfortunately, because of distortion in tube U3 it was only possible to measure the Kelvin work function immediately after out-gassing the cathode, i.e. in state 1.

The data for the temperature coefficient of the work function was obtained either from the Richardson plots or from effective work function plots, in both cases assuming the theoretical value of *A*.

Since the anode work function measurements are at a very early stage and little data is available, the results presented should be regarded as preliminary. Satisfactory measurements have been obtained from one experimental tube based on the shift in the retarding potential characteristic along the voltage axis when a reference surface was interposed for the anode under investigation. In this instance molybdenum was the reference surface and the cathode was uranium carbide.

Table 2 shows the series of seven measurements with this tube, each of which corresponds to the indicated number of hours with the cathode operated at 1850°K. From these results the anode surface appears to be covered with a film of evaporated material within

TABLE 2. ANODE WORK FUNCTIONS

Time (hr)	Work function (eV)
0	$4{\cdot}2 \pm 0{\cdot}15$
24	$2{\cdot}9 \pm 0{\cdot}15$
45	$2{\cdot}9 \pm 0{\cdot}15$
77	$3{\cdot}2 \pm 0{\cdot}15$
105	$2{\cdot}9 \pm 0{\cdot}15$
125	$3{\cdot}1 \pm 0{\cdot}15$
145	$3{\cdot}2 \pm 0{\cdot}15$

a few hours; over a period of 145 hr this remains at a constant work function of about three electron volts. Typical data used in the determination of the voltage shift is also shown on Fig. 3 where the two retarding potential curves were plotted for a cathode temperature of 1300°K.

4. DISCUSSION OF THE RESULTS

After a temperature correction had been applied to the work function measurements derived from the Richardson line technique so that they apply to 300°K, a considerable discrepancy still exists with the results from the Kelvin technique; averages of 3·0 as compared with 3·8 eV in the case of uranium carbide and 2·7 compared with 3·6 for zirconium carbide. An obvious explanation of these results is in terms of patches of differing work function at the cathode surfaces. The Kelvin method is then a measure of an arithmetic average over the area of the high and low work function patches, while the emission measurements reflect an average work function but heavily weighted towards the areas of greatest emission. On assuming that the surface is composed of only two components, one of high and one of low work function, and allotting an arbitrary value to the high work function patches, it is possible to calculate the areas occupied by the two constituents. If the arbitrary value is 4·5 eV for both the uranium and the zirconium carbides then the emitting areas of the cathodes are about 50 per cent. Such an interpretation is only possible if the emission measurements made at the intersection points between the retarding and the accelerating potential regions correspond to the case 1 accelerating fields discussed by Herring and Nichols [1]. Provided that the patch dimensions are large (about 1 mm dia.) this seems to be possible. The uranium carbide measurements of Haas and Jensen [8] using high accelerating fields which were without doubt case 1 fields, are in good agreement with the present work as far as the Richardson line work function is concerned but their measurements indicate very much smaller patch dimensions. Haas and Jensen in fact attempted to use the emission

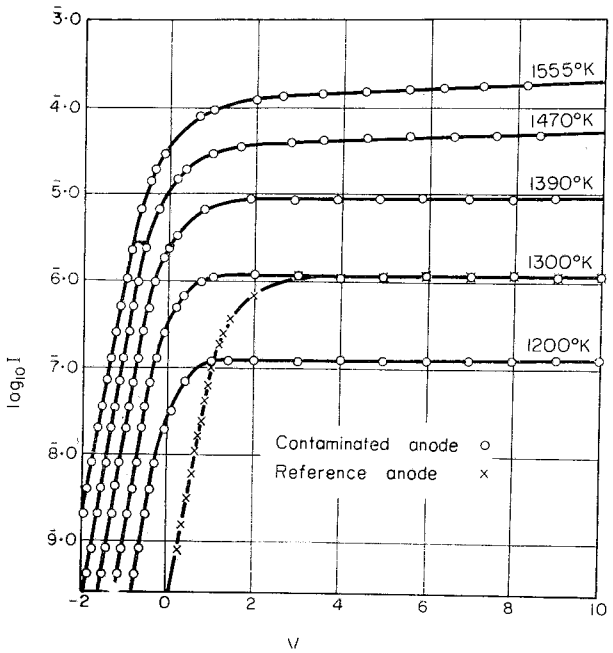

FIG. 3. Emission characteristics as used in the Richardson calculations and also the anode work function measurements.

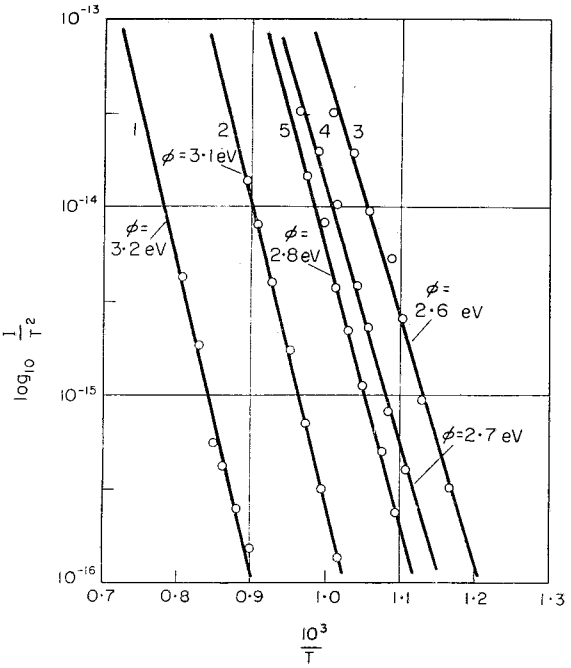

FIG. 4. Richardson lines for tube U3 containing a uranium carbide cathode. The line for state 1 has been displaced to the left.

values obtained at the intersection point in order to estimate the average work function of the emitter, that is accepting this point as corresponding to case 2 accelerating fields. Had this been true in our measurements then agreement should be expected between the Kelvin and the Richardson line measurements.

It is interesting to speculate concerning the nature of the material that is evaporating from the uranium carbide cathodes on to the anode surface. One explanation might be that uranium monocarbide evaporates from the cathode to form a uniform layer on the anode with a true work function corresponding roughly to the thermionic work function measurements on the patchy cathodes, about 3 eV. An explanation which is thought more probable in this laboratory is that uranium is evaporating from the cathode which condenses on the relatively cold anode causing a reduction in its work function. Rivière [9] has measured the work functions of evaporated uranium films using the Kelvin technique and finds a reproducible value of $3{\cdot}208 \pm 0{\cdot}013$ eV. Where contamination of these films is possible by uranium monoxide the work function falls and eventually reaches a limiting value of $3{\cdot}085 \pm 0{\cdot}005$ eV. The presence of uranium monoxide in the uranium carbide cathodes has been established, and it is therefore quite possible that some oxide contamination of the anode could take place by evaporation to account for the agreement between the work functions in Table 2 and Rivière's value of 3·085 eV.

Such evaporation of uranium at 1800°K would be expected to proceed very rapidly at 2300°K and might explain the poisoning effects observed in this laboratory and elsewhere in this temperature range. Perhaps the uranium dicarbide that might be left behind on the poisoned cathode is also the material responsible for the high work function patches on the active cathodes described above. All this of course is conjecture but it is along these lines that further experiments will be conducted in this laboratory.

Acknowledgements—The authors are pleased to acknowledge the help and advice of the Direct Conversion Group of the Atomic Energy Research Establishment, Harwell, who also financed the work. The assistance of Mr. A. A. Fuller of Research and Development Services, Wareham, Dorset, England, who prepared the cathode surfaces is also gratefully acknowledged. Finally thanks are due to Professors G. W. Hutchinson and A. M. Taylor for the facilities provided.

REFERENCES

[1] C. Herring and M. H. Nichols, *Rev. Mod. Phys.* **21**, 185 (1949).
[2] C. Herrmann and S. Wagener, *The Oxide Coated Cathode*, Vol. 2, Chapman and Hall, London (1951).
[3] P. A. Anderson, *Phys. Rev.* **47**, 958 (1935).
[4] S. Dushman, M. H. Rowe, J. Ewald and C. A. Kidner, *Phys. Rev.* **25**, 338 (1925).
[5] J. C. Rivière, *Proc. Phys. Soc.* B, **70**, 676 (1957).
[6] Engelhard Industries Ltd., London.
[7] A. Venema and M. Bandringa, *Philips Tech. Rev.* **20**, 145 (1958).
[8] G. A. Haas and J. T. Jensen, *J. Appl. Phys.* **31**, 1231 (1960).
[9] J. C. Rivière, *Proc. Phys. Soc.* **80**, 116 (1962).

Reprinted from JOURNAL OF APPLIED PHYSICS, Vol. 34, No. 7, 2111–2112, July, 1963

Anode Work Function Changes Caused by Sublimation from Barium Oxide under Applied Anode Potentials

B. J. HOPKINS AND K. J. ROSS
Department of Physics, The University, Southampton, England
(Received 25 February 1963)

MEASUREMENTS of the sublimation rate from barium oxide similar to those described recently by Florio[1] are reported in this communication. Further, the potential to which the anode is raised above the cathode during the evaporation can profoundly affect the shape of the anode work function versus time curves.

Platinum, Pt–Rh thermocouples were fitted to the platinum bases used in our work, which were then outgassed in vacuum at 1500°K until the pressure fell below 10^{-7} Torr. Finally, they were sprayed with a suspension of barium carbonate containing a nitrocellulose binder. Tungsten strip anodes were fabricated and hinged such that they could be moved magnetically through 180° into a region of the experimental tube remote from the cathode. The use of a radio-frequency heater for cleaning the strips permitted the anode to be maintained at a uniform temperature just below the melting point for extended periods, thus ensuring a clean surface before each run. The work function of the clean tungsten was assumed to be 4.5 eV.

The experimental tubes were continuously pumped on a vacuum system of the type described by Venema and Bandringa.[2] Cleaning of the anode surface never caused the pressure in the system to exceed 10^{-9} Torr.

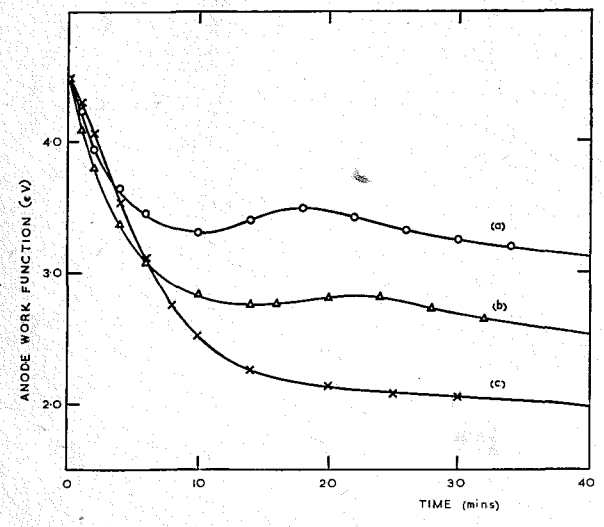

FIG. 1. The change in work function of a tungsten anode vs time of exposure to the sublimate from a barium oxide-coated platinum cathode at a temperature of 1173°K. Curve (a) was obtained early in the cathode life; curve (b) after the application of various anode potentials for a period of approximately 120 h; curve (c) was obtained with a potential of +100 V applied to the anode during the sublimation.

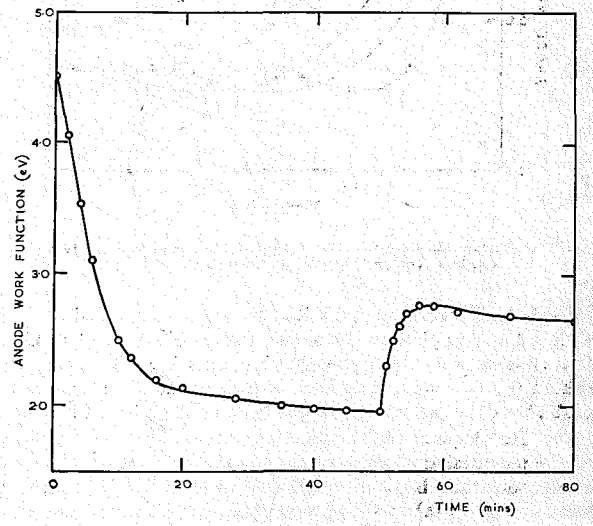

FIG. 2. A curve identical with that in Fig. 1(c) except that after 50 min the anode potential was removed.

The measurement technique of this investigation was similar to that used for the low-temperature data of Florio; sublimation at an elevated cathode temperature for a fixed period, then cooling the cathode for a point in the plot of anode work function (ϕ_A) against time. The success of this method for following changes in the anode work function requires constancy of the electron temperature during the measurements. The retarding potential plots before and after completion of each curve of anode work function versus time were always parallel and so indicated that changes in the electron temperature were less than 5%. Agreement between the electron temperature and the thermocouple reading was usually better than 10%.

The carbonates were decomposed to oxide by pyrolysis at 1173°K over a period of 48 h. Positive potentials of 4, 20, 50, 75, and 100 V were each successively applied to the anode for 24 h with the cathode at 1173°K. Following each 24-h treatment a curve of anode work function versus time was determined.

Some of the most interesting points arising from our measurements are:

(a) Immediately following the decomposition of the carbonate to oxide, curves such as the one shown in Fig. 1 (curve a) were obtained. A spread of ±0.1 eV on the ϕ_A scale and ±5 sec on the time scale was found from tube-to-tube. The final minimum work function of 3.0 eV was reached after a period of about 7 h with the

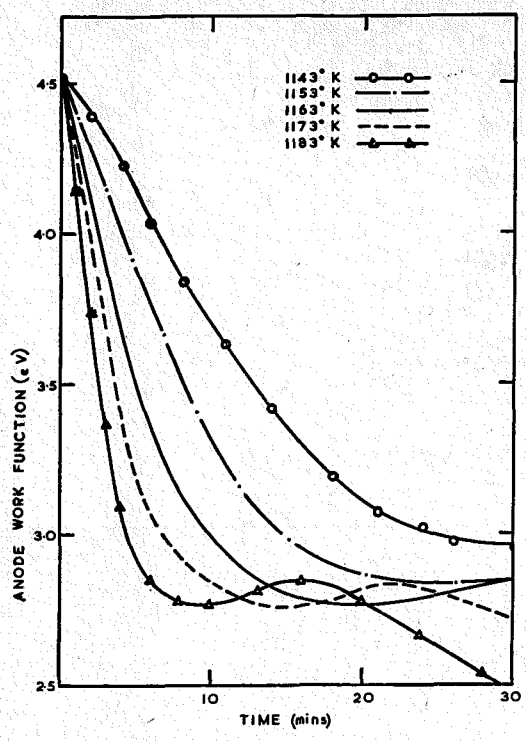

FIG. 3. Curves showing the rate of contamination of a clean tungsten anode vs temperature of the barium oxide cathode.

cathode temperature at 1173°K. After the final period of 24 h, with +100 V applied to the anode, curve (b) of Fig. 1 resulted. It is obvious from this curve that not only has the whole curve shifted to lower work functions, but also that the height of the peak above the first minimum has been reduced by a factor of 2.

(b) The shape of the curves of ϕ_A versus time was dependent on the potential applied to the anode during the sublimation. For anode potentials between −100 and +30 V, curves similar to those in Fig. 1 [(a) and (b)] were obtained. When the anode potential exceeded +30 V not only was the inflexion completely removed, but an appreciably lower anode work function resulted. The mean final anode work function for anode potentials exceeding +30 V was 2.0 eV.

(c) A reduction of the anode potential from +100 V to zero during sublimation caused the change in work function shown in Fig. 2. The final shape of the curve then followed closely that of curve (b) in Fig. 1.

(d) After completion of the cathode processing described above, about 120 h at 1173°K with the anode at the various potentials between 4 and 100 V, sublimation data (with no voltage applied to the anode) were prepared from a family of curves such as those shown in Fig. 3. All of these curves had the same shape as the curves in Fig. 1 [(a) and (b)] though at the lower temperatures the first minimum had not been reached on the figure. The method was essentially the same as that described by Florio, though our plots were prepared by measuring the time required at each temperature to reduce the anode work function by a fixed amount in the region before the first minimum. Within the temperature range 1143° to 1183°K the activation energy of the sublimation process was 4.9±0.2 eV. Published data[3–6] indicate activation energies of 3.8, 3.75, 3.8, and 3.75, respectively, though the data of Pelchowitch[7] show a spread from 4.08 to 4.96 eV.

The interpretation of the experimental data is not straightforward since the application of an anode potential can have several effects. Electron bombardment of the anode deposits can lead to their decomposition when the electron energy exceeds about 4 eV.[8,9] Current flow through the barium oxide matrix can cause its dissociation and under certain conditions the products of dissociation find their way to the anode. The electric field between the anode and cathode can also cause orientation of the barium oxide dipoles on the anode surface. Finally, some of these materials may be mobile on the anode surface since the temperature during the sublimation without an anode potential is about 400°K, but an increase to 500°K occurs with an anode potential of +100 V.

It is a pleasure to acknowledge many helpful discussions with Dr. C. H. B. Mee during the course of this work.

[1] J. V. Florio, J. Appl. Phys. **34**, 200 (1963).
[2] A. Venema and M. Bandringa, Philips Tech. Rev. **20**, 145 (1958–59).
[3] A. Claasen and C. F. Veenemans, Z. Physik. **80**, 342 (1933).
[4] J. P. Blewett, N. A. Liebhafsky, and E. F. Hennelly, J. Chem. Phys. **7**, 478 (1939).
[5] N. D. Morgulis, Soviet Phys.—Solid State (English Transl.) **1**, 1029 (1960).
[6] L. T. Aldrich, J. Appl. Phys. **22**, 1168 (1951).
[7] I. Pelchowitch, Philips Res. Rept. **9**, 42 (1954).
[8] D. A. Wright, Brit. J. Appl. Phys. **5**, 108 (1954).
[9] G. H. Metson, *Advances in Electronics and Electron Physics* (Academic Press Inc., New York, 1956), Vol. 8.